

Application of the crystalline sponge method for metabolite structure elucidation

Dissertation

zur Erlangung des Grades
des Doktors der Naturwissenschaften
der Naturwissenschaftlich-Technischen Fakultät
der Universität des Saarlandes

von

Apothekerin Lara Annette Rosenberger

Saarbrücken

2022

Tag des Kolloquiums: 19. September 2022
Dekan: Prof. Dr. Jörn Eric Walter
Berichterstatter: Prof. Dr. Rolf W. Hartmann
Prof. Dr. Anna K. H. Hirsch
Akad. Mitglied: Dr. Stefan Boettcher
Vorsitz: Prof. Dr. Rolf Müller

Die vorliegende Arbeit wurde von Juni 2018 bis Juni 2021 unter Anleitung von Herrn Dr. Lassina Badolo in der Abteilung Drug Metabolism and Pharmacokinetics (DMPK) des pharmazeutisch-chemischen Unternehmens Merck KGaA in Darmstadt in Kollaboration mit Univ. Prof. Dr. Rolf W. Hartmann und Univ. Prof. Dr. Anna K. H. Hirsch in der Fachrichtung Pharmazeutische und Medizinische Chemie der Naturwissenschaftlich-Technischen Fakultät der Universität des Saarlandes sowie am Helmholtz-Institut für Pharmazeutische Forschung Saarland (HIPS) angefertigt.

Acknowledgements

Throughout the experimental part and the writing of this dissertation I have received a great deal of support.

I would first like to thank my supervisor, Dr. Lassina Badolo, for his continuous support of my doctoral study, for his persistent enthusiasm for my research project, motivating speeches and valuable expertise regarding scientific questions and methodology. His guidance pushed me to successfully explore innovative approaches and to grow beyond what I thought my limits are, making my PhD time to an inspiring experience. Likewise, I would like to thank my supervisors Prof. Dr. Rolf W. Hartmann and Prof. Dr. Anna K. H. Hirsch for their support and advice through all the stages of my PhD project.

I would also like to thank my colleagues from the DMPK department, Ralf-Erwin Licht, Marlene Hagel, Ulrich Seibl, Katharina Reber, Benedikt Lang and Christian Stelz for their excellent laboratory support and kind integration into the team. Furthermore, I would like to thank Dr. Hanno Schieferstein, Dr. Jonny Nachtigall, Dr. Holger Scheible and Birikiti Kidane for their experimental support and our scientific discussions which directed me to think outside of the box. I would like to extend my thanks to Dr. Katrin Georgi and Dr. Klaus Urbahns for their advice and administrative support of the PhD study. Additionally, I would like to thank my PhD colleague Lena Preiss for the time we spent together in the lab, and in social settings.

My sincere thanks also go to the members of the Crystal-Do project. Thereby, I would like to thank Dr. Clemens Kühn for incorporating me into his lab and the team activities, as well as for the trust and the opportunity I was given to independently and limitless conduct my research work using the project's resources and equipment. I also would like to express my gratitude to Dr. Carolina von Essen for the transfer of knowledge and her guidance in the field of crystallography, as well as for the steadily support of my project and proofreading of my thesis. Furthermore, I would like to thank Dr. Anupam Khutia for his introduction and training of soaking experiments and Steffen Blauenburg for the continuous supply of crystalline sponge material. I am also thankful to Deborah Steinle, Dr. Judith Jenniches and Allen-Jeffrey Bonaldi for their kind technical support in the lab.

I am indebted also to several colleagues from different laboratories at Merck KGaA. I gratefully recognize Axel-Walter Thomasberger for his guidance and support regarding chromatographic separation techniques, as well as Alena Sommer, Christian Kolb, Renate Henkes and Dr. Andrea Unzue Lopez for their help with organic synthesis. I also had the pleasure to work with Dr. Andreas Marx, who

Acknowledgements

conducted and evaluated the NMR measurements. I also want to recognize Ruben Numrich, who supported me during his pharmaceutical internship with the provision of data.

Lastly, my appreciation also goes to my parents and my sister for their unconditional and unequivocal support, as well as regular encouragement at every stage of this journey.

Summary

The identification of metabolites during drug discovery and development can play a crucial role to understand their contribution to efficacy and safety. To investigate the metabolism of new drug candidates in human as early as possible, different *in vitro* systems from human origin are used. Standard structural elucidation tools like liquid chromatography-mass spectrometry, single-crystal X-ray diffraction or nuclear magnetic resonance spectroscopy are either limited in providing the complete structure of metabolites or require a larger amount of material not available from *in vitro* incubations. A new technology to overcome these limitations was introduced by Makoto Fujita in 2013 and is commonly known as the crystalline sponge method. The usage of a pre-existing crystal allows the complete crystallographic identification of small molecules at the atomic level by encapsulation of only nanogram amount of analyte material without the need for crystallization of the analyte itself.

In this thesis, the structural elucidation of metabolites generated from *in vitro* incubations using the crystalline sponge method is described. First, the analysis of an active pharmaceutical ingredient and its known metabolites demonstrated, that the crystalline sponge technology is a valuable method to identify the complete structure of trace amounts of analytes isolated from incubation matrices. The crystallographic data provided the exact position of metabolism for phase I and phase II metabolites. The technology was further used to identify various known and unknown metabolites of the anthelmintic drug praziquantel, which has been used for treatment of the parasitic flatworm of the genus *Schistosoma* for several decades. Moreover, to optimize the soaking process of the crystalline sponge method, which is the key element of the technology, an affinity screening to prioritize the optimal soaking conditions for individual analytes without time-consuming X-ray diffraction measurements, was developed.

Zusammenfassung

Die Identifizierung von Metaboliten während der Arzneimittelforschung und -entwicklung spielt eine wichtige Rolle um deren Beteiligung an der Wirksamkeit und Unbedenklichkeit zu verstehen. Um den humanen Metabolismus von neuen Wirkstoffkandidaten so früh wie möglich zu untersuchen, werden verschiedene *in vitro* Systeme humanen Ursprungs verwendet. Konventionelle Strukturaufklärungsmethoden wie Flüssigchromatographie gekoppelt mit Massenspektrometrie, Einkristall-Röntgenstrukturanalyse oder Kernspinresonanzspektroskopie sind einerseits begrenzt in ihrem Informationsgehalt in Bezug auf die vollständige Metabolitenstruktur oder benötigen eine hohe Menge an Probenmaterial, welches durch *in vitro* Inkubationen nicht zur Verfügung steht. Eine Möglichkeit zur Überwindung dieser Einschränkungen wurde 2013 von Makoto Fujita vorgestellt und ist allgemein bekannt als Crystalline Sponge Methode. Die Verwendung eines bereits vorhandenen Kristalls erlaubt die kristallografische Bestimmung von kleinen Molekülen auf atomarer Ebene durch die Aufnahme von Nanogramm Mengen an Analytmaterial in das Kristallgitter und vermeidet dadurch die Notwendigkeit eines Einkristalls des Analyten.

In der vorliegenden Dissertation wurde die Strukturaufklärung von Metaboliten aus *in vitro* Inkubationen unter Verwendung der Crystalline Sponge Methode beschrieben. Zunächst wurde anhand eines pharmazeutischen Wirkstoffes und seiner bekannten Metabolite veranschaulicht, dass die Crystalline Sponge Technologie eine nützliche Methode zur Bestimmung der vollständigen Struktur von geringen Mengen isolierter Analyten aus Inkubationsmatrizes darstellt. Die kristallografischen Daten bestimmten die exakte Position des Metabolismus für die vorliegenden Phase I und Phase II Metaboliten. Die Technologie wurde weiterhin zur Strukturaufklärung von bereits bekannten, sowie unbekanntem Metaboliten des anthelmintischen Arzneistoffes Praziquantel verwendet, welcher seit vielen Jahrzehnten für die Behandlung des parasitären Plattwurms der Gattung *Schistosoma* eingesetzt wird. Um den entscheidenden Schritt der Crystalline Sponge Methode zu optimieren, wurde des Weiteren ein Affinitätsscreening zur Priorisierung der optimalen Methodenparameter für individuelle Analyten ohne Einsatz von zeitaufwendigen Röntgenkristallstrukturmessungen entwickelt.

Publications included in this thesis

Publication 1: Lara Rosenberger, Carolina von Essen, Anupam Khutia, Clemens Kühn, Klaus Urbahns, Katrin Georgi, Rolf W. Hartmann, and Lassina Badolo; Crystalline sponges as a sensitive and fast method for metabolite identification: Application to gemfibrozil and its phase I and II metabolites. *Drug Metab. Dispos.* 48, 587–593 (2020).

Publication 2: Lara Rosenberger, Carolina von Essen, Anupam Khutia, Clemens Kühn, Katrin Georgi, Anna K. H. Hirsch, Rolf W. Hartmann, and Lassina Badolo; Crystalline sponge affinity screening: A fast tool for soaking condition optimization without the need of X-ray diffraction analysis. *Eur. J. Pharm. Sci.* 164, 105884 (2021).

Publication 3: Lara Rosenberger, Judith Jenniches, Carolina von Essen, Anupam Khutia, Clemens Kühn, Andreas Marx, Katrin Georgi, Anna K. H. Hirsch, Rolf W. Hartmann, and Lassina Badolo; Metabolic profiling of S-praziquantel: Structure elucidation using the crystalline sponge method in combination with mass spectrometry and nuclear magnetic resonance. *Drug Metab. Dispos.* 50, 320–326 (2022).

Contribution Report

Publication 1:

- Participated in research design and compound selection
- Conducted *in vitro* experiments, chromatographic separation and purification
- Performed part of the crystalline sponge soaking experiments, X-ray diffraction measurements and was involved in crystallographic evaluation
- Wrote main parts of the manuscript and experimental section, prepared most of the figures

Publication 2:

- Participated in research design
- Selected test compounds for evaluation of screening method
- Performed the crystalline sponge affinity screening experiments and UPLC-MS² measurements
- Conducted X-ray diffraction measurements and did most of the crystallographic evaluation and finalization
- Wrote main parts of the manuscript and experimental section, prepared most of the figures

Publication 3:

- Participated in research design and compound selection
- Conducted *in vitro* experiments, chromatographic separation and purification
- Performed the crystalline sponge soaking experiments and X-ray diffraction measurements
- Accomplished main part of the crystallographic data evaluation and finalization
- Wrote the manuscript and experimental section, prepared most of the figures

Abbreviations

ADH	alcohol dehydrogenase
ADME	absorption, distribution, metabolism and excretion
AF	affinity factor
ALDH	aldehyde dehydrogenase
AOX	aldehyde oxidase
API	active pharmaceutical ingredient
CO	carbon monoxide
CI	chemical ionization
CS	crystalline sponge
CSD	Cambridge Structural Database
CS-XRD	crystalline sponge method
CYP450	cytochrome P450
Da	dalton
DMPK	drug metabolism and pharmacokinetics
EI	electron ionization
EMA	European Medicines Agency
ESI	electrospray ionization
FDA	Food and Drug Administration
FMO	flavin-containing monooxygenase
GSH	glutathione
LC-MS	liquid chromatography-mass spectrometry
LLOD	lower limit of detection
MALDI	matrix-assisted laser desorption ionization
MAO	monoamine oxidase
MetID	metabolite identification
mDa	millidalton
MIST	metabolites in safety testing
MOF	metal-organic framework
MS	mass spectrometry
MS ²	tandem mass spectrometry

Abbreviations

m/z	mass-to-charge ratio
NADPH	nicotinamide adenine dinucleotide phosphate (reduced form)
NAPQI	<i>N</i> -acetyl- <i>p</i> -benzoquinone imine
NCE	new chemical entity
NMR	nuclear magnetic resonance
PAPS	3'-phosphoadenosine-5'-phosphosulfate
pm	picometre
PZQ	praziquantel
Q	quadrupole mass filter
QIT	quadrupole ion trap
QqQ	triple-quadrupole
SC-XRD	single-crystal X-ray diffraction
TOF	time-of-flight
tpt	2,4,6-tris(4-pyridyl)-1,3,5-triazine
UDPGA	uridine diphosphate α -D-glucuronic acid
UGT	uridine diphosphate-glucuronosyltransferase
UPLC	ultra-performance liquid chromatography

Table of Contents

Acknowledgements	IV
Summary	VI
Zusammenfassung.....	VII
Publications included in this thesis	VIII
Contribution Report	IX
Abbreviations	X
1. Introduction.....	1
1.1 Metabolism of Xenobiotics	1
1.2 Metabolite identification in drug discovery and development.....	3
1.3 Structural elucidation of small molecules	5
1.3.1 Mass spectrometry.....	5
1.3.2 Single-crystal X-ray diffraction	7
1.4 Crystalline sponge method.....	9
2. Aim and Scope	12
3. Results	13
3.1 Chapter A: Crystalline sponges for metabolite identification	13
3.2 Chapter B: Crystalline sponge affinity screening.....	21
3.3 Chapter C: Metabolic profiling of S-praziquantel using crystalline sponges.....	30
4. Final Discussion	38
4.1 Structural elucidation of APIs and metabolites using CS-XRD	38
4.1.1 Gemfibrozil and its phase I and II metabolites.....	38
4.1.2 S-PZQ and its hydroxylated phase I metabolites.....	41
4.2 CS Affinity Screening	43
5. Conclusions and Outlook.....	46
6. References.....	48
7. Appendix.....	54
7.1 Supporting Information Chapter A.....	54
7.2 Supporting Information Chapter B.....	67
7.3 Supporting Information Chapter C.....	95

1. Introduction

1.1 Metabolism of Xenobiotics

Xenobiotics are chemical substances, not naturally produced within a living organism and without a physiological function. Through evolution, the human body has developed different defense mechanisms to prevent their entering (*e.g.*, absorption, transporter proteins) or to remove potentially toxic compounds (*e.g.*, metabolism, elimination through bile and urine). The fate of a drug within an organism is commonly described with the abbreviation ADME (absorption, distribution, metabolism and excretion) and contains the processes of its disposition.¹ The aim of metabolism is the enzyme-mediated conversion of lipophilic compounds (good absorption through biological barriers) to hydrophilic metabolites (increased water solubility and renal excretion). These biotransformation reactions can be classified as functionalization reactions (phase I transformation) and conjugation reactions (phase II transformation) (Figure 1).²

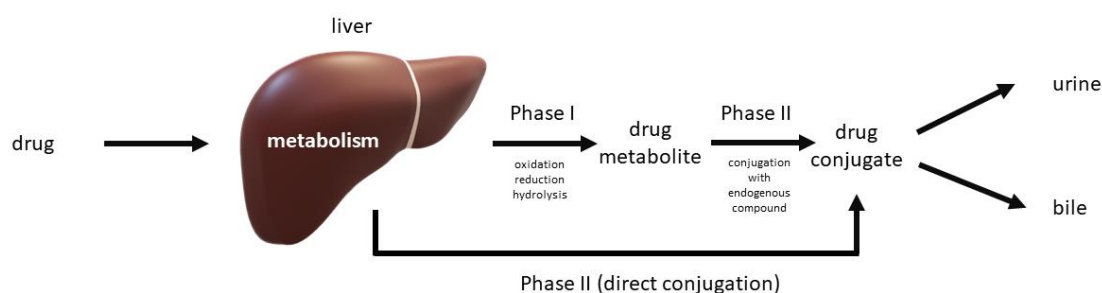


Figure 1: Phase I and Phase II biotransformation of drugs.

Phase I metabolism reactions introduce a functional group into the xenobiotic molecular structure or modify an already existing group (*e.g.*, -OH, -NH₂, -SH) and include oxidation, reduction and hydrolysis reactions. These reactions are catalyzed by drug metabolizing enzymes including the cytochrome P450 (CYP450) isozymes, the amine oxidases (*e.g.*, flavin-containing monooxygenase (FMO), monoamine oxidase (MAO)), molybdenum-based oxidases (*e.g.*, aldehyde oxidase (AOX)), reductases (*e.g.*, alcohol dehydrogenase (ADH), aldehyde dehydrogenase (ALDH)) and hydrolases (*e.g.*, esterases, amidases).^{3,4} The liver is the major site of metabolism but the enzymes are also located in *e.g.*, lung, kidney or the gut wall. The enzymes which play an important and major role in the metabolism of drugs and endogenous compounds and are ubiquitous across different species, are the CYP450 (P = pigment/porphyrin; λ_{\max} = 450 nm with CO as ligand) microsomal monooxygenases.^{5,6} This superfamily of enzymes is a hexa-coordinated ferric complex, with heme as prosthetic group and Fe³⁺ as central

Introduction

atom and catalyzes the introduction of one oxygen into the substrate (RH) while the second oxygen is reduced to water ($\text{RH} + \text{O}_2 + \text{NADPH} + \text{H}^+ \rightarrow \text{ROH} + \text{H}_2\text{O} + \text{NADP}^+$).³ The reduced cofactor nicotinamide adenine dinucleotide phosphate (NADPH) is needed as an electron donor during this reaction.⁷ CYP450 enzymes are highly expressed in the liver and mainly located in the lipid bilayer of microsomes, which are subcellular vesicle-like artifacts of the endoplasmic reticulum.⁸ Currently, 57 CYP450 enzymes are known in humans and are classified in 18 families and various subfamilies.^{9,10} The major enzymes responsible for the metabolism of drugs are CYP3A4, CYP2D6, CYP2C9, CYP2C19 and CYP1A2.^{2,11}

Phase II conjugation reactions comprise the addition of an endogenous molecule (substrate) like glucuronic acid, glutathione (GSH; a peptide of three amino acids), sulfate, acetate or amino acids directly to an already existing functional group or after a preceding oxidative phase I modification. As these molecules consist of polar groups, the conjugation to the xenobiotic compound results not only in an increase in polarity (except the addition of acetate) but also in an increase of the molecular weight (*e.g.*, +176 Da for glucuronic acid) and the degree of ionization at physiological pH to facilitate their elimination.³ During the reaction phase II enzymes, the so called transferases, catalyze the transfer of a substrate from an activated cofactor. In case of the glucuronidation reaction for example, D-glucuronic acid is transferred from the cofactor uridine diphosphate α -D-glucuronic acid (UDPGA) by the enzyme UDP-glucuronosyltransferase (UGT).¹² The site of metabolism varies within the cell. Cytosolic reactions include sulfonations, N-acetylations and amino acid conjugations. GSH conjugation occurs in various compartments of the cytoplasm.^{2,13} Glucuronidations take place in the endoplasmic reticulum as the active site of the UGT enzymes is located on the inside with a single transmembrane domain and a COO^- cytosolic tail.¹⁴ Subsequent to phase II reactions, the generated conjugates may be further metabolized. GSH conjugates, as an example, can be further biotransformed to acetylcysteine (mercapturic acid) conjugates by degradation of GSH of the amino acids glutamate and glycine by gamma-glutamyl transpeptidases and dipeptidases in a two-step reaction.^{15,16} Cleavage of glucuronic acid and sulfate conjugates through hydrolysis by intestinal flora can convert the metabolite back to its phase I modification or origin molecular structure.¹⁷

While the aim of metabolism tends to remove potentially toxic compounds, the mentioned functionalization and conjugation reactions may result not only in the pharmacological deactivation of a xenobiotic. Metabolites without, with similar, or with increased pharmacological activity (*e.g.*, morphine 6-glucuronide, desloratadine), compared to their parent compound, or toxic metabolites (*e.g.*, *N*-acetyl-*p*-benzoquinone imine (NAPQI)) are possible consequences of the structural modifications.¹⁸ The possibility of metabolic activation led to the idea of metabolizing a compound into its pharmacologically active drug after administration and to the concept of so-called "prodrugs".² Drug metabolism may also lead to the formation of electrophilic intermediates (*e.g.*, epoxides,) which

Introduction

tend to covalently bind nucleic acids and proteins, and results in mutagenicity, carcinogenesis, teratogenesis, cell damage and immune responses as a result of haptention of reactive metabolites to proteins.^{19,20}

1.2 Metabolite identification in drug discovery and development

From first synthesis to finally reaching the market, a drug candidate must pass a number of stages to ensure its efficacy, safety and tolerability. As drug development is an expensive and time-consuming process, inappropriate new chemical entities (NCEs) need to be identified in the early stage. Drug metabolism and pharmacokinetic (DMPK) studies (*e.g.*, metabolic stability, bioavailability, metabolic or toxicological profile) in early discovery and development are thereby an essential tool to select a favorable drug candidate.²¹

The characterization (detection, identification and quantification) of clinically relevant metabolites plays thereby an important role in the investigation of potential safety risks to humans. For that purpose, regulatory agencies, like the U.S. FDA (Food and Drug Administration) and the European Medicines Agency (EMA) drafted guidelines to support the pharmaceutical industry in the implementation of metabolism studies to understand the formation pathways of metabolites.^{22,23} In 2008, the FDA released such recommendations with the formal guidance for the safety testing of drug metabolites (MIST guideline).²² The document addresses the need for the assessment of human relevant metabolic profiles in preclinical species, which can vary quantitatively and qualitatively across the species if the metabolites are only formed in humans (rare) or formed in disproportionately higher levels in human compared to the animal test systems (common). Therefore, the guideline encourages the identification of metabolic differences between animal species and humans as early as possible to avoid problems in later development phases.

Traditionally, identification and quantification of human metabolites is conducted late during phase I or phase II of clinical development in a single-dose radiolabeled (¹⁴C) study, delaying further clinical trials if additional safety evaluation of metabolites are needed.²⁴ As an alternative, a multiple ascending dose trial during phase I can be used to collect plasma samples at steady state for metabolite identification (MetID) and quantification to evaluate if a human metabolite exceeds 10% of the parent drug's systemic exposure.²⁵ A radiolabeled study in humans in a later phase will then confirm the results obtained on the major circulating metabolites.²⁶

Strategies to assess metabolism and elucidate the structure of metabolites early at the preclinical stage are conducted routinely to provide information on the rate and kind of metabolism and the number of metabolites formed, allowing the modification of the parent compound for improved metabolic properties (*e.g.*, clearance, bioavailability, toxic potential).²⁷ In early discovery, different *in vitro*

Introduction

systems from various species (*e.g.*, human, mouse, rat, monkey) are used to investigate metabolic stability. As the highest levels of CYP enzymes is expressed in the liver, liver cells (hepatocytes) or subcellular fractions (microsomes, S9, cytosol) are the systems of choice.³ Hepatocytes are useful to examine phase I and phase II metabolism as well as metabolic membrane transporter effects but need to be freshly prepared or cryopreserved to retain their activity, which decreases otherwise within a few hours.^{28,29} Centrifugation at 9,000 g breaks the cell membrane of the hepatocytes and separates the soluble enzymes and fragmented endoplasmic reticulum (microsomes) in solution from the sedimented cellular debris. The supernatant, also called S9 fraction, contains the cytosolic and microsomal enzymes and is used for phase I and phase II metabolism studies but needs the addition of cofactors (*e.g.*, NADPH, UDPGA, PAPS, Acetyl CoA) to start the enzymatic reaction.^{13,30} Microsomes are the major subcellular fractions used as an *in vitro* system in metabolic stability studies. They contain the most important drug metabolizing enzymes and are therefore useful to study CYP450 metabolism and phase II conjugation reactions by addition of the appropriate cofactors (*e.g.*, NADPH, UDPGA).³¹ Besides the mentioned systems, heterologously expressed enzymes are important tools to identify and understand the role of individual enzymes in the detoxification of xenobiotics. These recombinant enzymes are used to assess an inhibitory or inductive potential of a drug candidate and to predict the path of metabolism as an interindividual variability of CYP enzymes in human may influence the kinetic parameters of a drug.³² There are four host cell systems commonly used for the expression of CYP enzymes. Bacterial systems (*e.g.*, *Escherichia coli*), yeast systems (*e.g.*, *Saccharomyces cerevisiae*), insect cell systems and mammalian cell lines are mainly used to express an individual CYP enzyme or in combination with one or both of its redox partners (*i.e.*, oxidoreductase, cytochrome *b₅*).^{33,34} To analyze the structure of metabolites only present in trace amounts in the incubation solution, state-of-the-art tools like liquid chromatography-mass spectrometry (LC-MS) are used for rapid analysis directly from incubation matrix. Especially modern approaches like tandem mass spectrometry (MS²) and time-of-flight (TOF) systems are used in metabolism studies as very sensitive and high resolution tools.²⁷

1.3 Structural elucidation of small molecules

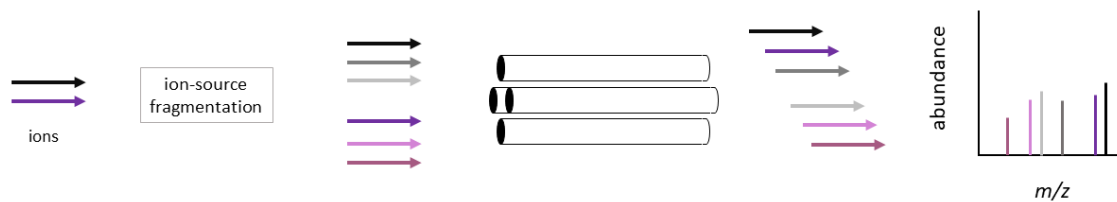
1.3.1 Mass spectrometry

The goal of analytical chemistry is the investigation of chemical material regarding its constituents like character (*e.g.*, form, chemical bonds), quantity (concentration) or structure (arrangement of atoms).³⁵ A variety of methods and instruments were developed over the years to tackle these tasks.

A technology playing an important role in the analysis of small molecules and proteins is mass spectrometry (MS). In principle, MS allows the generation and separation of ions from both organic and inorganic analytes for qualitative and quantitative detection by their mass-to-charge ratio (m/z) and abundance.³⁶ Different ionization techniques (*e.g.*, electrospray ionization (ESI), electron ionization (EI), chemical ionization (CI), matrix-assisted laser desorption ionization (MALDI)) were developed to ionize the samples and are used depending on the application and type of analyte.³⁶ The typical instrumentation setting of a mass spectrometer consists of an ion source, a mass analyzer and a detector.³⁵ After ionization and transfer of the analyte into the gas phase, the atoms or molecules are separated according to their mass in the mass analyzer.³⁷ Several types of mass analyzers (*e.g.*, quadrupole mass filter (Q), TOF, quadrupole ion trap (QIT), orbitrap) are available and differ in terms of *e.g.*, resolution, mass accuracy, sensitivity, mass range, speed or ion-source type (pulsed/continuous mode). The quadrupole mass analyzer is used as a mass filter by letting exclusively ions in a certain mass range pass while a mass spectrum is acquired by scanning the defined range and counting the ions at each m/z (Figure 2).³⁷ Using a QIT, selected ions can be trapped by a potential well for accumulation or storage to perform additional experiments before ejecting them for detection.³⁶ The basic principle of a TOF analyzer is the separation of ions based on the time difference between a well-defined start signal and a generated pulse when the ions arrive at the detector after their flight along a field-free drift region of known distance.³⁶ A technique used for its high sensitivity and selectivity for complex bioanalytical samples containing numerous analytes is MS², a multistage combination of two analyzer quadrupoles (Q1 and Q3) and a gas-filled collision cell for fragmentation in between (q2).³⁷ Two stages of m/z analysis are conducted with the triple-quadrupole (QqQ) system, using Q1 to scan for precursor ions (parent compound) and Q3 for fragments of the parent compound, the so-called product ions. The analyte of interest is selected in Q1 as precursor ion before undergoing a controllable low-energy collision-induced dissociation in q2 and a transmission of its particular product ion in Q3 (Figure 2).³⁵

Introduction

a) MS



b) MS²

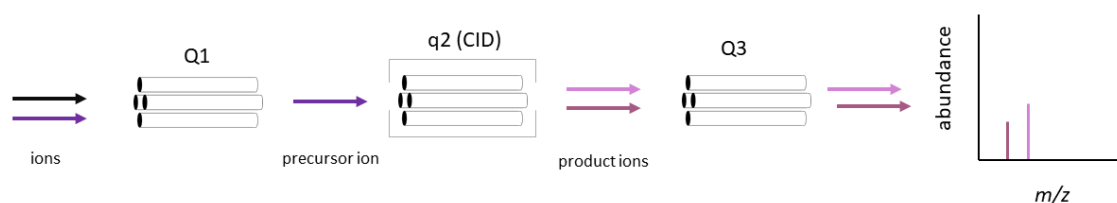


Figure 2: Principle of a) the single quadrupole mass analyzer and b) the triple-quadrupole mass spectrometer.

The availability of sensitive, high-resolution (± 5 -10 ppm) MS systems (*e.g.*, TOF or hybrid Q-TOF systems) coupled with liquid chromatography allowed a major improvement of MetID processes over the past decades.²⁷ A high mass accuracy in the sub-mDa region and a high resolution allow the classification and data-filtering of target analytes from matrix ions through changes in the molecular formula composition and thereby in a change of the accurate mass.²⁵ By determining the mass defect, the difference between the exact and nominal m/z value, a differentiation between metabolites and endogenous components is possible, whereby phase I and phase II metabolites typically fall within a defined mass defect window (*e.g.*, ± 50 mDa).³⁸ As the structure and molecular weight of the parent drug is known, changes in m/z values can give an indication on the kind of structural modification. A hydroxylation for example introduces an oxygen atom into the molecular structure, resulting in a m/z increase of 16 Da. The comparison of characteristic fragment ions from metabolites with the fragmentation pattern of their parent compound allows to limit the position of biotransformation to a certain part of the molecule based on the shift of m/z values.³

Besides the developments in instrumentation, *in silico* models were implemented to aid in the prediction of drug metabolism studies. Different commercially available software programs can be used as stand-alone software (*e.g.*, MetaSite, METEOR), as LC-MS integrated software (*e.g.*, MetaboLynx, UNIFI) or literature database dependent software (*e.g.*, Accelrys Metabolism).²⁷ Computational tools like MetaSite predict the site of metabolism through investigation of possible interactions between the target compound and the active site of the major human CYP enzymes.³⁹ Software packages like UNIFI screen the MS chromatograms for known phase I and II modifications and the associated increase and decrease of m/z values relative to the parent.⁴⁰

Introduction

Although MS is widely used in MetID studies, often the gained data alone does not provide sufficient information for a complete structural elucidation of metabolites. Additional tools like nuclear magnetic resonance (NMR), chemical derivatization or H/D-exchange for detailed information are then necessary.²¹ NMR analysis allows to define the exact position of metabolism as a complementary tool to MS data but requires high purity of target compounds from *in vitro* and *in vivo* samples in the microgram scale and thus time-consuming semi-preparative isolation and purification is needed.

1.3.2 Single-crystal X-ray diffraction

Single-crystal X-ray diffraction (SC-XRD) is a widely used method for the direct identification and characterization of chemical and biological compounds by determining the arrangement of atoms in a crystalline structure. The technique gives information on various structural parameters as the connectivity, the conformation, bond lengths and angles or the density of a substance.⁴¹ It also plays an important role in the unambiguous determination of absolute configurations because of the anomalous scattering effect from heavy atoms (*e.g.*, sulfur, chlorine) included in the molecular structure.^{42,43} The requirement using SC-XRD for structure determination is to crystallize the substance of interest as a single crystal of high quality.⁴¹ Time-consuming crystallization procedures and a sufficient amount of compound material are therefore required.⁴² This excludes the investigation of non-crystalline molecules like amorphous solids, powders, liquids and gases.

It was shown that crystals are built as a set of three-dimensional atomic coordinates, a so-called crystal lattice, which scatters X-rays with $\lambda = 50\text{-}300\text{ pm}$, corresponding with the interatomic distance of $100\text{-}300\text{ pm}$ ($1\text{-}3\text{ \AA}$).^{41,44} A crystal lattice can be described by its unit cell, the smallest pattern of atoms which contains all symmetry elements and can constitute the complete crystal structure by repeating translations. The unit cell can be described by six parameters, the lattice constants a , b and c representing the x , y and z axis, respectively, and the angles α , β and γ between the edges (Figure 3).⁴⁵ A crystal can be classified in one of seven crystal systems (triclinic, monoclinic, orthorhombic, tetragonal, trigonal, hexagonal and cubic). Their respective lattice parameters differ in cell edges and cell angles depending on their symmetry.⁴¹

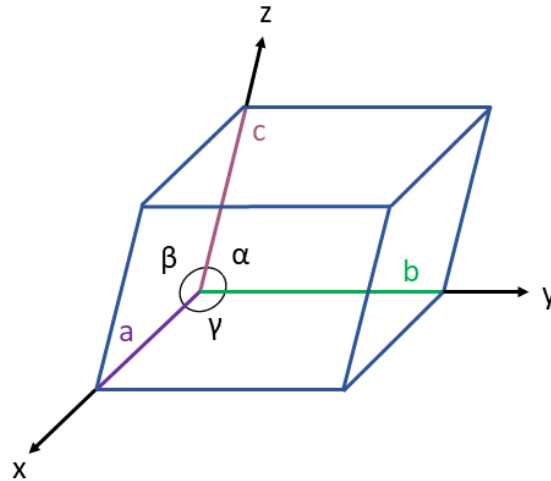


Figure 3: Unit cell with lattice constants.

To determine a crystal structure, electromagnetic radiation of short wavelength, the so-called X-rays, are used.⁴² A monochromatic beam of X-rays is thereby scattered by each point of the crystal lattice. Depending on the reflection angle and the spacing between the lattice planes (hkl), characteristic diffraction phenomena are observed which can be described with the Bragg equation.⁴⁶ The position and intensity of reflexes can directly be correlated with the electron density distribution in the lattice and thus with the atom type and position in the crystal.⁴²

To perform an XRD analysis, the X-rays are generated in the diffractometer under vacuum by impinging of electrons on an anode metal plate usually made of Mo or Cu and thus the emission of X-ray photons with defined wavelength. In comparison to a sealed high vacuum tube, modern systems are equipped with a rotating anode open system coupled with a continuous pumping system for the high vacuum to considerably increase the intensity of the XRD instrument. To measure the high number of reflections dependent on the position of X-ray beam and crystal, area detector systems are used.⁴¹ The general components of a SC-XRD instrument are shown in Figure 4.

Introduction



Figure 4: Example of a single-crystal X-ray diffractometer with X-ray source, goniometer head for crystal mounting, a cryostream for sample cooling and an area detector with beam stop for detection. (figure adapted from L. Rosenberger et al., 2020)⁴⁷

After data collection, each reflection is processed and corrected using a data reduction software to describe the lattice points and to select the optimal crystal system.⁴¹ Crystal structures are then modelled from electron density using a structure solution and refinement program (*e.g.*, OLEX2, ShelXle) for analysis and visualization.^{48,49} The finalized crystal structures may be deposited into one of the available public databases to share and benefit from the scientific results worldwide. The Cambridge Structural Database (CSD) for example contains the results of organic and organometallic compounds and is available in many countries.⁴²

The SC-XRD as a direct technique to assign the exact position of structural changes in a molecular scaffold would be beneficial for MetID studies. However, metabolites are only present in trace amounts in *in vitro* incubations and *in vivo* samples and cannot meet the requirements for crystallization processes to obtain a single crystal of suitable size and shape.

1.4 Crystalline sponge method

An approach to overcome the limitation of crystallization and to make nanogram to a few microgram amounts of compound material observable by conventional SC-XRD was introduced in 2013 by Makoto Fujita and is commonly known as the “crystalline sponge method” (CS-XRD).⁵⁰ Instead of crystallizing the compound of interest as a single crystal, the method uses a pre-existing porous metal complex $[(\text{Co}(\text{NCS})_2)_3(\text{tpt})_4 \cdot x(\text{solvent})]_n$ or $[(\text{ZnX}_2)_3(\text{tpt})_2 \cdot x(\text{solvent})]_n$ ($X=\text{Cl}, \text{I}$; $\text{tpt}=2,4,6\text{-tris}(4\text{-pyridyl})\text{-}1,3,5\text{-triazine}$), termed metal-organic framework (MOF), as a host crystal.^{51–53} The crystalline sponges (CS) consist of an inorganic metal salt (*e.g.*, ZnCl_2 , ZnI_2 , $\text{Co}(\text{NCS})_2$) coordinated to a tpt as organic ligand,

Introduction

forming a three-dimensional porous framework (Figure 5). The crystal structure allows weak supramolecular interactions like hydrogen and halogen bonding of the pyridyl protons (H-bond donors) and chloride/iodine atoms (H-bond acceptors) as well as hydrophobic, charge-transfer, C–H– π and π – π interactions with the electron-deficient tpt ligand.^{54,55} The high molecular-binding ability of the framework results in the inclusion and repetitive positioning of analyte molecules (“guest”) in each CS pore, allowing the guest to contribute to the diffraction pattern and making the target structure observable for conventional XRD analysis. The rod-shaped crystals are around 100 – 300 μm long and contain inert solvent molecules (*e.g.*, n-hexane, cyclohexane) in their cavities, which can be replaced by target guest molecules.⁵⁶ The pore size of approximately 5 x 8 Å allows the accommodation of small organic molecules, whereby expansion of the flexible framework upon guest inclusion was observed.⁵⁷ The small size of the crystals and therefore the number of guest-accessible voids requires only nanogram of compound material for XRD analysis, making CS-XRD a sensitive technology. In addition, the method can be used for the analysis of liquids and volatile gases, which are not crystallizable as single crystals and therefore unapproachable for traditional XRD.^{50,58}

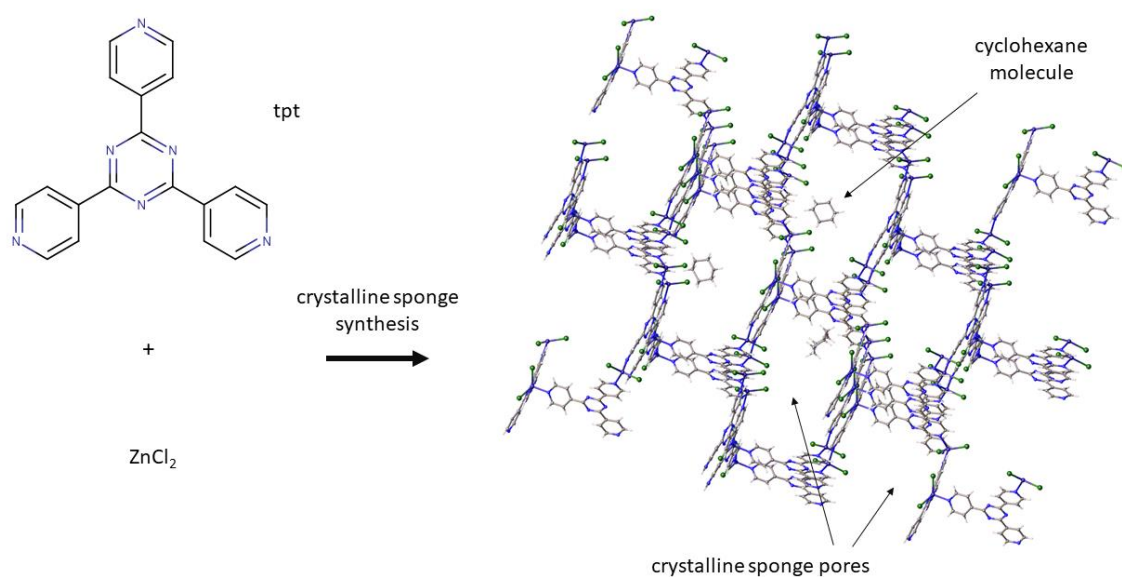


Figure 5: Three-dimensional porous network of crystalline sponge $[(\text{ZnCl}_2)_3(\text{tpt})_2 \cdot x(\text{cyclohexane})]_n$ (tpt=2,4,6-tris(4-pyridyl)-1,3,5-triazine)

Many porous coordination polymers or MOFs are known and topic of research because of their rich structural chemistry and potential for broad practical applications.^{59,60} However, only a limited number has the potential to function as a CS regarding guest inclusion and repetitive guest orientation in the CS pores. To be a potential new CS, a crystal candidate requires to crystallize in high diffraction-quality, to have large cavities to accommodate guest analytes, low porosity to warrant stability during guest

Introduction

soaking and the potential for host-guest interactions. Furthermore small thermal movement and low-symmetry groups to avoid target molecules across symmetry planes and rotation axes enhance structure determination of host and guest.^{54,61}

During a “soaking” process, the target analyte molecules are absorbed into the pores of the CS, enriched and regularly ordered by intermolecular, noncovalent interactions between framework and analyte (“guest soaking”).^{62,63} To achieve a successful trapping of a guest compound, the optimization of soaking conditions (*e.g.*, sponge type, solvent, soaking duration, temperature and analyte concentration) for each analyte is needed, as not all classes of compounds are compatible with the CS and the affinity of guest to the framework is rather unpredictable.⁵⁷

Since the introduction of the sponge technology in 2013, the CS-XRD has been used to confirm and elucidate the structures of compounds in different fields of application. To demonstrate the advantage regarding analytes normally impossible to crystallize or in need of further derivatization, the CS-XRD was used for volatile compounds and liquids, like oily analyte material.^{58,64,65} Besides structural elucidation of active pharmaceutical ingredients (APIs), unstable reaction intermediates and chemical synthesis products were successfully observed in the cavities of the CS.^{55,66,67} The requirement of only nanogram of sample material facilitates the structural analysis of compounds only available in trace amounts, *e.g.*, natural products. These compounds are usually obtained in small amounts in complex mixtures and need lengthy isolation and purification processes using semi-preparative HPLC. Using the CS-XRD, different research groups were able to successfully elucidate the structures of natural material like plant components from orange peel and red algae, a scarce marine sponge product (miyakosyne A) or metabolic products prepared from intramolecular C-S bond formation by cytochrome P450 enzymes and enzymatic reductions with baker’s yeast.^{50,68–70} In the context of drug discovery and development, the CS-XRD may be a promising analytical technique for structural elucidation of new drug candidates and their structurally related compounds.

2. Aim and Scope

Structural elucidation of compounds only available in low quantity from *in vitro* systems in early drug discovery and development is still a challenging task. State-of-the-art tools like NMR and LC-MS dramatically improved over the past years but are still limited regarding low amount of material (NMR) or the determination of the exact position of metabolism (MS). To achieve structure determination of metabolites already at early stages in drug development projects, a fast (few days) method with high information density and sensitivity in the nanogram range is needed.

The objective of this thesis was the evaluation of CS-XRD for complete structural elucidation of metabolites generated from *in vitro* incubations of APIs. This should be achieved by generation of metabolites from *in vitro* incubation with human or animal tissues, separation and purification using semi-preparative HPLC and structural elucidation using the CS-XRD.

In the first part of this work, we wanted to investigate the applicability of CS-XRD for the structural elucidation of metabolites from small drugs. Therefore, we conducted *in vitro* incubation experiments with rat and human liver microsomes for the generation of metabolites followed by isolation and purification of the target compounds using semi-preparative HPLC. Gemfibrozil was chosen as a tool compound as the metabolic pathway was known from the literature. We used the reference material of the API and one phase I and phase II metabolite, respectively, for first analysis and the optimization of soaking conditions. Thereupon, we generated two additional phase I gemfibrozil metabolites from *in vitro* incubation for structural elucidation with CS-XRD. The results are described in Chapter 3.1.

In the second part of this thesis we aimed at the optimization of soaking conditions. We established a screening method based on the affinity of guest analyte to CS framework prior to time-consuming XRD experiments. Therefore, we conducted parallel guest soaking of individual test compounds and mixtures using various soaking parameters. Thereafter, we prioritized the optimal soaking conditions for final XRD measurements by estimation of analyte concentration in the CS pores using UPLC-MS² (ultra-performance LC-MS²) analysis. The workflow and results of the affinity screening method are shown in Chapter 3.2.

The third part of this thesis covered the structural characterization of structurally unknown metabolites using CS-XRD. Therefore, we examined a variety of mono-hydroxylated derivatives of praziquantel (PZQ), an anthelmintic drug. *In vitro* incubation of enantiopure *S*-PZQ was conducted with human liver microsomes, and the generated metabolites were isolated and purified using an extensive chromatographic separation process. Additionally to CS-XRD, we conducted UPLC-qTOF-MS and NMR analysis for comparison of the used analytical methods. The results of these efforts are described in Chapter 3.3.

3. Results

3.1 Chapter A: Crystalline sponges for metabolite identification

Title:

Crystalline sponges as a sensitive and fast method for metabolite identification: Application to gemfibrozil and its phase I and II metabolites

Authors:

Lara Rosenberger, Carolina von Essen, Anupam Khutia, Clemens Kühn, Klaus Urbahns, Katrin Georgi, Rolf W. Hartmann, and Lassina Badolo;

Bibliographic Data:

Drug Metabolism and Disposition,

Volume 48, Issue 7, Pages 587-593,

Accepted April 20, **2020**,

Doi: 10.1124/DMD.120.091140

This is an open access article distributed under the CC BY Attribution 4.0 International license.

Crystalline Sponges as a Sensitive and Fast Method for Metabolite Identification: Application to Gemfibrozil and its Phase I and II Metabolites[§]

Lara Rosenberger, Carolina von Essen, Anupam Khutia, Clemens Kühn, Klaus Urbahns, Katrin Georgi, Rolf W. Hartmann, and Lassina Badolo

Discovery and Development Technologies (DDTech) (L.R., K.U., K.G., L.B.) and Innovation Center (C.v.E., A.K., C.K.), Merck KGaA, Darmstadt, Germany; and Department of Drug Design and Optimization (DDOP), Helmholtz-Institute for Pharmaceutical Research Saarland (HIPS)-Helmholtz Centre for Infection Research (HZI), Saarbrücken, Germany (L.R., R.W.H.)

Received March 3, 2020; accepted April 20, 2020

ABSTRACT

Understanding the metabolism of new drug candidates is important during drug discovery and development, as circulating metabolites may contribute to efficacy or cause safety issues. In the early phase of drug discovery, human *in vitro* systems are used to investigate human relevant metabolism. Though conventional techniques are limited in their ability to provide complete molecular structures of metabolites (liquid chromatography mass spectrometry) or require a larger amount of material not available from *in vitro* incubation (nuclear magnetic resonance), we here report for the first time the use of the crystalline sponge method to identify phase I and phase II metabolites generated from *in vitro* liver microsomes or S9 fractions. Gemfibrozil was used as a test compound. Metabolites generated from incubation with microsomes or S9 fractions, were fractionated using online fraction collection. After chromatographic purification and fractionation of the generated metabolites, single crystal X-ray diffraction of crystalline sponges was used to identify the structure

of gemfibrozil metabolites. This technique allowed for complete structure elucidation of 5'-CH₂OH gemfibrozil (M1), 4'-OH gemfibrozil (M2), 5'-COOH gemfibrozil (M3), and the acyl glucuronide of gemfibrozil, 1-O-β-glucuronide (M4), the first acyl glucuronide available in the Cambridge Crystallographic Data Centre. Our study shows that when optimal soaking is possible, crystalline sponges technology is a sensitive (nanogram amount) and fast (few days) method that can be applied early in drug discovery to identify the structure of pure metabolites from *in vitro* incubations.

SIGNIFICANCE STATEMENT

Complete structure elucidation of human metabolites plays a critical role in early drug discovery. Low amounts of material (nanogram) are only available at this stage and insufficient for nuclear magnetic resonance analysis. The crystalline sponge method has the potential to close this gap, as demonstrated in this study.

Introduction

During the process of drug discovery and development, assessing the identity of drug metabolites is crucial to understand the contribution of metabolites to efficacy or safety (Nedderman, 2009; Zhang et al., 2009). Guidelines have been drafted by regulatory agencies (EMA, 2013; FDA, 2016) to help the pharmaceutical industry to apply the right strategy regarding metabolites in safety assessment. The key element in all these guidances is to protect patients and healthy human volunteers from potentially toxic metabolites with a focus on human metabolites that are either absent in preclinical species or circulate in these animals at much lower concentrations than in humans (Ma and Chowdhury, 2011). It is therefore of paramount importance during drug development to gain an understanding of metabolism of new chemical entities in humans as early as possible. To achieve this, *in vitro* systems from human origin (e.g., microsomes or hepatocytes) are used to metabolize the new active

pharmaceutical ingredients (API) in drug discovery research (Brandon et al., 2003; Fasinu et al., 2012). Samples generated from these systems are analyzed with liquid chromatography (LC)-mass spectrometry (MS) of different types [e.g., tandem MS (MS²) and tandem time-of-flight] by drawing inferences from fragmentation patterns to assess metabolism (Prakash et al., 2007; Prasad et al., 2011). Although MS techniques have reached extreme sensitivity, these techniques fail in many situations, e.g., to identify the complete structure of metabolites. This forces scientists to use NMR, a less sensitive technique, requiring larger amounts of material (usually microgram to milligram range) (Murai et al., 2004), which is therefore not always suitable for analyzing samples from *in vitro* origin.

Besides NMR and LC-MS, another technique would be single crystal X-ray diffraction (XRD), a direct technique that provides structural information at the atomic level by measuring electron density as diffraction pattern of a single crystal (Massa, 2004). Single crystal XRD can even provide information on the absolute configuration of chiral centers but has the intrinsic limitation because of requirements of single crystals of suitable sizes and shape. The process of crystallization

<https://doi.org/10.1124/dmd.120.091140>.

[§]This article has supplemental material available at dmd.aspetjournals.org.

ABBREVIATIONS: API, active pharmaceutical ingredient; CS, crystalline sponge; CS-XRD, crystalline sponge method; DME, 1,2-dimethoxyethane; HPLC, high performance liquid chromatography; LC, liquid chromatography; MS, mass spectrometry; MS², tandem mass spectrometry; R_{int}, internal R-value; R₁, residual factor; tpt, 2,4,6-tris(4-pyridyl)-1,3,5-triazine; UDPGA, uridine 5'-diphosphoglucuronic acid; UPLC, ultra-performance liquid chromatography; XRD, X-ray diffraction.

is a time-consuming procedure that requires availability of sufficient amounts of materials and cannot be performed with amorphous solids, liquids, or volatile analytes. One approach to overcome the limitation of crystallization is the application of microcrystal electron diffraction from powder (Jones et al., 2018; Kunde and Schmidt, 2019). This technique requires solid material at a higher amount.

For structural elucidation of metabolites in solution, a method with the information density of X-ray crystallography and the sensitivity in the nanogram range is needed for human-related metabolites at this early stage of drug development research. In 2013, Makoto Fujita published a new technique commonly known as “crystalline sponge method” (CS-XRD), which enables crystal structure determination without crystallization with only a nanogram to few microgram amount of analytes (Inokuma et al., 2013). In one specific case, only 80 ng of material were sufficient to clearly elucidate the X-ray structure of the analyte, and presumably even smaller amounts are possible for synchrotron X-ray diffraction instruments. The CS-XRD uses pre-existing crystals of porous metal coordination complexes $[(ZnX_2)_3 \cdot (tpt)_2 \cdot x(\text{solvent})]_n$ ($X=Cl$; $tpt=2,4,6\text{-tris}(4\text{-pyridyl})\text{-}1,3,5\text{-triazine}$), which can absorb organic molecules in its pores and make them observable by conventional single crystal X-ray crystallography. Via diffusion (“soaking”), the analyte (“guest”) is absorbed into the pores of porous CS and regularly ordered by intermolecular, noncovalent interactions (“guest soaking”) (Inokuma et al., 2013; Inokuma et al., 2016; Sakurai et al., 2017). As a result, the repetitive positioning of the analytes in each pore of the framework serves for structural analysis via X-ray diffraction. For a successful CS-XRD experiment, regular order of the analyte is important. Functionalization of the APIs (e.g., hydroxylation, demethylation) increases the type of noncovalent interactions with the framework and therefore increases the chances of regular order. This even works for otherwise noncrystallizable compounds (Hoshino et al., 2016). The CS-XRD has been shown to be able to successfully elucidate the structure of APIs (Sakurai et al., 2017), products from biosynthesis catalyzed by cytochrome P450 enzymes (Morita et al., 2020), natural plant products (Wada et al., 2018), and metabolic products prepared by reductive dichlorination of an insecticide as well as keton reduction of a steroid hormone with baker’s yeast (Inokuma et al., 2016), but it has not been applied for drug-related material generated by incubation of API’s with human or animal tissues before.

In this study, we apply the crystalline sponge technology for complete structure identification of gemfibrozil phase I and phase II metabolites after incubation with liver microsomes or S9. Rat systems were used, however, and the formation of the same metabolites were confirmed in human liver S9.

Materials and Methods

Chemicals and Reagents. Gemfibrozil (Fig. 1) was purchased from Acros Organics (NJ), and its metabolite 4’OH gemfibrozil was synthesized from WuXi AppTec Co., Ltd. (Wuhan, China). Gemfibrozil glucuronide was purchased from Toronto Research Chemicals (Toronto, Canada). Di-potassium hydrogen phosphate, potassium dihydrogen phosphate, magnesium chloride hexahydrate, dimethylsulfoxide, cyclohexane, methanol, nitrobenzene, nicotinamide adenine dinucleotide phosphate disodium salt (NADP- Na_2), water (ultra-high-performance LC-MS grade), and acetonitrile (ultra-high-performance LC-MS grade) were purchased from Merck KGaA (Darmstadt, Germany). Zinc chloride, 1,2-dimethoxyethane (DME), alamethicin, uridine 5’-diphosphoglucuronic acid trisodium salt (UDPGA- Na_3), and formic acid were purchased from Sigma Aldrich Chemie GmbH (Steinheim, Germany). Dihydronicotinamide adenine dinucleotide phosphate tetrasodium salt (NADPH- Na_4) was purchased from AppliChem (Darmstadt, Germany), and 2,4,6-tri(4-pyridyl)-1,3,5-triazine (tpt) was purchased from abcr GmbH (Karlsruhe, Germany). Female WistarHan rat liver microsomes (R6500, pool of 225), female rat liver S9 (R3500.S9, pool of 100), and mixed gender human liver S9 (H0620.S9, pool of 50) were obtained

from Sekisui XenoTech (Kansas City), and mixed gender human liver microsomes (Ultrapool, pool of 150) were purchased from Corning (Corning)

Metabolism of Gemfibrozil by Rat/Human Liver Microsomes, Rat/Human Liver S9. The oxidation reaction of gemfibrozil was conducted with rat liver microsomes (0.5 mg/ml) in 50 mM potassium phosphate buffer (pH 7.4) containing 1 mM magnesium chloride and 20/200 μM substrate. After 5 minutes of preincubation (37°C, 150 rpm), the reaction was initiated by the addition of NADPH (1.5 mM) dissolved in 50 mM potassium buffer, and the mixture was incubated for another 3 hours (final volume: 5.40 ml). The reaction was terminated by adding one volume of cold acetonitrile and then centrifuged (4000g, 1 hour, 4°C) to sediment the precipitated proteins. The aliquots (100 μl) of the supernatant were injected onto high-performance LC (HPLC)-MS for separation and fractionation.

The oxidation of gemfibrozil with rat and human liver S9 fraction was conducted similar to the incubation with microsomes. Differences were the protein concentration of 1.0 mg/ml, the addition of NADPH and NADP⁺ (1.5 mM) as cofactors, and the incubation time (6 hours).

To generate gemfibrozil glucuronide, human liver microsomes were treated with alamethicin (4°C, 20 minutes, final concentration: 25 $\mu\text{g}/\text{ml}$), a channel-forming peptide to increase the metabolite formation. The reaction was initiated by the addition of UDPGA (1.5 mM) as cofactor.

HPLC-MS. The supernatants were analyzed on an Acquity Arc HPLC system combined with an isocratic solvent manager, a single quadrupole MS, and a fraction manager (Waters Corporation, Milford). The LC system included a quaternary solvent manager, a sample manager, and a 2998 photodiode array detector. The isocratic solvent manager was used with a 1:50 splitter. Samples were analyzed with electrospray ionization mass spectrometry in the negative ion mode. The following source parameters were used: probe temperature, 600°C; capillary voltage, 0.8 V; cone voltage, 3.0 V; and sampling frequency, 2 Hz. Ions were acquired in an MS acquisition range from m/z 100 to m/z 650 in continuum mode.

HPLC separations were achieved on two Chromolith Performance RP18e columns as first chromatographic system (100–4.6 mm; Merck KGaA) and Purospher Star RP18e Hibar HR column as second system (100–2.1 mm, 2 μm ; Merck KGaA) at a column oven temperature of 25°C. For the first purification, elution was performed at a flow rate of 1.0 ml/min over a period of 30 minutes with a mixture of solvent A (water + 0.1% formic acid) and solvent B (acetonitrile + 0.1% formic acid). Compounds were eluted using the following conditions: mobile phase B increased from 0% to 25% over 7 minutes, followed by a 13-minute linear gradient to 60% B and a linear gradient to 100% B in 5 minutes, returning to 0% B in 0.1 minute and re-equilibration at 0% B for 4.9 minutes. The first 6 minutes of eluent were directed to waste to reduce contamination, as it contains mainly microsomes and buffer salts from incubation matrix. For the second purification, elution was performed at a flow rate of 0.45 ml/min over a period of 15 minutes, using the following conditions: mobile phase B increased from 0% to 80% over 10 minutes, followed by linear gradient to 100% B in 2 minutes, returning to 0% B in 0.1 minute and re-equilibration at 0% B for 2.9 minutes. The eluate was subsequently split between the photodiode array detector and fraction manager (98%) and the mass spectrometer (2%). The MS flow was increased to 0.3 ml/min with a makeup solvent (90% water + 10% acetonitrile). The fractionation of the analytes was triggered by the mass values (m/z 265, m/z 279, and m/z 425) registered by the MS detector. Data acquisition and sample fractionation were performed using the software MassLynx 4.2 combined with FractionLynx.

Collected fractions were pooled, evaporated to dryness under nitrogen flow at 40°C, and resolubilized in acetonitrile/water (40/60%) for further purification. The fractions from the second purification step were evaporated to dryness for the soaking process.

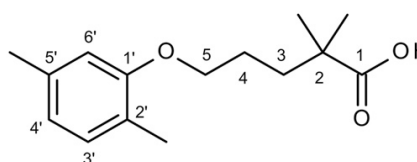


Fig. 1. Chemical structure of gemfibrozil.

Ultra-Performance LC-MS². The supernatants were analyzed on an Acquity UPLC Class I system (Waters Corporation) combined with a linear ion trap quadrupole (Qtrap 5500) mass spectrometer (AB Sciex LLC, Framingham). Samples were analyzed with an electrospray ion source in the negative ion mode. Source parameters were source temperature 600°C and ion spray voltage -4.5 kV. Ultra-performance LC (UPLC) separations were achieved on an Acquity UPLC BEH C18 column (1.7 μ m; 2.1 \times 50 mm; Waters Corporation) at a column oven temperature of 40°C. Elution was performed at a flow rate of 0.7 ml/min over a period of 5.2 minutes with a mixture of solvent A (water + 0.1% formic acid + 10 mM ammonium formate) and solvent B (acetonitrile). Compounds were eluted using the following conditions: mobile phase B increased from 30% to 50% between 0.1 and 4.0 minutes, followed by a 0.6-minute linear gradient to 100% B, returning to 30% B in 0.02 minutes and re-equilibration at 30% B for 0.58 minutes. After injection, the column effluent was directed to the waste for 0.2 minutes to reduce contamination. The software Analyst 1.6.3 was used for data acquisition.

Crystalline Sponge Method. The porous crystalline sponge $[(ZnCl_2)_3(apt)_2(cyclohexane)_x]_n$ was prepared according to the reported procedure (Biradha and Fujita, 2002; Ramadhar et al., 2015).

For guest soaking, one of the prepared $[(ZnCl_2)_3(apt)_2 \cdot x(cyclohexane)]_n$ single crystals was used as crystalline sponge and then transferred with 50 μ l cyclohexane to the sample vial. Reference material was prepared as 1 mg/ml solution in DME, 1 μ l of the solution pipetted into the sample vial, and the vial closed with a screw cap with septum seal (VWR, Darmstadt, Germany) and pierced with a syringe needle for slow evaporation of the solvent during guest inclusion. The samples were placed in an incubator at 50°C for 1 day. Soaking conditions for gemfibrozil glucuronide were conducted similarly. The volume of cyclohexane was reduced to 20 μ l, and the incubator temperature was 25°C. Incubation samples were prepared similarly to the reference material. Differences were that 40 μ l cyclohexane was transferred together with the crystal into the glass vial, which contained the pooled metabolite material. Four microliters of DME was added subsequently. The guest soaking for gemfibrozil glucuronide was performed using 20 μ l of cyclohexane at 25°C for 1 day.

Single crystal X-ray diffraction measurements were conducted by using a Rigaku Oxford Diffraction XtaLAB Synergy-R diffractometer, using Cu-K α X-ray radiation ($\lambda = 1.54184 \text{ \AA}$) equipped with a HyPix-6000HE/HyPix-Arc 150° Hybrid Photon Counting detector (Rigaku, Tokyo, Japan) at a temperature of 100 K with a Cryostream 800 nitrogen stream (Oxford Cryostreams, UK). The software CrysAlisPro (Rigaku Oxford Diffraction, 2018) was used for calculation of measurement strategy and data reduction (data integration, empirical and numerical absorption corrections, and scaling). Crystal structures were modeled using OLEX2 (Dolomanov et al., 2009), solved with SHELXT and refined by using SHELXL (Sheldrick, 2015). First, the refinement of the framework was performed by assigning atoms, modeling of disorder, applying anisotropic refinement, and adding of H atoms. The electron density of the guest molecules could safely be identified in the residual electron density after refinement of the framework. The amount of analyte in the sponge pores is modeled as occupancy of the respective atom coordinates, which is proportional to the observed electron density. The data quality of the measurement was assessed by R_{int} and the refined model of framework and analyte by R_1 . The R_1 value represents the agreement between calculated and observed model, and the R_{int} is the measure of precision/reproducibility, classifying the recorded reflections from different angles.

The complete process from analyte generation to processing crystallographic data are shown in Fig. 2.

Results

LC-MS Analysis of Gemfibrozil Metabolites Prepared by Incubation with Rat/Human Liver Microsomes and Rat/Human Liver S9. Gemfibrozil (Fig. 1) was chosen as a tool compound to assess the ability of the CS to elucidate the complete structures of metabolites obtained from in vitro incubation. Hydroxylation reactions were conducted by hydroxylases present in microsomes, and further oxidation to carboxylic acid was performed by alcohol and aldehyde dehydrogenases present in the cytosol part of S9 fraction. Formation of gemfibrozil glucuronide was conducted by uridine diphosphoglucuronosyltransferase

present in microsomes through conjugation with glucuronic acid (Zhang and Surapaneni, 2012) (Fig. 3).

After incubating gemfibrozil, the sample solution was tested with UPLC-MS-time-of-flight for metabolite identification. The settings applied on the MS-time-of-flight, did not allow for structure identification of neither the parent nor the metabolite. Further optimization was skipped, and the samples were rather analyzed on single quadrupole HPLC-MS and UPLC-MS² in multiple-reaction monitoring mode.

The HPLC-MS chromatogram of gemfibrozil, incubated with rat liver microsomes and liver S9 fraction in the presence of NADPH or NADPH/NADP⁺, showed the formation of two hydroxy- (M1 and M2) and one carboxy-gemfibrozil metabolite (M3). The three metabolites could not be observed in the absence of the cofactors, indicating that the metabolites were formed by enzymatic oxidation. All three metabolites detected in rat system were present in human liver S9 (Fig. 4). Gemfibrozil incubated with human liver microsomes in the presence of UDPGA showed the formation of a glucuronide (M4), which was only observable by addition of the cofactor. The metabolites M1 and M2 were detected at a deprotonated molecular mass $[M-H]^-$ of m/z 265. The m/z value was 16 Da higher than the $[M-H]^-$ ion of gemfibrozil (m/z 249), suggesting the addition of one oxygen to the molecular structure. M3 was detected as deprotonated molecule $[M-H]^-$ at m/z 279, suggesting a further addition of oxygen and loss of two hydrogens but giving no information about the site of metabolism. M4 was detected at a deprotonated molecular mass $[M-H]^-$ of m/z 425, indicating the addition of a glucuronic acid (176 Da).

To obtain more information, gemfibrozil and its metabolites were analyzed with UPLC-MS². Tuning of instrument parameters provided the optimal transition for 4'-OH gemfibrozil reference material and was also applied for detection of M1 gemfibrozil. Precursor ion and product ion were adjusted to measure M3 gemfibrozil. Collision-induced dissociation of gemfibrozil and its glucuronide generated a main product ion of m/z 121.0 (2',5'-dimethylphenoxy moiety). As a result of the loss of the glucuronide moiety, both compounds were measured with identical transition (m/z 249.1/121.0) but could be differentiated by their retention time. Hydroxygemfibrozil and carboxygemfibrozil were detected with m/z values of 137.2 and 151.0, respectively (Fig. 4), indicating that oxidation (+16 Da) and carboxylation (+30 Da) occurred at the 2',5'-dimethylphenoxy moiety and not at the chain of the carboxyalkyl group. This knowledge allowed to limit the metabolic position but could not give a more precise answer. However, CS-XRD provided precise information about the oxidation and glucuronidation sites as well as the structure of the metabolites.

Structural Elucidation of M1, M2, M3, and M4 Gemfibrozil by CS-XRD. A successful structure determination using the crystalline sponge method depends on various parameters, such as temperature, analyte concentration, duration of the soaking experiments, and solvent combinations during the soaking step (Hoshino et al., 2016). These parameters need to be optimized for each analyte. Different combinations of these parameters should be tried during this soaking process. Therefore, first analysis was conducted with 1000 ng for each experiment of commercially available gemfibrozil, 4'-hydroxy gemfibrozil, and gemfibrozil 1-O- β -glucuronide reference material to find the optimal soaking conditions for our tool compounds. The optimized soaking conditions were then applied to its metabolites generated from incubation. The reference material of 4'-hydroxy gemfibrozil was initially used to examine if this technology can be used for polar hydroxy and glucuronide metabolites.

Both the parent API and the reference metabolites 4'-hydroxy gemfibrozil (Fig. 5B) and gemfibrozil 1-O- β -glucuronide could successfully be structurally elucidated by CS-XRD using an in-house XRD system. The crystal structure of gemfibrozil revealed two molecules with

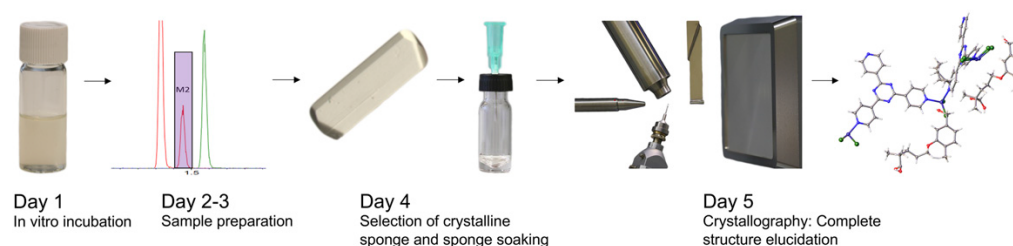


Fig. 2. Workflow of the metabolite identification processes using crystalline sponge technology.

occupancies of 100%, and the final R_1 and R_{int} values were 11.25% and 1.81%, respectively. The crystal structure of gemfibrozil 1-O- β -glucuronide revealed one molecule with occupancy of 100% and final R_1 and R_{int} values of 6.99% and 1.87%, respectively. Because of disorder, conformation of the glucuronide, i.e., the oxane ring and its substituents, cannot be determined. The presence of aliphatic rings in unfavorable conformations is often observed in the CS-XRD, especially for cyclohexane molecules. Nevertheless, the position of glucuronidation at the carboxylic acid function of gemfibrozil can be confirmed.

The successful results demonstrate that the application of the CS method can be expanded to the compounds containing highly polar hydrophilic groups introduced through metabolism of APIs, e.g., by using cytochrome P450 enzymes, despite the hydrophobic pore of the CS.

Next, the CS method was applied to metabolites obtained by incubation. Incubating gemfibrozil with rat liver microsomes for M1 and M2, rat liver S9 for M3, and human liver microsomes for M4 resulted in the formation of four metabolites in different quantities as described above. The reference material of 4'-OH gemfibrozil and gemfibrozil 1-O- β -glucuronide allowed the quantification of M2 and

M4, whereas the amounts of M1 and M3 were estimated. For pooling of M1, M3, and M4, an incubation solution of 20 μ M gemfibrozil was used, and 200 μ M gemfibrozil was used for M2. The direct use of the separated metabolites was not possible because of the sensitivity of the CS-XRD against impurities as already mentioned in previous publications (Inokuma et al., 2016; Kai et al., 2018). The impurities resulting from the incubation matrix that is necessary for preparation of metabolites by enzymatic reaction (e.g., salts, cofactor, microsomal stock solution) could not be separated by using only one purification step. Therefore, the pooled samples were further purified using a second column. CS soaking experiments were conducted with final amounts in a range of 500–1000 ng per experiment.

The soaking experiments of the obtained metabolites M1–M4 were carried out under the same conditions as used for the reference material. The soaked CS were then measured via XRD, and the crystallographic analysis clearly revealed the positions of hydroxylation, carboxylation, and glucuronidation. M1 exhibits relatively high electron density in close proximity to the 5'-methyl carbon atom forming a benzyl alcohol, which is further oxidized at the same position to form a benzoic acid (M3). M2 shows high electron density at position 4' of the 2',5'-dimethylphenoxy

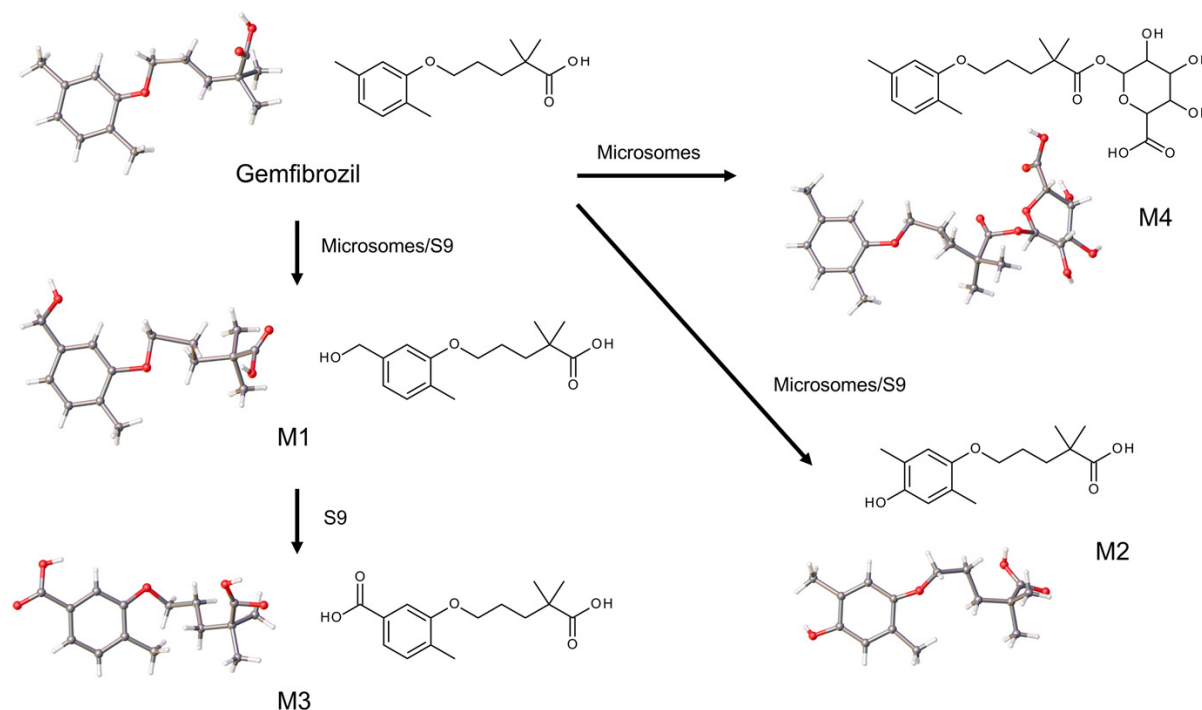


Fig. 3. Metabolic pathway of gemfibrozil; M1, 5'-CH₂OH gemfibrozil; M2, 4'-OH gemfibrozil; M3, 5'-COOH gemfibrozil; M4, gemfibrozil glucuronide.

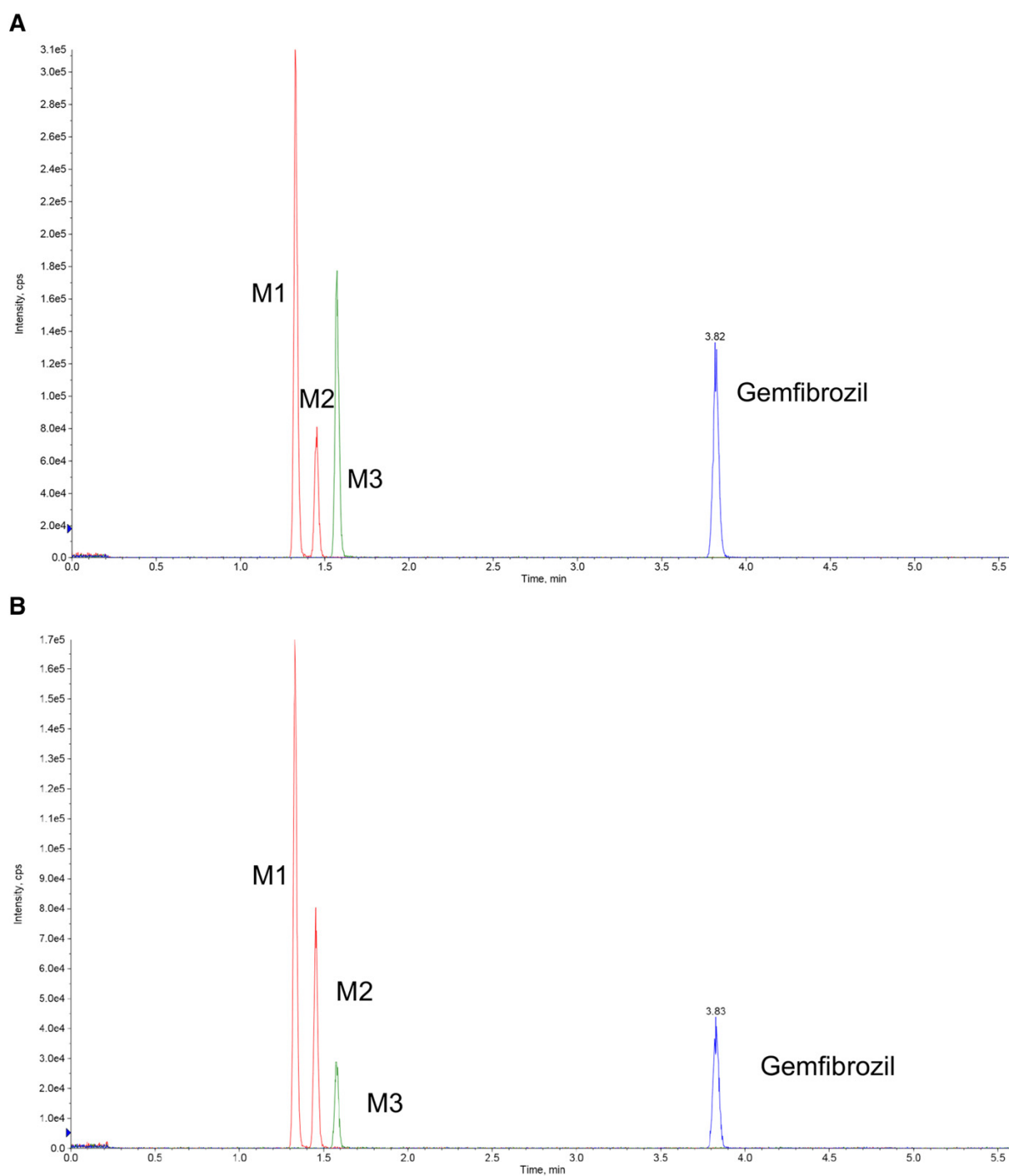


Fig. 4. Extracted ion chromatogram of multiple reaction monitoring (MRM) for gemfibrozil with rat liver S9 (A) and human liver S9 (B) in the presence of NADPH and NADP⁺ as cofactors. M1 (5'-CH₂OH gemfibrozil): *m/z* 265.0/137.2; M2 (4'-OH gemfibrozil): *m/z* 265.0/137.2; M3 (5'-COOH gemfibrozil): *m/z* 279.0/151.0; gemfibrozil: *m/z* 249.1/121.0.

moiety. The electron density map of the benzene core from gemfibrozil and its metabolites M1-M3 are shown in Fig. 5B. Two molecules of 5'-hydroxymethyl gemfibrozil and one cyclohexane were clearly assigned by its electron density in the asymmetric unit with occupancies of

100% (Fig. 5A). The modeled structure shows a R_1 value of 7.58% and a value of 2.18% for R_{int} . One guest is stabilized by π - π stacking interactions between its aromatic ring and the *tpt* ligand of the framework (distance 3.63 Å, angle 5.83°). Crystallographic data of 4'-hydroxy

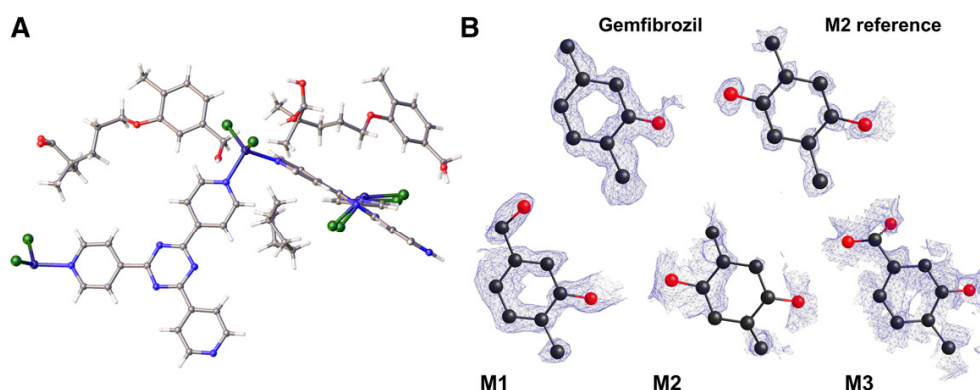


Fig. 5. (A) Asymmetric unit of $[(ZnCl_2)_2(tpf)_2]_n$ with two 5'-hydroxymethyl gemfibrozil molecules and one cyclohexane. (B) Electron density map F_o [contoured at 0.67σ (gemfibrozil), 0.65σ (M2 reference), 0.73σ (M1), 0.95σ (M2), 1.00σ (M3)] of benzene core from reference material and incubation samples.

gemfibrozil revealed one analyte molecule with occupancy of 44% (R_1 7.56%, R_{int} 2.09%) and two cyclohexane molecules. M2 interacts with the framework by π - π stacking interactions between the aromatic ring and the tpf ligand (distance 3.54 Å, angle 7.90°) as well as $CH\cdots Cl$ interactions (distance 2.50 Å) between the 5'-methylgroup of the analyte and the $ZnCl_2$ part of the framework (Fig. 6). The data of 5'-carboxygemfibrozil provided low electron density of the analyte but clearly confirmed the position of metabolism in comparison with the crystal structure obtained from 5'-hydroxymethylgemfibrozil (Fig. 5B). The XRD data of M4 showed the formation of an acyl glucuronide by conjugation of the carboxylic acid moiety of gemfibrozil with the C1-hydroxy group of glucuronic acid. This confirmed the position of glucuronidation, but because of low electron density of the analyte, the reference material was used to illustrate the structure in this publication. M3 and M4 could be assigned with low electron density compared with the hydroxy metabolites because of the higher polar and nucleophilic groups. The refined structures of gemfibrozil and its generated metabolites are shown in Fig. 3. Crystallographic data and ORTEP diagrams of the asymmetric unit of the framework and analyte are shown in the Supplemental Data.

Discussion

In summary, we were able to analyze the structure of three different phase I metabolites and one phase II acyl glucuronide of our tool

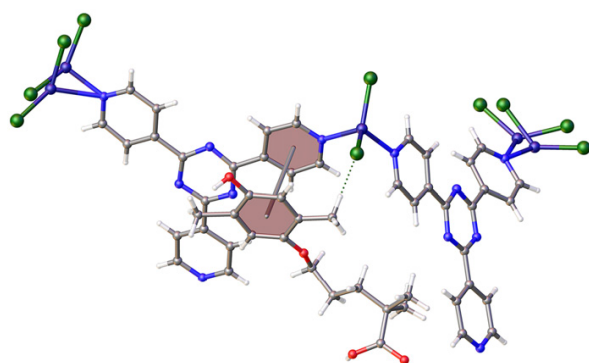


Fig. 6. The crystal structure of M2 gemfibrozil exhibits π - π stacking interactions (gray line) and $CH\cdots Cl$ interactions (green dashed line) between the analyte and the framework. Centroids are shown as gray spheres in the center of the benzene ring.

compound gemfibrozil at atomic level with only nanogram amounts of substance by using the crystalline sponge method. Data from MS analysis provided us information on the type of metabolism but could not pinpoint the exact position of the hydroxylation, carboxylation, or glucuronidation reaction. Only the crystallographic data showed that hydroxylation occurred at the 4'-C and 5'- CH_3 positions of the aromatic ring as well as further oxidation at position 5'- CH_3 to form a carboxylic acid and direct glucuronidation at the carboxylic acid moiety of the alkyl chain. The Cambridge Crystallographic Data Centre did not contain crystallographic data of an acyl glucuronide before and could be extended through M4 gemfibrozil.

The need to identify the structure of metabolites meets the need of industry to assess the contribution of drug metabolites to efficacy, toxicity, or drug-drug interactions. It also meets the requirements from regulatory agencies to ascertain that human metabolites are present in preclinical species used to assess drug safety. Acyl glucuronides especially play an important role in the assessment of drug-related risk factors, as they contain the risk to be potentially reactive metabolites. An intramolecular rearrangement process, so called "migration," leads to the formation of chemically reactive species that can covalently bind proteins (Bailey and Dickinson, 2003; Zhong et al., 2015).

The application of the crystalline sponge technology in structure elucidation is a convenient technology that can be applied in drug discovery to accelerate the metabolite identification processes and allow for using human-derived systems to identify human metabolites from in vitro incubation, years before clinical samples are available.

This technology is, however, in its infancy. Therefore, optimization of soaking conditions (time, solvent, and temperature) as well as assessing the purity required for compound is still needed. The amount of analyte per experiment was used in excess but could be reduced as in the original publication mentioned (Inokuma et al., 2013). It has also been described that not all compounds can be applied in this technology, as the size of the molecules may prevent them from entering the pores and their polarity may prevent some molecules to dissolve in the hydrophobic solvents typically used during soaking. It was therefore unclear if the technology would be applicable to drug metabolites resulting from phase I and especially phase II reactions. To answer this question, we used reference metabolites (M2 and M4 gemfibrozil) to confirm the ability of CS-XRD to assess the structure of phase I and phase II metabolites. Beside these two metabolites, we have applied this new technology to identify the structure of the two other unknown metabolites (M1 and M3

gemfibrozil), confirming its application in drug development of new chemical entities for which only the structure of the candidate molecule is known.

Our results show that the combination of CS-XRD with MS data offers a great opportunity for scientists in drug metabolism and pharmacokinetics to assess the structure of metabolites produced in low amounts from in vitro studies. The technology is also able to provide information on stereochemistry, offering a significant advantage over other techniques such as MS or NMR. In conclusion, we show that CS can be used to assess the structure of traces of drug-like molecules as well as their metabolites, showing promising application at different stages of drug development when complete structure elucidation is needed. Beside metabolites, this technology could also be applied to identify degradation products and impurities during drug product development.

Acknowledgments

The authors thank Andrea Unzue-Lopez for kindly providing 4'-OH gemfibrozil reference material and Axel-Walter Thomasberger, Ralf-Erwin Licht, Jonny Nachtigall, and Birikiti Kidane for their kind technical support in the laboratory. The authors also thank Anna K.H. Hirsch for her constructive comments of the manuscript.

Authorship Contributions

Participated in research design: All authors.

Conducted experiments: Rosenberger, von Essen, Khutia.

Contributed new reagents or analytic tools: Kühn, Urbahns.

Performed data analysis: Rosenberger, von Essen.

Wrote or contributed to the writing of the manuscript: Rosenberger, von Essen, Khutia, Kühn, Hartmann, Badolo.

References

- Bailey MJ and Dickinson RG (2003) Acyl glucuronide reactivity in perspective: biological consequences. *Chem Biol Interact* 145:117–137.
- Biradha K and Fujita M (2002) A springlike 3D-coordination network that shrinks or swells in a crystal-to-crystal manner upon guest removal or readsorption. *Angew Chem Int Ed Engl* 41:3392–3395.
- Brandon EFA, Raap CD, Meijerman I, Beijnen JH, and Schellens JHM (2003) An update on in vitro test methods in human hepatic drug biotransformation research: pros and cons. *Toxicol Appl Pharmacol* 189:233–246.
- Dolomanov OV, Bourhis LJ, Gildea RJ, Howard JAK, and Puschmann H (2009) OLEX2: a complete structure solution, refinement and analysis program. *J Appl Cryst* 42:339–341.
- EMA (2013) *Guideline on the Investigation of Drug Interactions*, European Medicines Agency, Amsterdam, Netherlands.
- Fasinu P, Bouic PJ, and Rosenkranz B (2012) Liver-based in vitro technologies for drug biotransformation studies - a review. *Curr Drug Metab* 13:215–224.
- FDA (2016) *Guidance for Industry: Safety Testing of Drug Metabolites*, US Department of Health and Human Services FDA, Center for Drug Evaluation and Research, Silver Spring, MD.
- Hoshino M, Khutia A, Xing H, Inokuma Y, and Fujita M (2016) The crystalline sponge method updated. *IUCrJ* 3:139–151.
- Inokuma Y, Ukegawa T, Hoshino M, and Fujita M (2016) Structure determination of microbial metabolites by the crystalline sponge method. *Chem Sci (Camb)* 7:3910–3913.
- Inokuma Y, Yoshioka S, Ariyoshi J, Arai T, Hitora Y, Takada K, Matsunaga S, Rissanen K, and Fujita M (2013) X-ray analysis on the nanogram to microgram scale using porous complexes [published correction appears in *Nature* (2013) 495:461–466]. *Nature* 501:262.
- Jones CG, Martynowycz MW, Hattné J, Fulton TJ, Stoltz BM, Rodriguez JA, Nelson HM, and Gonen T (2018) The CryoEM method MicroED as a powerful tool for small molecule structure determination. *ACS Cent Sci* 4:1587–1592.
- Kai K, Sogame M, Sakurai F, Nasu N, and Fujita M (2018) Collimonins A–D, unstable polyynes with antifungal or pigmentation activities from the fungus-feeding bacterium collimonas fungivorans Ter331. *Org Lett* 20:3536–3540.
- Kunde T and Schmidt BM (2019) Microcrystal electron diffraction (MicroED) for small-molecule structure determination. *Angew Chem Int Ed Engl* 58:666–668.
- Ma S and Chowdhury SK (2011) Analytical strategies for assessment of human metabolites in preclinical safety testing. *Anal Chem* 83:5028–5036.
- Massa W (2004) *Crystal Structure Determination*, Springer-Verlag GmbH, Heidelberg, Germany.
- Morita I, Mori T, Mitsuhashi T, Hoshino S, Taniguchi Y, Kikuchi T, Nagae K, Nasu N, Fujita M, Ohwada T, et al. (2020) Exploiting a C–N bond forming cytochrome P450 monooxygenase for C–S bond formation. *Angew Chem Int Ed Engl* 59:3988–3993.
- Murai T, Iwabuchi H, and Ikeda T (2004) Identification of gemfibrozil metabolites, produced as positional isomers in human liver microsomes, by on-line analyses using liquid chromatography/mass spectrometry and liquid chromatography/nuclear magnetic resonance spectroscopy. *J Mass Spectrom Soc Jpn* 52:277–283.
- Nedderman AN (2009) Metabolites in safety testing: metabolite identification strategies in discovery and development. *Biopharm Drug Dispos* 30:153–162.
- Prakash C, Shaffer CL, and Nedderman A (2007) Analytical strategies for identifying drug metabolites. *Mass Spectrom Rev* 26:340–369.
- Prasad B, Garg A, Takwani H, and Singh S (2011) Metabolite identification by liquid chromatography-mass spectrometry. *Trends Anal Chem* 30:360–387.
- Ramachar TR, Zheng SL, Chen YS, and Clardy J (2015) Analysis of rapidly synthesized guest-filled porous complexes with synchrotron radiation: practical guidelines for the crystalline sponge method. *Acta Crystallogr A Found Adv* 71:46–58.
- Rigaku Oxford Diffraction (2018) *CrysAlis PRO*, Rigaku Corporation, Tokyo, Japan.
- Sakurai F, Khutia A, Kikuchi T, and Fujita M (2017) X-ray structure analysis of n-containing nucleophilic compounds by the crystalline sponge method. *Chemistry* 23:15035–15040.
- Sheldrick GM (2015) Crystal structure refinement with SHELXL. *Acta Crystallogr C Struct Chem* 71:3–8.
- Wada N, Kersten RD, Iwai T, Lee S, Sakurai F, Kikuchi T, Fujita D, Fujita M, and Weng JK (2018) Crystalline-sponge-based structural analysis of crude natural product extracts. *Angew Chem Int Ed Engl* 57:3671–3675.
- Zhang D and Surapaneni S (2012) *ADME-Enabling Technologies in Drug Design and Development*, John Wiley & Sons, Inc., Hoboken, New Jersey.
- Zhang Z, Zhu M, and Tang W (2009) Metabolite identification and profiling in drug design: current practice and future directions. *Curr Pharm Des* 15:2220–2235.
- Zhong S, Jones R, Lu W, Schadt S, and Ottaviani G (2015) A new rapid in vitro assay for assessing reactivity of acyl glucuronides. *Drug Metab Dispos* 43:1711–1717.

Address correspondence to: Dr. Lassina Badolo, Merck KGaA, Frankfurter Str. 250, 64293 Darmstadt, Germany. E-mail: lassina.badolo@emdserono.com

Results

3.2 Chapter B: Crystalline sponge affinity screening

Title:

Crystalline sponge affinity screening: A fast tool for soaking condition optimization without the need of X-ray diffraction analysis

Authors:

Lara Rosenberger, Carolina von Essen, Anupam Khutia, Clemens Kühn, Katrin Georgi, Anna K. H. Hirsch, Rolf W. Hartmann, and Lassina Badolo

Bibliographic Data:

European Journal of Pharmaceutical Sciences,

Volume 164, Page 105884,

Accepted May 14, **2021**,

Doi: 10.1016/j.ejps.2021.105884

Reprinted with permission from European Journal of Pharmaceutical Sciences.

Copyright (2021) Elsevier B. V.



Contents lists available at ScienceDirect

European Journal of Pharmaceutical Sciences

journal homepage: www.elsevier.com/locate/ejps

Crystalline sponge affinity screening: A fast tool for soaking condition optimization without the need of X-ray diffraction analysis

Lara Rosenberger^{a,c,d}, Carolina von Essen^b, Anupam Khutia^b, Clemens Kühn^{b,*}, Katrin Georgi^a, Anna K.H. Hirsch^{c,d}, Rolf W. Hartmann^{c,d}, Lassina Badolo^a

^a Discovery and Development Technologies (DDTech), Merck KGaA, Frankfurter Strasse 250, 64293 Darmstadt, Germany

^b Innovation Center, Merck KGaA, Frankfurter Strasse 250, 64293 Darmstadt, Germany

^c Department of Drug Design and Optimization (DDOP), Helmholtz-Institute for Pharmaceutical Research Saarland (HIPS) - Helmholtz Centre for Infection Research (HZI), Campus EB.1, 66123 Saarbrücken, Germany

^d Department of Pharmacy, Saarland University, Campus EB.1, 66123 Saarbrücken, Germany

ARTICLE INFO

Keywords:

Crystalline sponge method
Metal organic framework
Host-guest chemistry
Single-crystal X-ray diffraction
Affinity screening
LC-MS²

ABSTRACT

Structural elucidation of small molecules only available in low quantity (nanogram) is one of the big advantages of the crystalline sponge method. The optimization of various soaking parameters is crucial for effective analyte absorption and repetitive positioning in the pores of the crystal. Time-consuming X-ray diffraction measurements are necessary for data collection and confirmation of successful guest inclusion. In this work, we report a screening method to select optimal soaking conditions without the need of single-crystal X-ray diffraction analysis for individual compounds and mixtures. 14 substances were chosen as test compounds. Parallel guest soaking of individual compounds and mixtures was conducted using various soaking conditions. After evaporation of solvent, excessive material was removed, and guest molecules released through dissolution of the framework. Liquid chromatography-tandem mass spectrometry allowed the estimation of analyte trapped in the pores and the selection of optimal soaking condition dependent on the highest amount of analyte to crystal size (affinity factor). The tool allowed subsequent crystallographic analysis of ten compounds with minimal experiment time. Additionally, a study to examine the lower limit of detection of the crystalline sponge method was conducted. Determination of two target analytes was possible using only 5 ng of sample. Our study shows the potential of an affinity screening to prioritize soaking parameters by estimation of the guest concentration in a single crystal for one or multiple target compounds within a short period of time.

1. Introduction

In recent years, continuous improvements of standard analytical techniques like liquid chromatography (LC)-mass spectrometry (MS), nuclear magnetic resonance (NMR) and single-crystal X-ray diffraction (XRD), or the development of new tools (e.g., microcrystal electron diffraction) have facilitated the determination of chemical structures of molecules. Although these experimental methods have been proven useful, they are still suffering from lack of sensitivity (NMR, XRD) or accuracy (LC-MS) and often fail to enable structure elucidation of

unknown molecules.

Single-crystal XRD analysis provides structural information at the atomic level but has the intrinsic limitation of growing single crystals, which requires a sufficient amount of material in the solid state (Massa, 2004). This disadvantage was addressed by Fujita and coworkers (Inokuma et al., 2013) by introducing the so called “crystalline sponge method” (CS-XRD). In this approach a porous metal coordination complex $[(ZnX_2)_3 \cdot (tpt)_2 \cdot x(\text{solvent})]_n$ ($X = \text{Cl}, \text{I}$; $tpt = 2,4,6\text{-tris}(4\text{-pyridyl})\text{-}1,3,5\text{-triazine}$) functions as a “host” crystal. The analyte (“guest”) is absorbed and regularly ordered in the pores of the three-dimensional

Abbreviations: AF, affinity factor; API, active pharmaceutical ingredient; CH, cyclohexane; CM, compound mixture; CS, crystalline sponge; CS-XRD, crystalline sponge method; DCM, dichloromethane; DME, 1,2-dimethoxyethane; DMSO, dimethyl sulfoxide; IS, internal standard; LC, liquid chromatography; MS, mass spectrometry; MS², tandem mass spectrometry; nH, n-hexane; NMR, nuclear magnetic resonance; R₁, residual factor; R_{int}, internal R-value; LLOD, lower limit of detection; TCM, trichloromethane; THF, tetrahydrofuran; UPLC, ultra-performance liquid chromatography; tpt, 2,4,6-tris(4-pyridyl)-1,3,5-triazine; XRD, X-ray diffraction.

* Corresponding author at: Merck KGaA, Frankfurter Str. 250, 64293 Darmstadt, Germany.

E-mail address: clemens.kuehn@merckgroup.com (C. Kühn).

<https://doi.org/10.1016/j.ejps.2021.105884>

Received 23 February 2021; Received in revised form 7 April 2021; Accepted 14 May 2021

Available online 20 June 2021

0928-0987/© 2021 Elsevier B.V. All rights reserved.

framework (“guest soaking”) and thus more readily accessible for XRD analysis. Thereby, not all classes of compounds are compatible with the available crystalline sponges (CS) and the affinity of each analyte for the framework is rather unpredictable and determines a low or high occupancy of analyte in the CS pores.

The field of applications of the CS-XRD has expanded since the publication of the original method in 2013. Besides structural elucidation of e.g., active pharmaceutical ingredients (API) (Sakurai et al., 2017), natural products (Li et al., 2019; Urban et al., 2016), volatile compounds (Zigon et al., 2017) or synthesis products (Duplan et al., 2016; Morita et al., 2020; Vinogradova et al., 2014), we recently applied this method for metabolite identification from *in vitro* incubation of gemfibrozil with liver microsomes from human and animal origin (Rosenberger et al., 2020). However, these drug-related materials are only available in small quantity from incubation and require isolation and purification of the target compound.

The crucial step of the CS-XRD is the individual optimization of soaking conditions for each analyte. It may take weeks to adjust the different soaking combinations of sponge type, organic solvent, soaking duration and temperature to achieve successful results. To examine successful analyte absorption and a regular order of guest molecules by intermolecular, noncovalent interactions (Brunet et al., 2017; Inokuma et al., 2016; Rissanen, 2017) with the CS framework, time-consuming XRD measurements are essential. The average measurement time of a standard system (e.g., SuperNova, Rigaku) requires around 24 hours per crystal and is thereby the limiting factor. To reduce the number of XRD experiments and to avoid unnecessary measurements for compounds with poor or no affinity for the sponges, a method to select the optimal soaking conditions without the usage of an XRD instrument is needed.

A first approach to prioritize analytes from a natural-product mixture was conducted by Wada et al. in 2018. Guest soaking of a crude plant extract was performed with five CS using one specific soaking condition. After completion of soaking, the crystals were further treated with cyclohexane for several days to extract the compounds from the framework. Comparison of HPLC-UV chromatograms before and after the CS soaking identified the analytes enriched in the pores of the framework. In our study the principle of analyzing trapped compound material prior to XRD analysis could be adapted for soaking condition optimization, by adjusting and screening the different parameters of the soaking process simultaneously.

In this study, we apply the CS affinity screening to 14 compounds to select the optimal soaking conditions by estimating the analyte concentration in the CS pores using LC-tandem MS (MS²) and without the need for XRD measurements. A selection of compounds was further analyzed as a mixture to reduce analysis time and investigate the influence of several analytes on the soaking conditions. To demonstrate that the amount of guest does not need to be applied in excess for CS-XRD, a lower limit of detection (LOD) study with reduced analyte concentration was conducted for four different analytes.

2. Material and methods

2.1. Chemicals and reagents

Acetaminophen (5), codeine (6), dehydro nifedipine (4), diclofenac (14), isoniazid (16), nifuroxazid (9), risperidone (11), orlistat (7), sildenafil (12), propranolol hydrochloride (21), zinc chloride, zinc iodide, 1,2-dimethoxyethane (DME), dimethyl sulfoxide (DMSO), ammonium formate and formic acid were purchased from Sigma Aldrich Chemie GmbH (Steinheim, Germany). Gemfibrozil (18) and carbamazepine (19) were purchased from Acros Organics (New Jersey, USA) and cyclohexane (cH), n-hexane (nH), methanol, acetone, dichloromethane (DCM), trichloromethane (TCM), tetrahydrofuran (THF), nitrobenzene, water (UPLC-MS grade) and acetonitrile (UHPLC-MS grade) were purchased from Merck KGaA (Darmstadt, Germany). 5-hydroxy omeprazole (13) was purchased from Biomol GmbH (Hamburg, Germany) and

doxorubicin (15) from Santa Cruz Biotechnology (Dallas, USA). Chlorpromazine hydrochloride (3), imipramine hydrochloride (10), doxorubicinone (8), irinotecan (17), and 4'-7-dimethoxyisoflavone (20) were obtained from VWR (Darmstadt, Germany). 2,4,6-tris(4-pyridyl)-1,3,5-triazine (tpt) was purchased from aber GmbH (Karlsruhe, Germany).

2.2. CS affinity screening/ CS-XRD

Reference material was prepared as 1 mg/ml solution in DME (5, 8, 12, 14, 15, 18 and 19), DCM (3, 4, 11, 10, 17 and 20) and TCM (6, 7 and 13). 0.33 mg/ml solution was prepared for 16 in DME and 9 in THF. The hydrochloride forms of 3 and 10 were converted to free amines.

Compound mixtures were prepared in lower concentration (final concentration: 0.1 mg/ml of 6; (334 nmol/ml) of additional compounds) to ensure an excess of crystal to analyte. Six analytes (334 nmol each) were mixed to generate compound mixture 1 (CM1: 5, 6, 12, 14, 16 and 17) and compound mixture 2 (CM2: 3, 6, 10, 14, 16 and 17).

The porous CS [(ZnCl₂)₃•(tpt)₂•x(solvent)]_n (solvent=cyclohexane (1a), n-hexane (1b)) and [(ZnI₂)₃•(tpt)₂•x(solvent)]_n (solvent=cyclohexane (2a), n-hexane (2b)) were prepared following the reported procedures (Biradha and Fujita, 2002; Ramadhar et al., 2015).

For guest soaking of single compounds, one of each prepared CS (1a, 1b, 2a and 2b) was transferred with 50 µl of solvent to a sample vial. 1 µl of the 1 mg/ml analyte solution or 3 µl of the 0.33 mg/ml solution was pipetted into the sample vials. The vials were closed with a screw cap with septum seal and pierced with a syringe needle for slow evaporation of the solvent using an incubator at 50 °C for 1 day. Soakings at lower temperature were prepared similarly with 25 µl solvent at 25 °C for 1 day. For guest soaking of CM1 and CM2 1 µl of the mixture, containing a negative control (17), was pipetted into the sample vials. All soaking conditions were prepared in triplicate (intra-assay n = 3).

After 1 day, the crystals were removed from the soaking vials and placed in a new vial. 1 ml of water was added, the vials were closed with a cap and shaken for a few seconds to remove not absorbed compound material from the surface of the CS. Compound 17 was used as a negative control in CM1 and CM2 to monitor this step, as its size prevents the molecules to enter the pores. After removing the liquid from the vials with a pipette, the crystal size (length x width) was measured using a microscope with attached camera (Leica, Wetzlar, Germany), as the amount of analyte within the CS depends on the available occupation sites. The crystal has a defined quantity of void space per unit cell (pores) and therefore the total accessible void volume increases with the crystal size. Measurement of the crystal height was not possible due to the limitation of the used microscope. To dissolve the framework of the crystal, 1 ml of dissolution medium (acetone, acetonitrile, methanol, water; 25% V/V each) was added and the solution placed in an incubator at 25 °C over night.

After complete CS dissolution and release of guest molecules, the sample solution was analyzed using UPLC-MS² in multiple-reaction monitoring mode. Prior tuning of instrument parameters provided the optimal transitions for each analyte (precursor ion and product ion in Table 2). Calibration curves of each analyte were prepared from stock solutions, using 21 as internal standard (IS). The ratio of amount of analyte over the crystal size was defined as affinity factor (AF) [fmol/µm²] and used to compare various soaking parameter combinations (Table 1). The three conditions, showing the highest mean AF for the target compound, were classified as optimal conditions and were used to

Table 1
Soaking conditions of affinity screening.

	50 °C	25 °C
ZnCl ₂ in cyclohexane (1a)	C _{cl-H,50}	C _{cl-H,25}
ZnCl ₂ in n-hexane (1b)	C _{cl-H,50}	C _{cl-H,25}
ZnI ₂ in cyclohexane (2a)	I _{cl-H,50}	I _{cl-H,25}
ZnI ₂ in n-hexane (2b)	I _{cl-H,50}	I _{cl-H,25}

determine the structure of the host-guest complex by XRD. Guest soaking for XRD analysis was performed as before. After evaporation of solvent and guest inclusion, the CS was mounted onto a single-crystal X-ray diffractometer and diffraction data was collected.

2.3. Preparation of calibration standards/sample preparation for UPLC-MS² analysis

A 10 nmol/l stock solution in DMSO was used to prepare calibration standard solutions of 1, 5, 10, 25, 50, 75, 100, 250 nmol/l for each analyte by diluting with acetonitrile/water (50/50%). **21** was added as IS, yielding a final concentration of 1 nmol/l. Calibration curves were obtained by plotting the peak area ratios of analyte to IS as a function of drug concentrations.

For sample preparation to 100 μ l of dissolved CS material, 10 μ l of IS and 890 μ l acetonitrile/water (50/50%) were added. The samples of the compound mixture were processed similarly, with the difference of 2 μ l of IS and 98 μ l acetonitrile/water (50/50%).

2.4. UPLC-MS²

The LC-MS² system consisted of an Acquity UPLC Class I system (Waters Corporation, Milford, USA) combined with a linear ion trap quadrupole (Qtrap 5500/6500+) mass spectrometer (AB Sciex LLC, Framingham, USA). Samples were analyzed with an electrospray ion source in the positive ionization mode. Source parameters were set at source temperature 600 °C and ion spray voltage 4.5 kV. The transitions were monitored using the multiple reaction monitoring mode. Chromatographic separation was achieved on an Acquity UPLC BEH C18 column (1.7 μ m; 2.1 \times 50 mm; Waters Corporation, Milford, USA) at a column oven temperature of 40 °C. Elution was performed at a flow rate of 0.8 ml/min over a period of 2.5 min with a mixture of solvent A (water + 0.1% formic acid + 10 mM ammonium formate) and solvent B (acetonitrile). Compounds were eluted using the following gradient: mobile phase B started isocratic for 0.1 min (5%) and increased from 5% to 100% between 0.1 min and 1.5 min, followed by elution with 100% B for 0.5 min, returning to 5% B in 0.01 min and re-equilibration at 5% B for 0.49 min. For the analysis of **4**, **5**, **6** and **16**, 30% B was used as starting condition at a flow rate of 0.7 ml/min. Mobile phase B increased from 30% B to 70% between 0.1 and 1.5 min, followed by a 0.5-min linear gradient to 100% B, returning to 30% B in 0.01 min and re-equilibration at 30% B for 0.49 min. For the analysis of **7** an isocratic

UPLC method (90% B) was used at a flow rate of 0.7 ml/min with a runtime of 1.70 min. The software Analyst 1.6.3 was used for data acquisition and processing.

2.5. XRD measurements

Single-crystal XRD measurements using a Rigaku Oxford Diffraction XtaLAB Synergy-R diffractometer and crystal structure modelling using OLEX2 (Dolomanov et al., 2009), SHELXT and SHELXL (Sheldrick, 2015) were conducted as described in detail in our previous work (Rosenberger et al., 2020).

The complete workflow of the affinity screening from optimization of soaking conditions to the final generation of crystallographic data is shown in Fig. 1.

3. Results

3.1. Single-compound screening for optimization of soaking conditions

In this study, optimization of soaking conditions was conducted for individual analytes, by varying different combinations of soaking parameters in parallel (Table 1). The analyte concentration per sponge (AF value) was used as selection criterion.

To demonstrate the potential of the CS affinity screening method, eleven APIs and three metabolites (3–16) with different size and polarity were selected as tool compounds. The estimation of guest concentration from dissolved sponge material using UPLC-MS² and the crystal-size measurement allowed the calculation of a mean AF [fmol/ μ m²] for each soaking condition and examined compound (optimal soaking conditions (1)–(3) in Table 2). To consider a correlation between these factors and the affinity to the CS, the highest mean AF values of analyte 3–16 are plotted in Fig. 2. Successful structure assignment in the CS pores using one of the optimal soaking conditions (1)–(3) is labeled as green datapoint (●), whereas unsuccessful XRD analysis is labeled as dark grey triangle (▲). Data shows that guest compounds with an AF value > 10 (3–8 and 10–12) resulted in successful XRD measurements (see 3.2 for detailed information on XRD experiments). In addition, data could be obtained demonstrating that compounds with AF values < 10 were not successful (13–16), except for 9, and could therefore be excluded from further investigation. Compound precipitation was observed for **9** after evaporation of solvent *CH*, correlating with its low solubility (0.33 mg/ml in THF) and resulting in a misleading lower AF

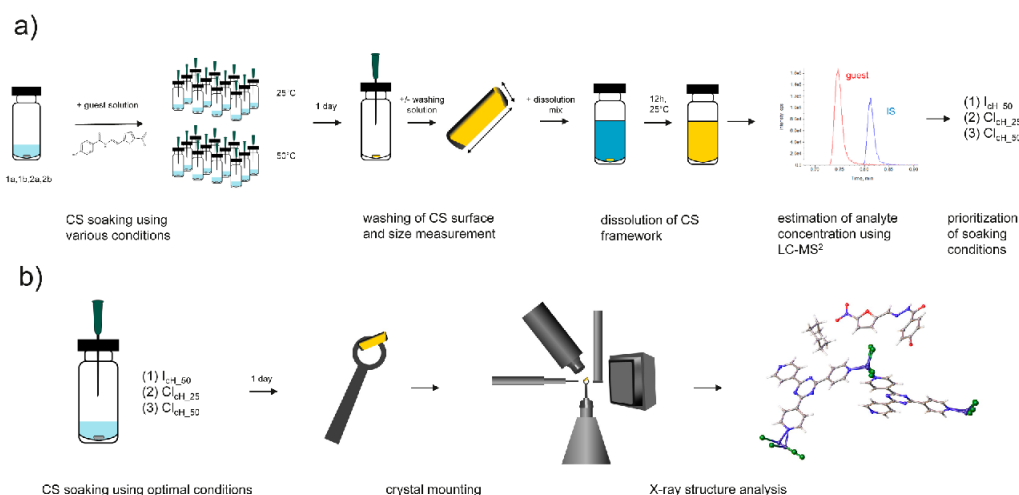
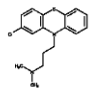
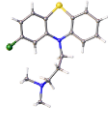
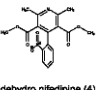
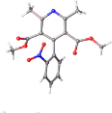
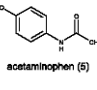
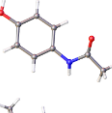
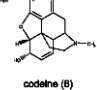
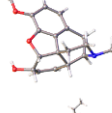
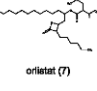
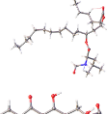
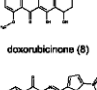
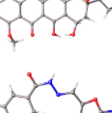
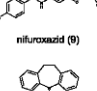
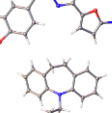
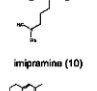
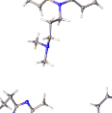
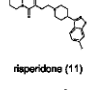
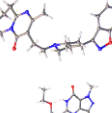
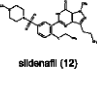
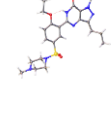
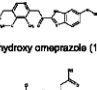
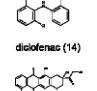
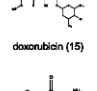
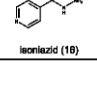


Fig. 1. Schematic workflow of a) CS affinity screening, b) CS-XRD using optimal soaking conditions (1)–(3).

Results

Table 2

a) Chemical structure of guest compounds; b) precursor and product ion for LC-MS² analysis in positive ionization mode; c) optimal soaking conditions (1) – (3) based on affinity screening; d) mean affinity factor of analyte concentration to crystal size ratio [fmol/μm²]; e) results of XRD measurements: + successful, - analyte not assignable, -* CS broken; f) molecular structure of guest compound observed in CS pores; g) selected crystallographic data of XRD measurements: (4) R_{int}, (5) R₁, (6) guest occupancy. ** optimal soaking condition was confirmed, but no data finalization was conducted as the host-guest structure has been reported before.

a) Compound	b) MS ² fragmentation (m/z)	c) Optimal soaking conditions	d) Mean affinity factor [fmol/μm ²]	e) XRD measurement	f) Molecular structure	g) Selected crystallographic data [%]
 chlorpromazine (3)	319.1/86.1	(1) I _{41,50} (2) Cl _{41,50} (3) I _{41,50}	(1) 48 (2) 33 (3) 25	(1) - (2) + (3) -		(4) 3.34 (5) 10.16 (6) 48 and 100
 delhydro nifedipine (4)	345.1/284.1	(1) I _{41,50} (2) I _{41,50} (3) Cl _{41,50}	(1) 19 (2) 10 (3) 6	(1) + (2) - (3) -		(4) 3.15 (5) 9.88 (6) 62
 acetaminophen (5)	152.1/110.0	(1) Cl _{41,25} (2) Cl _{41,50} (3) I _{41,50}	(1) 87 (2) 53 (3) 48	(1) + (2) + (3) -*		(4) 1.75 (5) 5.31 (6) 100
 codeine (6)	300.1/166.3	(1) I _{41,50} (2) I _{41,50} (3) Cl _{41,50}	(1) 28 (2) 19 (3) 19	(1) + (2) + (3) -		(4) 2.94 (5) 5.67 (6) 100 and 100
 orlistat (7)	486.5/319.5	(1) I _{41,25} (2) Cl _{41,25} (3) I _{41,50}	(1) 12 (2) 11 (3) 10	(1) + (2) + (3) +		(4) 4.58 (5) 7.22 (6) 82
 doxorubicinone (8)	413.0/310.9	(1) Cl _{41,50} (2) Cl _{41,50} (3) I _{41,50}	(1) 28 (2) 9 (3) 5	(1) + (2) - (3) -		(4) 1.37 (5) 8.05 (6) 49
 niluroxazid (9)	276.2/121.0	(1) I _{41,50} (2) Cl _{41,25} (3) Cl _{41,50}	(1) 4 (2) 4 (3) 3	(1) -* (2) + (3) +		(4) 1.57 (5) 6.49 (6) 53
 imipramine (10)	281.2/58.1	(1) I _{41,50} (2) Cl _{41,50} (3) I _{41,50}	(1) 38 (2) 29 (3) 29	(1) -* (2) + (3) -		**
 risperidone (11)	411.3/191.4	(1) I _{41,25} (2) Cl _{41,50} (3) I _{41,25}	(1) 11 (2) 10 (3) 9	(1) - (2) - (3) -*		(4) 3.06 (5) 9.66 (6) 48 and 54
 sildenafil (12)	475.3/283.1	(1) I _{41,50} (2) I _{41,50} (3) I _{41,25}	(1) 18 (2) 10 (3) 8	(1) + (2) + (3) -		(4) 5.00 (5) 11.99 (6) 69 and 100
 5-hydroxy omeprazole (13)	362.1/214.3	(1) I _{41,50} (2) Cl _{41,50} (3) I _{41,25}	(1) 3 (2) 2 (3) 1	(1) -* (2) - (3) -		
 diotofenaz (14)	296.0/215.0	(1) Cl _{41,50} (2) Cl _{41,50} (3) I _{41,50}	(1) 1 (2) 1 (3) 1	(1) - (2) -* (3) -*		
 doxorubicin (15)	544.2/361.1	(1) I _{41,50} (2) I _{41,25} (3) Cl _{41,25}	(1) 0 (2) 0 (3) 0	(1) -* (2) -* (3) -*		
 isoniazid (16)	138.1/79.1	(1) I _{41,25} (2) I _{41,50} (3) Cl _{41,25}	(1) 1 (2) 1 (3) 1	(1) - (2) -* (3) -*		

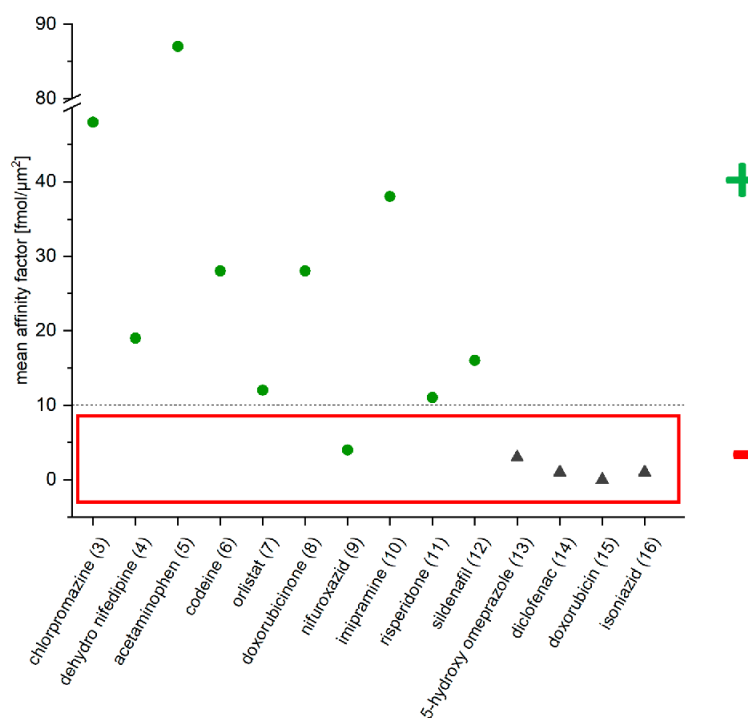


Fig. 2. Plot of highest mean affinity factors [fmol/μm²] of 3–16; CS-XRD successful ●, unsuccessful ▲.

number. Only dissolved guest molecules can diffuse into the crystal by guest exchange with solvent molecules filling the CS pores.

These results give a clear indication that the AF can be applied as exclusion criteria (+/-) to prioritize soaking parameters and decide if an XRD experiment should be conducted.

3.2. Structural elucidation of compounds by CS-XRD using optimal soaking conditions

The optimal soaking conditions prioritized by the affinity screening were applied to conduct the CS-XRD. Results were classified as + (analyte could be assigned successfully after guest inclusion; sponge crystallinity remains intact due to an exchange of solvent molecules to analyte molecules), as - (no analyte could be assigned (e.g., no repetitive order of target compound in CS pores) or only solvent (cH or nH) visible) and -* (crystals were damaged as a result of complete evaporation of solvent or nucleophilic attacks (e.g., aliphatic amino groups) and unusable for XRD measurements). The molecular structures as well as selected crystallographic data such as final R_1 (residual factor) values, R_{int} (internal R-value) values and guest occupancies are shown in Table 2.

One of the three proposed optimal soaking conditions resulted in a successful XRD measurement for compound 3, 4, 8 and 10. After refinement of the framework, the molecular structure of one guest could be clearly assigned from the residual electron density in the CS pores. First XRD measurements of compound 8 using $Cl_{nH_{50}}$, $Cl_{cH_{50}}$ and $I_{cH_{50}}$ for sample preparation were unsuccessful as no analyte was assignable and guest precipitation was observed after evaporation of solvent. As the AF showed a value > 10 and the crystal colour changed from colourless to slightly red after CS soaking and evaporation of nH, a solvent exchange was conducted to increase the compound solubility. Through further optimization by exchange of solvent DME to THF for condition

$Cl_{nH_{50}}$ one guest molecule could be clearly assigned. The affinity screening allowed a preselection of soaking condition $Cl_{nH_{50}}$ which was further optimized by adjusting the solvent to dissolve the analyte as an additional parameter.

XRD analysis of compounds 5, 6, 9 and 12 resulted in successful measurements for two of the three proposed optimal soaking conditions. Two molecules of 12 were clearly assigned in the asymmetric unit. The crystal structure of 6 revealed two molecules. The space group of the crystal changed from centrosymmetric $C2/c$ to chiral $C2$ after inclusion of 6 due to the enhanced anomalous scattering effect of heavy atoms (Cl and I) embedded in the framework (Flack and Bernardinelli, 1999; Yan et al., 2017). A reasonable Flack parameter of 0.025(3) was obtained, confirming the absolute configuration of 6. For compound 7, crystallographic analysis of the optimal soaking conditions $I_{cH_{25}}$, $Cl_{cH_{25}}$ and $I_{cH_{50}}$ resulted in a successful assignment of guest molecules.

To obtain the crystallographic data of compound 11, additional XRD measurements were necessary. No analyte could be assigned for the proposed optimal soaking conditions. By comparing the AF of the screened conditions (data not shown), similar AF values were observed and further XRD experiments were conducted. Thereby, the analyte structure was partly observed for condition $Cl_{cH_{25}}$ using the standard concentration of 1 μg. The structure of two analyte molecules could be completely assigned by increasing the amount of guest to 2 μg during guest soaking.

Crystallographic analysis of compound 13–16 was either not possible due to low crystal quality (crystals broken) or no analyte could be assigned, indicating poor affinity of test compound to the framework and confirming the results of the affinity screening.

Crystallographic data and ORTEP diagrams of the asymmetric unit including framework and analytes are shown in the Supplemental Data.

3.3. Screening of compound mixture for optimization of soaking conditions

After using the affinity screening to detect the optimal soaking parameters for single compounds, the application of the screening method to a mixture of analytes was examined. Two mixtures (CM1 and CM2) were prepared by selecting five compounds with AF values above and below 10. The three highest calculated AF values for each analyte are shown in Table 3. Soaking parameters, resulting in a successful assignment of guest analyte in already conducted XRD experiments, are highlighted in grey.

Compared to the screening of single compounds, lower AF values were observed for the compounds of the mixtures. A classification based on AF values (> 10) as conducted before was therefore not possible. For CM1 one of the three classified optimal soaking conditions for analytes 5, 6 and 12 is the same as that identified in the individual screening and resulted in a successful XRD measurement. Negative control 17 shows no affinity to the CS and was therefore used as a lower limit and exclusion limit. AF values of compounds 14 and 16 were comparable to negative control 17 and were therefore excluded from further analysis. Similar results were observed for compounds 6, 16 and negative control 17 in CM2. Guests 3 and 10 showed higher AF values compared to 17 but did not match the soaking parameters from the single compound analysis. Optimal conditions $Cl_{cH_{50}}$ and $Cl_{nH_{50}}$ were missed by applying the mixture. Compounds showing a greater AF value than the negative control, would need to be analyzed again using the single compound screening to identify the optimal soaking condition. This also applies for compound 14, as higher AF values were observed for CM2 but re-analysis would show no increase of AF by increasing the analyte concentration.

3.4. LLOD

To examine the LLOD of the CS-XRD, four analytes (5, 18, 19 and 20) were chosen as tool compounds. Guest soaking was conducted using soaking condition $Cl_{nH_{50}}$ for compound 18, $Cl_{cH_{50}}$ for 19 and 20, and $Cl_{cH_{25}}$ for 5. Analysis was started with 1000 ng. After observation of guest molecule in the pores, the amount of substance was continuously reduced to half. Thereby, it was observed that compound 18 was also visible down to 250 ng. For guest 19, the lower limit could even be decreased to 50 ng, where one analyte molecule was still clearly visible (occupancy: 100%; R_1 7.39% and R_{int} 1.76%). Surprisingly, when soaking compound 5 and 20 (occupancy: 34%; R_1 6.79% and R_{int}

2.71%), the amount of substance needed to assign a complete host-guest complexation could even further be reduced to only 5 ng. Close examination of intermolecular interactions between the host framework and the guest molecules from crystal structures confirm that some analytes like 5 or 20 tend to form strong non-covalent contacts (e.g., hydrogen bonds, π - π stacking) facilitating the inclusion of compound even using only a few ng of substance. A detailed analysis of the structures for intermolecular interactions can be taken from Supplemental Data.

4. Discussion

During the process of “guest soaking”, analyte molecules can be absorbed into the pores of the porous CS and regularly ordered due to the high molecular-binding ability of the framework (Mon et al., 2018; Zhang et al., 2020). This results in an inclusion and enrichment of target molecules in the CS pores. Typical interactions can be observed between the electron-deficient tpt ligand (π - π , CH- π) and I/Cl atoms as hydrogen-bond acceptors of the framework and the analytes (Ohmori et al., 2004; Hoshino et al., 2016). The stronger the interactions and therefore the affinity, the higher will be the occupancy of the compound of interest in the CS pores. The formation of these interactions is influenced by the analyte type and the parameters of the soaking condition, such as CS type (e.g., $[(ZnCl_2)_3 \cdot (tpt)_2 \cdot x(\text{solvent})]_n$, $[(ZnI_2)_3 \cdot (tpt)_2 \cdot x(\text{solvent})]_n$), solvent (e.g., cH, nH), temperature (e.g., 25 °C, 50 °C) and analyte concentration.

In summary, we were able to demonstrate that the affinity screening can be used as a practical tool to find the optimal soaking condition for individual analytes without the need of an XRD instrument. Screening of 14 compounds yielded in the successful analysis of ten guest analytes. First experiments were conducted by analyzing compound 3 and 10, which could successfully be structurally elucidated by CS-XRD in earlier works (Sakurai et al., 2017). The parameters known from literature ($Cl_{nH_{50}}$) could be confirmed for compound 10. For analyte 3, the combinations of soaking parameters, which result in sufficient interactions between host and guest, could be expanded for $Cl_{cH_{50}}$. By analyzing the AF values of 14 test compounds, it was observed that analytes showing an AF value > 10 likely interact with the CS pores, whereas it became clear that AF < 10 represents low or no host-guest interactions. By conducting the CS-XRD using the soaking condition showing the highest AF value, only one XRD measurement would have been sufficient for a successful structural elucidation of six compounds. Unnecessary time-consuming XRD experiments of compounds having low affinity to the CS and therefore low AF values can be avoided. The prioritization of soaking conditions allowed moreover a targeted adaptation of a further parameter (e.g., solvent, (THF)) to achieve successful structure elucidation, as demonstrated for tool compound 8. As this is a first approach to use the analyte concentration to optimize the soaking conditions, more data points are needed to confirm the exclusion criterion of AF 10.

It was also shown that the affinity screening of a mixture of compounds can be used as a first assessment to reduce analyte concentration and experimental time but cannot replace completely the screening of single compounds, as shown in CM2. Lower AF values were observed as a result of the reduced analyte concentration added during the CS soaking and therefore the amount of analyte gained from LC-MS² estimation (data not shown). The influence of excessive guest concentration and several analytes on the soaking process and regular order in the pores is yet unknown and needs further investigation. The application of the affinity screening for mixtures could be used as a prospective approach to optimize soaking parameters of unknown compounds not available as reference material prior to compound isolation and purification, e.g., metabolites from microsomal incubation only formed in low concentration. Unnecessary chromatographic purification of analytes showing low or no affinity could be avoided.

Literature shows, that the applied guest amount is inconsistent and differs amongst research groups and analytes (Hayashi et al., 2018;

Table 3
Mean AF values [fmol/ μm^2] from affinity screening of CM1 and CM2 for soaking conditions $Cl_{cH_{50}}$ - $Cl_{nH_{25}}$.

CM1						
Soaking Condition	Compound (5)	(6)	(12)	(14)	(16)	(17)
$Cl_{cH_{50}}$	13	3	4		1	1
$Cl_{nH_{50}}$						
$Cl_{cH_{25}}$	7					
$Cl_{nH_{25}}$						
$l_{cH_{50}}$	7	3	3	1	1	1
$l_{nH_{50}}$				2	1	
$l_{cH_{25}}$		3	3	1		1
$l_{nH_{25}}$						
CM2						
Soaking Condition	Compound (3)	(6)	(10)	(14)	(16)	(17)
$Cl_{cH_{50}}$		2			1	
$Cl_{nH_{50}}$						
$Cl_{cH_{25}}$	3	4	3	2	1	1
$Cl_{nH_{25}}$						0
$l_{cH_{50}}$	3	5	2	3	0	1
$l_{nH_{50}}$						
$l_{cH_{25}}$	2		2	2		
$l_{nH_{25}}$						

Kersten et al., 2017; Lee et al., 2017). Considering crystal size and possible positions in the sponge channels, analyte molecules can only be absorbed proportionally; any remaining substance precipitates on the vial surface. In 2013, Inokuma et al. demonstrated that only 80 ng of guest was sufficient to observe guest structure and presumed that analysis is still possible with even lower amounts. We have demonstrated that the amount of analyte per experiment does not need to be applied in excess for all analytes in general. Thereby, the crystallographic analysis of **5** and **20** was still successful using only 5 ng. This LLOD study showed that CS-XRD can be applied using only trace amounts of substance for compounds with high affinity to the framework.

The affinity screening is, however, a tool to estimate the analyte concentration and not a quantitative approach. Guest extraction from the outer layers of the CS during the washing of the crystal surface might reduce the effective concentration and the limitation of measuring width and length, but not the crystal height, influences the calculation of AF values. As the results are based on LC-MS analysis, the method shows the presence of analytes in the CS pores but gives no information of the regular order of guest molecules, as was observed for **11**. Guest molecules may be absorbed in the CS but cannot be positioned repetitively in each pore, which is a necessary requirement for a successful structure assignment using XRD.

The screening was also limited to the applied soaking parameters and number of compounds. To increase the success rate, the affinity screening method needs to be expanded for a wider range of experimental conditions. That includes the development of new types of CS with different binding sites and pore sizes to trap analytes with a higher molecular weight, as well as a selection of polar and unpolar solvents for the soaking process and compound solubility (e.g., nH, cH, pentane, DME, THF, DCM, TCM, water, methanol, ethanol). Furthermore, the method allows the investigation of soaking temperature and duration, as well as the necessary amount of analyte material. These expansions of the screening range have the potential to increase the success rate in future experiments.

5. Conclusions

In conclusion, the results show that the affinity screening can be used as a valuable tool for scientists using the CS-XRD for structural elucidation of small molecules. Optimal use of limited XRD measurement time can be achieved by prioritization of soaking conditions through simultaneous screening of various soaking parameters. The expansion to analyze a few compounds in a mixture can further reduce analyte amount and experiment time. The LLOD study demonstrated the potential of the CS technology to assess the structure of a molecule needing only a few ng of substance.

Authors contribution

Lara Rosenberger: Conceptualization, Methodology, Formal analysis, Writing - Original Draft, Project administration. Carolina von Essen: Conceptualization, Methodology, Formal analysis, Writing - Review & Editing, Project administration. Anupam Khutia: Conceptualization, Methodology, Writing - Review & Editing, Project administration. Clemens Kühn: Resources, Project administration, Writing - Review & Editing. Katrin Georgi: Resources, Writing - Review & Editing. Anna K.H. Hirsch: Supervision, Writing - Review & Editing. Rolf W. Hartmann: Supervision, Writing - Review & Editing. Lassina Badolo: Conceptualization, Methodology, Project administration, Supervision, Funding acquisition, Writing - Review & Editing.

Declaration of Competing Interest

The authors declare a conflict of interest. L. Rosenberger, C. v. Essen, A. Khutia, C. Kühn, K. Georgi and L. Badolo are employees of Merck

KGaA, Darmstadt, Germany.

Acknowledgment

The authors would like to thank Ruben Numrich, Deborah Steinle, Alena Sommer and Christian Kolb for their kind assistance and support in the laboratory, and Judith Jemichs for useful discussions and editorial help.

Supplementary materials

Supplementary material associated with this article can be found, in the online version, at doi:10.1016/j.ejps.2021.105884.

References

- Biradha, K., Fujita, M., 2002. A springlike 3D-coordination network that shrinks or swells in a crystal-to-crystal manner upon guest removal or readsorption. *Angew. Chem. Int. Ed. Engl.* 41, 3392–3395.
- Brunet, G., Safin, D.A., Aghaji, M.Z., Robeyns, K., Korobkov, I., Woo, T.K., Murugesu, M., 2017. Stepwise crystallographic visualization of dynamic guest binding in a nanoporous framework. *Chem. Sci.* 8, 3171–3177.
- Dolomanov, O.V., Bourhis, L.J., Gildea, R.J., Howard, J.A.K., Puschmann, H., 2009. OLEX2: a complete structure solution, refinement and analysis program. *J. Appl. Crystallogr.* 42, 339–341.
- Duplan, V., Hoshino, M., Li, W., Honda, T., Fujita, M., 2016. In situ observation of thiol michael addition to a reversible covalent drug in a crystalline sponge. *Angew. Chem. Int. Ed.* 55, 4919–4923.
- Hack, H.D., Bernardinelli, G., 1999. Absolute structure and absolute configuration. *Acta Crystallogr. A* 55, 908–915.
- Hayashi, Y., Ohara, K., Taki, R., Saeki, T., Yamaguchi, K., 2018. Combined analysis of 1,3-benzodioxoles by crystalline sponge X-ray crystallography and laser desorption/ionization mass spectrometry. *Analyst* 143, 1475–1481.
- Hoshino, M., Khutia, A., Xing, H., Inokuma, Y., Fujita, M., 2016. The crystalline sponge method update. *I.U.Cr.J* 3, 139–151.
- Inokuma, Y., Ukegawa, T., Hoshino, M., Fujita, M., 2016. Structure determination of microbial metabolites by the crystalline sponge method. *Chem. Sci.* 7, 3910–3913.
- Inokuma, Y., Yoshioka, S., Ariyoshi, J., Arai, T., Hitora, Y., Takada, K., Matsunaga, S., Rissanen, K., Fujita, M., 2013. X-ray analysis on the nanogram to microgram scale using porous complexes. *Nature* 495, 461–466.
- Corrigendum Inokuma, Y., Yoshioka, S., Ariyoshi, J., Arai, T., Hitora, Y., Takada, K., Matsunaga, S., Rissanen, K., Fujita, M., 2013. *Nature* 501, 262.
- Kersten, R.D., Lee, S., Fujita, D., Pluskal, T., Kram, S., Smith, J.E., Iwai, T., Noel, J.P., Fujita, M., Weng, J.K., 2017. A red algal bourbonane sesquiterpene synthase defined by microgram-scale NMR-coupled crystalline sponge X-ray diffraction analysis. *J. Am. Chem. Soc.* 139, 16838–16844.
- Lee, S., Hoshino, M., Fujita, M., Urban, S., 2017. Cyclooctatene A and B: absolute configuration determination and structural revision by the crystalline sponge method. *Chem. Sci.* 8, 1547–1550.
- Li, K., Yang, D.S., Gu, X.F., Di, B., 2019. Absolute configuration determination of asarinin by synchrotron radiation with crystalline sponge method. *FitoTerapia* 134, 135–140.
- Massa, W., 2004. Crystal Structure Determination. Springer-Verlag GmbH, Heidelberg.
- Mon, M., Bruno, R., Ferrando-Soria, J., Bartela, L., Di Donna, L., Talia, M., Lappano, R., Maggolini, M., Armentano, D., Pardo, E., 2018. Crystallographic snapshots of host-guest interactions in drugs@metal-organic frameworks: towards mimicking molecular recognition processes. *Mater. Horiz.* 5, 683–690.
- Morita, I., Mori, T., Mitsuhashi, T., Hoshino, S., Taniguchi, Y., Kikuchi, T., Nagae, K., Nasu, N., Fujita, M., Ohwada, T., Abe, I., 2020. Exploiting a C-N bond forming cytochrome P450 monooxygenase for C-S bond formation. *Angew. Chem. Int. Ed. Engl.* 59, 3988–3993.
- Ohmori, O., Kawano, M., Fujita, M., 2004. Crystal-to-crystal guest exchange of large organic molecules within a 3D coordination network. *J. Am. Chem. Soc.* 126, 16292–16293.
- Ramadhari, T.R., Zheng, S.L., Chen, Y.S., Clardy, J., 2015. Analysis of rapidly synthesized guest-filled porous complexes with synchrotron radiation: practical guidelines for the crystalline sponge method. *Acta Crystallogr. A Found. Adv.* 71 (Pt 1), 46–58.
- Rissanen, K., 2017. Crystallography of encapsulated molecules. *Chem. Soc. Rev.* 46, 2638–2648.
- Rosenberger, L., von Essen, C., Khutia, A., Kühn, C., Urbahn, K., Georgi, K., Hartmann, R.W., Badolo, L., 2020. Crystalline sponges as a sensitive and fast method for metabolite identification: application to gemfibrozil and its phase I and II metabolites. *Drug. Metab. Dispos.* 48, 587–593.
- Sakurai, F., Khutia, A., Kikuchi, T., Fujita, M., 2017. X-ray structure analysis of n-containing nucleophilic compounds by the crystalline sponge method. *Chem. Eur. J.* 23, 15035–15040.
- Sheldrick, G.M., 2015. Crystal structure refinement with SHELXL. *Acta Crystallogr. C Struct. Chem.* 71, 3–8.
- Urban, S., Brkjdaca, R., Hoshino, M., Lee, S., Fujita, M., 2016. Determination of the absolute configuration of the pseudo-symmetric natural product elatylene by the crystalline sponge method. *Angew. Chem. Int. Ed.* 55, 2678–2682.

Results

L. Rosenberger et al.

- Vinogradova, E.V., Müller, P., Buchwald, S.L., 2014. Structural reevaluation of the electrophilic hypervalent iodine reagent for trifluoromethylthiolation supported by the crystalline sponge method for X-ray analysis. *Angew. Chem. Int. Ed.* 53 (12), 3125–3128.
- Wada, N., Kersten, R.D., Iwai, T., Lee, S., Sakurai, S., Kikuchi, T., Fujita, D., Fujita, M., Weng, J.K., 2018. Crystalline-sponge-based structural analysis of crude natural product extracts. *Angew. Chem. Int. Ed. Engl.* 57, 3671–3675.

European Journal of Pharmaceutical Sciences 164 (2021) 105884

- Yan, K., Dubey, R., Arai, T., Inokuma, Y., Fujita, M., 2017. Chiral crystalline sponges for the absolute structure determination of chiral guests. *J. Am. Chem. Soc.* 139, 11341–11344.
- Zhang, S.Y., Fairen-Jimenez, D., Zaworotko, M.J., 2020. Structural elucidation of the mechanism of molecular recognition in chiral crystalline sponges. *Angew. Chem.* 132, 17753–17759.
- Zigon, N., Kikuchi, T., Ariyoshi, J., Inokuma, Y., Fujita, M., 2017. Structural elucidation of trace amounts of volatile compounds using the crystalline sponge method. *Chem. Asian. J.* 12, 1057–1061.

Results

3.3 Chapter C: Metabolic profiling of *S*-praziquantel using crystalline sponges

Title:

Metabolic profiling of *S*-praziquantel: Structure elucidation using the crystalline sponge method in combination with mass spectrometry and nuclear magnetic resonance

Authors:

Lara Rosenberger, Judith Jenniches, Carolina von Essen, Anupam Khutia, Clemens Kühn, Andreas Marx, Katrin Georgi, Anna K. H. Hirsch, Rolf W. Hartmann, and Lassina Badolo

Bibliographic Data:

Drug Metabolism and Disposition,

Volume 50, Issue 4, Pages 320-326,

Accepted January 15, **2022**,

Doi: 10.1124/DMD.121.000663

This is an open access article distributed under the CC BY Attribution 4.0 International license.

Supplemental material to this article can be found at:
<http://dmd.aspetjournals.org/content/suppl/2022/02/03/dmd.121.000663.DC1>

1521-009X/50/4/320-326\$35.00
 DRUG METABOLISM AND DISPOSITION
 Copyright © 2022 by The Author(s)

dx.doi.org/10.1124/dmd.121.000663
 Drug Metab Dispos 50:320-326, April 2022

This article is distributed under the terms of the CC BY Attribution 4.0 International license.

Metabolic Profiling of S-praziquantel: Structure Elucidation Using the Crystalline Sponge Method in Combination with Mass Spectrometry and Nuclear Magnetic Resonance[§]

Lara Rosenberger, Judith Jenniches, Carolina von Essen, Anupam Khutia, Clemens Kühn, Andreas Marx, Katrin Georgi, Anna K. H. Hirsch, Rolf W. Hartmann, and Lassina Badolo

Merck KGaA, Darmstadt, Germany (L.R., J.J., C.v.E., A.K., C.K., A.M., K.G., L.B.); Helmholtz-Institute for Pharmaceutical Research Saarland (HIPS) - Helmholtz Centre for Infection Research (HZI), Saarbrücken, Germany (L.R., A.K.H.H., R.W.H.); and Department of Pharmacy, Saarland University, Saarbrücken, Germany (L.R., A.K.H.H., R.W.H.)

Received September 2, 2021; accepted January 15, 2022

ABSTRACT

Praziquantel (PZQ) is the drug of choice for treatment of the neglected tropical disease schistosomiasis. Although the drug has been extensively used over several decades and its metabolism well studied (several oxidative metabolites are known from literature), the knowledge of the complete structure of some of its metabolites remains elusive. Conventional techniques, such as nuclear magnetic resonance or liquid chromatography mass spectrometry were used in the past to investigate phase I and phase II metabolites of PZQ. These techniques are either limited to provide the complete molecular structure (liquid chromatography mass spectrometry) or require large amount of sample material (NMR), which are not always available when *in vitro* systems are used for investigation of the metabolites. In this study, we describe new structures of S-PZQ metabolites generated *in vitro* from human liver microsomes using the crystalline sponge method. After chromatographic separation and purification of the oxidative metabolites, ultra-performance liquid chromatography-quadrupole time-of-flight mass spectrometry analysis was

conducted to narrow down the position of oxidation to a certain part of the molecule. To determine the exact position of hydroxylation, single-crystal X-ray diffraction analysis of the crystalline sponges and absorbed analyte was used to identify the structure of S-PZQ and its metabolites. The crystalline sponge method allowed for complete structure elucidation of the known metabolites S-*trans*-4'-hydroxy-PZQ (M1), S-*cis*-4'-hydroxy-PZQ (M2) and S-/R-11b-hydroxy-PZQ (M6) as well as the unknown metabolites S-9-hydroxy-PZQ (M3) and S-7-hydroxy-S-PZQ (M4). For comparison of structural elucidation techniques, one metabolite (M3) was additionally analyzed using NMR.

SIGNIFICANCE STATEMENT

The information content of the metabolic pathway of praziquantel is still limited. The crystalline sponge method allowed the complete structural elucidation of three known and two unknown metabolites of S-praziquantel, using only trace amounts of analyte material, as demonstrated in this study.

Introduction

Schistosomiasis is a neglected tropical disease caused by a parasitic flatworm of the genus *Schistosoma* and affects almost 240 million people worldwide, with a high prevalence in Africa. The World Health Organization implemented a program for schistosomiasis control over the past 40 years and recommends the anthelmintic drug praziquantel (PZQ) as the treatment of choice for all forms of the disease (WHO, 2011, 2020). PZQ is currently used as a racemic formulation in therapy; however, the activity is mainly associated with the *R*-enantiomer (Meister et al., 2014; Kovač et al., 2017). Although the drug has been known and extensively used since the early 1980s, the information content of the metabolic pathway is limited. Enantioselective transformation of

R-PZQ and *S*-PZQ has been explored in various studies, showing different metabolic profiles for both enantiomers (Wang et al., 2014; Vendrell-Navarro et al., 2020; Park et al., 2021). Several mono-oxidized (+16 Da) and secondary oxidative metabolites (+32 and +14 Da) are known from the literature, but most of their complete structures are still unknown. The main metabolite in human is 4'-hydroxy-PZQ and the position of hydroxylation was identified both in *cis* and *trans* configuration (Nleya et al., 2019). Two more metabolites have been described as 8-hydroxy-PZQ and 11b-hydroxy-PZQ by isolation from human urine and *in vitro* recombinant human P450 reactions, using NMR for data analysis (Schepmann and Blaschke, 2001; Vendrell-Navarro et al., 2020). Additional metabolites have been analyzed using different liquid chromatography mass spectrometry (LC-MS) systems, giving information of the type of metabolism (*i.e.*, hydroxylation, dehydrogenation and glucuronidation) and allowing to narrow down the site of metabolism to a certain part of the molecule (Lerch and Blaschke, 1998; Huang et al., 2010; Wang et al., 2014). Despite the advantage of LC-MS techniques to reach high sensitivity for sample analysis from *in vitro* origin, these techniques failed to identify the complete structure of metabolites.

This work received no external funding.

The authors declare a conflict of interest. L.R., J.J., C.v.E., A.K., C.K., A.M., K.G. and L.B. are employees of Merck KGaA, Darmstadt, Germany.
[dx.doi.org/10.1124/dmd.121.000663](https://doi.org/10.1124/dmd.121.000663)

§ This article has supplemental material available at dmd.aspetjournals.org.

ABBREVIATIONS: CS, crystalline sponge; CS-XRD, crystalline sponge method; HLM, human liver microsome; HPLC, high-performance liquid chromatography; LC-MS, liquid chromatography-mass spectrometry; PZQ, praziquantel; qTOF, quadrupole time-of-flight mass spectrometry; R_f , residual factor; R_{int} , internal R-value; tpt, 2,4,6-tris(4-pyridyl)-1,3,5-triazine; UPLC, ultra-performance liquid chromatography.

A new approach for structural elucidation of compounds was introduced in 2013 by Makoto Fujita and is commonly known as the “crystalline sponge method” (CS-XRD) (Inokuma et al., 2013). The method enables crystal structure determination without the limitation of crystallization with only nanogram to a few microgram of analyte material. A metal coordination complex $[(ZnX_2)_3(\text{tpt})_2]_n \cdot x(\text{solvent})_m$ ($X=I$; $\text{tpt}=2,4,6\text{-tris}(4\text{-pyridyl})\text{-}1,3,5\text{-triazine}$) is used as a pre-existing crystal and functions as a host. During a “soaking process”, the analyte (guest) is absorbed into the pores of the three-dimensional framework via diffusion and regularly ordered by intermolecular, noncovalent interactions and thus accessible for X-ray diffraction analysis (Inokuma et al., 2016; Brunet et al., 2017; Sakurai et al., 2017). We recently demonstrated that CS-XRD is a valuable tool, which can be applied to identify the exact position of metabolism for phase I and phase II metabolites generated in low amounts from *in vitro* incubation (Rosenberger et al., 2020).

In this study, we apply the CS-XRD for the determination of the absolute structures of *S*-PZQ and six of its hydroxylated metabolites after incubation with human liver microsome (HLM).

Materials and Methods

Chemicals and Reagents. *S*-PZQ, *S*-*cis*-4'-hydroxy-PZQ and *S*-*trans*-4'-hydroxy-PZQ were obtained from Merck KGaA small molecule library. Dipotassium hydrogen phosphate, potassium dihydrogen phosphate, magnesium chloride hexahydrate, cyclohexane, *n*-hexane, dihydronicotinamide adenine dinucleotide phosphate tetrasodium salt, DMSO- d_6 , water (ultra-high-performance LC-MS grade), and acetonitrile (ultra-high-performance LC-MS grade) were purchased from Merck KGaA (Darmstadt, Germany). Zinc iodide, 1,2-dimethoxyethane, and formic acid were purchased from Sigma Aldrich Chemie GmbH (Steinheim, Germany). Tpt was purchased from abcr GmbH (Karlsruhe, Germany). Mixed gender HLM (Ultrapool, pool of 150) were purchased from Corning (Corning, USA).

Metabolism of *S*-PZQ by HLM. The hydroxylation of *S*-PZQ was conducted with an incubation mixture containing 0.5 mg/ml of HLM, 50 mM of potassium phosphate buffer (pH 7.4), 1 mM of magnesium chloride, and 200 μM of substrate. After 5 minutes of preincubation (37°C, 150 rpm), the reaction was initiated by the addition of nicotinamide adenine dinucleotide phosphate (NADPH, 1.5 mM), and the mixture was incubated for another 24 hours (final volume: 5.40 ml). After 6 hours, the reaction was boosted by addition of NADPH (1.5 mM).

The reaction was quenched by adding one volume of ice-cold acetonitrile and the precipitated proteins were removed by centrifugation at 4000 g for 1 hour at 4°C. The supernatant was evaporated to dryness (nitrogen flow, 40°C) and resolubilized in acetonitrile/water (20:80). 100 μl aliquots were used for purification and fractionation by high-performance liquid chromatography coupled with mass spectrometry (HPLC-MS).

Ultra-Performance Liquid Chromatography-Quadrupole Time-of-Flight Mass Spectrometry. The supernatants were analyzed on a Waters Acquity ultra-performance liquid chromatography (UPLC) system combined with a Xevo G2-S qTOF (Waters Corporation). Analysis was performed with an electrospray ion source in positive ion mode. For MS scan, the quadrupole time-of-flight mass spectrometry (qTOF) was operating with a source temperature at 150°C, a desolvation temperature at 600°C and a capillary voltage at 0.5 kV. For full-scan MS mode, the collision energy was set to 4 V, and the mass range was set to m/z 100 to 1000. For MS/MS studies, qTOF MS^e acquisition was conducted using a collision energy ranging from 25 to 40 V.

Metabolite separation was achieved on a chiral Lux Cellulose-2 column (150-2 mm, 3 μm ; Phenomenex) equipped with a Lux Cellulose-2 precolumn (3 mm inner diameter; Phenomenex) at a flow rate of 0.45 ml/min over a period of 20 minutes using solvent A (water + 0.1% formic acid) and solvent B (acetonitrile + 0.1% formic acid) as mobile phases. The column oven temperature was set to 40°C. Elution was performed using a gradient from 20 to 90% B in 15 minutes, 90 to 95% B in 0.2 minutes, 95% B for 2.1 minutes, returning to 20% B in 0.1 minutes and re-equilibration at 20% B for 2.6 minutes. The software UNIFI version 1.9.4 (Waters Corporation) was used

to support the identification of metabolites. The metabolites were evaluated for mass error (≤ 4 ppm), fragmentation pattern and retention time.

HPLC-MS. The supernatants were analyzed and fractionated on an Acquity Arc HPLC system (Waters Corporation). The equipment components were described in detail in our previous work (Rosenberger et al., 2020).

Samples were analyzed with electrospray ionization mass spectrometry in positive ionization mode within an acquisition range from m/z 100 to m/z 650 in continuum mode and a sampling frequency of 2 Hz. The capillary voltage and the cone voltage were set to 0.8 V and 10.0 V, respectively. The probe temperature was set to 600°C. The mass value of m/z 329 was registered by the MS detector and triggered the fractionation of the target analytes. The software MassLynx 4.2 and FractionLynx were used for data acquisition and sample fractionation.

HPLC separation for M4 and M6 PZQ was performed with two Chromolith Performance RP18e columns (100-4.6 mm; Merck KGaA) for primary chromatographic purification and one Purospher Star RP18e Hibar HR column (100-2.1 mm, 2 μm ; Merck KGaA) as second chromatographic system. The column oven temperature was set to 25°C. For the first purification, elution was performed at a flow rate of 1.0 ml/min using solvent A (water) and solvent B (acetonitrile) as mobile phases. The analytes were eluted over a period of 30 minutes, using a multi-segmented gradient from 0% to 25% B in 7 minutes, 25% to 30% B in 3 minutes, 30% to 80% B in 10 minutes, 80% B for 5 minutes, returning to 0% B in 0.1 minutes, and re-equilibration at 0% B for 4.9 minutes. The eluent was directed to the waste during the first 5 minutes to reduce contamination. For the second purification, elution was performed at a flow rate of 0.45 ml/min over a period of 15 minutes, applying the following gradient: mobile phase 0% to 60% for 10 minute, 60% B to 100% B in 2 minute; 100% to 0% B in 0.1 minutes and re-equilibration at 0% B for 2.9 minutes.

HPLC separation for M3, M5, and additionally M6 PZQ was achieved using an additional third purification step. The further purification was performed using the Lux Cellulose-2 column and gradient described as before. Differences were the column oven temperature of 25°C and the solvent A (water) and solvent B (acetonitrile) as mobile phases.

Following each chromatographic separation step, the collected fractions were pooled, evaporated to dryness at 40°C under nitrogen flow and resolubilized in acetonitrile/water (20:80) for further purification. After final purification, the collected fractions from each metabolite were combined and evaporated to dryness to conduct the crystalline sponge (CS) soaking and NMR measurement.

CS-XRD. The porous CS $[(ZnI_2)_3(\text{tpt})_2]_n \cdot x(\text{cyclohexane})_m$ (**1a**) and $[(ZnI_2)_3(\text{tpt})_2]_n \cdot x(\text{n-hexane})_m$ (**1b**) were prepared according to the procedures known from literature (Biradha and Fujita, 2002; Ramadhar et al., 2015).

For guest soaking of *S*-PZQ, a single crystal of **1a** was transferred with 50 μl of cyclohexane to a glass vial. After addition of 2 μl of dissolved analyte solution (1 mg/ml in 1,2-dimethoxyethane), the sample vial was closed with a screw cap and the septum seal was pierced with a syringe needle, before placing it in an incubator at 50°C for 1 day. Following evaporation of solvent, the vial was placed without a needle for 2 days at 4°C to increase guest occupancy and hence the chirality transfer from the guest molecules to the CS framework. For *S*-*trans*-4'-hydroxy-PZQ, one crystal of **1b** was used and analyzed after evaporation of *n*-hexane after 1 day. The soaking condition for *S*-*cis*-4'-hydroxy-PZQ was adjusted by reducing the volume of *n*-hexane to 25 μl , the temperature for solvent evaporation to 25°C and the soaking time to 3 days by using a syringe needle with smaller diameter. Soaking of incubation samples (about 1–2 μg) was conducted similarly to the reference material. Two microliters of 1,2-dimethoxyethane, 50 μl of cyclohexane and one CS (**1a**) were pipetted into the vial, which contained the pooled metabolite material. The incubator temperature was set to 50°C and the evaporation time was one day.

Single-crystal X-ray diffraction measurements were performed by using a Rigaku Oxford Diffraction XtaLAB Synergy-R diffractometer (Cu-K α , $\lambda = 1.54184$ Å) at a temperature of 100 K and crystal structure modeling using OLEX2 (Dolomanov et al., 2009), SHELXT, and SHELXL (Sheldrick, 2015) were conducted as described in detail in our previous work (Rosenberger et al., 2020). The software ShelXle was used to generate the electron density maps of *S*-PZQ and its hydroxy metabolites (Hübschle et al., 2011).

NMR of PZQ Metabolite M3. Structural elucidation of metabolite M3 was performed at 298 K using a 700 MHz Bruker Avance III equipped with a 5-mm cryocooled triple resonance probe. The isolated metabolite (about 15 μg) was dissolved in 200 μl of DMSO- d_6 and transferred into a 3 mm NMR tube.

The ^1H NMR spectrum was acquired with 64 k time domain points, a spectral width of 20 ppm, a relaxation delay of 10 seconds, and 1024 scans. Edited heteronuclear single quantum coherence NMR spectrum was recorded with 1024×256 time domain data points over a spectral width of 12 ppm in the t_2 and 165 ppm in the t_1 dimension. The homonuclear correlation spectroscopy NMR spectrum was acquired with 1024×256 time domain data points over a spectral width of 12 ppm in the t_2 and t_1 dimension. The rotating frame Overhauser enhancement effect spectroscopy NMR spectrum was recorded with 1024×256 time domain data points over a spectral width of 12 ppm in the t_2 and t_1 dimension. The software MestReNova version 14.1.0 (Mestrelab Research) was used for data analysis.

Results

UPLC-qTOF Analysis of *S*-PZQ Metabolites Prepared by Incubation with HLM. Both enantiomers of PZQ (Fig. 1) were incubated with HLM for 24 hour respectively, for metabolite profiling and identification (data not shown). *S*-PZQ showed an increased formation of metabolites and was therefore chosen for further analysis. During the study of metabolic stability, the UPLC-qTOF chromatogram of *S*-PZQ, incubated with HLM in the presence of NADPH, showed the formation of several oxidative metabolites (+16, +32 and +14 Da), which is in line with already published data (Huang et al., 2010; Wang et al., 2014). The incubation of *S*-PZQ without cofactor was conducted in parallel and showed no formation of metabolites, indicating their generation by enzymatic reaction. The analysis presented in this study, however, focuses on six monohydroxylated metabolites of *S*-PZQ (M1–M6).

The metabolites M1–M6 were detected at a protonated molecular mass $[\text{M}+\text{H}]^+$ of m/z 329. The increased m/z value of 16 Da, compared with the $[\text{M}+\text{H}]^+$ ion of the parent (m/z 313), suggested the addition of one oxygen to the molecular scaffold.

The mono-oxidized metabolites were further analyzed based on their MS/MS spectra and accurate mass measurements (Fig. 2, Supplemental Table 1). The mass spectrum ($[\text{M}+\text{H}]^+$) of M1 and M2 showed similar fragment ion peaks as the parent compound. The main fragment ions at m/z 203 and m/z 174 were assigned to the “core moiety” (i.e., hexahydro-pyrazino [2,1-*a*]isoquinolin-4-one), indicating that the oxidation occurred at the cyclohexane ring. Metabolites M1 and M2 were identified as *S-trans*-4'-hydroxy-PZQ and *S-cis*-4'-hydroxy-PZQ by comparison of the respective retention time with the reference material.

The main fragment ions at m/z 219, m/z 190, m/z 162 and m/z 148, observed in the spectra of both M3 and M5, were assigned to an oxidized core moiety, indicating that the hydroxylation occurred somewhere at the tetrahydro-isoquinoline ring system. The full-scan mass spectrum of metabolites M4 and M6 showed the abundant ion m/z 311, representing a predominant loss of water ($329 \rightarrow 311$). In addition, both metabolites fragmented to form characteristic ions of m/z 201, m/z 144 and m/z 130, indicating a spontaneous water loss of the fragment ions observed for M3 and M5. The loss of water is predominantly

observed for aliphatic hydroxylation, whereas it is less common for hydroxylation reactions, which occur on phenyl rings (Ramanathan et al., 2000; Holčapek et al., 2010). Therefore, it is likely that the addition of one oxygen occurred in the aliphatic part of the core moiety and not on the aromatic benzene.

The tandem mass spectrometry fragmentation pattern allowed to limit the oxidation to a certain part of the molecule but could not reveal the actual positions of hydroxylation. The metabolite structures of *S*-PZQ were therefore further analyzed using CS-XRD and NMR.

Structural Elucidation of *S*-PZQ Metabolites (M1–M4 and M6) by CS-XRD. For successful structure determination using CS-XRD, the optimization of soaking conditions (e.g., CS type, solvent, temperature, time) is the crucial step. Thereby, various parameters need to be examined for every analyte (Hoshino et al., 2016). The optimal soaking parameters for *S*-PZQ were selected by conducting a CS affinity screening and examining the affinity of target analyte to CS framework using two CS types $[(\text{ZnI}_2)_3(\text{tpt})_2]_n \cdot x(\text{solvent})_m$ and $[(\text{ZnCl}_2)_3(\text{tpt})_2]_n \cdot x(\text{solvent})_m$; solvent = cyclohexane, *n*-hexane) at three different temperatures (50°C, 25°C, 4°C) (data not shown). The screening method has been described in detail in our previous work (Rosenberger et al., 2021). The optimal soaking conditions were then applied for *S*-PZQ and its mono-oxidized metabolites. To increase the occupancy of the analyte in the CS pores and to maximize the intermolecular interactions between CS framework and guest molecules, the soaking time was further adjusted for some analytes.

The parent active pharmaceutical ingredient and the reference metabolites *S-trans*-4'-hydroxy-PZQ (M1) and *S-cis*-4'-hydroxy-PZQ (M2) could successfully be structurally elucidated with CS-XRD using a conventional X-ray diffractometer. The crystal structure of *S*-PZQ revealed one guest molecule with an occupancy of 64% and one additional cyclohexane molecule with final residual factor (R_1) and internal R-factor (R_{int}) values of 8.23% and 3.08%, respectively. A Flack parameter of 0.234(8) was obtained, suggesting that the absolute configuration PZQ is *S*. One molecule of metabolite M1 was assigned by its electron density in the asymmetric unit with an occupancy of 52% (R_1 6.58% and R_{int} 3.86%, $\chi = 0.229(8)$). First analysis of the reference material M2 resulted in the determination of the hydroxy group at the 4'-cyclohexyl moiety in *trans* configuration. Pharmacokinetic data from previous studies showed the preferred formation of M1 and a *cis* to *trans* interconversion (Nleya et al., 2019; Vendrell-Navarro et al., 2020). To influence the less favored axial position of the substituent as little as possible, the soaking process was further optimized by decreasing the temperature to 25°C. As a result, one guest molecule in *cis* configuration could be assigned to M2 (occupancy 54%, R_1 5.85%, R_{int} 2.86%, $\chi = 0.328(8)$).

Next, CS-XRD was applied to the mono-hydroxylated metabolites of *S*-PZQ generated by in vitro incubation. The formation of several metabolites in different quantities was observed, necessitating an extensive chromatographic separation and purification process to fractionate the very closely eluting metabolites (Fig. 3A). To generate the sample amount in high purity, M4 and M6 were purified using two different chromatographic columns. M3 and M5 were thereby detected as one peak, requiring further separation using a third column (Fig. 3B). To estimate the amounts of M3–M6, the MS (for M3 and M5) and UV (for M4 and M6) signals of the reference material M2 were used. Thereby, an increase in the UV-VIS absorption maxima was observed for M3 (278 nm) and M5 (281 nm) compared with *S*-PZQ or M6 (263 nm), indicating an aromatic hydroxylation at the benzene moiety.

To reveal the exact position of hydroxylation, the soaking experiments were conducted under similar conditions as used for the parent compound to elucidate the structure of metabolites M3–M6. XRD measurements of the soaked CS allowed the crystallographic analysis of the metabolite structures. M6 shows high electron density at position 11b of

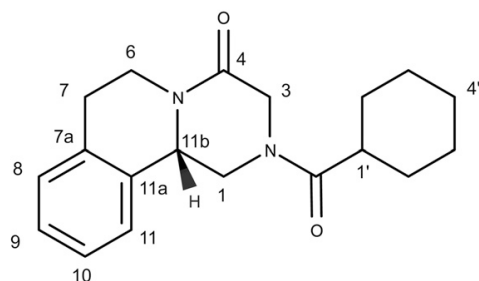


Fig. 1. Chemical structure of *S*-praziquantel.

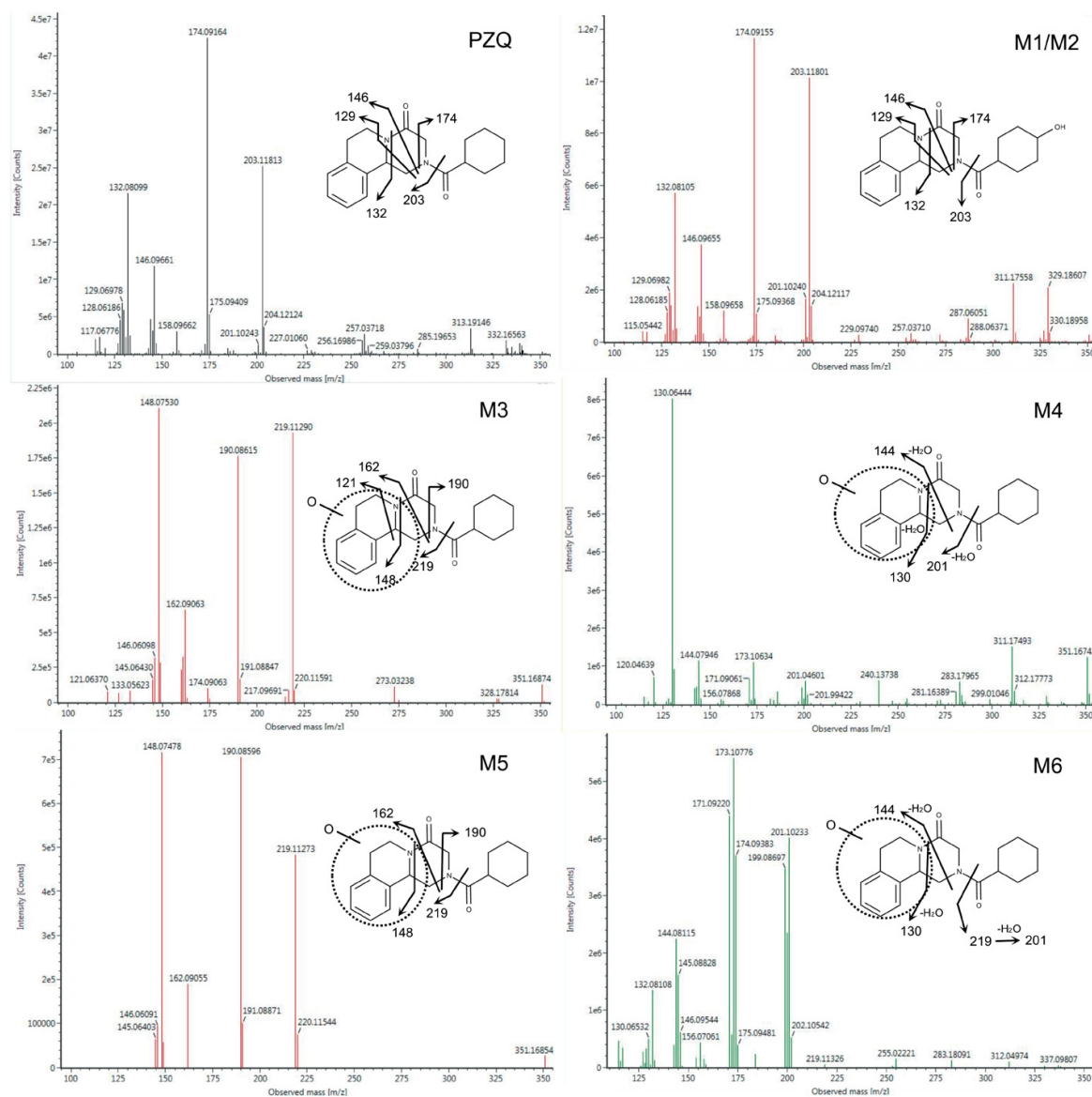


Fig. 2. Tandem mass spectrometry spectra and proposed structures of *S*-praziquantel and its metabolites M1–M6.

the isoquinoline ring system, confirming the structure elucidated via NMR in previous works (Vendrell-Navarro et al., 2020). High electron density in close proximity to the isoquinoline part was also observed for M4 at position 7 and M3 at position 9. Metabolite M5 shows diffuse electron density in the CS pores, but no structure could be successfully assigned. The electron density map of the “core moiety” from *S*-PZQ and its successfully elucidated metabolites are shown in Fig. 4.

Crystallographic data of M3 revealed one analyte molecule with an occupancy of 60% (R_1 5.53%, R_{int} 1.52%, $\chi = 0.204(7)$) and two cyclohexane molecules.

The crystal structure of M4 revealed one molecule with an occupancy of 76%, three cyclohexane molecules, and final R_1 and R_{int} values of

4.99% and 1.45%, respectively. The addition of one oxygen at position 7 of the molecule caused the creation of a second chiral center, which could be determined as *S* configuration indicated on the Flack parameter value of 0.191(7).

As already observed for the other metabolites and the parent compound, M6 was expected to be enantiopure. Surprisingly, an inconclusive Flack parameter of 0.5, indicating a racemic mixture, was observed. Furthermore, when analyzing the CS pores, both *S*- and *R*-11b-hydroxy-PZQ (occupancy 40% and 30%) were observed (R_1 5.92%; R_{int} 2.48%). The observation was further confirmed by chiral chromatography with the separation of both enantiomers. After chromatographic separation and purification, both enantiomers were

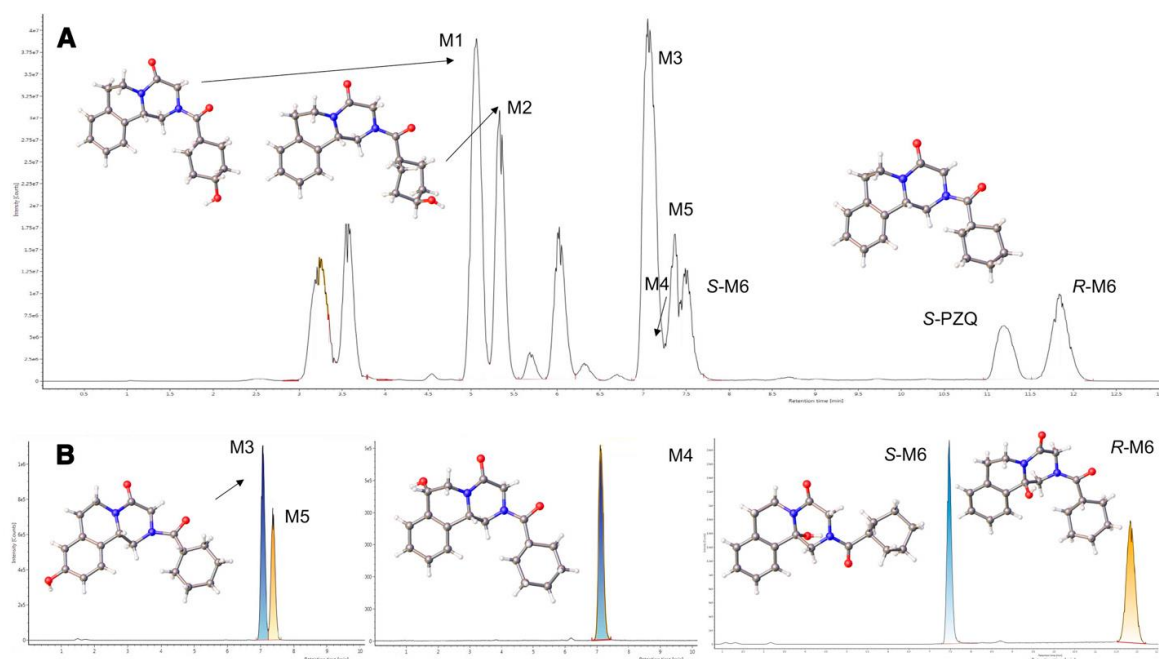


Fig. 3. Full-scan liquid chromatography mass spectrometry chromatograms of *S*-praziquantel (PZQ) incubated with human liver microsome for 24 hours in the presence of nicotinamide adenine dinucleotide phosphate as cofactor on a Lux Cellulose-2 column (A) and PZQ metabolites M3–M6 after semi-preparative high-performance liquid chromatography separation and fractionation (B); M1, *S*-*trans*-4'-hydroxy-PZQ; M2, *S*-*cis*-4' hydroxy-PZQ, M3, *S*-9-hydroxy-PZQ; M4, *S*-7-hydroxy-*S*-PZQ; M5, still unknown; M6, *S*-11b-hydroxy-PZQ and *R*-11b-hydroxy-PZQ.

examined separately by CS-XRD. The soaking experiment of the first enantiomer of M6 showed the presence of one *S*-11b-hydroxy-PZQ molecule, but due to low occupancy of the analyte and therefore an insufficient chirality transfer from guest molecules to the host framework, the resulting inconclusive Flack value did not allow the confirmation of the chiral center. However, when analyzing the second enantiomer, one molecule of *R*-11b-hydroxy-PZQ (occupancy 100%) could be observed in the CS pores (R_1 7.32%; R_{int} 3.69%, $\chi =$

0.221(8)), hence indicating the identification of the first enantiomer to be in *S* configuration.

The refined crystallographic structures of *S*-PZQ and its hydroxy metabolites are shown in Fig. 3. Crystallographic data, ORTEP diagrams of the asymmetric unit including CS framework and analytes, reciprocal *h0l* layers and Flack parameters before and after using solvent masking are shown in the Supplemental Data (Supplemental Fig. 1–22).

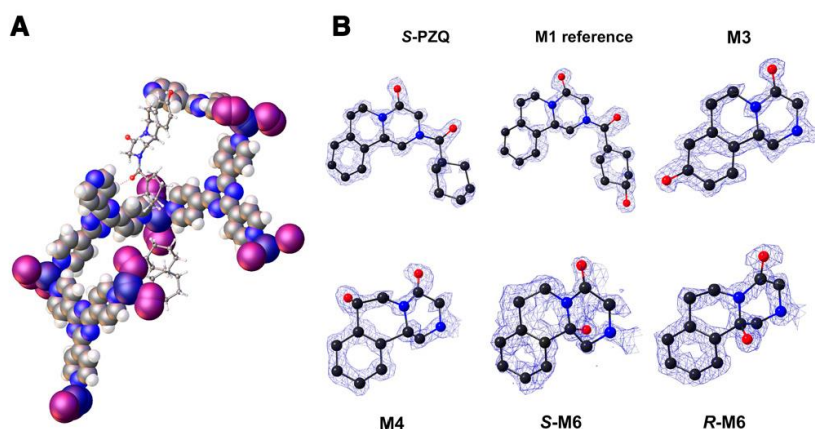


Fig. 4. (A) Asymmetric unit of $[(ZnI_2)_3(tpz)_2]_n$ with one *S*-9-hydroxy praziquantel (M3) and two cyclohexane molecules. The crystal structure exhibits C–H...O (red dashed line) interactions between the hydroxy metabolite and the crystalline sponge framework. (B) Electron density map F_0 [contoured at 2.02σ (*S*-praziquantel), 2.00σ (M1 reference), 2.61σ (M3), 1.94σ (M4), 1.89σ (*S*-M6), 2.54σ (*R*-M6)] of the complete molecule of *S*-praziquantel and M1, as well as the core moiety of the incubation samples M3, M4, *S*-M6 and *R*-M6.

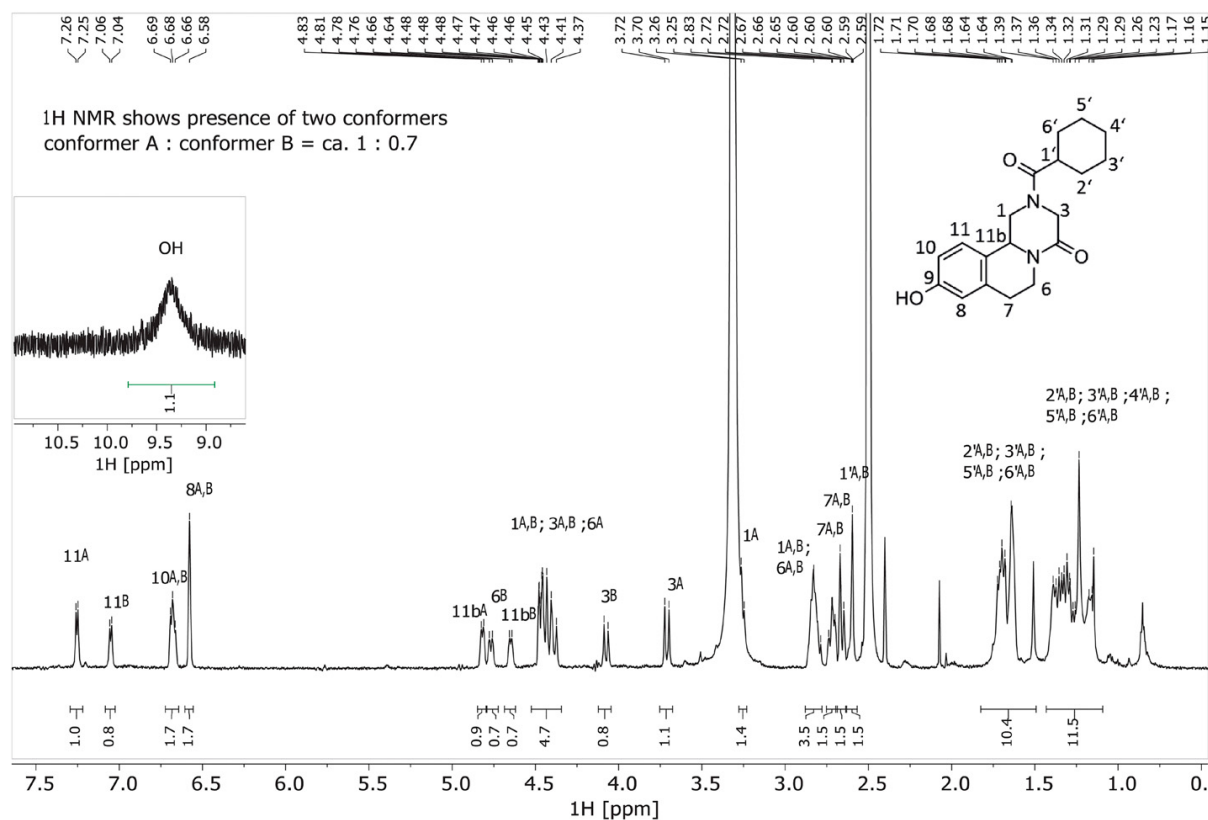


Fig. 5. 700 MHz ^1H NMR spectrum of *S*-9-hydroxy praziquantel (M3).

Characterization of M3 by NMR. Additional to CS-XRD experiments, M3 was further isolated to characterize the structure by NMR analysis (Supplemental Data). The results confirmed the position of hydroxylation at position 9 of the benzene moiety. The following signals were assigned to the structure in the ^1H NMR measurement (700 MHz, $\text{DMSO}-d_6$). The NMR spectra indicated the presence of two conformers, which are indicated in the following assignment by superscript A and B. The numbering is depicted in Fig. 5: δ 7.25 (d, $J = 8.3$ Hz, 1H, 11^A), 7.05 (d, $J = 8.5$ Hz, 1H, 11^B), 6.72–6.64 (m, 2H, 10^{A,B}), 6.58 (s, 2H, 8^{A,B}), 4.82 (d, $J = 10.4$ Hz, 1H, 11b^A), 4.77 (d, $J = 13.1$ Hz, 1H, 6^B), 4.65 (d, $J = 10.6$ Hz, 1H, 11b^B), 4.52–4.34 (m, 5H, 1^{A,B}, 3^{A,B}, 6^A), 4.08 (d, $J = 17.2$ Hz, 1H, 3^B), 3.71 (d, $J = 17.7$ Hz, 1H, 3^A), 3.26 (d, $J = 12.9$ Hz, 1H, 1^A), 2.88–2.78 (m, 4H, 1^{A,B}, 6^{A,B}), 2.75–2.69 (m, 2H, 7^{A,B}), 2.74–2.70 (m, 2H, 7^{A,B}), 2.60–2.58 (m, 2H, 1^{A,B}), 1.80–1.58 (m, 8H, 2^{A,B}, 3^{A,B}, 5^{A,B}, 6^{A,B}), 1.44–1.11 (m, 10H, 2^{A,B}, 3^{A,B}, 4^{A,B}, 5^{A,B}, 6^{A,B}). The ^1H NMR spectrum of M3 showed three aromatic proton signals (one singlet at δ 6.58 and two duplets at δ 7.25 and δ 6.72–6.64). The coupling pattern indicated a substitution of one benzene hydrogen with a hydroxyl group at either position 9 or 10. rotating frame Overhauser enhancement effect spectroscopy cross-correlations of H-7 to H-8 and H-11b to H-11 were observable. Since H-8 showed singlet multiplicity and H-11 duplet multiplicity, the substitution can be unambiguously assigned to position 9 (Fig. 5, Supplemental Fig. 23–27).

Discussion

In summary, we were able to elucidate the absolute structure of three known and two unknown hydroxy metabolites of *S*-PZQ using

CS-XRD. UPLC-qTOF analysis and target-structure prediction of the fragmentation pattern allowed us to determine the type of metabolism and to limit the position of hydroxylation to a certain part of the molecule. However, only the crystallographic data could give information about the stereochemistry and pinpoint the exact position of the inserted hydroxy groups at the 4'-C position of the cyclohexane moiety (M1 and M2) as well as the 7-C (M4), 9-C (M3) and 11b-C (M6) positions at the core moiety. The structure of metabolite M3 was furthermore confirmed by NMR analysis.

The large number of different metabolites and impurities from the *in vitro* incubation matrix (e.g., buffer salts, cofactor, microsomal stock solution) required a lengthy semi-preparative sample separation and purification process as well as the selection of different columns. Metabolites M3, M4, and M5 were coeluting in the first chromatographic purification step. The application of a second column allowed the separation of M4, which could be successfully identified as *S*-7-hydroxy-*S*-PZQ. First experiments of the second peak using CS-XRD were unsuccessful. Only diffuse electron density could be observed in the CS pores, indicating successful guest inclusion, but no regular order of analyte molecules, which is a necessary requirement for the assignment of guest compounds. From our experience, additional impurities in analyte material investigated with CS-XRD could lead to such behavior. Therefore, a third chromatographic step was conducted for further purification, which allowed the detection of an additional metabolite and thus the separation of M3 and M5. CS-XRD analysis of M3 allowed to identify the position of hydroxylation at 9-C of the aromatic ring. The crystallographic analysis of M5, however, did not reveal the

structure of the metabolite as a guest molecule in the CS pores, but MS and UV-VIS data strongly indicated that the hydroxylation occurred at the aromatic benzene ring. The structure of metabolite M6, which is known from literature, was confirmed, and the presence of both enantiomers *in vitro* was shown. The analysis of both enantiomers as a racemic mixture and individually after chiral separation allowed the determination of the respective configuration as *S*-11b-hydroxy-PZQ and *R*-11b-hydroxy-PZQ.

The application of CS-XRD for *S*-PZQ and its metabolites demonstrates that this technology can be applied for metabolite identification studies in drug discovery in which metabolites are only available in trace amounts from *in vitro* incubation. In comparison with the CS analysis, a high amount of substance was needed to conduct the NMR spectrum of M3, prolonging the lengthy sample purification process from days to weeks to collect sufficient analyte material. Furthermore, no information of the absolute configuration was obtained. The low abundance of metabolite M4 in the incubation solution only allowed the chromatographic preparation of 1–2 µg of sample material, which is insufficient for complete structure analysis by NMR. However, the CS-XRD could be applied and allowed the successful determination of M4.

Our results show that CS-XRD in combination with MS data are a valuable tool for absolute structure identification of metabolites in early phases of drug discovery and development, it constitutes a powerful tool for human metabolite identification from *in vitro* incubations and allows earlier risk mitigations associated with metabolites in safety testing guidelines (FDA, 2016). The technology was able to provide new knowledge of the metabolism of PZQ, which has been used for the treatment of schistosomiasis for decades. The structural information at the atomic level were gained using only trace amounts of analyte material, outlining a significant advantage in comparison with other techniques like MS or NMR. Thus, we successfully confirmed the structure of three known hydroxy metabolites and elucidated the complete molecular scaffold of two unknown metabolites of *S*-PZQ.

To fully benefit from this technology, further investigation of the CS method is still needed to expand the chemical space of possible guest analytes by applying new types of CS with different binding sites and pore sizes to successfully encapsulate a wide range of target analytes in the CS pores and thus to successfully elucidate their complete structure.

Acknowledgments

The authors gratefully thank Ralf-Erwin Licht for his excellent experimental contribution on metabolite profiling. We also acknowledge Holger Scheible, Dominique Perrin, Hanno Schieferstein and Benedikt Lang for useful discussions and support of this study.

Authorship Contributions

Participated in research design: Rosenberger, Badolo.

Conducted experiments: Rosenberger.

Contributed new reagents or analytic tools: Kühn, Georgi.

Performed data analysis: Rosenberger, Jenniches, Marx.

Wrote or contributed to the writing of the manuscript: Rosenberger, Jenniches, von Essen, Khutia, Kühn, Marx, Hirsch, Hartmann, Badolo.

References

- Biradha K and Fujita M (2002) A springlike 3D-coordination network that shrinks or swells in a crystal-to-crystal manner upon guest removal or readsorption. *Angew Chem Int Ed Engl* 41:3392–3395.
- Brunet G, Safin DA, Aghaji MZ, Robeyns K, Korobkov I, Woo TK, and Murugesu M (2017) Stepwise crystallographic visualization of dynamic guest binding in a nanoporous framework. *Chem Sci (Camb)* 8:3171–3177.
- Dolomanov OV, Bourhis LJ, Gildea RJ, Howard JAK, and Puschmann H (2009) OLEX2: a complete structure solution, refinement and analysis program. *J Appl Cryst* 42:339–341 International Union of Crystallography.
- FDA (2016) *Safety Testing of Drug Metabolites - Guidance for Industry*, US Department of Health and Human Services FDA Center for Drug Evaluation and Research, Silver Spring, MD.
- Holčápek M, Jirásko R, and Lísa M (2010) Basic rules for the interpretation of atmospheric pressure ionization mass spectra of small molecules. *J Chromatogr A* 1217:3908–3921.
- Hoshino M, Khutia A, Xing H, Inokuma Y, and Fujita M (2016) The crystalline sponge method updated. *IUCr* 3:139–151.
- Huang J, Bathena SPR, and Alnouti Y (2010) Metabolite profiling of praziquantel and its analogs during the analysis of *in vitro* metabolic stability using information-dependent acquisition on a hybrid triple quadrupole linear ion trap mass spectrometer. *Drug Metab Pharmacokin* 25:487–499.
- Hübschle CB, Sheldrick GM, and Dittrich B (2011) ShelXle: a Qt graphical user interface for SHELXL. *J Appl Cryst* 44:1281–1284.
- Inokuma Y, Ukegawa T, Hoshino M, and Fujita M (2016) Structure determination of microbial metabolites by the crystalline sponge method. *Chem Sci (Camb)* 7:3910–3913.
- Inokuma Y, Yoshioka S, Ariyoshi J, Arai T, Hitora Y, Takada K, Matsunaga S, Rissanen K, and Fujita M (2013) X-ray analysis on the nanogram to microgram scale using porous complexes [published correction appears in *Nature* (2013) 501:262]. *Nature* 495:461–466.
- Kovač J, Vargas M, and Keiser J (2017) *In vitro* and *in vivo* activity of *R*- and *S*-praziquantel enantiomers and the main human metabolite trans-4-hydroxy-praziquantel against *Schistosoma haematobium*. *Parasit Vectors* 10:365.
- Lorch C and Blaschke G (1998) Investigation of the stereoselective metabolism of praziquantel after incubation with rat liver microsomes by capillary electrophoresis and liquid chromatography-mass spectrometry. *J Chromatogr B Biomed Sci Appl* 708:267–275.
- Meister I, Ingram-Sieber K, Cowan N, Todd M, Robertson MN, Meli C, Patra M, Gasser G, and Keiser J (2014) Activity of praziquantel enantiomers and main metabolites against *Schistosoma mansoni*. *Antimicrob Agents Chemother* 58:5466–5472.
- Nieya L, Thelengwani R, Li XQ, Cavallin E, Isin E, Nhachi C, and Masimirembwa C (2019) The effect of ketoconazole on praziquantel pharmacokinetics and the role of CYP3A4 in the formation of *X*-OH-praziquantel and not 4-OH-praziquantel. *Eur J Clin Pharmacol* 75:1077–1087.
- Park SK, Friedrich L, Yahya NA, Rohr CM, Chukov EG, Maillard D, Rippmann F, Spangenberg T, and Marchant JS (2021) Mechanism of praziquantel action at a parasitic flatworm ion channel. *Sci Transl Med* 13:eabj5832.
- Ramadhani TR, Zheng SL, Chen YS, and Clardy J (2015) Analysis of rapidly synthesized guest-filled porous complexes with synchrotron radiation: practical guidelines for the crystalline sponge method. *Acta Crystallogr A Found Adv* 71:46–58.
- Ramanathan R, Su AD, Alvarez N, Blumenkrantz N, Chowdhury SK, Alton K, and Patrick J (2000) Liquid chromatography/mass spectrometry methods for distinguishing *N*-oxides from hydroxylated compounds. *Anal Chem* 72:1352–1359.
- Rosenberger L, von Essen C, Khutia A, Kühn C, Georgi K, Hirsch AKH, Hartmann RW, and Badolo L (2021) Crystalline sponge affinity screening: A fast tool for soaking condition optimization without the need of X-ray diffraction analysis. *Eur J Pharm Sci* 164:105884.
- Rosenberger L, von Essen C, Khutia A, Kühn C, Urbahn K, Georgi K, Hartmann RW, and Badolo L (2020) Crystalline Sponges as a Sensitive and Fast Method for Metabolite Identification: Application to Gemfibrozil and Its Phase I and II Metabolites. *Drug Metab Dispos* 48:587–593.
- Sakurai F, Khutia A, Kikuchi T, and Fujita M (2017) X-ray Structure Analysis of *N*-Containing Nucleophilic Compounds by the Crystalline Sponge Method. *Chemistry* 23:15035–15040.
- Schepmann D and Blaschke G (2001) Isolation and identification of 8-hydroxypraziquantel as a metabolite of the antischistosomal drug praziquantel. *J Pharm Biomed Anal* 26:791–799.
- Sheldrick GM (2015) Crystal structure refinement with SHELXL. *Acta Crystallogr C Struct Chem* 71:3–8.
- Vendrell-Navarro G, Scheible H, Lignet F, Burt H, Luepfert C, Marx A, Abila N, Swart P, and Perrin D (2020) Insights into Praziquantel Metabolism and Potential Enantiomeric Cytochrome P450-Mediated Drug-Drug Interaction. *Drug Metab Dispos* 48:481–490.
- Wang H, Fang ZZ, Zheng Y, Zhou K, Hu C, Krausz KW, Sun D, Idle JR, and Gonzalez FJ (2014) Metabolic profiling of praziquantel enantiomers. *Biochem Pharmacol* 90:166–178.
- World Health Organization (2011) Schistosomiasis: number of people treated in 2009. *Wkly Epidemiol Rec* 86:73–80.
- World Health Organization (2020) Schistosomiasis fact sheet. <https://www.who.int/news-room/fact-sheets/detail/schistosomiasis>.

Address correspondence to: Lara Rosenberger, Frankfurter Strasse 250, 64293 Darmstadt, Germany. E-mail: Lara.Rosenberger@emdgroup.com

4. Final Discussion

The aim of this thesis was the structural elucidation of metabolites generated from *in vitro* systems using CS-XRD. MetID plays a key role in drug discovery and development to protect patients from potentially toxic metabolites, which can occur at lower concentration in preclinical species or be absent in these animals compared to human.²³ Conventional techniques are often limited in their ability to identify the complete structures of metabolites (LC-MS) or require large amounts of material (NMR) and therefore not always suitable to analyze samples from *in vitro* incubations. CS-XRD has the advantage of providing structural information at the atomic level using only nanogram to a few microgram amounts of analyte material.⁵⁰ Hence, this technology is a promising tool to assess the structure of metabolites generated in low amounts from *in vitro* studies.

We successfully determined the exact metabolic positions for three different phase I metabolites and one phase II acyl glucuronide of our tool compound gemfibrozil using CS-XRD (Chapter 3.1). Thereafter, we used the CS technology for the structure determination of three known and two unknown phase I metabolites of *S*-PZQ (Chapter 3.3). Therefore, we established a workflow including *in vitro* incubation with liver microsomes (gemfibrozil, *S*-PZQ) and liver S9 (gemfibrozil), sample preparation using semi-preparative HPLC and LC-MS analysis, and finally structural determination with CS using SC-XRD.

Furthermore, we developed an affinity screening method to select the optimal soaking condition without the need of SC-XRD analysis (Chapter 3.2). Guest soaking of individual compounds and mixtures was conducted in parallel for various soaking parameters. The amount of analyte in the pores of the CS was estimated using LC-MS², and the optimal soaking condition prioritized dependent on the highest affinity factor (AF). Additionally, the lower limit of detection (LLOD) of CS-XRD was investigated using four tool compounds.

4.1 Structural elucidation of APIs and metabolites using CS-XRD

4.1.1 Gemfibrozil and its phase I and II metabolites

In the first part of this thesis, we applied CS-XRD for the structural elucidation of gemfibrozil and its phase I metabolites and phase II acyl glucuronide. Usually, standard tools for complete structural determination like NMR, SC-XRD or the chemical synthesis of target compounds require significant time and resources, limiting the application for compounds only available in trace amounts. Therefore, the optimization of available techniques and the exploration of new tools is continuously needed. In recent years, CS-XRD came into focus as a tool to analyze the absolute structure of different kinds of compounds like APIs, natural products or synthesis products, using only nanogram to a few

micrograms of compound material.^{55,64,69,71,72} This technique combines high information density of X-ray crystallography with a sensitivity in the nanogram range, and is therefore a promising tool for structural elucidation of human metabolites at early stages in drug discovery and development, where only low amounts of material (nanogram range) are available.

As the CS technique has not been applied to metabolites generated by incubation of APIs with human or animal tissues (*i.e.*, microsomes, S9 fraction, hepatocytes) before, it was unclear, if the rather hydrophobic nature of the crystalline framework would be able to encapsulate these analytes due to their hydrophilic nature as a result of metabolism.^{57,73} We therefore analyzed the reference material of gemfibrozil and its metabolites 4'-hydroxy gemfibrozil (**M2**) and gemfibrozil 1-O- β -glucuronide (**M4**) as a first approach. Furthermore, the reference material was used to select the optimal soaking conditions (*i.e.*, sponge type, solvent, temperature), which were afterwards applied to the metabolites generated from incubation. After soaking 1000 nanogram of reference material for 24 hours using one prepared $[(ZnCl_2)_3(tpt)_2 \cdot x(\text{cyclohexane})]_n$ single crystal, the structure of gemfibrozil, as well as its two metabolites were clearly visible in the CS pores. The successful results showed that CS-XRD can be applied for hydrophilic compounds with highly polar groups (*e.g.*, glucuronides), despite the hydrophobic pores of the CS. In the next step, we expanded the application of CS-XRD to metabolites generated by incubation.

The main part in this chapter was the implementation of a workflow from generation of metabolite material by *in vitro* incubation, over sample preparation using semi-preparative HPLC to crystal measurement with SC-XRD (Figure 6). The metabolic pathway of our tool compound gemfibrozil was known from the literature. Gemfibrozil undergoes extensive phase I and II metabolism, including hydroxylation of the 2',5'-dimethylphenoxy moiety, further oxidation to carboxylic acid and direct glucuronidation.^{74,75} Therefore, suitable incubation systems (*i.e.*, microsomes, S9 fraction), which contain the required microsomal and cytosolic enzymes and the addition of cofactors (*i.e.*, NADPH, NADP⁺, UDPGA) were specifically selected to catalyze the metabolic reactions (Figure 7). To increase the respective metabolite formation, the incubation parameters (*i.e.*, incubation time, protein and substrate concentration) were optimized prior the *in vitro* assays (data not shown).

Final Discussion

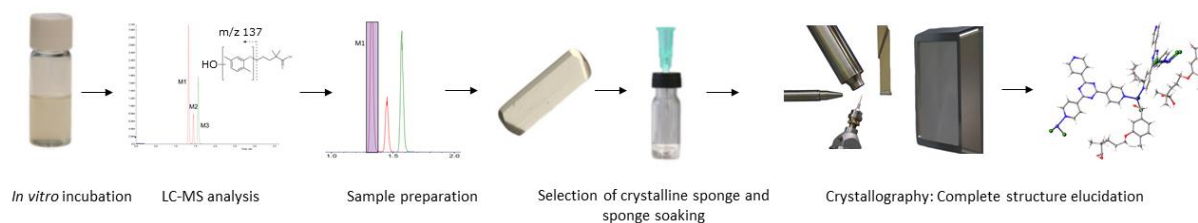


Figure 6: Workflow of MetID processes using the crystalline sponge method (figure adapted from L. Rosenberger et al., 2020.)⁴⁷

In the following step, we analyzed the incubation samples using different LC-MS techniques. The fragmentation of API and metabolites provided information about the kind of metabolism (*i.e.*, hydroxylation, carboxylation and glucuronidation) and limited the enzymatic oxidation to the 2',5'-dimethylphenoxy moiety, but was not able to pinpoint the exact position of metabolism. Therefore, we aimed to elucidate the complete structures using CS-XRD next. The sample purification of the target compounds was an important step, as CS-XRD is sensitive against impurities, which may cause damage to the crystal or even lead to the loss of crystallinity, occupy certain positions in the CS pores or influence the regular order of target analytes. The incubation matrix especially contains a large number of impurities, necessary for the enzymatic reaction, like buffer salts, cofactors or microsomal/cytosolic stock solution. Therefore, we purified the metabolites of interest twice *via* semi-preparative HPLC, using two different chromatographic columns. In order to achieve a high occupancy of guest analyte in the CS pores, we aimed to collect around 500–1000 nanogram of sample material for each compound.

The pooled incubation samples were then analyzed with CS-XRD applying the soaking conditions which were used for the reference material before. The obtained XRD data showed that hydroxylation occurred at the 4'-C (**M2** gemfibrozil) and 5'-CH₃ (**M1** gemfibrozil) positions of the benzene ring as well as the further oxidation to form a carboxylic acid at position 5'-CH₃ (**M3** gemfibrozil). **M4** gemfibrozil was determined as direct glucuronidation product at the carboxylic acid moiety of the alkyl chain. In combination with the MS data, which provided us information on the type of metabolism, we were able to assess the complete structures of four phase I and II metabolites of gemfibrozil using CS-XRD. The refined structures of gemfibrozil and its generated metabolites are summarized in Figure 7.

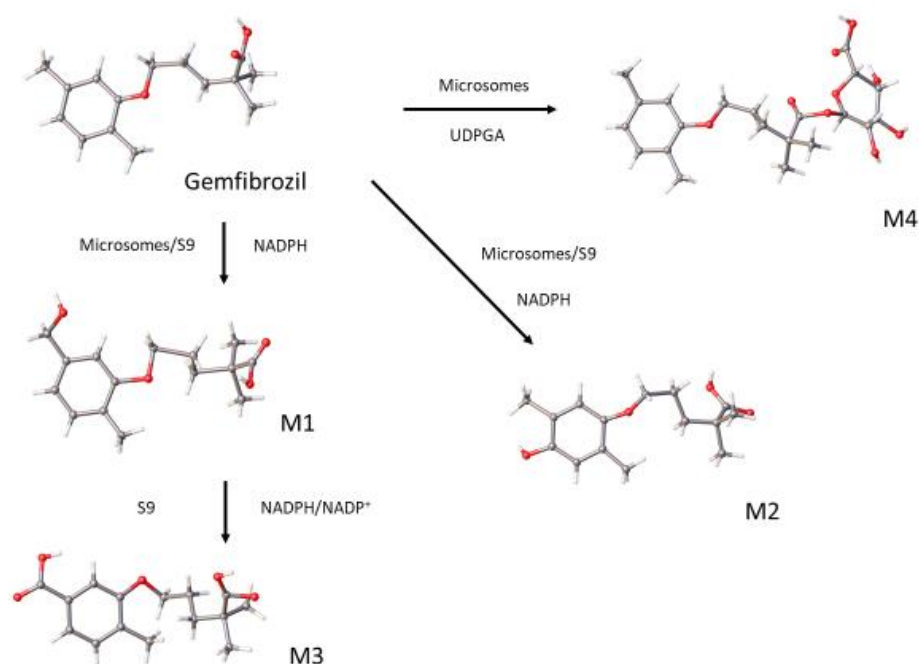


Figure 7: Metabolic pathway of gemfibrozil, 5'-CH₂OH-gemfibrozil (**M1**), 4'-OH-gemfibrozil (**M2**), 5'-COOH-gemfibrozil (**M3**) and gemfibrozil glucuronide (**M4**) (figure adapted from L. Rosenberger et al., 2020).⁴⁷

For the first part of this work, we applied the crystals to identify the structures of known metabolites to demonstrate, that CS-XRD is a promising tool to assess the structure of traces of drug-like molecules and their metabolites generated from *in vitro* studies.

4.1.2 S-PZQ and its hydroxylated phase I metabolites

As described in the first part of this work, CS-XRD can be a valuable tool for MetID studies from *in vitro* incubations. The goal of the next step was the application of the CS technology for the structural elucidation of unknown metabolites. PZQ, the drug of choice against the neglected tropical disease schistosomiasis, has been extensively used over the past decades. Several oxidative phase I metabolites (*e.g.*, hydroxylation, dehydrogenation) are known from metabolism studies, but the knowledge of the complete structure of some of these metabolites is still lacking.^{76–79}

It is known from the literature, that the enantioselective biotransformation of *R*-PZQ and *S*-PZQ leads to different metabolic profiles for both enantiomers.^{79,80} Therefore, we incubated *R*-PZQ and *S*-PZQ individually with human liver microsomes and NADPH as cofactor. To increase the respective metabolite formation, we optimized the incubation parameters (*i.e.*, incubation time, substrate concentration and addition of supplementary cofactor) prior to the *in vitro* assays (data not shown). *S*-PZQ thereby showed a higher formation of the unknown target metabolites and was therefore selected for further analysis. As the number of different metabolites generated *in vitro* was high, the

Final Discussion

chromatographic separation of coeluting analytes was challenging and an extensive chromatographic separation process needed to be conducted. Four unknown mono-oxidized metabolites were separated and purified by using three different chromatographic columns in tandem.

We then analyzed the pure analyte fractions by UPLC-qTOF-MS analysis to limit the position of hydroxylation to a certain part of the molecule but could not determine the exact position of metabolism.

To select the optimal soaking conditions for *S*-PZQ and its unknown metabolites to conduct CS-XRD, we examined the reference material of *S*-PZQ, using the prior developed CS affinity screening (data not shown).⁸¹ The optimal soaking conditions were then applied for *S*-PZQ and the reference material of the major metabolites *S-trans*-4'-hydroxy-PZQ (**M1**) and *S-cis*-4'-hydroxy-PZQ (**M2**). Next, we applied CS-XRD for structural elucidation of 11b-hydroxy-PZQ (**M6**), which was known from the literature.⁷⁹ Surprisingly, both enantiomers were observed in the CS pores with a Flack value of around 0.5, confirming the presence of the racemic mixture. After chiral separation, the absolute configuration of one enantiomer was determined as *R*, suggesting the other enantiomer to be in *S* configuration. After the successful structure assignment of **M1** PZQ and **M2** PZQ as well as the discovery of both enantiomers of **M6** PZQ, CS soaking experiments were conducted for the unknown metabolites **M3–M5**. The crystallographic data clearly revealed the position of hydroxylation for **M3** PZQ and **M4** PZQ at the 9-C position of the aromatic benzene and 7-C position of the non-aromatic part of *S*-PZQ, respectively. Furthermore, the newly introduced chiral center at position 7 of **M4** PZQ was indicated as *S* configuration. The structure of **M5** PZQ however, could not be determined as a guest molecule in the CS framework, as only diffuse electron density could be observed. The refined structures of *S*-PZQ and its analyzed phase I metabolites are summarized in Figure 8.

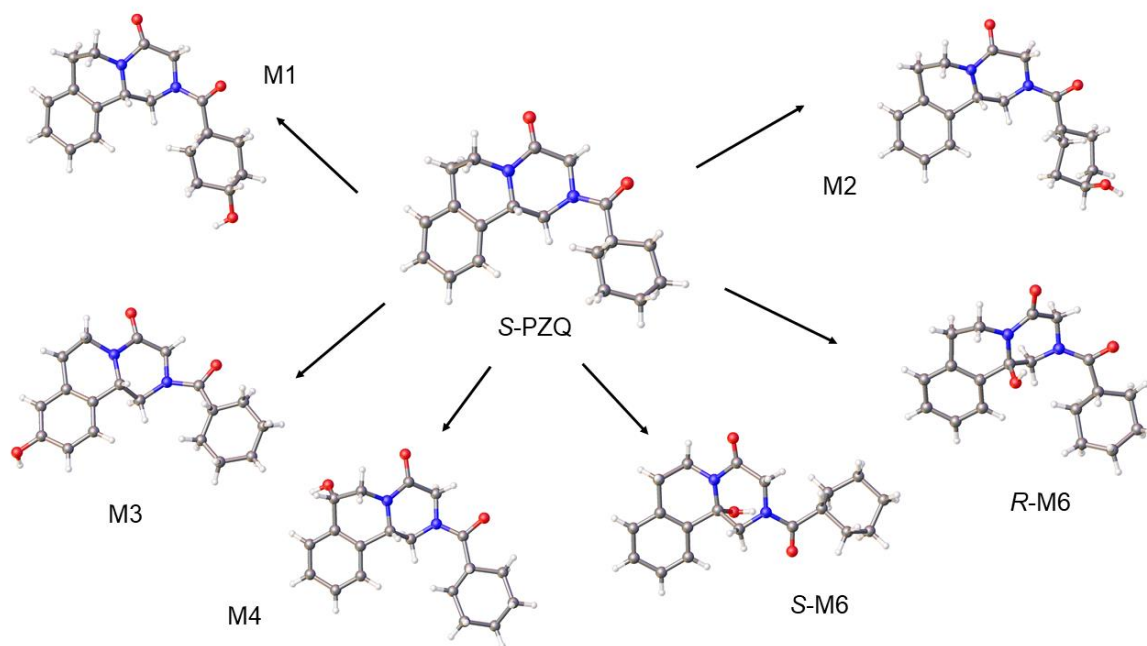


Figure 8: S-PZQ and its monohydroxy metabolites S-trans-4'-hydroxy-PZQ (**M1**), S-cis-4'-hydroxy PZQ (**M2**), S-9-hydroxy-PZQ (**M3**), S-7-hydroxy-S-PZQ (**M4**), S-11b-hydroxy-PZQ (**S-M6**) and R-11b-hydroxy-PZQ (**R-M6**) (figure adapted from L. Rosenberger et al., 2022).⁸²

Besides the UPLC-qTOF analysis of the fragmentation pattern, we performed the NMR analysis of **M3** PZQ in comparison to CS-XRD. The increased sample amount necessary to conduct an NMR spectrum, resulted in a prolonged sample collection period from days to weeks. Metabolite **M4** however, was only present in low abundance in the incubation solution and therefore did not allow the collection of sufficient analyte material for NMR analysis.

These results show that CS-XRD is a valuable tool for absolute structure elucidation of small molecules, generated by synthesis (*e.g.*, APIs) or nature (*e.g.*, natural products, metabolites) that are often available only in trace amounts.

4.2 CS Affinity Screening

The crucial step of CS-XRD is the optimization of soaking parameters (*i.e.*, sponge type, solvent, temperature, soaking duration) for successful guest inclusion and repetitive order of analyte in the CS pores to make the target structure visible for XRD analysis.^{55,70,83} Different combinations of soaking parameters must be tested to find the optimal conditions for each individual target analyte. Time-consuming XRD measurements (around 24 hours per crystal with a standard system) are thereby essential to determine if an analyte has been successfully absorbed into the pores of the crystalline framework. Therefore, it may take weeks to optimize the soaking process and to achieve successful results.

Final Discussion

In this chapter, we aimed at the development of a screening method to select the optimal soaking parameters based on the respective compound affinity prior to XRD measurements. During the soaking process, guest molecules can be absorbed from solution into the pores of the crystalline framework and arranged in a regular pattern through specific non-covalent host–guest interactions.^{50,84} This leads to an inclusion and enrichment of target sample in the CS. The occupancy of guest compound in the CS pores is thereby influenced by the parameters of the respective soaking condition. Based on the facts outlined, the determination of the amount of encapsulated analyte material in the CS pores dependent on the respective soaking condition permits the selection of the optimal soaking parameters for an individual target analyte. To determine the optimal soaking conditions, we developed a workflow from parallel guest soaking, over estimation of analyte material in the CS pores to the final generation of crystallographic data using SC-XRD (Figure 9).

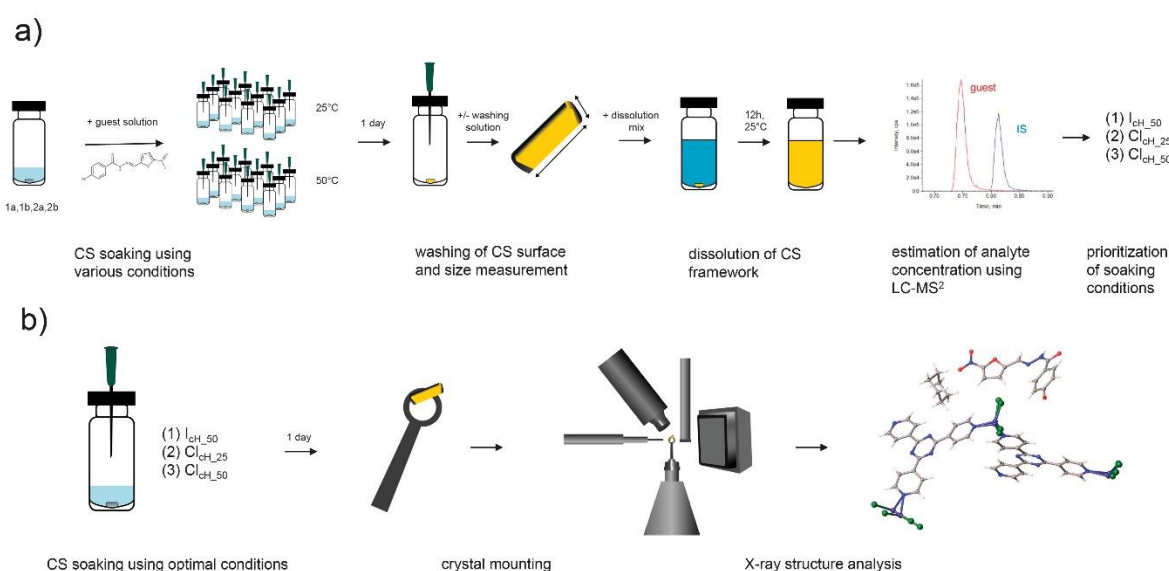


Figure 9: Workflow of a) CS affinity screening, b) CS-XRD using the optimal soaking conditions (1)–(3) (figure from L. Rosenberger et al., 2021).⁸¹

We analyzed 14 individual compounds using a series of eight different soaking conditions in parallel including two CS types (e.g., $[(ZnCl_2)_3 \cdot (tpt)_2 \cdot x(\text{solvent})]_n$, $[(ZnI_2)_3 \cdot (tpt)_2 \cdot x(\text{solvent})]_n$) in two solvents (cyclohexane, n-hexane) at two temperatures (25 °C, 50 °C). After soaking 1000 nanogram of analyte material with one crystal for one day, not absorbed compound was removed from the CS through a washing step to avoid false positive results because of analyte precipitation on the crystal surface. The crystal dimensions were measured to estimate the amount of analyte in relation to the crystal size, as the crystal has a defined quantity of void spaces per pores for guest exchange, which increase in relation to the crystal size. To release the guest molecules from the CS pores fast, the crystalline

Final Discussion

framework was dissolved using a dissolution medium before analyzing the sample solution using UPLC-MS².

We then compared the different soaking conditions by their respective AF, the ratio of estimated amount of analyte and crystal size, and selected the optimal conditions by the highest AF values for final XRD measurements. The crystallographic analysis of the optimal soaking conditions resulted in the successful structural elucidation of ten guest analytes using CS-XRD. Four compounds showed low or no affinity to the CS and no structure could be assigned.

By analyzing the highest AF values of 14 test compounds, we observed a difference between the analytes leading to successful crystallographic results and those resulting in unsuccessful XRD measurements. Analytes showing an AF value > 10 tend to interact with the host framework, whereas AF values < 10 represent low or no occupancy of guest molecules in the CS pores. This classification of soaking conditions by AF values and the exclusion criterion of AF 10 allows a reasonable decision to focus on analytes, which show interactions with the CS framework and to avoid unnecessary time-consuming XRD measurements for target compounds without affinity. As this work was a first proof-of-concept study to use the amount of analyte in the CS pores to select the optimal soaking conditions, more data points are needed to confirm the indicated exclusion criterion of AF 10.

After testing compounds individually, we investigated if the affinity screening method can be expanded for the analysis of a mixture of compounds as well. Therefore, we selected five of the already tested analytes with AF values above and below 10. The compounds were added for soaking in equimolar amounts, considering their molecular weight, and allowing each molecule equal opportunity to occupy a position within the porous framework. Furthermore, the analyte amount was reduced compared to the single compound soakings to ensure an excess of possible occupation sites in the crystal. The results showed that the prioritized optimal soaking conditions from the mixture did not match the results from the single compound soaking for all test compounds. Therefore, we concluded that the affinity screening of a compound mixture can be used as a first estimate but cannot replace the screening of single compounds in general. The influence of excessive analyte amount and the use of several compounds on the soaking process and the regular order of guest molecules in the CS pores is yet unknown and needs to be further investigated.

In addition, we examined the LLOD of CS-XRD using four different test compounds. The crystallographic analysis showed that only 5 nanogram were sufficient to unambiguously determine the structure of two guest analytes. These impressive results confirmed that CS-XRD is indeed a convenient technology for structure elucidation with the potential of analyzing only trace amounts of compound material (*e.g.*, metabolites, impurities) with high affinity for the crystalline framework.

5. Conclusions and Outlook

The aim of this thesis was to investigate the applicability of CS-XRD for the structural elucidation of small molecule drug metabolites generated from *in vitro* incubation. We successfully showed that the CS technology is a sensitive (nanogram amount) and fast (few days) method to pinpoint the exact position of metabolism for both phase I and phase II metabolites. Overall, we were able to apply CS-XRD to identify the structures of four different metabolites of our tool compound gemfibrozil, as well as three known and two unknown metabolites of *S*-PZQ. Furthermore, we developed an affinity screening method to prioritize soaking conditions without the use of time-consuming XRD measurements. The screening of a mixture of compounds led to promising results and could be used for future soaking parameter optimization of analytes not available as reference material, *e.g.*, impurities or metabolites from *in vitro* incubation only formed in low amounts.

As was shown in this thesis, CS-XRD has the potential to help scientists in their task of structural elucidation using only trace amounts of target analyte. However, this technology is still in its infancy, and therefore the method requires further development to expand its scope. While the MOF type used in this thesis is suitable for small organic molecules with a molecular weight less than 500 g/mol, it is limited in trapping larger molecules, molecules with nucleophilic moieties or compounds only soluble in highly polar solvents (*e.g.*, water).^{55,56} Moreover, not all target analytes interact with the framework to achieve a successful encapsulation or regular order of guest molecules in the CS pores, as the results of the CS affinity screening showed.

To expand the chemical space of guest molecules and hence the potential for additional interactions between host and guest, a variety of different MOF types with the characteristics of a CS, need to be developed. To modify the pore nature and as a result the possible interactions, Fujita and coworkers intercalated a cartridge molecule containing different functional groups as part of the framework, which can undergo chemical reactions and covalent binding with certain guest molecules.⁸⁵⁻⁸⁷ In 2020, Taniguchi *et al.* showed, that the CS framework can be protected from reactive compounds which are acidic, basic or nucleophilic by the addition of sulfonic acids to form ion-pairs prior to the CS soaking.⁸⁸

Besides the Zn_2/Cl_2 -tpt MOF introduced by Fujita, several research groups reported the design of new CS types in the past years. In 2016, Yaghi and coworkers showed that the Al-based chiral MOF-520 can be used for the analysis of analytes with functionalities as primary amines, phenols, vicinal diols, and carboxylic acids by their coordinative alignment to the framework.^{89,90} In 2019, Bacchi and coworkers reported the synthesis and a first solvent-to-guest exchange from the polar solvent *N,N*-dimethylformamide for their porous material PUM168.⁹¹ A water stable lanthanide MOF (RUM-2) was described by de Poel *et al.* in 2019, and its guest encapsulation capability was further demonstrated

Conclusions and Outlook

by Carmalt and coworkers thereafter.^{92,93} Another example for a CS, which can tolerate polar solvents and accommodates hydrophilic guests, was reported in 2016 by Ning *et al.* for a saccharide-based sugar sponge.⁹⁴

To detect new CS, a first screening by Inokuma *et al.* showed, that the CSD hosts a large number of porous materials and thereby potential candidates for new CS.⁶¹ To identify if one of the scored porous materials has the required properties to act and be called as a “crystalline sponge”, an extensive procedure of chemical synthesis, solvent screening, soaking optimization and crystallographic-data analysis is necessary to assess the promising findings but has the potential of detecting new sponge material in the future.

According to the current state, little is known about the possible correlation between the target structure, the soaking conditions and the successful encapsulation in the crystalline framework. In our opinion, more attention should be paid to the soaking process, which is the key step of CS-XRD. The knowledge of the influence of each individual soaking parameter in dependency of the physical and chemical analyte properties during this step, could help for future prediction of optimal soaking conditions. However, the necessary data quantity is currently too low to build such a data informatics platform for software-dependent data evaluation, as CS-XRD got introduced only some years ago and is currently not yet in a state for experimental high-throughput data generation. Nevertheless, the number of uploaded CS structures in the CSD increases constantly, and thereby approaching the possibility of an evaluation study in the near future.

6. References

1. Caldwell, J., Gardner, I. & Swales, N. An Introduction to Drug Disposition: The Basic Principles of Absorption, Distribution, Metabolism, and Excretion. *Toxicol. Pathol.* **23**, 102–114 (1995).
2. Talevi, A. & Quiroga, P. A. M. *ADME Processes in Pharmaceutical Sciences*. (Springer Nature Switzerland AG, 2018).
3. Zhang, D., Zhu, M. & Humphreys, W. G. *Drug Metabolism in Drug Design and Development*. (John Wiley & Sons, Inc., 2007).
4. Testa, B., Pedretti, A. & Vistoli, G. Foundation review: Reactions and enzymes in the metabolism of drugs and other xenobiotics. *Drug Discov. Today* **17**, 549–560 (2012).
5. Gibbons, G. F. The role of cytochrome P450 in the regulation of cholesterol biosynthesis. *Lipids* **37**, 1163–1170 (2003).
6. Omura, T. & Sato, R. The Carbon of Liver Microsomes: I. Evidence for its hemoprotein nature. *J. Biol. Chem.* **239**, 2370–2378 (1964).
7. Gordeziani, M. S., Varazi, T. G. & Pruidze, M. V. Structural–functional organization of cytochrome P450 containing monooxygenase and some aspects of modeling. *Ann. Agrar. Sci.* **14**, 82–94 (2016).
8. Shankar, K. & Mehendale, H. M. Cytochrome P450. *Encycl. Toxicol. Third Ed.* **1**, 1125–1127 (2014).
9. Zanger, U. M. & Schwab, M. Cytochrome P450 enzymes in drug metabolism: Regulation of gene expression, enzyme activities, and impact of genetic variation. *Pharmacol. Ther.* **138**, 103–141 (2013).
10. Nelson, D. R. & Nebert, D. W. Cytochrome P450 (CYP) Gene Superfamily. *eLS* **450**, 1–19 (2018).
11. Ingelman-Sundberg, M. Pharmacogenetics of cytochrome P450 and its applications in drug therapy: The past, present and future. *Trends Pharmacol. Sci.* **25**, 193–200 (2004).
12. Smith, D. A., Waterbeemd, H. van de & Walker, D. K. *Pharmacokinetics and Metabolism in Drug Design*. (Wiley-VCH Verlag GmbH, 2001).
13. Penner, N., Woodward, C. & Prakash, C. Appendix: Drug Metabolizing Enzymes and Biotransformation Reactions. *ADME-Enabling Technol. Drug Des. Dev.* 545–565 (2012).
14. Kauffman, F. C. *Conjugation - Deconjugation Reactions in Drug Metabolism and Toxicity. The American Journal of The Medical Sciences* Vol. 112 (Springer-Verlag Berlin Heidelberg, 1994).
15. Meister, A. *Advances in enzymology and related areas of molecular biology*. vol. 32 (John Wiley & Sons, Inc., 1969).
16. Bachhawat, A. K. & Kaur, A. Glutathione Degradation. *Antioxidants Redox Signal.* **27**, 1200–1216 (2017).
17. Koppel, N., Rekdal, V. M. & Balskus, E. P. Chemical transformation of xenobiotics by the human gut microbiota. *Science.* **356**, 1246–1257 (2017).
18. Gibson, G. G. & Skett, P. *Introduction to Drug Metabolism*. (Springer Science+Business Media Dordrecht, 1994).

References

19. Attia, S. M. Deleterious effects of reactive metabolites. *Oxid. Med. Cell. Longev.* **3**, 238–253 (2010).
20. Chipinda, I., Hettick, J. M. & Siegel, P. D. Haptenation: Chemical Reactivity and Protein Binding. *J. Allergy* **2011**, 1–11 (2011).
21. Prakash, C., Shaffer, C. L. & Nedderman, A. Analytical Strategies for identifying drug metabolites. *Mass Spectrom. Rev.* **26**, 340–369 (2007).
22. FDA. *Safety Testing of Drug Metabolites - Guidance for Industry.* (US Department of Health and Human Services FDA Center for Drug Evaluation and Research, 2016).
23. EMA. *Guideline on the investigation of drug interactions.* (European Medicine Agency, 2013).
24. Penner, N., Klunk, L. J. & Prakash, C. Human Radiolabeled Mass Balance Studies: Objectives, Utilities and Limitations. *Biopharm. Drug Dispos.* **30**, 185–203 (2009).
25. Ma, S. & Chowdhury, S. K. Analytical Strategies for Assessment of Human Metabolites in. *Anal. Chem.* **83**, 5028–5036 (2011).
26. Ma, S. & Chowdhury, S. K. A tiered approach to address regulatory drug metabolite-related issues in drug development. *Bioanalysis* **6**, 587–590 (2014).
27. Prasad, B., Garg, A., Takwani, H. & Singh, S. Metabolite identification by liquid chromatography-mass spectrometry. *TrAC - Trends Anal. Chem.* **30**, 360–387 (2011).
28. Houle, R., Raoul J., Lévesque, J.-F., Pang, S., Nicoll-Griffith, D. A. & Silva, J. M. Retention of transporter activities in cryopreserved, isolated rat hepatocytes. *Drug Metab. Dispos.* **31**, 447–451 (2003).
29. Hengstler, J. G., Utesch, D., Steinberg, P., Platt, K. L., Diener, B., Ringel, M., Swales, N., Fischer, T., Biefang, K., Gerl, M., Böttger, T. & Oesch, F. Cryopreserved primary hepatocytes as a constantly available in vitro model for the evaluation of human and animal drug metabolism and enzyme induction. *Drug Metab. Rev.* **32**, 81–118 (2000).
30. Kerns, E. H. & Di, L. *Drug-like Properties: Concepts, Structure Design and Methods.* (Elsevier Inc., 2008).
31. Kwon, Y. *Handbook of Essential Pharmacokinetics, Pharmacodynamics, and Drug Metabolism for Industrial Scientists.* (Kluwer Academic Publishers, 2001).
32. Krishna, R. *Applications of Pharmacokinetic Principles in Drug Development.* (Springer Science+Business Media, LLC, 2004).
33. Crespi, C. L. & Miller, V. P. The use of heterologously expressed drug metabolizing enzymes-state of the art and prospects for the future. *Pharmacol. Ther.* **84**, 121–131 (1999).
34. Gan, L., von Moltke, L. L., Trepanier, L. A., Harmatz, J. S., Greenblatt, D. J. & Court, M. H. Role of NADPH-cytochrome P450 reductase and cytochrome-b 5/NADH-b5 reductase in variability of CYP3A activity in human liver microsomes. *Drug Metab. Dispos.* **37**, 90–96 (2009).
35. Günzler, H. & Williams, A. *Handbook of Analytical Techniques. Handbook of Analytical Techniques* (John Wiley & Sons, Inc., 2001).
36. Gross, J. H. *Mass Spectrometry.* (Springer International Publishing, 2017).
37. Ekman, R., Silberring, J., Westman-Brinkmalm, A. M. & Kraj, A. *Mass Spectrometry: Instrumentation, Interpretation, and Applications.* (John Wiley & Sons, Inc., 2009).

References

38. Zhang, H., Zhang, D. & Ray, K. A software filter to remove interference ions from drug metabolites in accurate mass liquid chromatography/mass spectrometric analyses. *J. Mass Spectrom.* **38**, 1110–1112 (2003).
39. Cruciani, G., Carosati, E., De Boeck, B., Ethirajulu, K., Mackie, C., Howe, T. & Vianello, R. MetaSite: Understanding metabolism in human cytochromes from the perspective of the chemist. *J. Med. Chem.* **48**, 6970–6979 (2005).
40. Zhu, C., Wan, M., Cheng, H., Wang, H., Zhu, M. & Wu C. Rapid detection and structural characterization of verapamil metabolites in rats by UPLC – MSE and UNIFI platform. *Biomed. Chromatogr.* **34**, e4702 (2020).
41. Massa, W. *Crystal Structure Determination*. (Springer-Verlag Berlin Heidelberg GmbH, 2004).
42. Ladd, M. & Palmer, R. *Structure determination by X-ray Crystallography*. (Springer US, 2013).
43. Flack, H. D. & Bernardinelli, G. Absolute structure and absolute configuration. *Acta Crystallogr. Sect. A* **A55**, 908–915 (1999).
44. Waseda, Y., Matsubara, E. & Shinoda, K. *X-Ray Diffraction Crystallography*. *X-Ray Diffraction Crystallography* (Springer-Verlag Berlin Heidelberg, 2011).
45. Hoffmann, F. *Introduction to Crystallography*. (Springer International Publishing, 2020).
46. Borchardt-Ott, W. *Crystallography*. (Springer-Verlag Berlin Heidelberg, 2012).
47. Rosenberger, L., von Essen, C., Khutia, A., Kühn, C., Urbahns, K., Georgi, K., Hartmann, R.W. & Badolo, L. Crystalline sponges as a sensitive and fast method for metabolite identification: Application to gemfibrozil and its phase I and II metabolites. *Drug Metab. Dispos.* **48**, 587–593 (2020).
48. Dolomanov, O. V, Bourhis, L. J., Gildea, R. J., Howard, J. A. K. & Puschmann, H. OLEX2: a complete structure solution, refinement and analysis program. *J. Appl. Crystallogr.* **42**, 339–341 (2009).
49. Hübschle, C. B., Sheldrick, G. M. & Dittrich, B. ShelXle: a Qt graphical user interface for SHELXL. *J. Appl. Crystallogr.* **44**, 1281–1284 (2011).
50. Inokuma, Y., Yoshioka, S., Ariyoshi, J., Arai, T., Hitora, Y., Takada, K., Matsunaga, S., Rissanen, K. & Fujita, M. X-ray analysis on the nanogram to microgram scale using porous complexes. *Nature* **495**, 461–466 (2013) [published correction appears in *Nature* **501**:262].
51. Ramadhar, T. R., Zheng, S.-L., Chen, Y.-S. & Clardy, J. Analysis of rapidly synthesized guest-filled porous complexes with synchrotron radiation: Practical guidelines for the crystalline sponge method. *Acta Crystallogr. Sect. A Found. Crystallogr.* **71**, 46–58 (2015).
52. Biradha, K. & Fujita, M. A springlike 3D-coordination network that shrinks or swells in a crystal-to-crystal manner upon guest removal or readsorption. *Angew. Chemie - Int. Ed.* **41**, 3392–3395 (2002).
53. Inokuma, Y., Arai, T. & Fujita, M. Networked molecular cages as crystalline sponges for fullerenes and other guests. *Nat. Chem.* **2**, 780–783 (2010).
54. Rissanen, K. Crystallography of encapsulated molecules. *Chem. Soc. Rev.* **46**, 2638–2648 (2017).
55. Sakurai, F., Khutia, A., Kikuchi, T. & Fujita, M. X-ray Structure Analysis of N-Containing Nucleophilic Compounds by the Crystalline Sponge Method. *Chem. - Eur. J.* **23**, 15035–15040 (2017).

References

56. Inokuma, Y., Yoshioka, S., Ariyoshi, J., Arai, T. & Fujita, M. Preparation and guest-uptake protocol for a porous complex useful for 'crystal-free' crystallography. *Nat. Protoc.* **9**, 246–252 (2014).
57. Hoshino, M., Khutia, A., Xing, H., Inokuma, Y. & Fujita, M. The crystalline sponge method updated. *Acta Crystallogr. Sect. B* **3**, 139–151 (2016).
58. Zigon, N., Kikuchi, T., Ariyoshi, J., Inokuma, Y. & Fujita, M. Structural Elucidation of Trace Amounts of Volatile Compounds Using the Crystalline Sponge Method. *Chem. - An Asian J.* **12**, 1057–1061 (2017).
59. Furukawa, H., Cordova, K. E., O'Keeffe, M. & Yaghi, O. M. The chemistry and applications of metal-organic frameworks. *Science*. **341**, (2013).
60. Li, X., Semiramoth, N., Hall, S., Tefani, V., Josse, J., Laurent, F., Salzano, G., Foulkes, D., Brodin, P., Majlessi, L., Ghermani, N.-E., Maurin, G., Couvreur, P., Serre, C., Bernet-Camard, M.-F., Zhang, J. & Gref, R. Compartmentalized Encapsulation of Two Antibiotics in Porous Nanoparticles: an Efficient Strategy to Treat Intracellular Infections. *Part. Part. Syst. Charact.* **36**, 1–9 (2019).
61. Inokuma, Y., Matsumura, K., Yoshioka, S. & Fujita, M. Finding a New Crystalline Sponge from a Crystallographic Database. *Chem. - An Asian J.* **12**, 208–211 (2017).
62. Ohmori, O., Kawano, M. & Fujita, M. Crystal-to-Crystal Guest Exchange of Large Organic Molecules within a 3D Coordination Network. **126**, 16292–16293 (2004).
63. Brunet, G., Safin, D. A., Robeyns, K., Facey, G. A., Korobkov, I., Filinchuk, Y. & Murugesu M. Confinement effects of a crystalline sponge on ferrocene and ferrocene carboxaldehyde. *Chem. Commun.* **53**, 5645–5648 (2017).
64. Urban, S., Brkljača, R., Hoshino, M., Lee, S. & Fujita, M. Determination of the Absolute Configuration of the Pseudo-Symmetric Natural Product Elatenyne by the Crystalline Sponge Method. *Angew. Chemie - Int. Ed.* **55**, 2678–2682 (2016).
65. Kawahata, M., Komagawa, S., Ohara, K., Fujita, M. & Yamaguchi, K. High-resolution X-ray structure of methyl salicylate, a time-honored oily medicinal drug, solved by crystalline sponge method. *Tetrahedron Lett.* **57**, 4633–4636 (2016).
66. Duplan, V., Hoshino, M., Li, W., Honda, T. & Fujita, M. In Situ Observation of Thiol Michael Addition to a Reversible Covalent Drug in a Crystalline Sponge. *Angew. Chemie - Int. Ed.* **55**, 4919–4923 (2016).
67. Kai, K., Sogame, M., Sakurai, F., Nasu, N. & Fujita, M. Collimonins A-D, Unstable Polyynes with Antifungal or Pigmentation Activities from the Fungus-Feeding Bacterium *Collimonas fungivorans* Ter331. *Org. Lett.* **20**, 3536–3540 (2018).
68. Wada, N., Kersten, R. D., Iwai, T., Lee, S., Sakurai, F., Kikuchi, T., Fujita, D., Fujita, M. & Weng, J.-K. Crystalline-Sponge-Based Structural Analysis of Crude Natural Product Extracts. *Angew. Chemie - Int. Ed.* **57**, 3671–3675 (2018).
69. Morita, I., Mori, T., Mitsunashi, T., Hoshino, S., Taniguchi, Y., Kikuchi, T., Nagae, K., Nasu, N., Fujita, M., Ohwada, T. & Abe I. Exploiting a C–N Bond Forming Cytochrome P450 Monooxygenase for C–S Bond Formation. *Angew. Chemie - Int. Ed.* **59**, 3988–3993 (2020).
70. Inokuma, Y., Ukegawa, T., Hoshino, M. & Fujita, M. Structure determination of microbial metabolites by the crystalline sponge method. *Chem. Sci.* **7**, 3910–3913 (2016).

References

71. Li, K., Yang, D. S., Gu, X. F. & Di, B. Absolute configuration determination of asarinin by synchrotron radiation with crystalline sponge method. *Fitoterapia* **134**, 135–140 (2019).
72. Vinogradova, E. V., Müller, P. & Buchwald, S. L. Structural reevaluation of the electrophilic hypervalent iodine reagent for trifluoromethylthiolation supported by the crystalline sponge method for x-ray analysis. *Angew. Chemie - Int. Ed.* **53**, 3125–3128 (2014).
73. Habib, F., Tocher, D. A., Press, N. J. & Carmalt, C. J. Structure determination of terpenes by the crystalline sponge method. *Microporous Mesoporous Mater.* **308**, 110548 (2020).
74. Hermening, A., Gräfe, A. K., Baktir, G., Mutschler, E. & Spahn-Langguth, H. Gemfibrozil and its oxidative metabolites: Quantification of aglycones, acyl glucuronides, and covalent adducts in samples from preclinical and clinical kinetic studies. *J. Chromatogr. B* **741**, 129–144 (2000).
75. Thomas, B. F., Burgess, J. P., Coleman, D. P., Scheffler, N. M., Jeffcoat, A. R. & Dix, K. J. Isolation and identification of novel metabolites of gemfibrozil in rat urine. *Drug Metab. Dispos.* **27**, 147–157 (1999).
76. Huang, J., Bathena, S. P. R. & Alnouti, Y. Metabolite Profiling of Praziquantel and its Analogs During the Analysis of in vitro Metabolic Stability Using Information- Dependent Acquisition on a Hybrid Triple Quadrupole Linear Ion Trap Mass Spectrometer. *Drug Metab Pharmacokinet* **25**, 487–499 (2010).
77. Meier, H. & Blaschke, G. Capillary electrophoresis – mass spectrometry , liquid chromatography – mass spectrometry and nanoelectrospray-mass spectrometry of praziquantel metabolites. **748**, 221–231 (2000).
78. Schepmann, D. & Blaschke, G. Isolation and identification of 8-hydroxypraziquantel as a metabolite of the antischistosomal drug praziquantel. *J. Pharm. Biomed. Anal.* **26**, 791–799 (2001).
79. Vendrell-Navarro, G., Scheible, H., Lignet, F., Burt, H., Luepfert, C., Marx, A., Abia, N., Swart, P. & Perrin, D. Insights into Praziquantel Metabolism and Potential Enantiomeric Cytochrome P450-Mediated Drug-Drug Interaction. *Drug Metab. Dispos.* **48**, 481–490 (2020).
80. Wang, H., Fang, Z.-Z., Zheng, Y., Zhou, K., Hu, C., Krausz, K. W., Sun, D., Idle, J. R. & Gonzalez, F. J. Metabolic profiling of praziquantel enantiomers. *Biochem. Pharmacol.* **90**, 166–178 (2014).
81. Rosenberger, L., von Essen, C., Khutia, A., Kühn, C., Georgi, K., Hirsch, A. K. H., Hartmann, R. W. & Badolo, L. Crystalline sponge affinity screening: A fast tool for soaking condition optimization without the need of X-ray diffraction analysis. *Eur. J. Pharm. Sci.* **164**, 105884 (2021).
82. Rosenberger, L., Jenniches, J., von Essen, C., Khutia, A., Kühn, C., Marx, A., Georgi, K., Hirsch, A. K. H., Hartmann, R. W. & Badolo, L. Metabolic profiling of S-praziquantel: Structure elucidation using the crystalline sponge method in combination with mass spectrometry and nuclear magnetic resonance. *Drug Metab. Dispos.* **50**, 320-326 (2022).
83. Zhang, S., Fairen-jimenez, D. & Zaworotko, M. J. Structural Elucidation of the Mechanism of Molecular Recognition in Chiral Crystalline Sponges. **132**, 17753–17759 (2020).
84. Mon, M., Bruno, R., Ferrando-Soria, J., Bartella, L., Donna, L. D., Talia, M., Lappano, R., Maggolini, M., Armentano, D. & Pardo, E. Crystallographic snapshots of host-guest interactions in drugs@metal-organic frameworks: Towards mimicking molecular recognition processes. *Mater. Horizons* **5**, 683–690 (2018).
85. Kawano, M., Kawamichi, T., Haneda, T., Kojima, T. & Fujita, M. The Modular Synthesis of Functional Porous Coordination Networks. *J. Am. Chem. Soc.* **129**, 15418–15419 (2007).

References

86. Ohmori, O., Kawano, M. & Fujita, M. A Two-in-One Crystal: Uptake of Two Different Guests into Two Distinct Channels of a Biporous Coordination Network. *Angew. Chemie - Int. Ed.* **44**, 1962–1964 (2005).
87. Kawamichi, T., Kodama, T., Kawano, M. & Fujita, M. Single-Crystalline Molecular Flasks : Chemical Transformation with Bulky Reagents in the Pores of Porous Coordination Networks. *Angew. Chemie - Int. Ed.* **47**, 8030–8032 (2008).
88. Taniguchi, Y., Matsumoto, R. & Kadota, T. An Expansion of Crystalline Sponge X-ray Analysis to Elucidate the Molecular Structure of Reactive Compounds via Ion Pair Formation. *Chem. - A Eur. J.* **26**, 15799–15803 (2020).
89. Lee, S., Kapustin, E. A. & Yaghi, O. M. Coordinative alignment of molecules in chiral metal-organic frameworks. *Science* **353**, 808–811 (2016).
90. Pei, X., Bürgi, H. B., Kapustin, E. A., Liu, Y. & Yaghi, O. M. Coordinative Alignment in the Pores of MOFs for the Structural Determination of N-, S-, and P-Containing Organic Compounds including Complex Chiral Molecules. *J. Am. Chem. Soc.* **141**, 18862–18869 (2019).
91. Balestri, D., Mazzeo, P. P., Carraro, C., Demitri, N., Pelagatti, P. & Bacchi, A. Stepwise Evolution of Molecular Nanoaggregates Inside the Pores of a Highly Flexible Metal–Organic Framework. *Angew. Chemie* **131**, 17503–17511 (2019).
92. de Poel, W., Tinnemans, P., Duchateau, A. L. L., Honing, M., Rutjes, F. P. J. T., Vlieg, E. & de Gelder, R. The Crystalline Sponge Method in Water. *Chem. - A Eur. J.* **25**, 14999–15003 (2019).
93. Lunn, R. D. J., Tocher, D. A., Sidebottom, P. J., Montgomery, M. G., Keates, A. C. & Carmalt, C. J. Encapsulation of Aromatic Compounds and a Non-Aromatic Herbicide into a Gadolinium-Based Metal-Organic Framework via the Crystalline Sponge Method. *Cryst. Growth Des.* **20**, 7238–7245 (2020).
94. Ning, G. H., Matsumura, K., Inokuma, Y. & Fujita, M. A saccharide-based crystalline sponge for hydrophilic guests. *Chem. Commun.* **52**, 7013–7015 (2016).

7. Appendix

7.1 Supporting Information Chapter A

Supplemental Data for

Crystalline Sponges as a sensitive and fast method for metabolite identification:

Application to gemfibrozil and its phase I and II metabolites

Lara Rosenberger, Carolina von Essen, Anupam Khutia, Clemens Kühn, Klaus Urbahns,
Katrini Georgi, Rolf W. Hartmann, Lassina Badolo

Department of Drug Metabolism and Pharmacokinetics (DMPK), Merck KGaA, Frankfurter
Strasse 250, 64293 Darmstadt, Germany (L.R., K.U., K.G., L.B.)

Innovation Center, Merck KGaA, Frankfurter Strasse 250, 64293 Darmstadt, Germany (C.v.E.,
A.K., C.K.)

Department of Drug Design and Optimization (DDOP), Helmholtz-Institute for Pharmaceutical
Research Saarland (HIPS)-Helmholtz Centre for Infection Research (HZI), Campus E8.1,
66123 Saarbrücken, Germany (L.R., R.W.H.)

Single crystal X-ray diffraction experiments

Single crystal X-ray diffraction measurements were conducted on a Rigaku Oxford Diffraction XtaLAB Synergy-R diffractometer using Cu-K α X-ray radiation ($\lambda = 1.54184 \text{ \AA}$), equipped with a HyPix-6000HE (M1 gemfibrozil, M2 gemfibrozil, M3 gemfibrozil and M4 gemfibrozil) or HyPix-Arc 150° (gemfibrozil) Hybrid Photon Counting (HPC) detector (Rigaku, Tokyo, Japan) at a temperature of 100 K using a Cryostream 800 nitrogen stream (Oxford Cryostreams, UK). The software CrysAlisPro ver. 171.39.46 (M1 gemfibrozil, M2 gemfibrozil, M3 gemfibrozil and M4 gemfibrozil) and ver. 171.41.48a (gemfibrozil) was used for calculation of measurement strategy and data reduction (data integration, empirical and numerical absorption corrections and scaling). The software ShelXle was used to generate the electron density maps F_o to verify the position of metabolism (Hübschle et al., 2011). Isocontour levels are described as σ (square root of the average variance of the density).

Crystal structure analysis

All crystal structures were modeled using OLEX2 (Dolomanov et al., 2009), solved with SHELXT ver. 2014/5 and refined using SHELXL ver. 2018/1 (Sheldrick, 2015). Figures of framework and analyte were created using OLEX2. Non-hydrogen atoms were refined anisotropically. Hydrogen atoms were fixed using the riding model. Populations of the guests in the crystal were modelled by least-square refinement of a guest/solvent disorder model under the constraint that the sum of them should equal to 100%. When a reasonable guest/solvent disorder model could not be built due to severe disorder of the solvent molecules, the guest populations were set to 100% (s.o.f. = 1). In this case, overestimation is unavoidable if the actual occupancy is less than 100% leading to high large displacement parameters compared to the framework (Hoshino et al., 2016). Number of restraints was tried to minimize and applied without changing the standard deviation. Solvent cyclohexane molecules in the pores were found in the difference electron density map and refined using the restraints (DFIX, DANG, SIMU and ISOR). These molecules are expected to be severely disordered due their

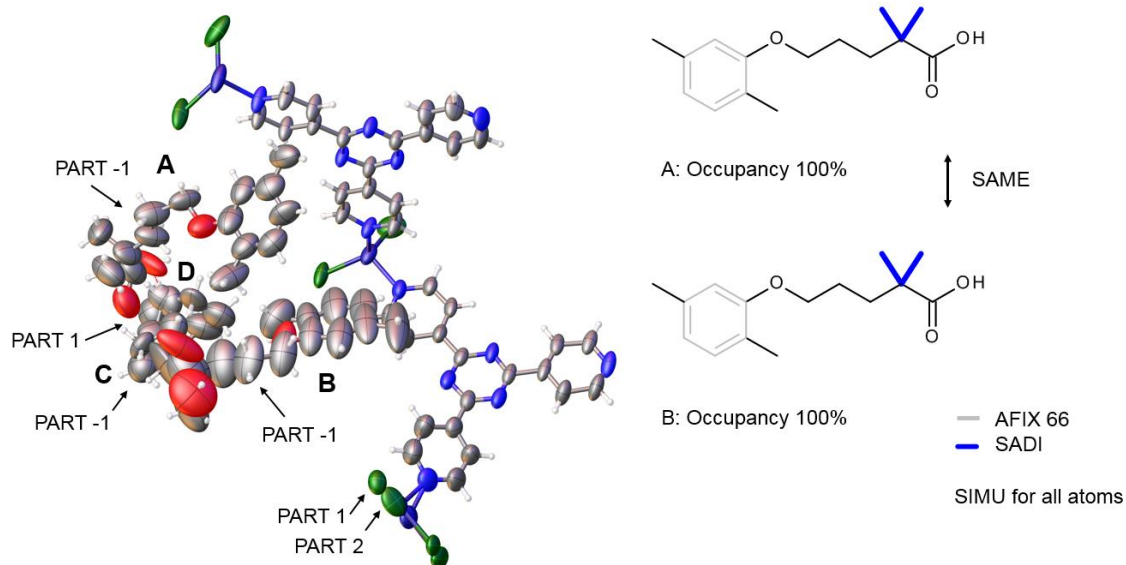
high thermal motion. Due to their averaged structure of various geometry and orientation, some cyclohexane molecules are distorted to energetically-unfavorable (boat-shaped or twisted) structures. Some “Alert A” notifications were found in the validation program CheckCIF. Those alerts are derived from short intermolecular contacts of hydrogen atoms between solvent molecule (cyclohexane) and the crystalline sponge framework, guest molecule, and other solvent molecules, and are unavoidable due to severe disorder. The comments for the alerts are described in the CIFs using the validation response form (vrf).

The present crystal structures are not used for exact structure analysis. They are used to confirm structure proposals derived from information obtained from mass spectrometry and knowledge of the parent structure. Therefore, details of the crystals structure (bond lengths, angles, etc.) will not be discussed.

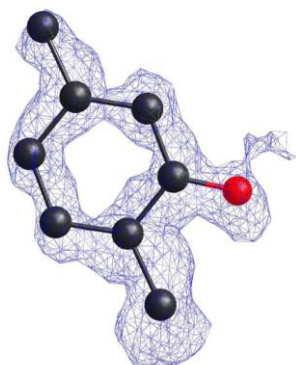
Crystallographic data for gemfibrozil

Crystal size: 131 × 83 × 59 μm^3 , refined formula: $\text{C}_{55}\text{H}_{55}\text{Cl}_6\text{N}_{12}\text{O}_3\text{Zn}_3$, formula weight (M_r) = 1344.24 g/mol, yellow needle, crystal system: Monoclinic, space group $C2/c$, $Z = 8$, 14170 unique reflections merged from recorded 47910 ones ($2.695^\circ < \theta < 71.380^\circ$) were used for structural analysis ($R_{\text{int}} = 0.0181$). Lattice parameters, R-factor on $F^2 > 2\sigma(F^2)$, weighted R-factor, and goodness-of-fit are follows: $a = 33.6364(5) \text{ \AA}$, $b = 14.36600(10) \text{ \AA}$, $c = 32.0319(4) \text{ \AA}$, $\beta = 102.8500(10)^\circ$, $V = 15090.8(3) \text{ \AA}^3$, $R = 0.1125$, $wR_2 = 0.3255$, $S = 1.102$. Calculated density is 1.183 g cm^{-3} . Linear absorption coefficient (μ) is 3.409 mm^{-1} . Residual electron density (max/min) is $0.865/-0.471 \text{ e\AA}^{-3}$. CCDC number 1983846. The ORTEP diagram of the asymmetric unit of the framework and gemfibrozil is shown in Supplemental Figure 1.

The framework is refined without using restraints. One ZnCl_2 moiety is disordered and refined using disorder model. Two guest molecules (A, B) were found in the asymmetric unit. Two additional cyclohexane molecules (C, D) can be found in the asymmetric unit. Both analytes are located very close to the symmetry centers (inversion and $C2$ axis, respectively) and are refined using PART -1 command to avoid calculation of bonds between symmetry related atoms. The analyte occupancy is 100%. The geometry of both molecules is related by SAME command. The benzene ring was fixed using AFIX 66. Two C-C single bonds were restrained using SADI command. No other geometrical restrains were used in the refinement of the analyte molecules. SIMU was applied for all analyte molecules. Applied restraints can be taken from Supplemental Fig. 1. Supplemental Fig. 2 shows the electron density map of the aromatic part of one gemfibrozil molecule taken from the crystal structure.



Supplemental Fig. 1. ORTEP diagram with 50% probability of the asymmetric unit of gemfibrozil; restraints and constraints applied in the refinement of gemfibrozil



Supplemental Fig. 2. Electron density map F_o of the benzene core from gemfibrozil (contoured at the 0.67σ level)

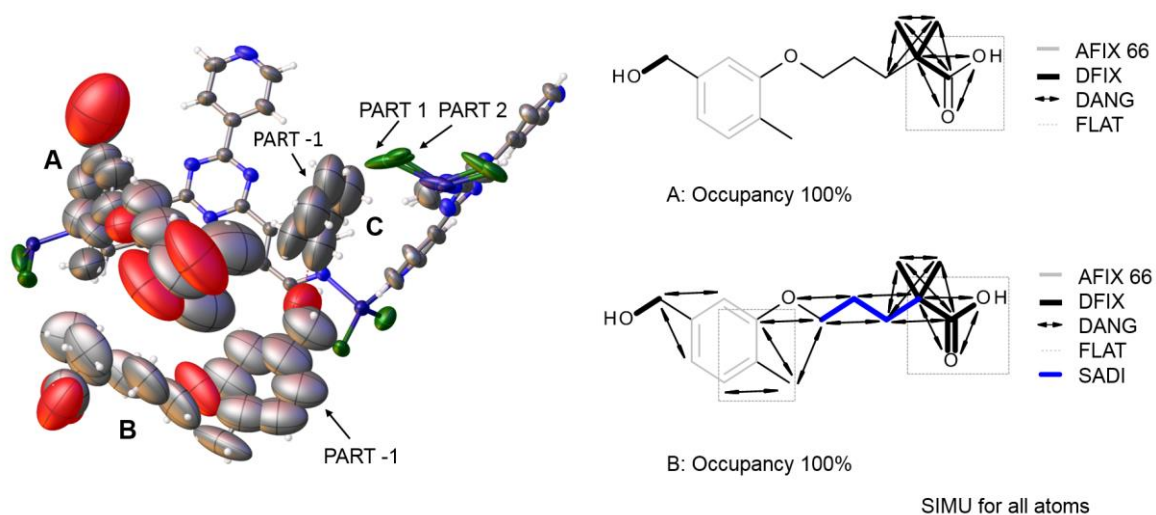
Crystallographic data for M1 gemfibrozil

Crystal size: 163 × 76 × 54 μm³, refined formula: C₆₂H₆₃Cl₆N₁₂O₆Zn₃, formula weight (M_r) = 1475.05 g/mol, yellow needle, crystal system: Monoclinic, space group C2/c, Z = 8, 13144 unique reflections merged from recorded 42219 ones (2.692° < θ < 67.080°) were used for structural analysis (R_{int} = 0.0218). Lattice parameters, R-factor on F² > 2σ (F²), weighted R-factor and goodness-of-fit are follows: a = 33.5373(8) Å, b = 14.3660(2) Å, c = 31.4546(9) Å, β = 101.801(3) °, V = 14834.4(6) Å³, R = 0.0758, wR₂ = 0.2571, S = 1.056. Calculated density is 1.321 gcm⁻³. Linear absorption coefficient (μ) is 3.547. Residual electron density (max/min) is 0.703/-0.622 eÅ⁻³. CCDC number 1983847. The ORTEP diagram of the asymmetric unit of the framework and M1 gemfibrozil is shown in Supplemental Fig. 3.

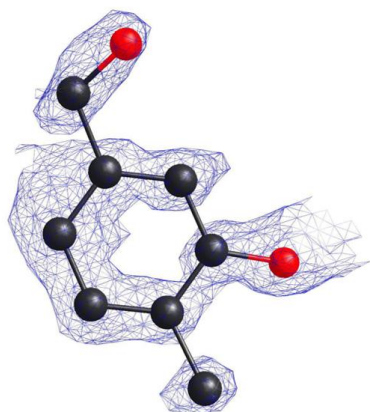
The framework is refined without using restraints. One ZnCl₂ moiety is disordered and refined using disorder model. Two guest molecules were found in the asymmetric unit. One molecule (A) is ordered at general position with modeled occupancy of 100% because solvent disorder models could not be built due to high disorder. The other molecule (B) is disordered at special position (C2 axis) and refined using PART -1 command and s.o.f. = 0.5. One cyclohexane molecule (C) is disordered on special position (C2 axis) and refined using PART -1 command and s.o.f. = 0.5. Some restraints were applied for refinement of the analyte and solvent molecules. Both guest molecules were refined with applying SIMU (for complete molecules). The restraints used for the refinement are summarized in Supplemental Fig. 3. The benzene part of both molecules could be refined with minor restraints and the presence of oxidation at the 5'-methyl carbon is clearly visible from electron density maps (Supplemental Fig. 4). The positions of carbon atoms in the alkyl chains had to be restrained to their theoretical values applying DFIX and DANG commands due to high mobility and not resolved disorder with solvent molecules of these parts. In the present study, the task of the crystalline sponge method was the determination of positions of oxidation during metabolization and the position could be determined without any doubts. The combination of knowledge of the parent structure, information from mass spectrometry and crystalline sponge analysis leads to a

Appendix

successful structure elucidation. For a full structural analysis of this compound without any prior knowledge of the composition, soaking conditions should be optimized for higher occupancy leading to improved data.



Supplemental Fig. 3. ORTEP diagram with 50% probability of the asymmetric unit of M1 gemfibrozil; restraints and constraints applied in the refinement of M1 gemfibrozil

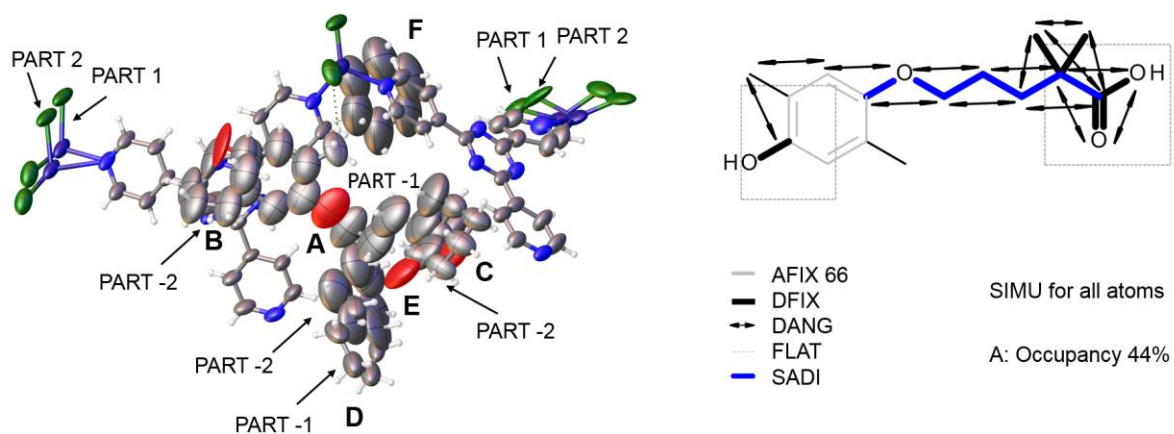


Supplemental Fig. 4. Electron density map F_o of the benzene core from M1 gemfibrozil (contoured at the 0.73σ level)

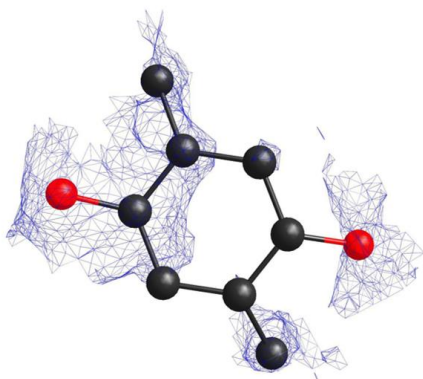
Crystallographic data for M2 gemfibrozil

Crystal size: 295 × 144 × 120 μm³, refined formula: C₅₂H₅₃Cl₆N₁₂O₁Zn₃, formula weight (M_r) = 1262.43 g/mol, light yellow needle, crystal system: Monoclinic, space group *C2/c*, Z = 8, 12268 unique reflections merged from recorded 38793 ones (3.373° < θ < 67.076°) were used for structural analysis (R_{int} = 0.0209). Lattice parameters, R-factor on F² > 2σ(F²), weighted R-factor, and goodness-of-fit are follows: a = 31.8982(5) Å, b = 14.4063(2) Å, c = 30.4802(6) Å, β = 98.783(2)°, V = 13842.5(4) Å³, R = 0.0756, wR₂ = 0.2381, S = 1.084. Calculated density is 1.212 gcm⁻³. Linear absorption coefficient (μ) is 3.658 mm⁻¹. Residual electron density (max/min) is 0.644/-0.610 eÅ⁻³. CCDC number 1983848. The ORTEP diagram of the asymmetric unit of the framework and M2 gemfibrozil is shown in Supplemental Fig. 5.

The framework exhibits disorder of two ZnCl₂ parts. In one case, displacement parameters of respective atoms were restrained using the DELU command. One guest molecule (A) can be found in the asymmetric unit disordered with two cyclohexane (B, C) molecules. Two additional cyclohexane molecules, one disordered with a second cyclohexane (D, E) and one without disorder (F) can be found in the asymmetric unit. The analyte and cyclohexane molecules lie near the center of symmetry (*C2* axis). Therefore, the analyte is refined using PART -1 with s.o.f. = 0.5x(FVAR#4) and the disordered cyclohexane molecules are refined using PART -2 with s.o.f. = 0.5x(1-FVAR#4). This leads to an analyte occupancy of 44%. AFIX 66 was applied to the benzene ring, and DFIX and DANG were used for some bonds and angles of the guest (see Supplemental Fig. 5). Due to missing hydrogen bond acceptors near phenyl and carboxylic acid alcohol function and low occupancy, a stable refinement for the respective hydrogen atom was not possible. SIMU was applied for both analyte molecules. The oxidation of the benzene ring in 4-position during metabolization is clearly visible from electron density maps (Supplemental Fig. 6).



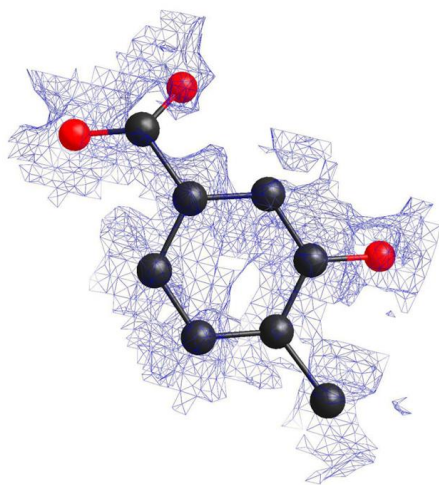
Supplemental Fig. 5. ORTEP diagram with 50% probability of the asymmetric unit of M2 gemfibrozil; restraints and constraints applied in the refinement of M2 gemfibrozil



Supplemental Fig. 6. Electron density map F_o of the benzene core from M2 gemfibrozil (contoured at the 0.95σ level)

Crystallographic data for M3 gemfibrozil

The framework can be refined without using restraints. One disordered ZnCl_2 moiety is modeled using the disorder model. Applying solvent masking implemented in OLEX2 after complete framework refinement, one void with $V= 969 \text{ \AA}^3$ and 264 electrons per asymmetric unit can be found. This is consistent with the presence of 1.5 molecules of M3 and one cyclohexane molecule (273 electrons). Electron density assignable to a benzene core can be found. Careful investigation of the electron density map around the benzene core revealed electron density assignable to a carboxylic acid function in 5 position (Supplemental Fig. 7). Due to low occupancy and high disorder, the complete analyte molecule could not be modeled. Information obtained from MS indicated a two-fold oxidation, presumably to a carboxylic acid and the structure obtained from the crystalline sponge method confirmed the position of oxidation.



Supplemental Fig. 7. Electron density map F_o of the benzene core from M3 gemfibrozil (contoured at the 1.00σ level)

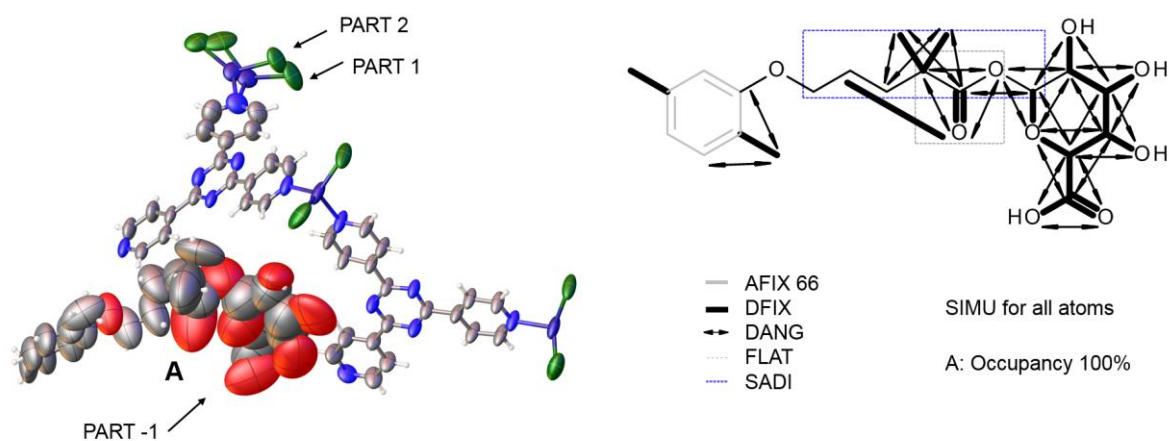
Crystallographic data for M4 gemfibrozil

Crystal size: 200 × 97 × 26 μm³, refined formula: C₄₇H₃₉Cl₆N₁₂O₅Zn₃, formula weight (M_r) = 1246.70 g/mol, colourless needle, crystal system: Monoclinic, space group C2/c, Z = 8, 12853 unique reflections merged from recorded 39917 ones (2.742° < θ < 67.079°) were used for structural analysis (R_{int} = 0.0187). Lattice parameters, R-factor on F² > 2σ(F²), weighted R-factor, and goodness-of-fit are follows: a = 32.8136(6) Å, b = 14.42330(10) Å, c = 31.0646(5) Å, β = 100.840(2)°, V = 14439.9(4) Å³, R = 0.0699, wR₂ = 0.2481, S = 1.026. Calculated density is 1.147 gcm⁻³. Linear absorption coefficient (μ) is 3.544 mm⁻¹. Residual electron density (max/min) is 0.724/-0.460 eÅ⁻³. CCDC number 1983849. The ORTEP diagram of the asymmetric unit of the framework and M4 gemfibrozil is shown in Supplemental Fig. 8.

The framework exhibits disorder of one ZnCl₂ part refined using the disorder model. One guest molecule (A) can be found in the asymmetric unit near the center of symmetry (C₂ axis) and refined using PART -1 command with s.o.f. = 0.5. The analyte occupancy was modeled to 100% as no disordered solvent molecules could be assigned. AFIX 66 was applied to the benzene ring, and DFIX and DANG were used for some bonds and angles of the guest (see Supplemental Fig. 8). The guest molecule was refined with applying SIMU. Additional electron density was found that could not be assigned due to disorder. Contribution of this electron density was removed using solvent masking algorithm implemented in OLEX2. A solvent mask was calculated and 648 electrons were found in a volume of 2548 Å³ in one void per unit cell. This is consistent with the presence of 1.5 cyclohexane molecules per asymmetric unit which account for 576 electrons per unit cell. The analyte was used as enantiopure material. Although it is in general possible to determine absolute structures with the crystalline sponge method, we were not able to determine the absolute structure of gemfibrozil glucuronide. Due to disorder, conformation of the glucuronide, i. e. oxane and substituents cannot be determined. The presence of aliphatic rings in unfavorable conformations is often observed in the crystalline sponge method especially for cyclohexane molecules. Nevertheless, the position of glucuronidation at the carboxylic acid function of gemfibrozil can be confirmed.

Appendix

Material obtained from incubation was used for a soaking experiment. The crystal structure shows electron density assignable to gemfibrozil glucuronide. Due to high disorder and low analyte occupancy, a stable model could not be obtained. Therefore, the structure obtained from reference material is presented.



Supplemental Fig. 8. ORTEP diagram with 50% probability of the asymmetric unit of M4 gemfibrozil; restraints and constraints applied in the refinement of M4 gemfibrozil

References

- Dolomanov OV, Bourhis LJ, Gildea RJ, Howard JAK, and Puschmann H (2009) OLEX2: a complete structure solution, refinement and analysis program. *J Appl Crystallogr* 42: 339-341.
- Hübschle CB, Sheldrick GM, and Dittrich B (2011) ShelXle: a Qt graphical user interface for SHELXL. *J Appl Crystallogr* 44(Pt 6): 1281-1284.
- Sheldrick GM (2015) Crystal structure refinement with SHELXL. *Acta Crystallogr C Struct Chem* 71: 3-8.

7.2 Supporting Information Chapter B

Supplementary Material for

Crystalline Sponge Affinity Screening: A Fast Tool for Soaking Condition Optimization without the Need of X-ray Diffraction Analysis

Lara Rosenberger^{a,c,d}, Carolina von Essen^b, Anupam Khutia^b, Clemens Kühn^{b*}, Katrin Georgi^a,
Anna K. H. Hirsch^{c,d}, Rolf W. Hartmann^{c,d}, Lassina Badolo^a

^a Discovery and Development Technologies (DDTech), Merck KGaA, Frankfurter Strasse 250,
64293 Darmstadt, Germany

^b Innovation Center, Merck KGaA, Frankfurter Strasse 250, 64293 Darmstadt, Germany

^c Department of Drug Design and Optimization (DDOP), Helmholtz-Institute for Pharmaceutical
Research Saarland (HIPS) - Helmholtz Centre for Infection Research (HZI), Campus E8.1,
66123 Saarbrücken, Germany

^d Department of Pharmacy, Saarland University, Campus E8.1, 66123 Saarbrücken, Germany

***Corresponding author:** Dr. Clemens Kühn, Merck KGaA, Frankfurter Str. 250, 64293
Darmstadt, Germany

E-mail address: clemens.kuehn@merckgroup.com (C. Kühn)

Preparation of crystalline sponges

The porous crystalline sponges $[(\text{ZnCl}_2)_3 \cdot (\text{tpt})_2 \cdot x(\text{solvent})]_n$ (solvent=cyclohexane (**1a**), n-hexane (**1b**)) and $[(\text{ZnI}_2)_3 \cdot (\text{tpt})_2 \cdot x(\text{solvent})]_n$ (solvent=cyclohexane (**2a**), n-hexane (**2b**)) were prepared following the reported procedures (Biradha and Fujita, 2002; Ramadhar et al., 2015).

Single crystal X-ray diffraction experiments

Single crystal X-ray diffraction measurements were conducted on a Rigaku Oxford Diffraction XtaLAB Synergy-R diffractometer using Cu-K α X-ray radiation ($\lambda = 1.54184 \text{ \AA}$), equipped with a HyPix-6000HE (**1a•3**, **2a•7**, **1a•11** and **1a•20**) or HyPix-Arc 150° (**2a•4**, **1a•5**, **2a•6**, **1b•8**, **1a•9**, **2a•12** and **1b•19**) Hybrid Photon Counting (HPC) detector (Rigaku, Tokyo, Japan) at a temperature of 100 K using a Cryostream 800 nitrogen stream (Oxford Cryostreams, Oxford, UK). The software CrysAlisPro ver. 1.171.39.46 (**1a•3** and **2a•7**), ver. 1.171.41.48a (**1a•5** and **1b•19**), 1.171.41.68a (**2a•4**, **2a•6**, **1b•8**, **1a•9** and **2a•12**) and ver. 1.171.41.76a (**1a•11** and **1a•20**) was used for calculation of measurement strategy and data reduction (data integration, empirical and numerical absorption corrections and scaling).

Crystal structure analysis

All crystal structures were modelled using OLEX2 (Dolomanov et al., 2009), solved with SHELXT ver. 2014/5 and refined using SHELXL ver. 2018/1 (Sheldrick, 2015). Figures of framework and analyte were created using OLEX2. Non-hydrogen atoms were refined anisotropically. Hydrogen atoms were fixed using the riding model. Populations of the guests in the crystal were modelled by least-square refinement of a guest/solvent disorder model under the constraint that the sum of them should be equal to 100%. When a reasonable guest/solvent disorder model could not be built due to severe disorder of the solvent molecules, the guest populations were set to 100% (s.o.f. = 1). In this case, overestimation is unavoidable if the actual occupancy is less than 100% leading to large displacement parameters compared

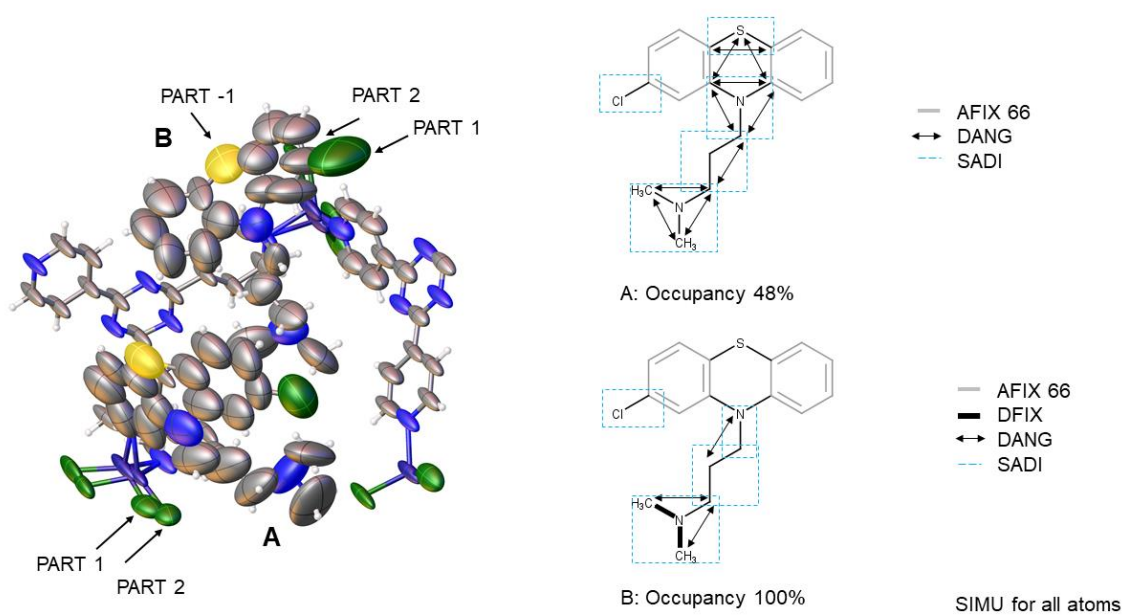
to the framework (Hoshino *et al.*, 2016). Constraints and restraints were applied using the default standard deviations. The number of used constraints and restraints was tried to minimize. Solvent cyclohexane and n-hexane molecules in the pores were found in the difference electron density map and refined using the restraints (DFIX, DANG, SIMU, RIGU and SADI). These molecules are expected to be severely disordered due to their high thermal motion. Due to their averaged structure of various geometry and orientation, some cyclohexane molecules are distorted to energetically-unfavorable (boat-shaped or twisted) structures. Some “Alert A” notifications were found with the validation program CheckCIF. Those alerts are derived from short intermolecular contacts of hydrogen atoms between a solvent molecule (cyclohexane or n-hexane) and the crystalline sponge framework, guest molecule, and other solvent molecules, and are unavoidable due to severe disorder. The comments for the alerts are described in the CIFs using the validation response form (vrf).

The quality indicators for the crystalline sponge crystal structures often are not as good as those of many conventional single crystal structures. However, in many cases, the atomic connectivity and identity can unequivocally be determined and several examples have been published which exhibit decent quality indicators including displacement ellipsoids (Sanna *et al.*, 2015; Cuenca *et al.*, 2016; Inokuma *et al.*, 2016). The data quality of the crystalline sponge method is in any case sufficient to confirm a known structure or changes in the molecular scaffold of a known structure, as was shown for example for the metabolite identification study of gemfibrozil (Rosenberger *et al.*, 2020), the analysis of α -humulene oxidation products (Zigon *et al.*, 2015) and metabolic products from fermentation with baker’s yeast (Inokuma *et al.*, 2016).

Crystallographic data for 1a•3 (chlorpromazine)

Crystal size: 194 × 112 × 76 μm³, refined formula: C_{52.62}H_{42.58}Cl_{6.98}N_{13.96}S_{0.98}Zn₃, formula weight (M_r) = 1345.24 g/mol, colourless needle, crystal system: monoclinic, space group C2/c, Z = 8, 13413 unique reflections merged from recorded 49921 ones (3.350° < θ < 67.078°) were used for structural analysis (R_{int} = 0.0334). Lattice parameters, R-factor on F² > 2σ (F²), weighted R-factor, and goodness-of-fit are as follows: a = 34.071(3) Å, b = 14.3799(3) Å, c = 31.673(3) Å, β = 103.437(9)°, V = 15093.2(19) Å³, R = 0.1016, wR₂ = 0.2191, S = 0.933. Calculated density is 1.184 gcm⁻³. Linear absorption coefficient (μ) is 3.946 mm⁻¹. Residual electron density (max/min) is 0.77/-0.60 eÅ⁻³. CCDC number 2051013. The ORTEP diagram of the asymmetric unit of **1a•3** is shown in Supplemental Figure 1.

The framework is refined using the constraint EADP for one disordered ZnCl₂ moiety. Two ZnCl₂ moieties are disordered and refined using disorder model. Two guest molecules (A, B) were found in the asymmetric unit. The analyte occupancy of A is 48%. One molecule (B) is disordered at special position (inversion) and refined using PART -1 command and s.o.f. = 0.5. The benzene rings were fixed using AFIX 66 and DFIX, DANG and SADI were used for some bonds and angles of the guest (see Supplemental Fig. 1). SIMU was applied for all analyte molecules. Applied restraints can be taken from Supplemental Fig. 1. Additional electron density was found that could not be assigned due to disorder. Contribution of this electron density was removed using solvent masking algorithm implemented in OLEX2. A solvent mask was calculated and 40 electrons were found in a volume of 174 Å³ in one void per asymmetric unit. This is consistent with the presence of 0.8 cyclohexane molecules per asymmetric unit.



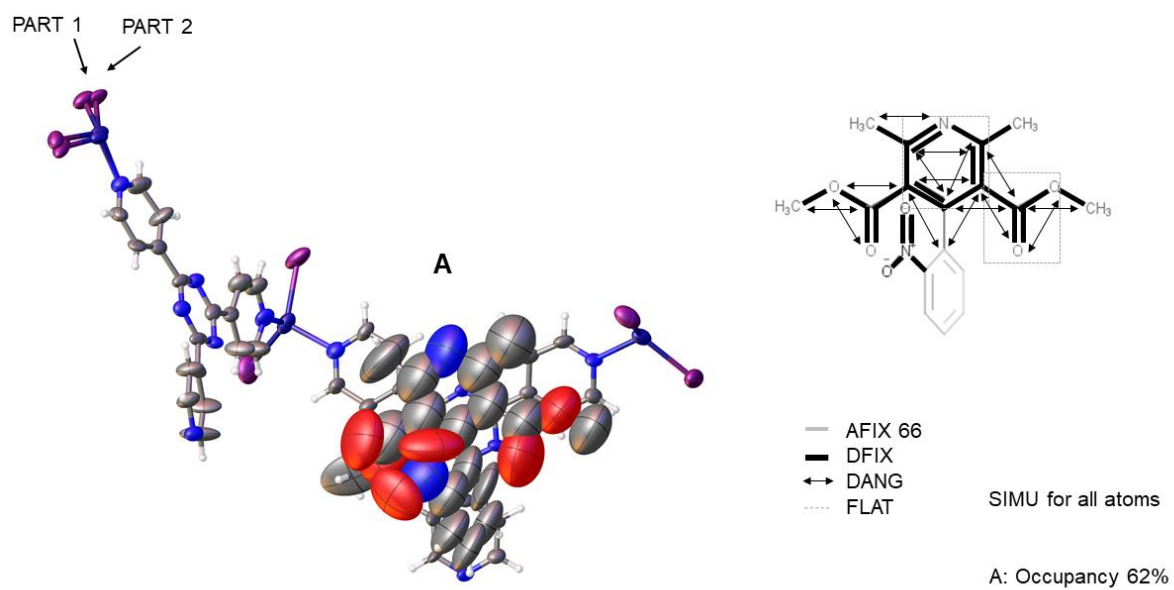
Supplemental Fig. 1. ORTEP diagram with 50% probability of the asymmetric unit of **1a•3**; restraints and constraints applied in the refinement of **1a•3**

Crystallographic data for 2a•4 (dehydro nifedipine)

Crystal size: 124 × 106 × 74 μm^3 , refined formula: $\text{C}_{53}\text{H}_{40}\text{I}_6\text{N}_{14}\text{O}_6\text{Zn}_3$, formula weight (M_r) = 1926.50 g/mol, colourless needle, crystal system: monoclinic, space group $C2/c$, $Z = 8$, 15242 unique reflections merged from recorded 66055 ones ($2.937^\circ < \theta < 74.346^\circ$) were used for structural analysis ($R_{\text{int}} = 0.0315$). Lattice parameters, R-factor on $F^2 > 2\sigma(F^2)$, weighted R-factor, and goodness-of-fit are as follows: $a = 34.6182(10) \text{ \AA}$, $b = 14.9265(3) \text{ \AA}$, $c = 30.6790(8) \text{ \AA}$, $\beta = 101.247(3)^\circ$, $V = 15548.3(7) \text{ \AA}^3$, $R = 0.0988$, $wR_2 = 0.2242$, $S = 1.038$. Calculated density is 1.646 gcm^{-3} . Linear absorption coefficient (μ) is 20.175 mm^{-1} . Residual electron density (max/min) is $1.65/-1.34 \text{ e\AA}^{-3}$. CCDC number 2051009. The ORTEP diagram of the asymmetric unit of **2a•4** is shown in Supplemental Figure 2.

The framework is refined using the constraint EADP for one disordered Zn atom. One ZnI_2 moiety is disordered and refined using disorder model. One guest molecule (A) with an occupancy of 62% was found in the asymmetric unit. The benzene ring was fixed using AFIX 66. DFIX and DANG and were used for some bonds and angles of the guest. In addition, FLAT was applied for the pyridine ring and neighboring ester moiety. SIMU was applied for all atoms of the molecule. Applied restraints can be taken from Supplemental Fig. 2. Calculation of solvent mask was used and 153 electrons were found in a volume of 556 \AA^3 in one void per asymmetric unit. This is consistent with the presence of 3.5 cyclohexane molecules per asymmetric unit which account for 1344 electrons per unit cell.

Appendix

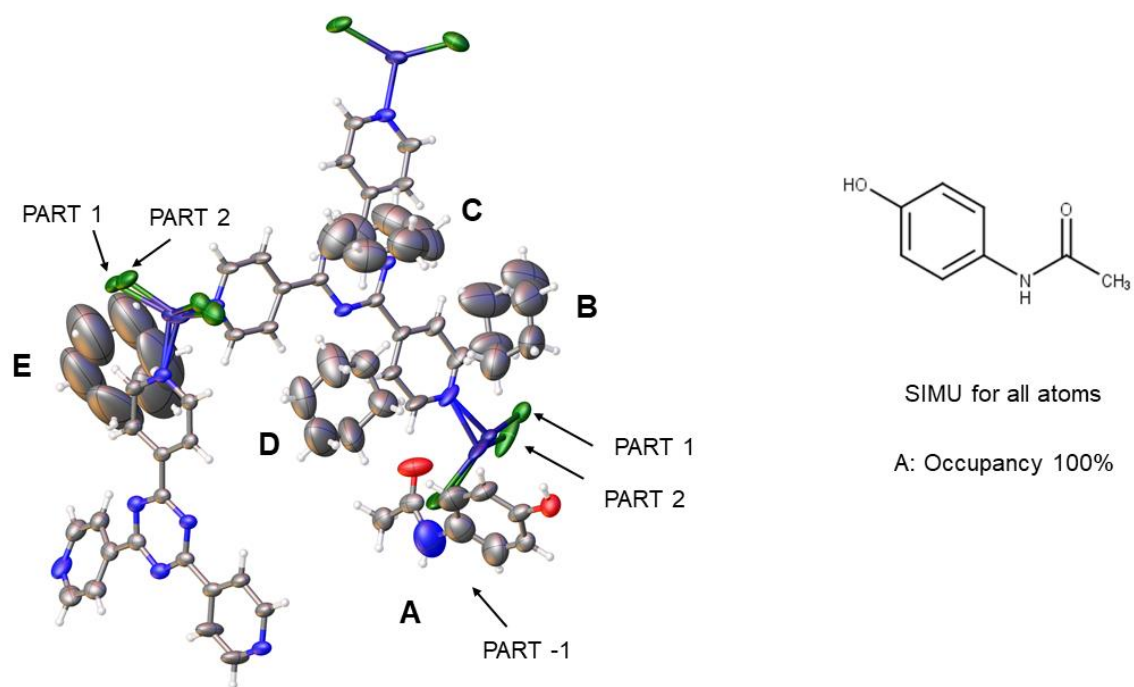


Supplemental Fig. 2. ORTEP diagram with 50% probability of the asymmetric unit of **2a•4**; restraints and constraints applied in the refinement of **2a•4**

Crystallographic data for 1a•5 (acetaminophen)

Crystal size: 171 × 110 × 69 μm^3 , refined formula: $\text{C}_{64}\text{H}_{76.5}\text{Cl}_6\text{N}_{12.5}\text{OZn}_3$, formula weight (M_r) = 1445.68 g/mol , yellow needle, crystal system: monoclinic, space group $C2/c$, $Z = 8$, 13835 unique reflections merged from recorded 53687 ones ($3.342^\circ < \theta < 74.531^\circ$) were used for structural analysis ($R_{\text{int}} = 0.0175$). Lattice parameters, R-factor on $F^2 > 2\sigma(F^2)$, weighted R-factor, and goodness-of-fit are as follows: $a = 32.6417(4) \text{ \AA}$, $b = 14.51920(10) \text{ \AA}$, $c = 30.6464(4) \text{ \AA}$, $\beta = 101.2080(10)^\circ$, $V = 14247.3(3) \text{ \AA}^3$, $R = 0.0531$, $wR_2 = 0.1541$, $S = 1.044$. Calculated density is 1.348 gcm^{-3} . Linear absorption coefficient (μ) is 3.626 mm^{-1} . Residual electron density (max/min) is $0.84/-0.46 \text{ e\AA}^{-3}$. CCDC number 2051269. The ORTEP diagram of the asymmetric unit of **1a•5** is shown in Supplemental Fig. 3.

The framework is refined without using restraints. Two ZnCl_2 moieties are disordered and refined using disorder model. One guest molecule (A) and four additional cyclohexane molecules (B-E) can be found in the asymmetric unit. The analyte lies near the center of symmetry ($C2$ axis) and is refined using PART -1. This leads to an analyte occupancy of 100%. SIMU was applied to the analyte molecule (Supplemental Fig. 3). Hydrogen bonding interactions could be observed for compound **5** between the terminal methyl group of the analyte and the ZnCl_2 of the framework ($\text{C-H}\cdots\text{Cl}$; distance 1.74 \AA) as well as between the keton moiety and the tpt ligand ($\text{C-H}\cdots\text{O}$; distance 2.22 \AA).

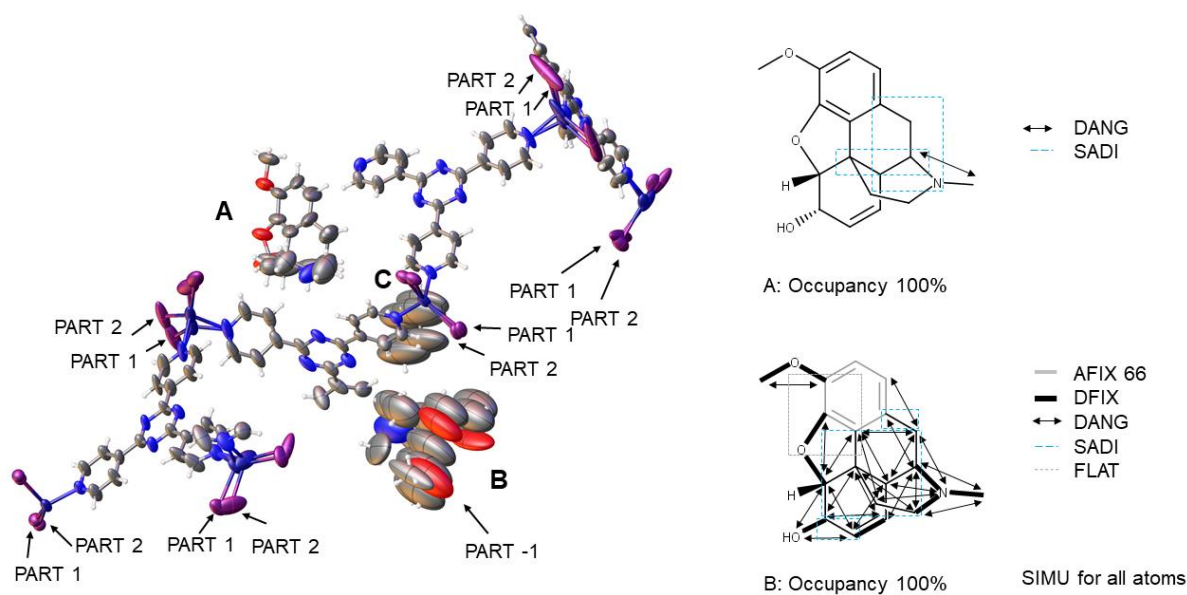


Supplemental Fig. 3. ORTEP diagram with 50% probability of the asymmetric unit of **1a•5**; restraints and constraints applied in the refinement of **1a•5**

Crystallographic data for 2a•6 (codeine)

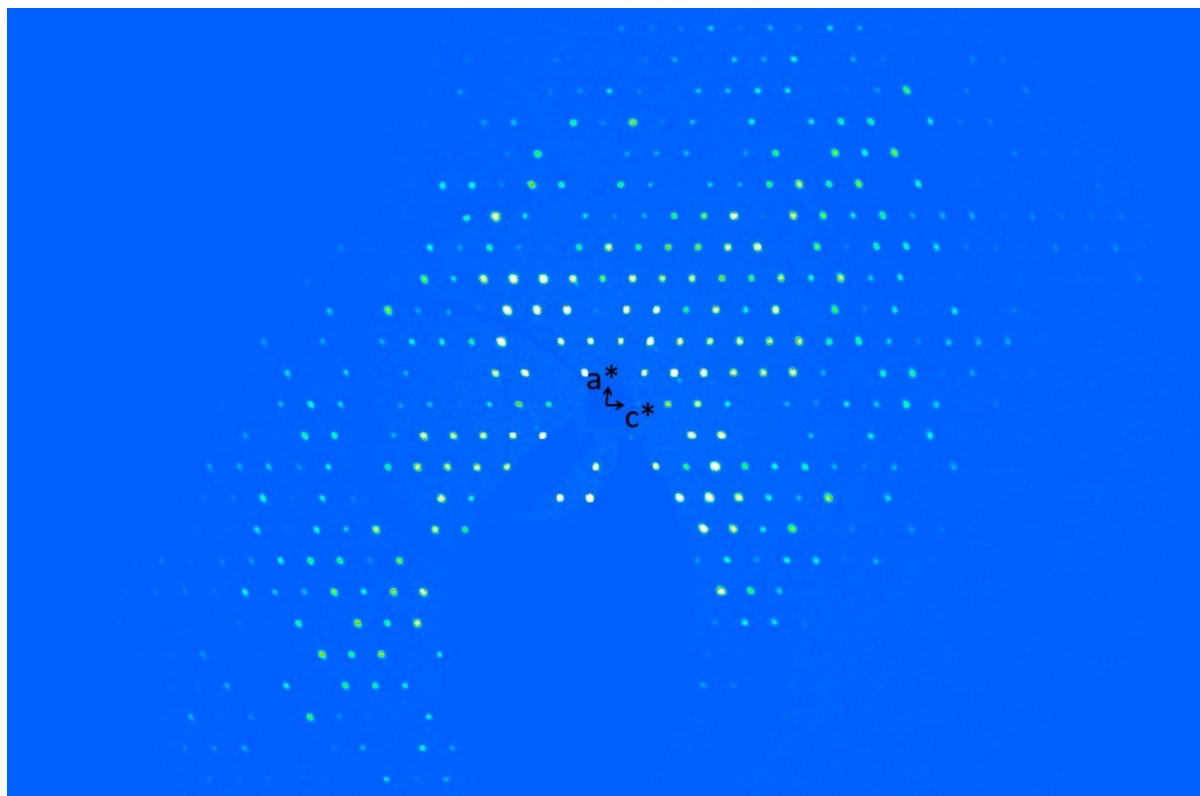
Crystal size: $193 \times 81 \times 73 \mu\text{m}^3$, refined formula: $\text{C}_{105}\text{H}_{91.5}\text{I}_{12}\text{N}_{25.5}\text{O}_{4.5}\text{Zn}_6$, formula weight (M_r) = 3697.55 g/mol , light yellow needle, crystal system: monoclinic, space group $C2$, $Z = 4$, 29183 unique reflections merged from recorded 149010 ones ($3.044^\circ < \theta < 74.446^\circ$) were used for structural analysis ($R_{\text{int}} = 0.0294$). Lattice parameters, R-factor on $F^2 > 2\sigma(F^2)$, weighted R-factor, goodness-of-fit, and Flack parameter (calculated from 9471 Parsons' quotients) are as follows: $a = 34.4052(3) \text{ \AA}$, $b = 14.98760(10) \text{ \AA}$, $c = 29.5017(2) \text{ \AA}$, $\beta = 100.2100(10)^\circ$, $V = 14971.7(2) \text{ \AA}^3$, $R = 0.0567$, $wR_2 = 0.1597$, $S = 1.060$, $\chi = 0.025(3)$. Calculated density is 1.640 gcm^{-3} . Linear absorption coefficient (μ) is 20.877 mm^{-1} . Residual electron density (max/min) is $1.41/-1.51 \text{ e\AA}^{-3}$. CCDC number 2051307. The ORTEP diagram of the asymmetric unit of **2a•6** is shown in Supplemental Fig. 4.

The framework is refined using the commands SADI for one ZnI_2 moiety, SIMU for some I atoms and EADP for two disordered I atoms. The framework exhibits disorder of six ZnI_2 parts refined using the disorder model. Two guest molecules (A, B) and one cyclohexane molecule (C) were found in the asymmetric unit. The analyte occupancy of A is 100%. The second molecule (B) is disordered at special position ($C2$ axis) and refined using PART -1 command and s.o.f. = 0.5. DANG and SADI was applied for analyte A. AFIX66 was applied to the benzene ring and DFIX, DANG and SADI were used for some bonds and angles of guest B (see Supplemental Fig. 4). Both guest molecules were refined with applying SIMU. Additional electron density was found that could not be assigned due to disorder. Contribution of this electron density was removed using solvent masking algorithm implemented in OLEX2. A solvent mask was calculated, and 96 electrons were found in a volume of 420 \AA^3 in one void per asymmetric unit. This is consistent with the presence of 2 cyclohexane molecules per asymmetric unit.

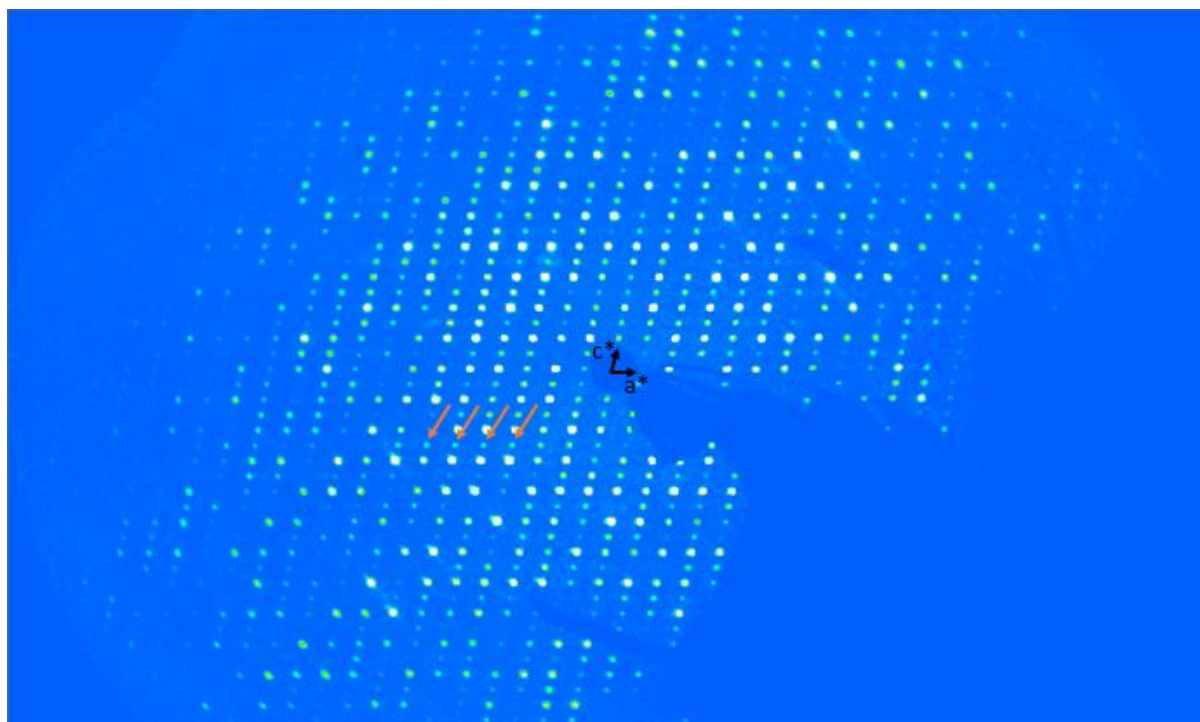


Supplemental Fig. 4. ORTEP diagram with 50% probability of the asymmetric unit of **2a•6**; restraints and constraints applied in the refinement of **2a•6**

Compound **6** was used as enantiomerically pure substance. Several examples have shown that the crystalline sponge method can be used to determine the absolute structure of soaked analytes because soaking of chiral molecules lead to lowering of the symmetry from $C2/c$ to $C2$ or $P2_1$ (Hoshino et al., 2016; Zigon et al., 2015). To assure the correct space group assignment during data processing, extinction rules for C centering (hkl , $h+k=\text{odd}$) and the existence of the c glide plane ($h0l$, $l=\text{odd}$) were evaluated. The reciprocal space of **2a•6** was inspected for the $h0l$ layer, clearly revealing Bragg spots $h=2n$ and $l=n$. Therefore, the data reduction and structure solution were executed for space group $C2$. For typical $C2/c$ example for comparison see Supplemental Fig. 5, after soaking see Supplemental Fig. 6.



Supplemental Fig. 5. Reciprocal $h0l$ layer of a typical crystalline sponge crystal before soaking in $C2/c$. Absence of $h=\text{odd}$ and $l=\text{odd}$ reflexes is clearly visible.

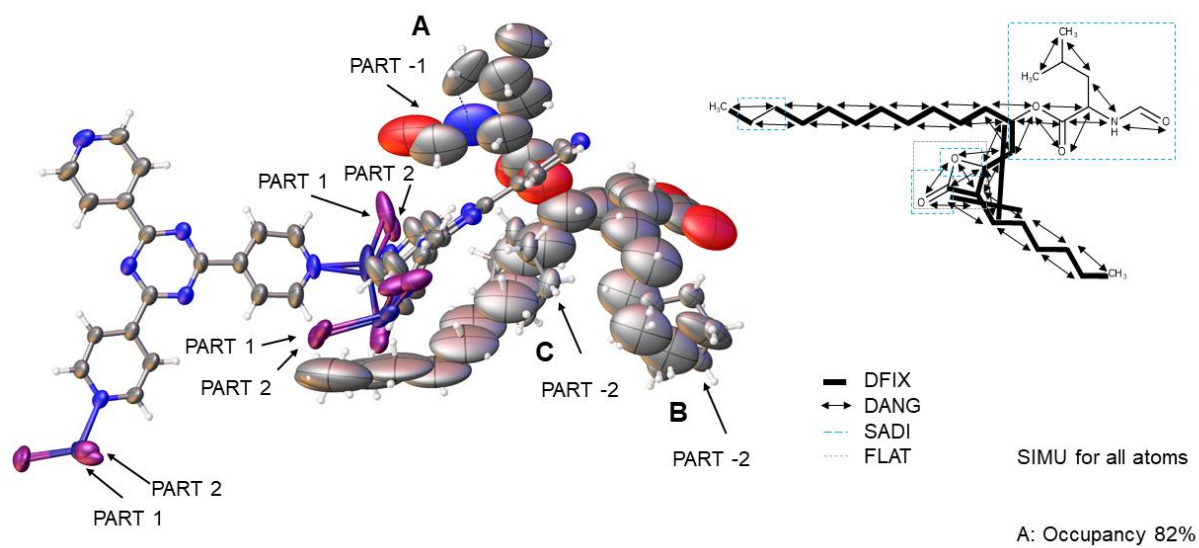


Supplemental Fig. 6. Reciprocal $h0l$ layer after soaking **6** into crystalline sponge. Reflexes at $h=2n$ and $l=n$ (highlighted with orange arrows) clearly visible.

Crystallographic data for 2a•7 (orlistat)

Crystal size: 161 × 93 × 62 μm³, refined formula: C_{48.94}H_{68.89}I₆N_{12.41}O_{2.04}Zn₃, formula weight (M_r) = 1821.28 g/mol, colourless needle, crystal system: monoclinic, space group C2/c, Z = 8, 15103 unique reflections merged from recorded 49594 ones (2.613° < θ < 75.674°) were used for structural analysis (R_{int} = 0.0456). Lattice parameters, R-factor on F² > 2σ (F²), weighted R-factor, and goodness-of-fit are as follows: a = 34.3807(8) Å, b = 14.9845(2) Å, c = 30.1529(8) Å, β = 100.353(2)°, V = 15281.1(6) Å³, R = 0.0722, wR₂ = 0.2186, S = 1.046. Calculated density is 1.583 gcm⁻³. Linear absorption coefficient (μ) is 20.432 mm⁻¹. Residual electron density (max/min) is 1.06/-0.91 eÅ⁻³. CCDC number 2051278. The ORTEP diagram of the asymmetric unit of **2a•7** is shown in Supplemental Figure 7.

The framework is refined using one restrain (DFIX) and exhibits disorder of three ZnI₂ parts. One guest molecule (A) can be found in the asymmetric unit disordered with two cyclohexane (B, C) molecules. The analyte and solvent molecules lie near the center of symmetry (C2 axis) and A is therefore refined using PART -1 with s.o.f. = 0.5x(FVAR#5). The cyclohexane molecules are refined using PART -2 with s.o.f. = 0.5x(1-FVAR#5). This leads to an analyte occupancy of 82%. The positions of carbon atoms in the alkyl chains and the lactone ring had to be restrained to their theoretical values applying DFIX, SADI and DANG commands due to high mobility. In addition, FLAT was applied for the lactone ring (see Supplemental Fig. 7). Two intramolecular hydrogen bonds could be observed by the short C–H⋯O distance (2.30 Å) and C–H⋯N distance (2.02 Å).



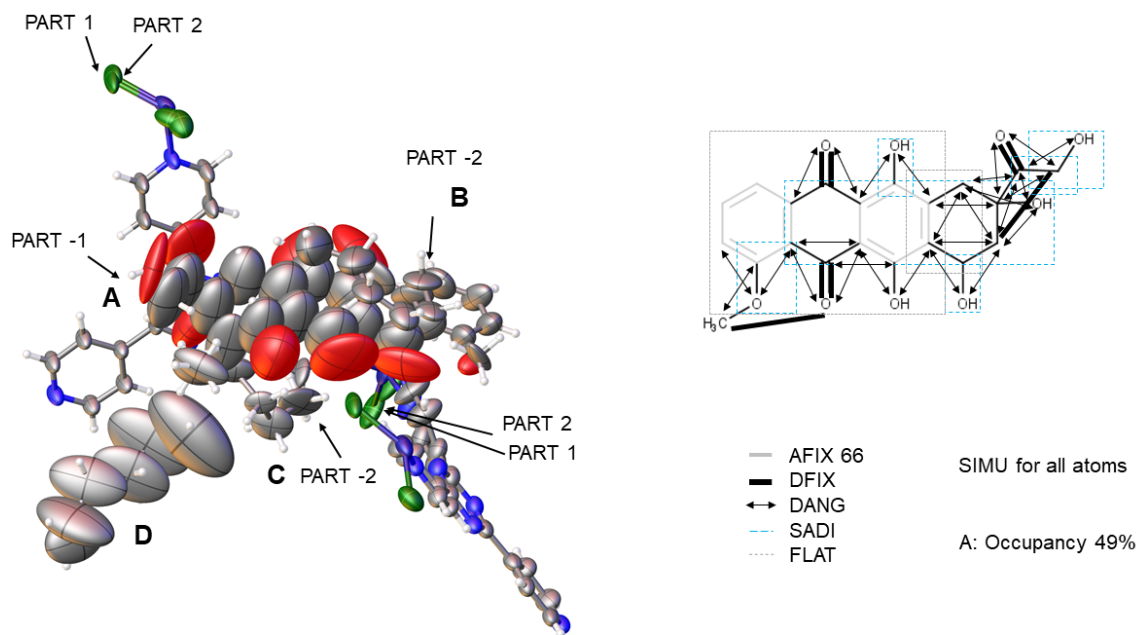
Supplemental Fig. 7. ORTEP diagram with 50% probability of the asymmetric unit of **2a•7**; restraints and constraints applied in the refinement of **2a•7**

Crystallographic data for 1b•8 (doxorubicinone)

Crystal size: 228 × 124 × 86 μm^3 , refined formula: $\text{C}_{50.2}\text{H}_{55.49}\text{Cl}_6\text{N}_{12}\text{O}_{2.21}\text{Zn}_3$, formula weight (M_r) = 1271.10 g/mol, red needle, crystal system: monoclinic, space group $C2/c$, $Z = 8$, 14083 unique reflections merged from recorded 49240 ones ($2.76^\circ < \theta < 74.57^\circ$) were used for structural analysis ($R_{\text{int}} = 0.0137$). Lattice parameters, R-factor on $F^2 > 2\sigma(F^2)$, weighted R-factor, and goodness-of-fit are as follows: $a = 32.5418(4) \text{ \AA}$, $b = 14.37930(10) \text{ \AA}$, $c = 31.3438(3) \text{ \AA}$, $\beta = 100.2560(10)^\circ$, $V = 14432.3(3) \text{ \AA}^3$, $R = 0.0805$, $wR_2 = 0.2542$, $S = 1.055$. Calculated density is 1.170 gcm^{-3} . Linear absorption coefficient (μ) is 3.526 mm^{-1} . Residual electron density (max/min) is $1.34/-0.70 \text{ e\AA}^{-3}$. CCDC number 2051280. The ORTEP diagram of the asymmetric unit of **1b•8** is shown in Supplemental Figure 8.

The framework is refined without using restraints and exhibits disorder of two ZnCl_2 parts. One guest molecule (A) can be found in the asymmetric unit disordered with two n-hexane (B, C) molecules. One additional n-hexane molecule without disorder (D) can be found in the asymmetric unit. The analyte and two n-hexane molecules lie near the center of symmetry ($C2$ axis). Therefore, the analyte is refined using PART -1 with s.o.f. = $0.5x(\text{FVAR}\#3)$ and the disordered n-hexane molecules are refined using PART -2 with s.o.f. = $0.5x(1-\text{FVAR}\#3)$. This leads to an analyte occupancy of 49%. AFIX 66 was applied to the benzene ring, and DFIX and DANG were used for some bonds and angles of the guest. C-C and C-O bonds were restrained using SADI command. In addition, FLAT was applied for four-membered ring system (see Supplemental Fig. 8). SIMU was applied for all analyte molecules. Intramolecular hydrogen bonding was observed by the short O–H \cdots O distance (1.98 \AA) between two hydroxy groups intermolecular hydrogen bonding was indicated between one hydroxy group of the analyte and one pyridine hydrogen of the framework (C–H \cdots O; distance 2.23 \AA).

Appendix

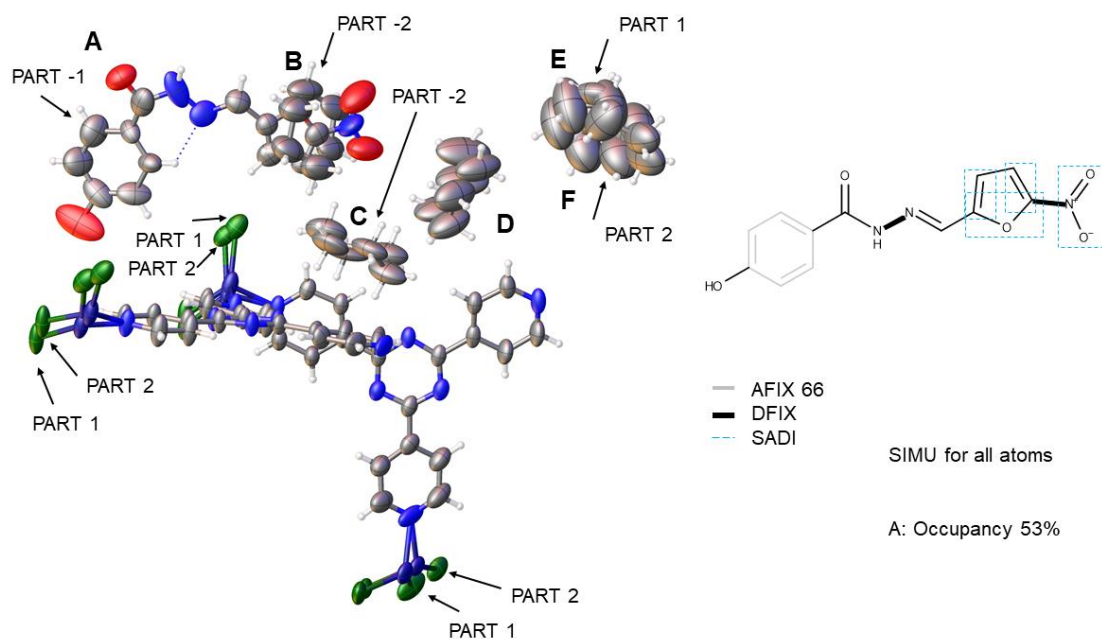


Supplemental Fig. 8. ORTEP diagram with 50% probability of the asymmetric unit of **1b•8**; restraints and constraints applied in the refinement of **1b•8**

Crystallographic data for 1a•9 (nifuroxazid)

Crystal size: 170 × 130 × 100 μm³, refined formula: C_{50.93}H_{50.95}Cl₆N_{12.79}O_{1.32}Zn₃, formula weight (M_r) = 1272.17 g/mol, light orange needle, crystal system: monoclinic, space group C2/c, Z = 8, 13624 unique reflections merged from recorded 56635 ones (3.359° < θ < 74.631°) were used for structural analysis (R_{int} = 0.0157). Lattice parameters, R-factor on F² > 2σ (F²), weighted R-factor, and goodness-of-fit are as follows: a = 32.2222(4) Å, b = 14.46130(10) Å, c = 30.4099(4) Å, β = 100.4930(10)°, V = 13933.3(3) Å³, R = 0.0649, wR₂ = 0.1985, S = 1.060. Calculated density is 1.213 gcm⁻³. Linear absorption coefficient (μ) is 3.648 mm⁻¹. Residual electron density (max/min) is 0.89/-0.57 eÅ⁻³. CCDC number 2051286. The ORTEP diagram of the asymmetric unit of **1a•9** is shown in Supplemental Figure 9.

The framework is refined using the constraint EADP for one ZnCl₂ moiety. Three ZnCl₂ moieties are disordered and refined using disorder model. One guest molecule (A) can be found in the asymmetric unit disordered with two cyclohexane (B, C) molecules. Two additional cyclohexane molecules, one without disorder (D) and one disordered with a second cyclohexane (E, F) and can be found in the asymmetric unit. The analyte molecule and the two cyclohexane molecules lie near the center of symmetry (C2 axis). Therefore, the analyte is refined using PART -1 with s.o.f. = 0.5x(FVAR#6) and the disordered cyclohexane molecules are refined using PART -2 with s.o.f. = 0.5x(FVAR#6) and s.o.f. = 0.5x (1-FVAR#6). This leads to an analyte occupancy of 53%. AFIX 66 was applied to the benzene ring, and DFIX and SADI were used for some bonds of the guest (see Supplemental Fig. 9). Intramolecular hydrogen bonding was indicated by the short C–H⋯N distance (2.18 Å) between one nitrogen and the benzene ring.



Supplemental Fig. 9. ORTEP diagram with 50% probability of the asymmetric unit of **1a•9**; restraints and constraints applied in the refinement of **1a•9**

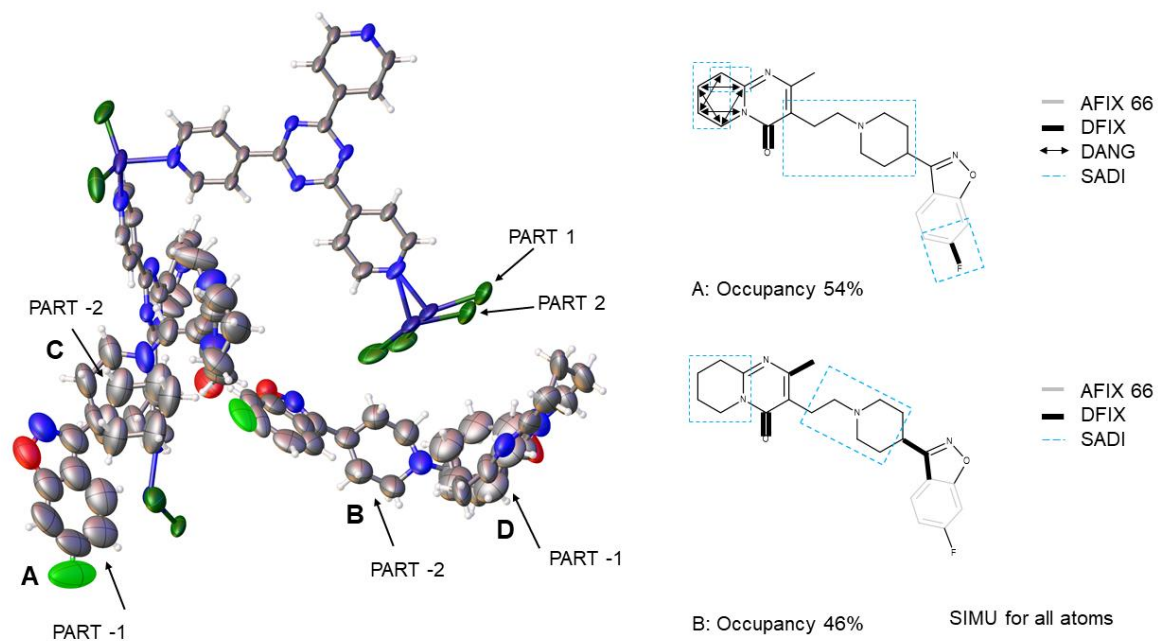
Crystallographic data for **1b•10** (imipramine)

Successful elucidation of host-guest complex **1b•10** was shown by CS-XRD in earlier works (Sakurai et al., 2017). Obtained crystallographic data corresponds to already published results.

Crystallographic data for 1a•11 (risperidone)

Crystal size: 137 × 80 × 47 μm³, refined formula: C_{50.5}H_{43.5}Cl₆F_{0.5}N₁₄OZn₃, formula weight (M_r) = 1280.80 g/mol, colourless needle, crystal system: monoclinic, space group C2/c, Z = 8, 14467 unique reflections merged from recorded 52253 ones (2.879° < θ < 77.113°) were used for structural analysis (R_{int} = 0.0306). Lattice parameters, R-factor on F² > 2σ (F²), weighted R-factor, and goodness-of-fit are as follows: a = 32.9196(8) Å, b = 14.4178(2) Å, c = 31.2975(8) Å, β = 101.249(2)°, V = 14569.3(6) Å³, R = 0.0986, wR₂ = 0.2854, S = 1.090. Calculated density is 1.168 gcm⁻³. Linear absorption coefficient (μ) is 3.506 mm⁻¹. Residual electron density (max/min) is 0.89/-0.60 eÅ⁻³. CCDC number 2051287. The ORTEP diagram of the asymmetric unit of **1a•11** is shown in Supplemental Figure 10.

The framework is refined using the constraint EADP for one ZnCl₂ moiety. One ZnCl₂ moiety is disordered and refined using disorder model. Two guest molecules (A and B) can be found in the asymmetric unit disordered with two cyclohexane (B, C) molecules. All guest molecules lie near the center of symmetry (C2 axis). Therefore, analyte A is refined using PART -1 with s.o.f. = 0.5x(FVAR#3) and the disordered cyclohexane molecule (C) is refined using PART -2 with s.o.f. = 0.5x(1-FVAR#3). The second analyte molecule (B) is refined using PART -2 with s.o.f. = 0.5x(1-FVAR#3) and the disordered cyclohexane molecule (D) is refined using PART -1 with s.o.f. = 0.5x(FVAR#3). This leads to an analyte occupancy of 54% for analyte A and 46% for analyte B. AFIX 66 was applied to the benzene ring, and DFIX and DANG were used for some bonds and angles of the guest. C-C, C-N and C-F bonds were restrained using SADI command (see Supplemental Fig. 10). SIMU was applied for all analyte molecules. Compound **11** interacts with the framework by C–H ⋯N interactions (distance 1.96 Å) between the pyrimidine of the analyte and the tpt of the framework.



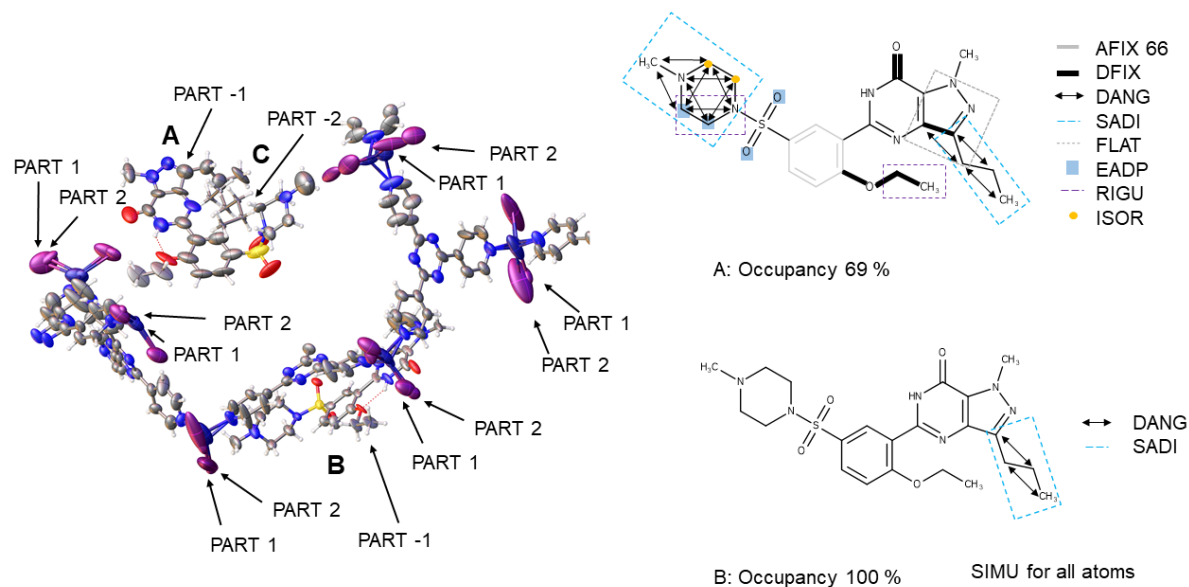
Supplemental Fig. 10. ORTEP diagram with 50% probability of the asymmetric unit of **1a•11**; restraints and constraints applied in the refinement of **1a•11**

Crystallographic data for 2a•12 (sildenafil)

Crystal size: 303 × 174 × 64 μm³, refined formula: C_{91.53}H_{76.55}I₁₂N_{29.07}O_{3.38}S_{0.84}Zn₆, formula weight (M_r) = 3580.06 g/mol, colourless needle, crystal system: monoclinic, space group *P2/c*, Z = 4, 29303 unique reflections merged from recorded 124098 ones (2.665° < θ < 74.336°) were used for structural analysis (R_{int} = 0.0500). Lattice parameters, R-factor on F² > 2σ (F²), weighted R-factor, and goodness-of-fit are as follows: a = 33.6086(6) Å, b = 15.0556(2) Å, c = 29.9880(4) Å, β = 99.423(2)°, V = 14969.1(4) Å³, R = 0.1199, wR₂ = 0.3401, S = 1.019. Calculated density is 1.589 gcm⁻³. Linear absorption coefficient (μ) is 20.968 mm⁻¹. Residual electron density (max/min) is 2.08/-1.82 eÅ⁻³. CCDC number 2051288. The ORTEP diagram of the asymmetric unit of **2a•12** is shown in Supplemental Figure 11.

The framework is refined using the restraints SADI (for some tpt C atoms), DFIX (between one Zn and one C atom) and SIMU (for one disordered ZnI₂ moiety and some atoms of a pyridine ring). The framework exhibits disorder of six ZnI₂ parts refined using the disorder model. Two guest molecules (A, B), one disordered with a n-hexane (C), were found in the asymmetric unit. The analyte occupancy of A and B are 69% and 100%, respectively. The analyte molecules lie near the center of symmetry (C₂ axis) and were refined using command PART - 1 with s.o.f. = 0.5x(FVAR#8) (A) and PART -1 with s.o.f. = 0.5 (B). The disordered n-hexane molecule (C) is refined using PART -2 with s.o.f. = 0.5x(1-FVAR#8). AFIX66 was applied to the benzene ring and DFIX, DANG and SADI were used for some bonds and angles of guest A. FLAT was used for the pyrazole ring and RIGU for the ethyl side chain. In addition, RIGU, ISOR and EADP was applied to the piperazine ring and sulfur dioxide oxygen atoms of the guest. DANG and SADI was applied for analyte B. Both guest molecules were refined with applying SIMU. Applied restraints can be taken from Supplemental Fig. 11. Additional electron density was found that could not be assigned due to disorder. Contribution of this electron density was removed using solvent masking algorithm implemented in OLEX2. A solvent mask was calculated per asymmetric unit and 18 and 70 electrons were found in a volume of 108 Å³ and 311 Å³, respectively. This is consistent with the presence of 2 n-hexane molecules per

asymmetric unit. Intramolecular hydrogen bonding was indicated by the short N–H···O distance (1.82 Å and 1.94 Å) between one ether and one secondary nitrogen group.



Supplemental Fig. 11. ORTEP diagram with 50% probability of the asymmetric unit of **2a•12**; restraints and constraints applied in the refinement of **2a•12**

Crystallographic data for **1a•18** (gemfibrozil)

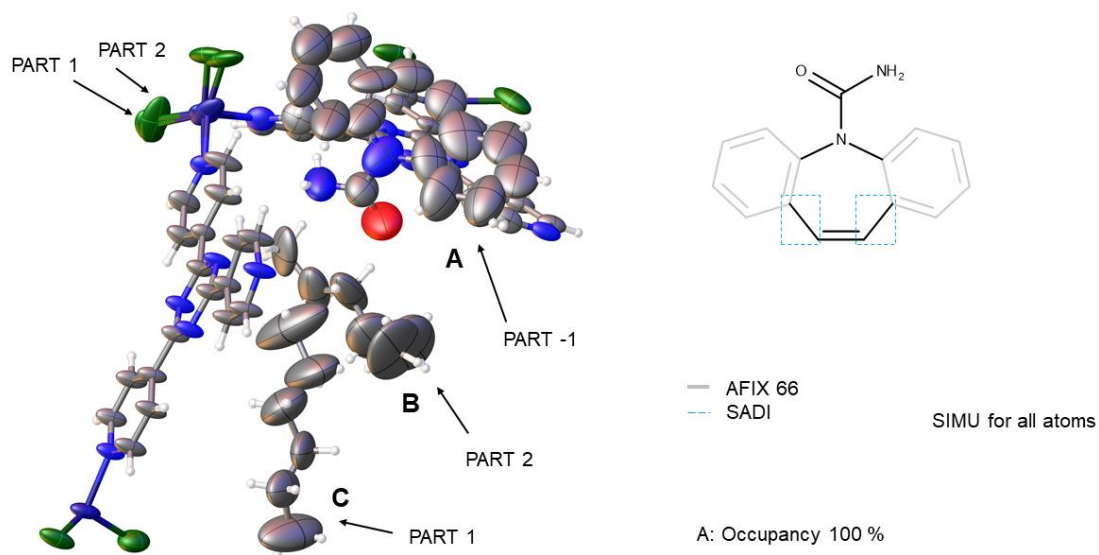
Successful elucidation of host-guest complex **1a•18** was shown by CS-XRD in our previous work (Rosenberger et al., 2020). Obtained crystallographic data corresponds to already published results.

Crystallographic data for 1b•19 (carbamazepine)

Crystal size: 150 × 70 × 58 μm³, refined formula: C_{49.5}H₄₄Cl₆N₁₃O_{0.5}Zn₃, formula weight (M_r) = 1237.78 g/mol, colourless needle, crystal system: monoclinic, space group C2/c, Z = 8, 13842 unique reflections merged from recorded 45415 ones (2.748° < θ < 74.535°) were used for structural analysis (R_{int} = 0.0176). Lattice parameters, R-factor on F² > 2σ (F²), weighted R-factor, and goodness-of-fit are as follows: a = 32.6483(4) Å, b = 14.40370(10) Å, c = 30.8462(4) Å, β = 99.8950(10)°, V = 14289.8(3) Å³, R = 0.0739, wR₂ = 0.2415, S = 1.034. Calculated density is 1.151 gcm⁻³. Linear absorption coefficient (μ) is 3.538 mm⁻¹. Residual electron density (max/min) is 1.27/-0.47 eÅ⁻³. CCDC number 2051333. The ORTEP diagram of the asymmetric unit of **1b•19** is shown in Supplemental Figure 12.

The framework exhibits disorder of one ZnCl₂ part. One guest molecule (A) and two additional n-hexane molecules (B and C) can be found in the asymmetric unit. The analyte lies near the center of symmetry (C2 axis) and is refined using PART -1. This leads to an analyte occupancy of 100%. Solvent molecules B and C are disordered and refined using PART 1 with s.o.f. = (FVAR#3) and PART 2 with s.o.f. = (1-FVAR#3). The benzene rings of molecule A were fixed using AFIX 66 and two C-C bonds were restrained using SADI. SIMU was applied for all atoms of the analyte molecule (Supplemental Fig. 12). A solvent mask was calculated per asymmetric unit and 52 electrons were found in a volume of 250 Å³. This is consistent with the presence of 1 n-hexane molecule per asymmetric unit.

Appendix

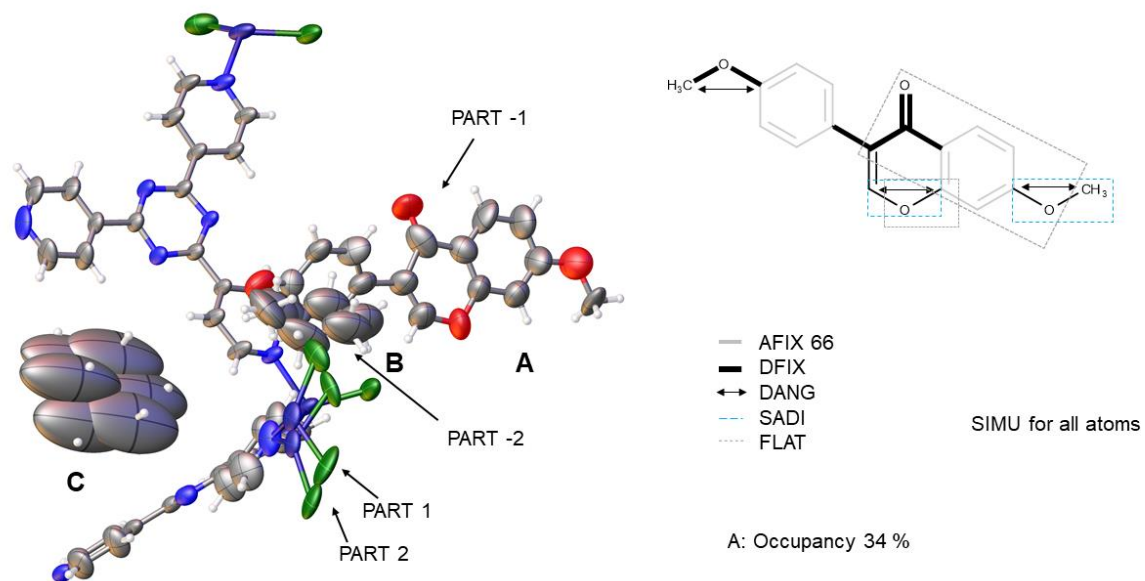


Supplemental Fig. 12. ORTEP diagram with 50% probability of the asymmetric unit of **1b•19**; restraints and constraints applied in the refinement of **1b•19**

Crystallographic data for 1a•20 (4'-7-dimethoxyisoflavone)

Crystal size: 154 × 80 × 46 μm³, refined formula: C_{46.89}H_{47.83}Cl₆N₁₂O_{0.69}Zn₃, formula weight (M_r) = 1199.22 g/mol, colourless needle, crystal system: monoclinic, space group C2/c, Z = 8, 13822 unique reflections merged from recorded 46345 ones (2.76° < θ < 76.723°) were used for structural analysis (R_{int} = 0.0271). Lattice parameters, R-factor on F² > 2σ (F²), weighted R-factor, and goodness-of-fit are as follows: a = 32.5199(12) Å, b = 14.4610(3) Å, c = 30.5970(12) Å, β = 100.056(3)°, V = 14167.8(8) Å³, R = 0.0679, wR₂ = 0.2066, S = 1.045. Calculated density is 1.124 gcm⁻³. Linear absorption coefficient (μ) is 3.548 mm⁻¹. Residual electron density (max/min) is 0.91/-1.31 eÅ⁻³. CCDC number 2051294. The ORTEP diagram of the asymmetric unit of **1a•20** is shown in Supplemental Figure 13.

The framework is refined without using restraints and exhibits disorder of one ZnCl₂ part. One guest molecule (A) can be found in the asymmetric unit disordered with one cyclohexane (B) molecule. One additional cyclohexane molecule without disorder (C) can be found in the asymmetric unit. The analyte and one cyclohexane molecule were disordered at special position (inversion). Therefore, the analyte is refined using PART -1 with s.o.f. = 0.5x(FVAR#3) and the disordered cyclohexane molecule is refined using PART -2 with s.o.f. = 0.5x(1-FVAR#3). This leads to an analyte occupancy of 34%. AFIX 66 was applied to the benzene rings, and DFIX and DANG were used for some bonds and angles of the guest. C-O bonds were restrained using SADI command and FLAT was applied for the fused ring system (see Supplemental Fig. 13). SIMU was applied for all analyte molecules. A solvent mask was calculated and 115 electrons were found in a volume of 430 Å³ in one void per asymmetric unit, consisting with the presence of 2.5 cyclohexane molecules. It was observed that guest **20** is stabilized by π-π stacking interactions between its aromatic ring and the tpt ligand of the framework (distance 3.31 Å, angle 16.33°). Intramolecular hydrogen bonding was indicated by the short C-H...O distance (2.32 Å) between one oxygen and one benzene ring and intermolecular hydrogen bonding was observed between one ether group of the analyte and one pyridine hydrogen of the framework (C-H...O; distance 2.27 Å).



Supplemental Fig. 13. ORTEP diagram with 50% probability of the asymmetric unit of **1a•20**; restraints and constraints applied in the refinement of **1a•20**

References

- Biradha, K., Fujita, M., 2002. A springlike 3D-coordination network that shrinks or swells in a crystal-to-crystal manner upon guest removal or readsorption. *Angew. Chem. Int. Ed. Engl.* 41, 3392–3395.
- Cuenca, A.B., Zigon, N., Duplan, V., Hoshino, M., Fujita, M., Fernández, E., 2016. Undeniable Confirmation of the syn-Addition Mechanism for Metal-Free Diboration by Using the Crystalline Sponge Method. *Chem. Eur. J.* 22, 4723–4726.
- Dolomanov, O.V., Bourhis, L.J., Gildea, R.J., Howard, J.A.K., Puschmann, H., 2009. OLEX2: a complete structure solution, refinement and analysis program. *J. Appl. Crystallogr.* 42, 339-341.
- Hoshino, M., Khutia, A., Xing, H., Inokuma, Y., Fujita, M., 2016. The crystalline sponge method update. *I.U.Cr.J.* 3, 139-151.
- Inokuma, Y., Ukegawa, T., Hoshino, M., Fujita, M., 2016. Structure determination of microbial metabolites by the crystalline sponge method. *Chem. Sci.* 7, 3910–3913.
- Ramadhar, T.R., Zheng, S.L., Chen, Y.S., Clardy, J., 2015. Analysis of rapidly synthesized guest-filled porous complexes with synchrotron radiation: practical guidelines for the crystalline sponge method. *Acta. Crystallogr. A Found. Adv.* 71(Pt 1), 46–58.
- Rosenberger, L., von Essen, C., Khutia, A., Kühn, C., Urbahns, K., Georgi, K., Hartmann, R.W., Badolo, L., 2020. Crystalline sponges as a sensitive and fast method for metabolite identification: application to gemfibrozil and its phase I and II metabolites. *Drug. Metab. Dispos.* 48, 587-593.
- Sakurai, F., Khutia, A., Kikuchi, T., Fujita, M., 2017. X-ray structure analysis of n-containing nucleophilic compounds by the crystalline sponge method. *Chem. Eur. J.* 23, 15035-15040.
- Sanna, E., Escudero-Adán, E.C., Bauzá, A., Ballester, P., Frontera, A., Rotger, C., Costa, A., 2015. A crystalline sponge based on dispersive forces suitable for X-ray structure determination of included molecular guests. *Chem. Sci.* 6, 5466–5472.

Appendix

Sheldrick, G.M., 2015. Crystal structure refinement with SHELXL. *Acta Crystallogr. C Struct. Chem.* 71, 3-8.

Zigon, N., Hoshino, M., Yoshioka, S., Inokuma, Y., Fujita, M., 2015. Where is the Oxygen? Structural Analysis of α -Humulene Oxidation Products by the Crystalline Sponge Method. *Angew. Chem. Int. Ed.* 54, 9033–9037.

7.3 Supporting Information Chapter C

Supplemental Data for

Metabolic profiling of S-praziquantel: Structure elucidation using the crystalline sponge method in combination with mass spectrometry and nuclear magnetic resonance

Lara Rosenberger, Judith Jenniches, Carolina von Essen, Anupam Khutia, Clemens Kühn, Andreas Marx, Katrin Georgi, Anna K. H. Hirsch, Rolf W. Hartmann, Lassina Badolo

Merck KGaA, Frankfurter Strasse 250, 64293 Darmstadt, Germany (L.R., J.J., C.v.E., A.K., C.K., A.M., K.G., L.B.)

Helmholtz-Institute for Pharmaceutical Research Saarland (HIPS) - Helmholtz Centre for Infection Research (HZI), Campus E8.1, 66123 Saarbrücken, Germany (L.R., A.K.H.H., R.W.H.)

Department of Pharmacy, Saarland University, Campus E8.1, 66123 Saarbrücken, Germany (L.R., A.K.H.H., R.W.H.)

Preparation of crystalline sponges

The porous crystalline sponges $[(ZnI_2)_3 \cdot (tpt)_2]_n \cdot x(\text{cyclohexane})_m$ (**1a**) and $[(ZnI_2)_3 \cdot (tpt)_2]_n \cdot x(\text{n-hexane})_m$ (**1b**), were prepared following the reported procedures (Biradha and Fujita, 2002; Ramadhar et al., 2015).

Single-crystal X-ray diffraction experiments

Single crystal X-ray diffraction measurements were conducted on a Rigaku Oxford Diffraction XtaLAB Synergy-R diffractometer using Cu-K $_{\alpha}$ X-ray radiation ($\lambda = 1.54184 \text{ \AA}$), equipped with a HyPix-Arc 150° Hybrid Photon Counting (HPC) detector (Rigaku, Tokyo, Japan) at a temperature of 100 K using a Cryostream 800 nitrogen stream (Oxford Cryostreams, UK). The software CrysAlisPro ver. 171.41.68a (S-/R-M6 praziquantel), ver. 171.41.99 (M1 praziquantel, R-M6 praziquantel) and ver. 171.41.113a (S-praziquantel, M2 praziquantel, M3 praziquantel and M4 praziquantel) was used for calculation of measurement strategy, data reduction (data integration, empirical and numerical absorption corrections and scaling) and the generation of the $h0l$ layers. The software ShelXle was used to generate the electron density maps F_o to verify the position of metabolism (Hübschle et al., 2011). Isocontour levels are described as σ (square root of the average variance of the density).

Crystal structure analysis

All crystal structures were modeled using OLEX2 (Dolomanov et al., 2009), solved with SHELXT ver. 2014/5 and refined using SHELXL ver. 2018/1 (Sheldrick, 2015). Figures of framework and analyte were created using OLEX2. Non-hydrogen atoms were refined anisotropically. Hydrogen atoms were fixed using the riding model. Populations of the guests in the crystal were modelled by least-square refinement of a guest/solvent disorder model under the constraint that the sum of them should equal to 100%. The number of used

constraints and restraints was tried to minimize and applied without changing the standard deviation. Solvent cyclohexane molecules in the pores were found in the difference electron density map and refined using the restraints (DFIX, DANG, SIMU, RIGU and SADI). These molecules are expected to be severely disordered due their high thermal motion. Due to their averaged structure of various geometry and orientation, some cyclohexane molecules are distorted to energetically-unfavorable (boat-shaped or twisted) structures. One “Alert A” notification was found by the validation program CheckCIF. This alert is derived from undefined solvent molecules is unavoidable due to severe disorder. The comments for the alerts are described in the CIFs using the validation response form (vrf).

Solvent masking algorithm was applied during structure refinement. The Flack parameters before and after solvent masking including their estimated standard deviations are described (Classic Flack method).

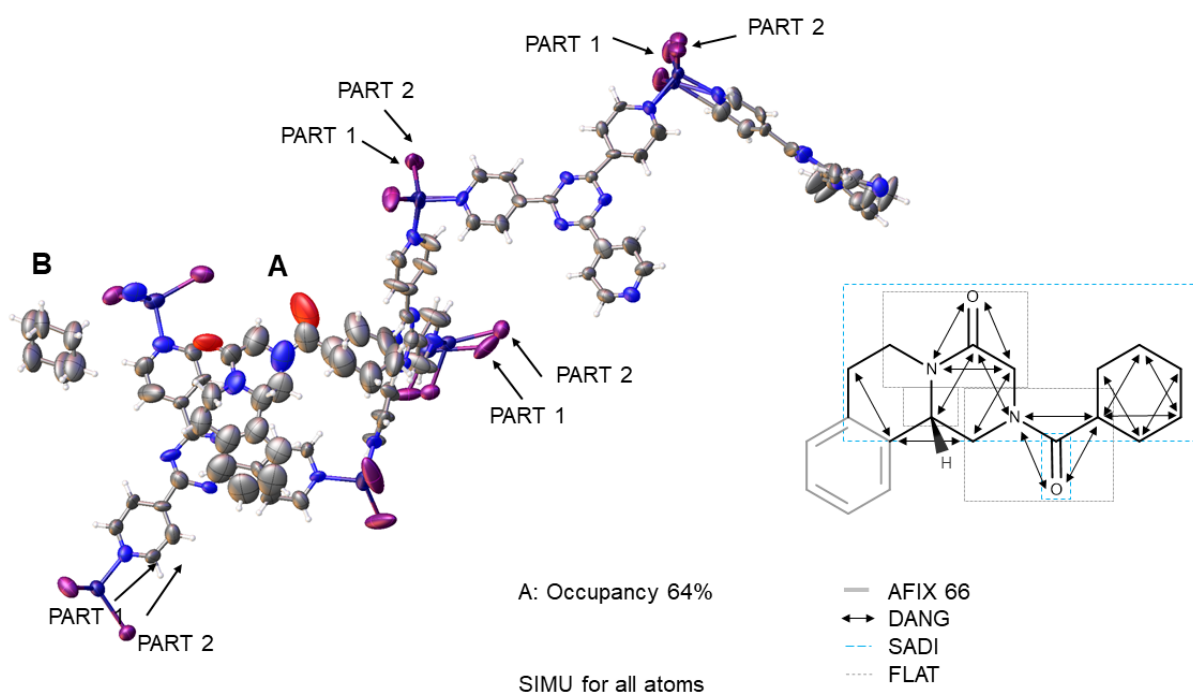
The present crystal structures are not used for exact structure analysis. They are used to confirm structure proposals derived from information obtained from mass spectrometry and knowledge of the parent structure. Therefore, details of the crystals structure (bond lengths, angles, etc.) will not be discussed.

Crystallographic data for 1a•S-praziquantel (after solvent masking)

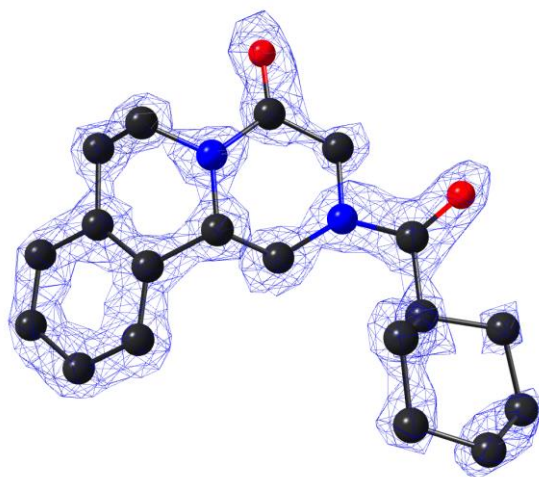
Crystal size: 342 × 180 × 97 μm³, refined formula: C_{87.57}H_{69.78}I₁₂N_{25.28}O_{1.28}Zn₆, formula weight (M_r) = 3411.76 g/mol, light yellow needle, crystal system: monoclinic, space group C2, Z = 4, 27315 unique reflections merged from recorded 145718 ones (2.579° < θ < 67.078°) were used for structural analysis (R_{int} = 0.0308). Lattice parameters, R-factor on F² > 2σ (F²), weighted R-factor, and goodness-of-fit are as follows: a = 35.2195(4) Å, b = 14.7904(2) Å, c = 32.5945(4) Å, β = 103.339(1)°, V = 16520.8(4) Å³, R = 0.0823, wR₂ = 0.2695, S = 1.123. Calculated density is 1.372 gcm⁻³. Linear absorption coefficient (μ) is 18.857 mm⁻¹. Residual electron density (max/min) is 1.95/-1.24 eÅ⁻³. The Flack parameters for S-praziquantel before and after using solvent masking were χ = 0.146(9) and χ = 0.234(8), respectively. CCDC number 2104973. The ORTEP diagram of the asymmetric unit of the framework and S-praziquantel is shown in Supplemental Figure 1.

The framework is refined using the constraint EADP for some disordered ZnI₂ moieties, as well as the commands SADI and DANG for some tpt rings. Three ZnI₂ moieties are disordered and refined using disorder model. One guest molecule (A) with an occupancy of 64% and one solvent molecule (B) were found in the asymmetric unit. The benzene ring was fixed using AFIX 66. The C=O double bonds, C-C and C-N single bonds were restrained using SADI command. DANG was used for some angles of the guest. In addition, FLAT was applied for the two cyclic amide functional groups. SIMU was applied for all analyte molecules. Applied restraints can be taken from Supplemental Fig. 1. Additional electron density was found that could not be assigned due to disorder. Contribution of this electron density was removed using solvent masking algorithm implemented in OLEX2. A solvent mask was calculated and 428 electrons were found in a volume of 1622 Å³ in one void per asymmetric unit. This is consistent with the presence of 9 cyclohexane molecules per asymmetric unit. Supplemental Fig. 2 shows the electron density map of the S-praziquantel molecule taken from the crystal structure. The parent compound interacts with the CS framework by C-H...O interactions (distance 2.49 Å) between the aromatic ring of the tpt ligand and the carbonyl group of the analyte.

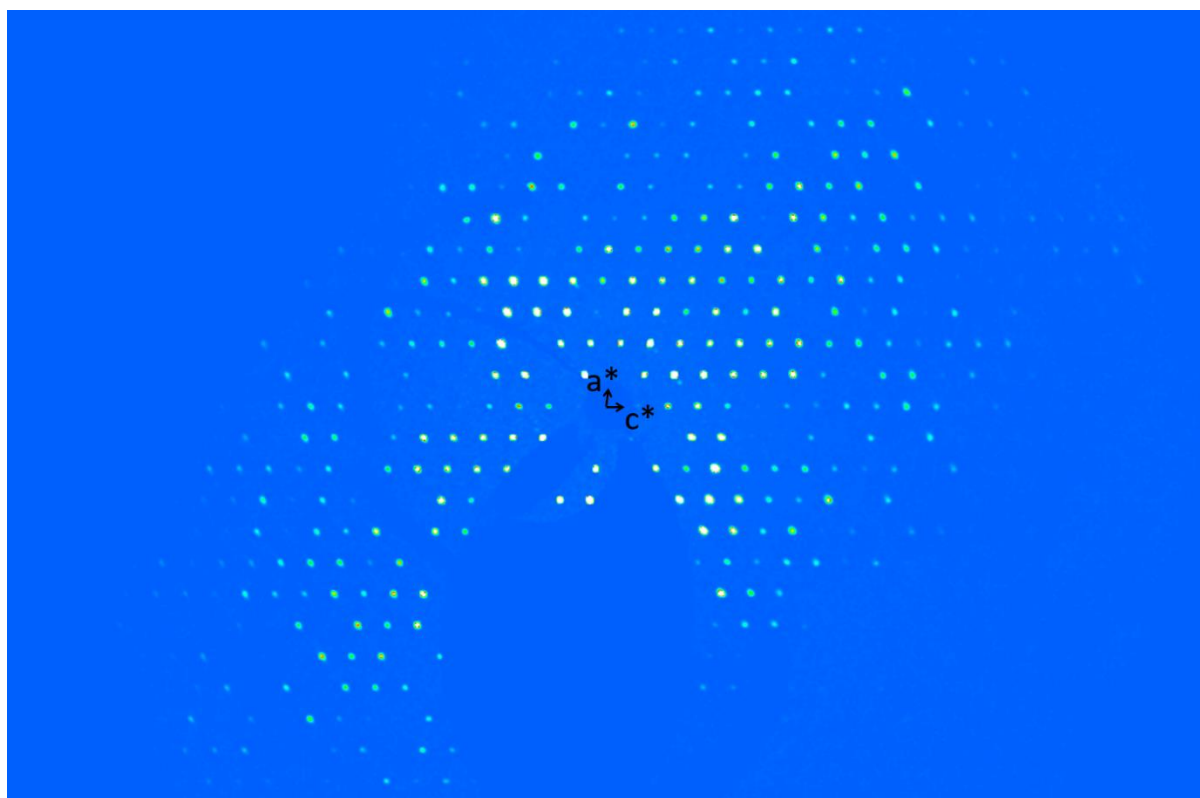
S-praziquantel was used as enantiomerically pure substance. Several examples have shown that the crystalline sponge method can be used to determine the absolute structure of soaked analytes because soaking of chiral molecules lead to lowering of the symmetry from $C2/c$ to $C2$ or $P2_1$ (Hoshino et al., 2016; Zigon et al., 2015). To assure the correct space group assignment during data processing, extinction rules for C centering (hkl , $h+k=\text{odd}$) and the existence of the c glide plane ($h0l$, $l=\text{odd}$) were evaluated. The reciprocal space of **1a**•**S-praziquantel** was inspected for the $h0l$ layer, clearly revealing Bragg spots $h=2n$ and $l=n$. Therefore, the data reduction and structure solution were executed for space group $C2$. For typical $C2/c$ example for comparison see Supplemental Fig. 3, after soaking see Supplemental Fig. 4.



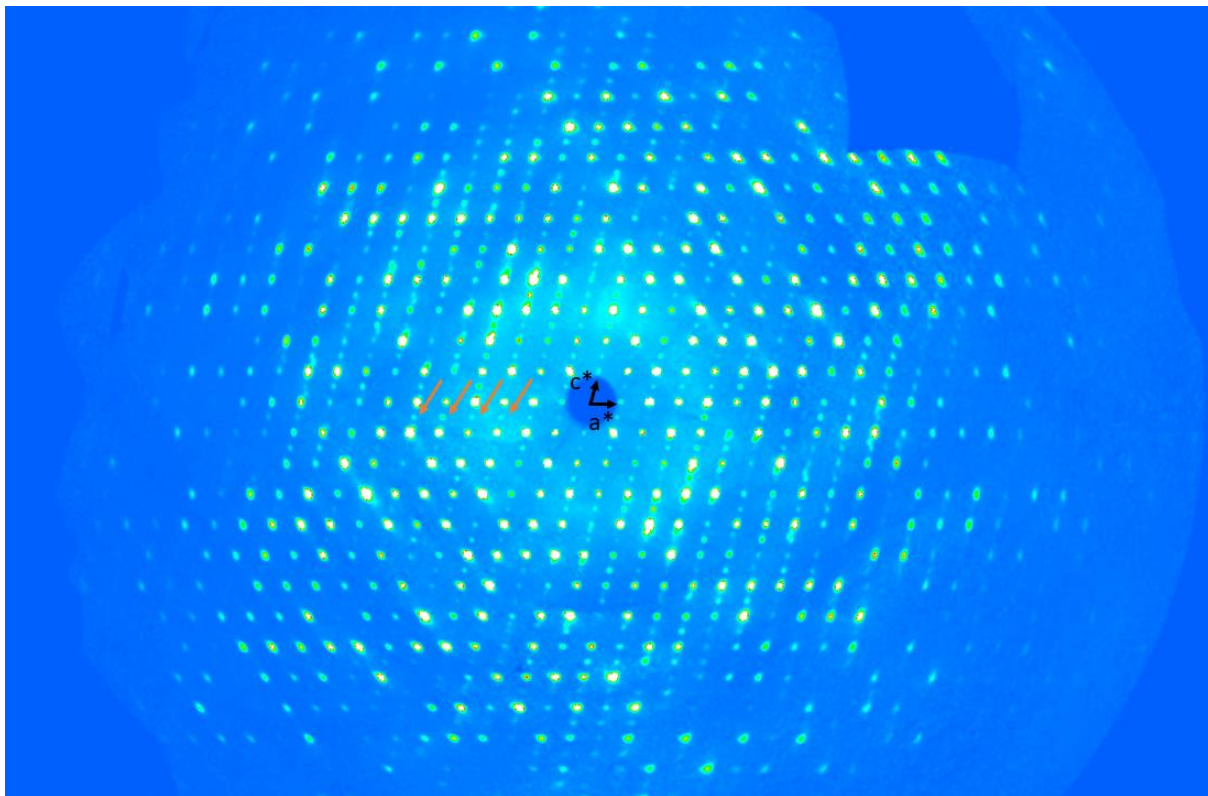
Supplemental Fig. 1. ORTEP diagram with 50% probability of the asymmetric unit of **1a**•**S-praziquantel**; restraints and constraints applied in the refinement of **S-praziquantel**



Supplemental Fig. 2. Electron density map F_o of **S-praziquantel** (contoured at the 2.02σ level)



Supplemental Fig. 3. Reciprocal $h0l$ layer of a typical crystalline sponge crystal before soaking in $C2/c$. Absence of $h=$ odd and $l=$ odd reflexes is clearly visible.



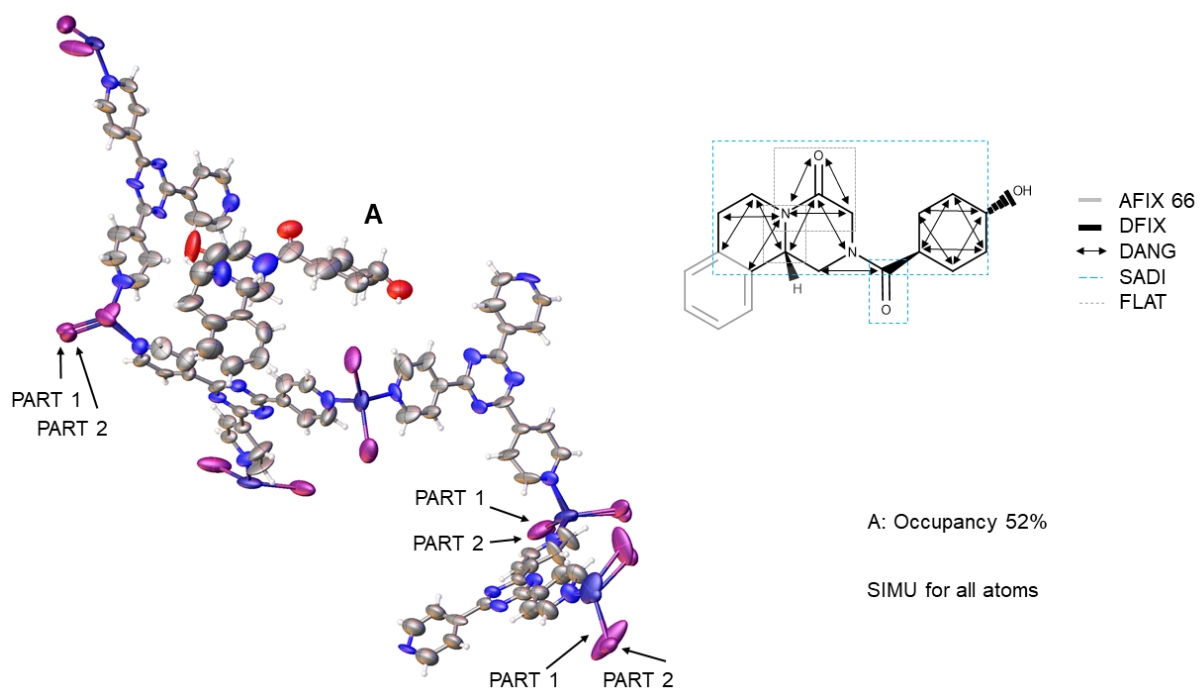
Supplemental Fig. 4. Reciprocal $h0l$ layer after soaking **S-praziquantel** into the crystalline sponge. Reflexes at $h=2n$ and $l=n$ (highlighted with orange arrows) clearly visible.

Crystallographic data for 1b•S-*trans*-4'-hydroxy-praziquantel (M1) (after solvent masking)

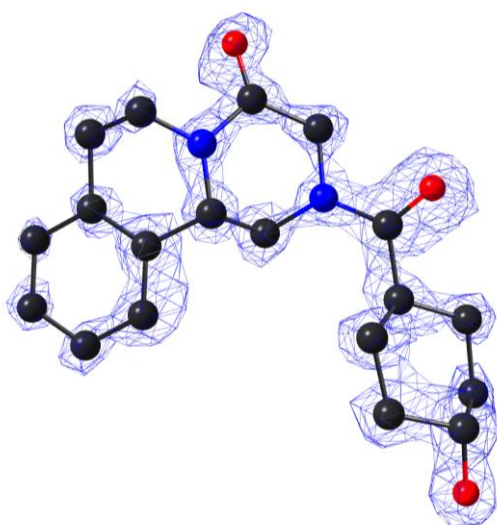
Crystal size: 253 × 213 × 97 μm³, refined formula: C_{81.95}H_{60.57}I₁₂N_{25.05}O_{1.57}Zn₆, formula weight (M_r) = 3336.32 g/mol, yellow needle, crystal system: Monoclinic, space group C2, Z = 4, 27092 unique reflections merged from recorded 134281 ones (2.631° < θ < 67.074°) were used for structural analysis (R_{int} = 0.0386). Lattice parameters, R-factor on F² > 2σ (F²), weighted R-factor and goodness-of-fit are as follows: a = 34.1212(5) Å, b = 14.9488(2) Å, c = 30.3783(6) Å, β = 100.163(2)°, V = 15252.0(4) Å³, R = 0.0658, wR₂ = 0.2218, S = 1.083. Calculated density is 1.453 gcm⁻³. Linear absorption coefficient (μ) is 20.413. Residual electron density (max/min) is 1.32/-1.08 eÅ⁻³. The Flack parameters for *S-trans*-4'-hydroxy praziquantel before and after using solvent masking were χ = 0.179(10) and χ = 0.229(8), respectively. CCDC number 2104977. The ORTEP diagram of the asymmetric unit of the framework and M1 praziquantel is shown in Supplemental Fig. 5.

The framework is refined using the restraint SIMU and constraint EADP for some carbon and nitrogen atoms of the tpt rings. Three ZnI₂ moieties are disordered and refined using disorder model. One guest molecule was found in the asymmetric unit with an occupancy of 52%. The benzene ring was fixed using AFIX 66 and DFIX, DANG, SADI and FLAT were used for some bonds and angles of the guest (see Supplemental Fig. 5). In addition, the guest molecule was refined by applying SIMU (for the complete molecule). A solvent mask was calculated and 255 electrons were found in a volume of 1024 Å³ in one void per asymmetric unit. This is consistent with the presence of 5 n-hexane molecules per asymmetric unit. The oxidation of the cyclohexane ring in position 4' in *trans* configuration is clearly visible from electron density maps (Supplemental Fig. 6).

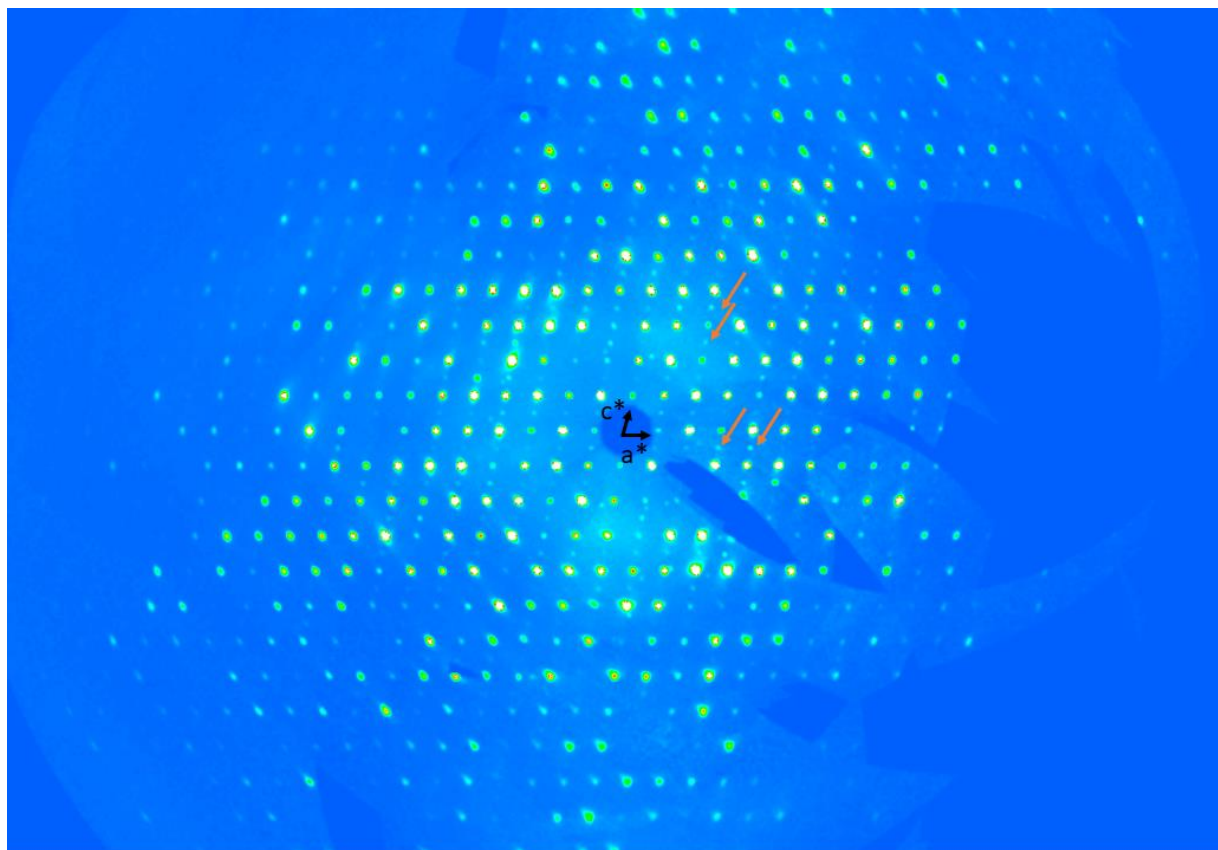
S-trans-4'-hydroxy praziquantel was used as enantiomerically pure substance. The reciprocal space of **1b•M1** was inspected for the *h0l* layer, revealing Bragg spots $h=2n$ and $l=n$ (Supplemental Fig.7).



Supplemental Fig. 5. ORTEP diagram with 50% probability of the asymmetric unit of **1b•M1 praziquantel**; restraints and constraints applied in the refinement of **M1 praziquantel**



Supplemental Fig. 6. Electron density map F_o of **M1 praziquantel** (contoured at the 2.00σ level)



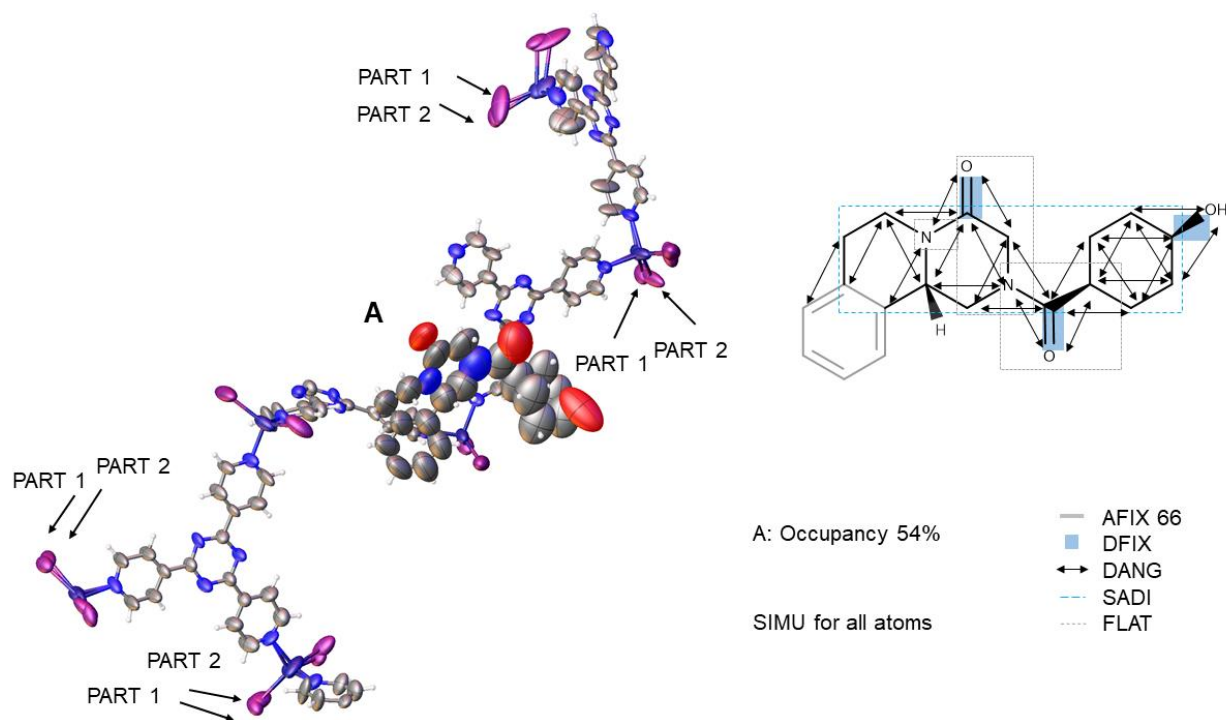
Supplemental Fig. 7. Reciprocal $h0l$ layer after soaking **S-trans-4'-hydroxy-praziquantel** into the crystalline sponge. Reflexes at $h=2n$ and $l=n$ (highlighted with orange arrows) visible.

Crystallographic data for 1b•S-cis-4'-hydroxy-praziquantel (M2) (after solvent masking)

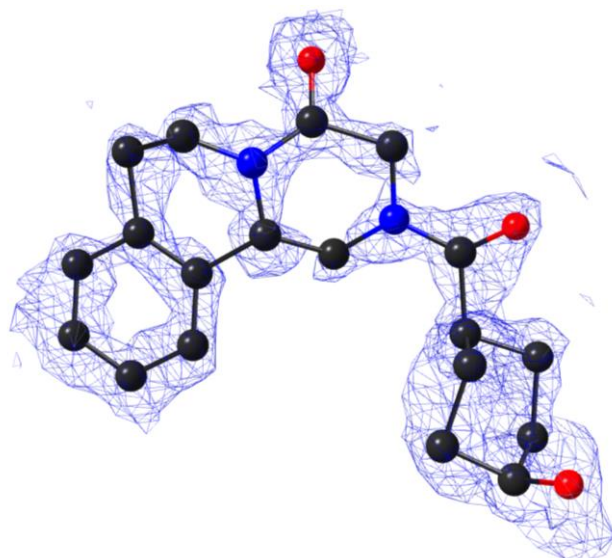
Crystal size: 264 × 136 × 112 μm³, refined formula: C_{81.87}H_{60.87}I₁₂N_{25.07}O_{1.61}Zn₆, formula weight (M_r) = 3336.89 g/mol, yellow needle, crystal system: Monoclinic, space group C2, Z = 4, 27270 unique reflections merged from recorded 189002 ones (2.711° < θ < 67.078°) were used for structural analysis (R_{int} = 0.0286). Lattice parameters, R-factor on F² > 2σ(F²), weighted R-factor, and goodness-of-fit are as follows: a = 34.7979(5) Å, b = 14.9056(2) Å, c = 30.9525(3) Å, β = 101.311(1)°, V = 15742.7(4) Å³, R = 0.0585, wR₂ = 0.2003, S = 1.101. Calculated density is 1.408 gcm⁻³. Linear absorption coefficient (μ) is 19.777 mm⁻¹. Residual electron density (max/min) is 0.87/-0.58 eÅ⁻³. The Flack parameters for S-cis-4'-hydroxy praziquantel before and after using solvent masking were χ = 0.180(9) and χ = 0.328(8), respectively. CCDC number 2104978. The ORTEP diagram of the asymmetric unit of the framework and M2 praziquantel is shown in Supplemental Fig. 8.

The framework is refined using the constraint EADP for four carbon atoms. The framework exhibits disorder of four ZnI₂ parts. One guest molecule (A) can be found in the asymmetric unit with an occupancy of 54%. AFIX 66 was applied to the benzene ring, and DFIX, DANG, SADI and FLAT were used for most bonds and angles of the guest (see Supplemental Fig. 8). SIMU was applied for the analyte molecule. A solvent mask was calculated and 440 electrons were found in a volume of 1544 Å³ in one void per asymmetric unit. This is consistent with the presence of 8.5 n-hexane molecules per asymmetric unit. The oxidation of the cyclohexane ring in position 4' in cis configuration is clearly visible from electron density maps (Supplemental Fig. 9).

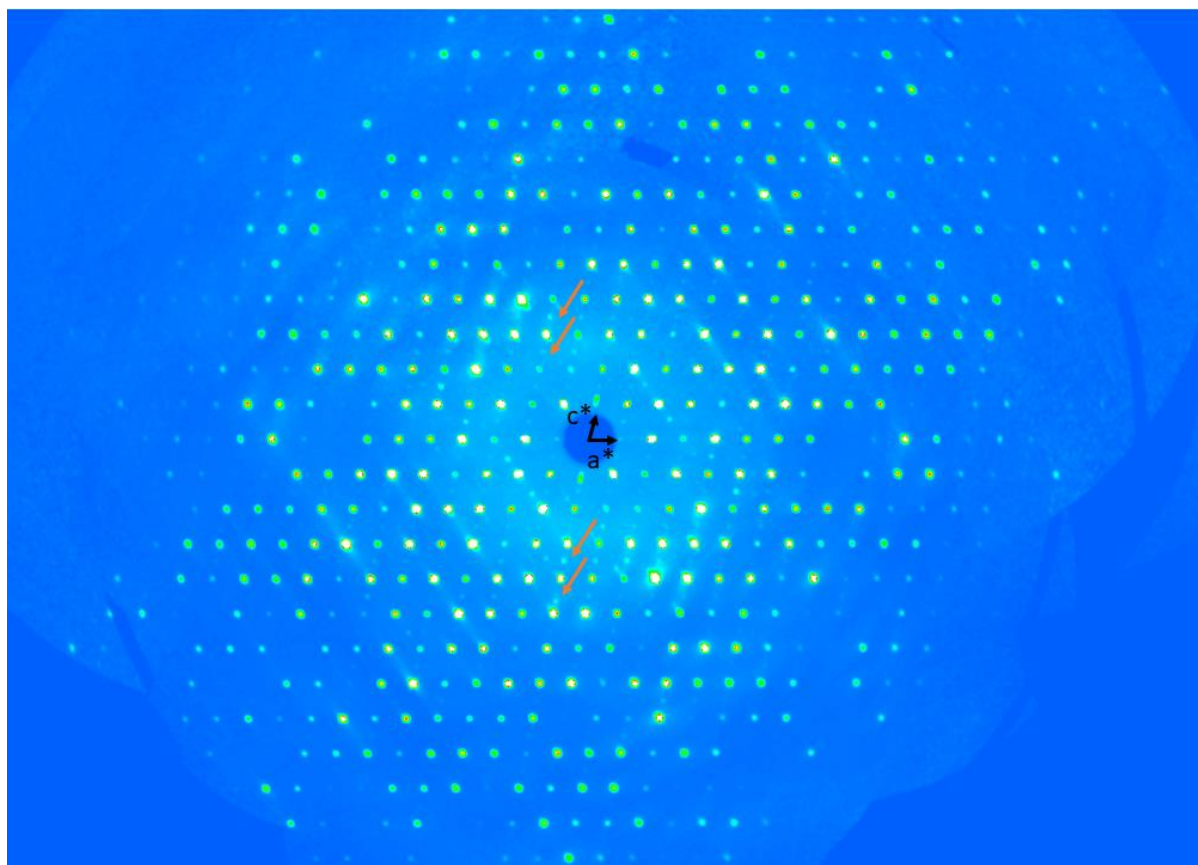
S-cis-4'-hydroxy praziquantel was used as enantiomerically pure substance. The reciprocal space of **1b•M2** was inspected for the *h0l* layer, revealing Bragg spots *h=2n* and *l=n* (Supplemental Fig.10).



Supplemental Fig. 8. ORTEP diagram with 50% probability of the asymmetric unit of **1b•M2 praziquantel**; restraints and constraints applied in the refinement of **M2 praziquantel**



Supplemental Fig. 9. Electron density map F_o of **M2 praziquantel** (contoured at the 3.70σ level)



Supplemental Fig. 10. Reciprocal $h0l$ layer after soaking **S-cis-4'-hydroxy-praziquantel** into the crystalline sponge. Reflexes at $h=2n$ and $l=n$ (highlighted with orange arrows) visible.

Crystallographic data for 1a•S-9-hydroxy-praziquantel (M3) (after solvent masking)

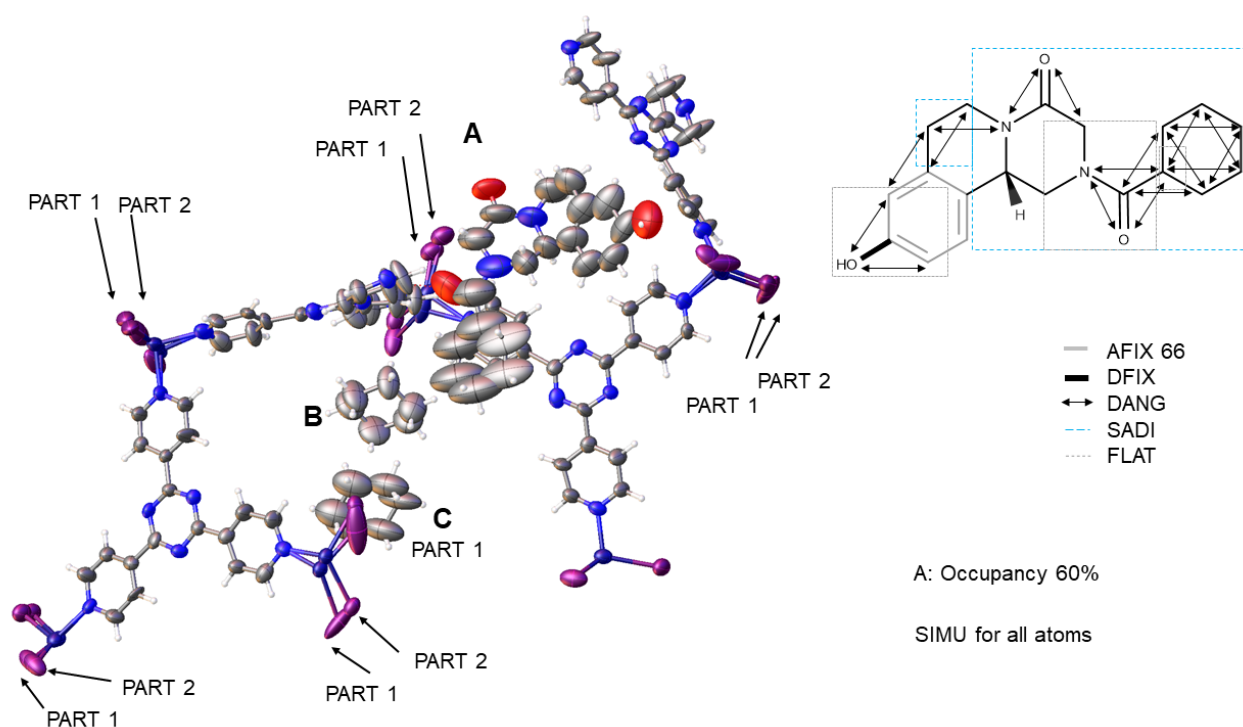
Crystal size: 178 × 120 × 71 μm^3 , refined formula: $\text{C}_{91.82}\text{H}_{79.01}\text{I}_{12}\text{N}_{25.2}\text{O}_{1.8}\text{Zn}_6$, formula weight (M_r) = 3478.97 g/mol , colorless needle, crystal system: Monoclinic, space group $C2$, $Z = 4$, 23994 unique reflections merged from recorded 68432 ones ($2.583^\circ < \theta < 67.081^\circ$) were used for structural analysis ($R_{\text{int}} = 0.0152$). Lattice parameters, R-factor on $F^2 > 2\sigma(F^2)$, weighted R-factor, and goodness-of-fit are as follows: $a = 35.1163(6)$ Å, $b = 14.8449(2)$ Å, $c = 32.1504(6)$ Å, $\beta = 103.042(2)^\circ$, $V = 16327.6(5)$ Å³, $R = 0.0553$, $wR_2 = 0.1716$, $S = 1.113$. Calculated density is 1.415 gcm^{-3} . Linear absorption coefficient (μ) is 19.093 mm^{-1} . Residual electron density (max/min) is 1.02/-1.05 $\text{e}\text{\AA}^{-3}$. The Flack parameters for S-9-hydroxy praziquantel before and after using solvent masking were $\chi = 0.111(9)$ and $\chi = 0.204(7)$, respectively. CCDC number 2107215. The ORTEP diagram of the asymmetric unit of the framework and M3 praziquantel is shown in Supplemental Fig. 11.

The framework is refined using the constraint EADP for some disordered ZnI_2 moieties and the restraint SIMU for some carbon atoms. Five ZnI_2 moieties are disordered and refined using the disorder model. One guest molecule (A) and two cyclohexane molecules (B and C) were found in the asymmetric unit. The analyte occupancy is 60%. Solvent molecule C is disordered with one ZnI_2 moiety and refined using PART 1 command. Some restraints were applied for refinement of the analyte and solvent molecules (DFIX, SADI, FLAT and DANG). The guest molecule was refined by applying SIMU (for complete molecule). The restraints used for the refinement are summarized in Supplemental Fig. 11. The benzene part of the molecule could be refined with minor constraints (AFIX 66) and the presence of oxidation at position 9 of the aromatic ring is clearly visible from the electron density map (Supplemental Fig. 12). The position of hydroxylation had to be restrained to its theoretical values by applying DFIX and DANG commands due to high mobility and not resolved disorder with solvent molecules at this part. Intermolecular hydrogen bonds could be observed by the C-H...O distance (2.17 Å) between the framework and the carbonyl of the analyte. A solvent mask was calculated and

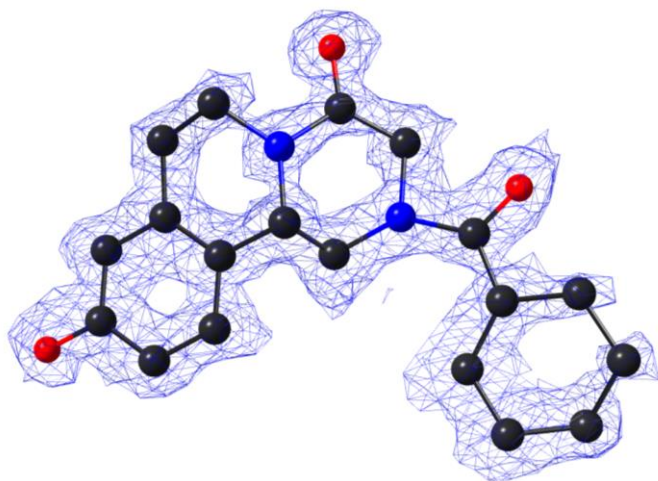
418 electrons were found in a volume of 1342 Å³ in one void per asymmetric unit. This is consistent with the presence of 8.5 cyclohexane molecules per asymmetric unit.

In the present study, the task of the crystalline sponge method was the determination of the hydroxy positions after *in vitro* incubation of the parent compound. The position of metabolism could be determined unambiguously. The combination of known parent structure, mass spectrometry and crystalline sponge analysis leads therefore to a successful structure elucidation. Furthermore, NMR analysis of the metabolite confirms the structure.

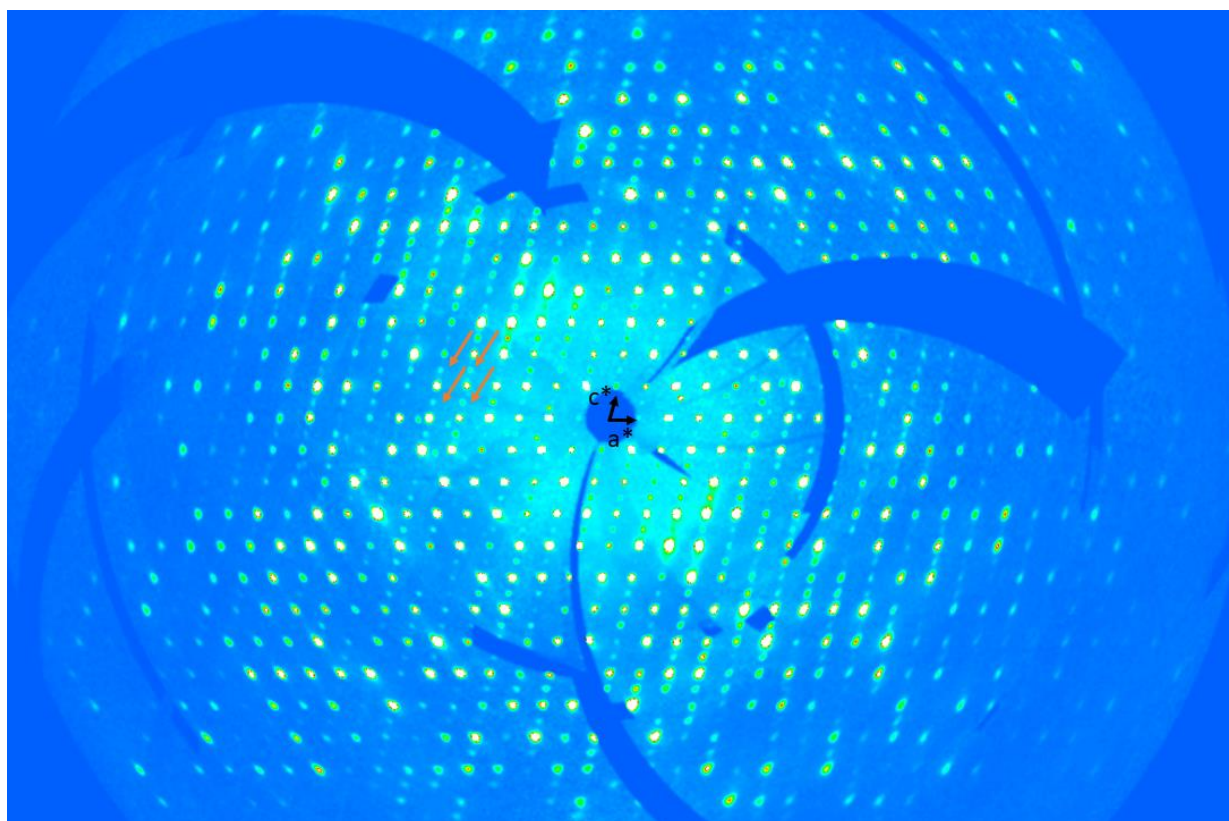
S-9-hydroxy praziquantel was isolated from incubation of enantiomerically pure S-praziquantel. The reciprocal space of **1b•M3** was inspected for the *h0l* layer, clearly revealing Bragg spots $h=2n$ and $l=n$ (Supplemental Fig.13).



Supplemental Fig. 11. ORTEP diagram with 50% probability of the asymmetric unit of **1a•M3 praziquantel**; restraints and constraints applied in the refinement of **M3 praziquantel**



Supplemental Fig. 12. Electron density map F_o of **M3 praziquantel** (contoured at the 3.33σ level)



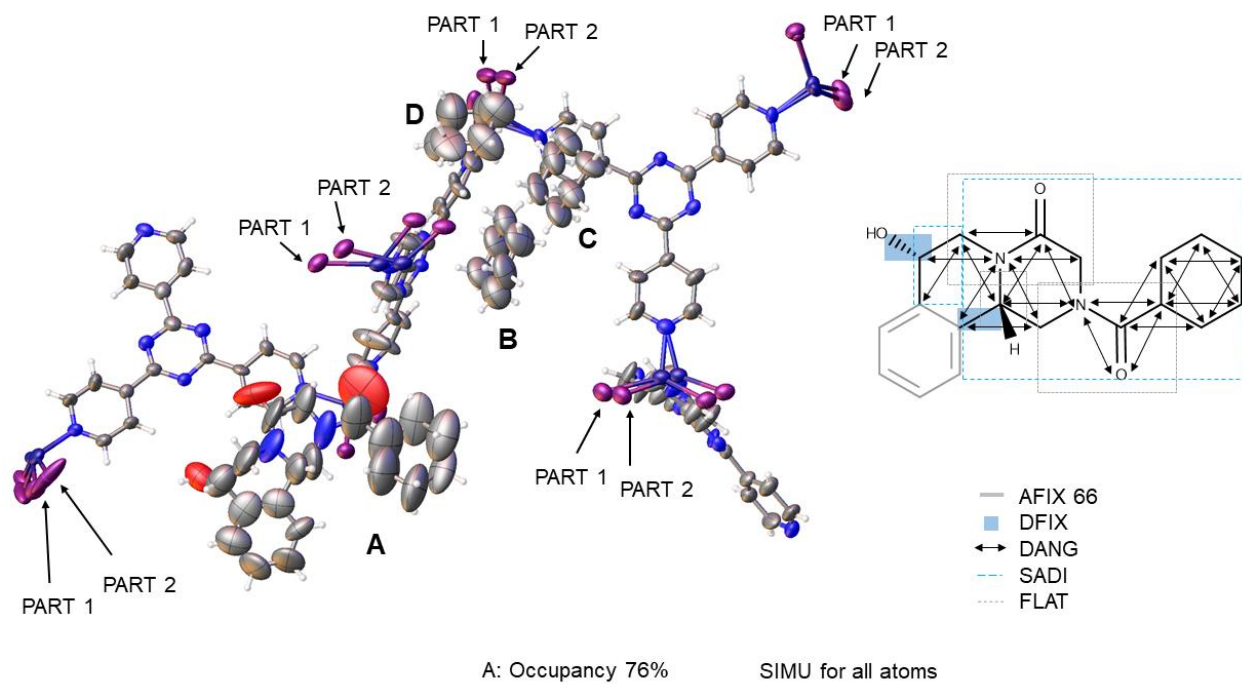
Supplemental Fig. 13. Reciprocal $h0l$ layer after soaking **S-9-hydroxy-praziquantel** into the crystalline sponge. Reflexes at $h=2n$ and $l=n$ (highlighted with orange arrows) clearly visible.

Crystallographic data for 1a•S-7-hydroxy-S-praziquantel (M4) (after solvent masking)

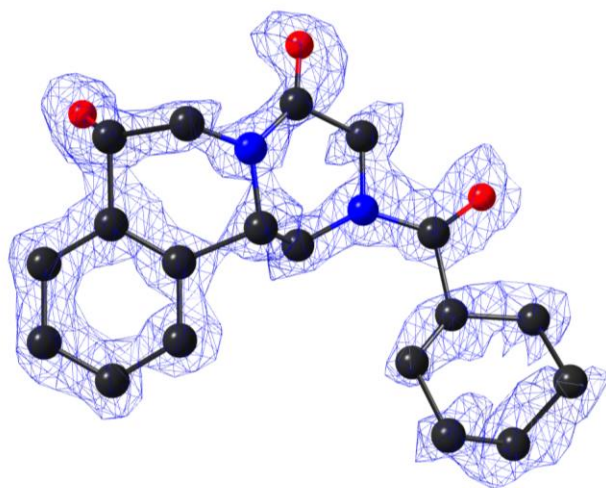
Crystal size: 198 × 142 × 89 μm³, refined formula: C_{100.54}H_{94.49}I₁₂N_{25.51}O_{2.27}Zn₆, formula weight (M_r) = 3611.29 g/mol, colorless needle, crystal system: Monoclinic, space group C2, Z = 4, 24684 unique reflections merged from recorded 54687 ones (2.573° < θ < 67.08°) were used for structural analysis (R_{int} = 0.0145). Lattice parameters, R-factor on F² > 2σ(F²), weighted R-factor, and goodness-of-fit are as follows: a = 35.2848(5) Å, b = 14.7872(2) Å, c = 32.3789(4) Å, β = 103.223(1)°, V = 16446.2(4) Å³, R = 0.0499, wR₂ = 0.1491, S = 1.089. Calculated density is 1.458 gcm⁻³. Linear absorption coefficient (μ) is 18.979 mm⁻¹. Residual electron density (max/min) is 0.94/-1.07 eÅ⁻³. The Flack parameters for S-7-hydroxy S-praziquantel before and after using solvent masking were χ = 0.092(8) and χ = 0.191(7), respectively. CCDC number 2107216. The ORTEP diagram of the asymmetric unit of the framework and M4 praziquantel is shown in Supplemental Fig. 14.

The framework exhibits disorder of five ZnI₂ parts refined using the disorder model. One guest molecule (A) with an occupancy of 76% and three additional cyclohexane molecules (C, D and E) can be found in the asymmetric unit. The benzene ring of molecule A was fixed using AFIX 66 and the non-aromatic rings had to be restrained using SADI, DFIX, DANG and FLAT (Supplemental Fig. 14). SIMU was applied for all atoms of the analyte molecule. A solvent mask was calculated and 272 electrons and 50 electrons were found in a volume of 1040 Å³ and 147 Å³, respectively, in two voids per asymmetric unit. This is consistent with the presence of 5.5 and 1 cyclohexane molecules per asymmetric unit. The electron density map clearly showed the introduction of an additional atom at position 7 of the non-aromatic part of the structure (Supplemental Fig. 15). The distance of the C-O bond had to be restrained using DFIX.

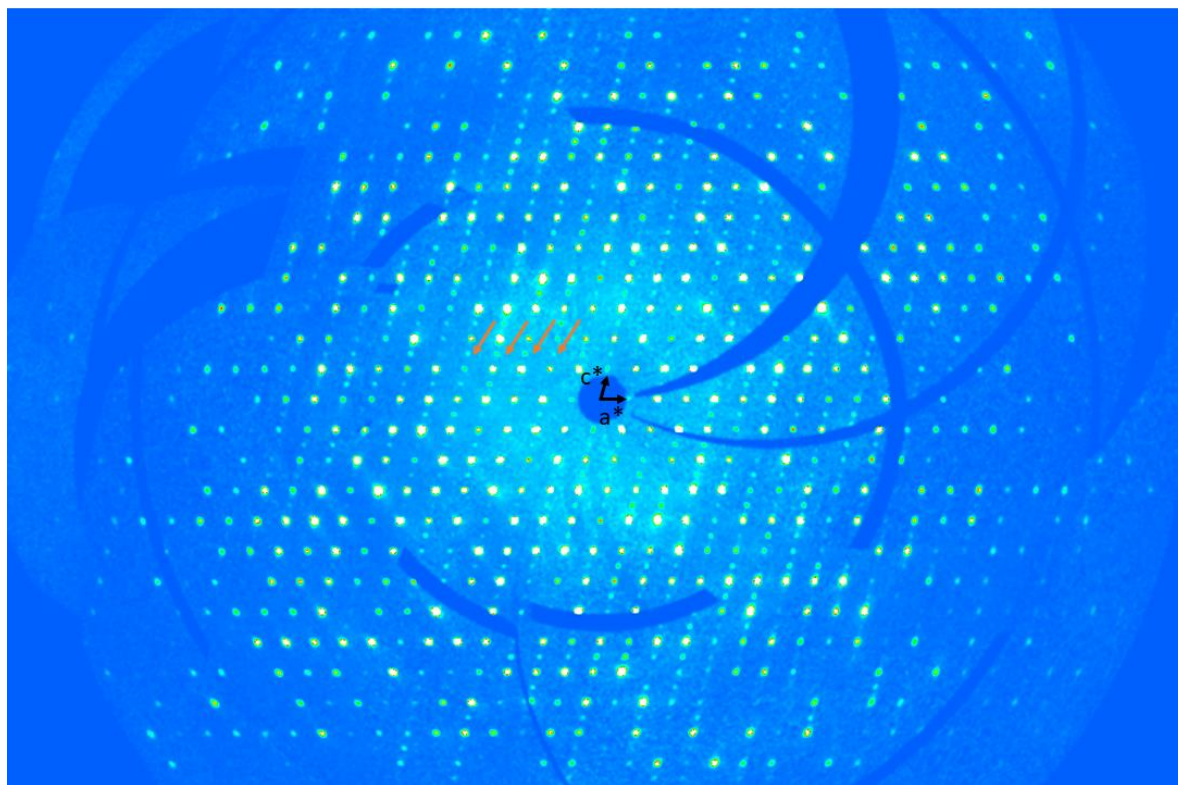
S-7-hydroxy S-praziquantel was isolated from incubation of enantiomerically pure S-praziquantel. The reciprocal space of **1b•M4** was inspected for the *h0l* layer, clearly revealing Bragg spots *h=2n* and *l=n* (Supplemental Fig.16).



Supplemental Fig. 14. ORTEP diagram with 50% probability of the asymmetric unit of **1a•M4 praziquantel**; restraints and constraints applied in the refinement of **M4 praziquantel**



Supplemental Fig. 15. Electron density map F_o of **M4 praziquantel** (contoured at the 2.11σ level)



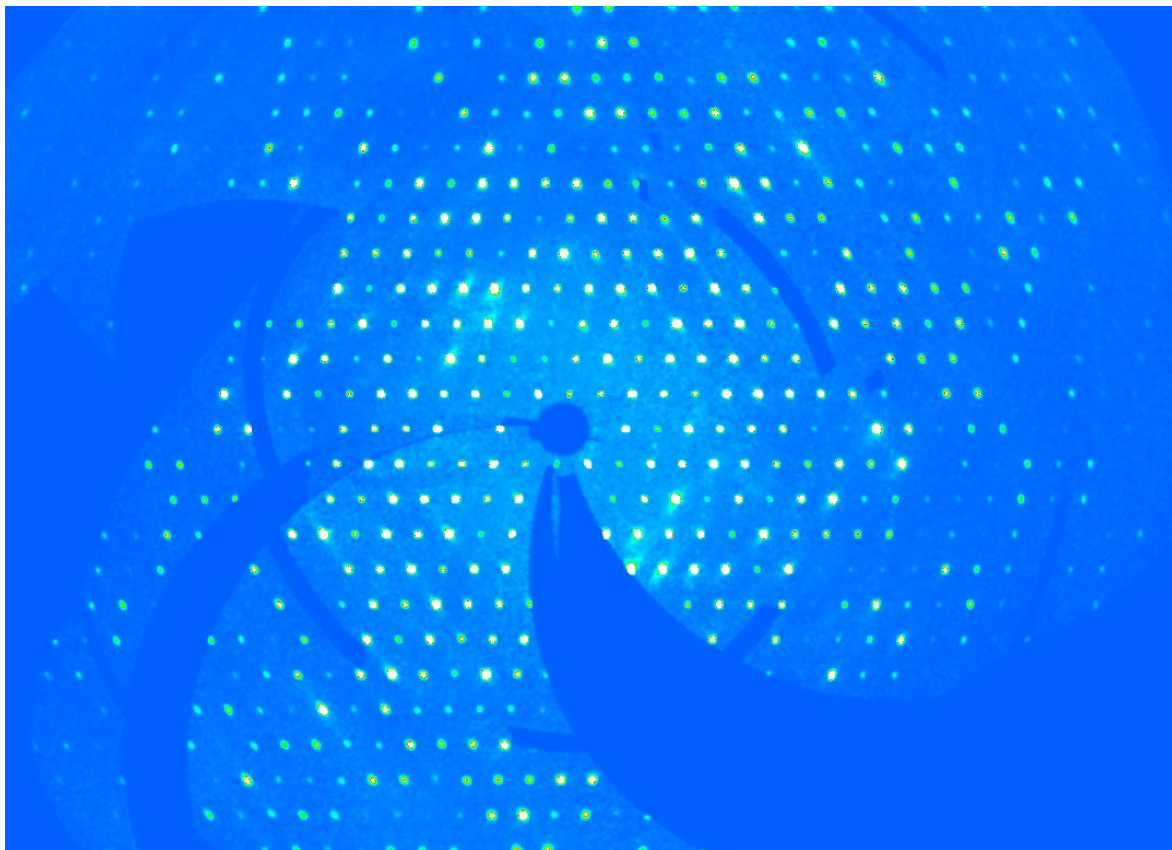
Supplemental Fig. 16. Reciprocal $h0l$ layer after soaking **S-7-hydroxy-S-praziquantel** into the crystalline sponge. Reflexes at $h=2n$ and $l=n$ (highlighted with orange arrows) visible.

Crystallographic data for 1a•S-11b-hydroxy-praziquantel and R-11b-hydroxy-praziquantel (S-/R-M6)

Crystal size: 339 × 172 × 90 μm³, refined formula: C_{45.46}H_{35.94}I₆N_{12.99}O_{1.49}Zn₃, formula weight (M_r) = 1745.61 g/mol, yellow needle, crystal system: Monoclinic, space group C2/c, Z = 8, 14979 unique reflections merged from recorded 53191 ones (2.610° < θ < 74.592°) were used for structural analysis (R_{int} = 0.0248). Lattice parameters, R-factor on F² > 2σ(F²), weighted R-factor, and goodness-of-fit are as follows: a = 34.4208(4) Å, b = 15.0229(1) Å, c = 30.2656(3) Å, β = 100.421(1)°, V = 15392.2(3) Å³, R = 0.0592, wR₂ = 0.1890, S = 1.090. Calculated density is 1.507 gcm⁻³. Linear absorption coefficient (μ) is 20.264 mm⁻¹. Residual electron density (max/min) is 1.67/-0.99 eÅ⁻³. CCDC number 2104985. The ORTEP diagram of the asymmetric unit of the framework and S-/R-M6 praziquantel is shown in Supplemental Fig. 17.

The framework is refined without restraints. The framework exhibits disorder of three ZnI₂ part refined using the disorder model. Two guest molecules (A) and (B) can be found in the asymmetric unit. Guest A is disordered at special position (inversion) and refined using PART -1 command and s.o.f. = 0.5x(FVAR#5). This leads to an analyte occupancy of 40%. An additional guest molecule (B), disordered with one ZnI₂ moiety, was observed, and is refined as PART 1 with a fixed occupancy of 30%. AFIX 66 was applied to the benzene rings, and DFIX, SADI, DANG and FLAT were used for some bonds and angles of the guest (Supplemental Fig. 17). The guest molecules were refined by applying SIMU. Additional electron density was observed for both guest molecules in position 11b in either S or R configuration of the non-aromatic ring system and was assigned as hydroxylation (+16 Da) (Supplemental Fig. 18). The introduced oxygens were restrained using the command DFIX (A, B) and DANG (B).

The reciprocal space of **1a•S-/R-M6** was inspected for the *h0l* layer, revealing the absence of Bragg spots *h=2n* and *l=n* (Supplemental Fig.19) and confirming the centrosymmetric space group C2/c.



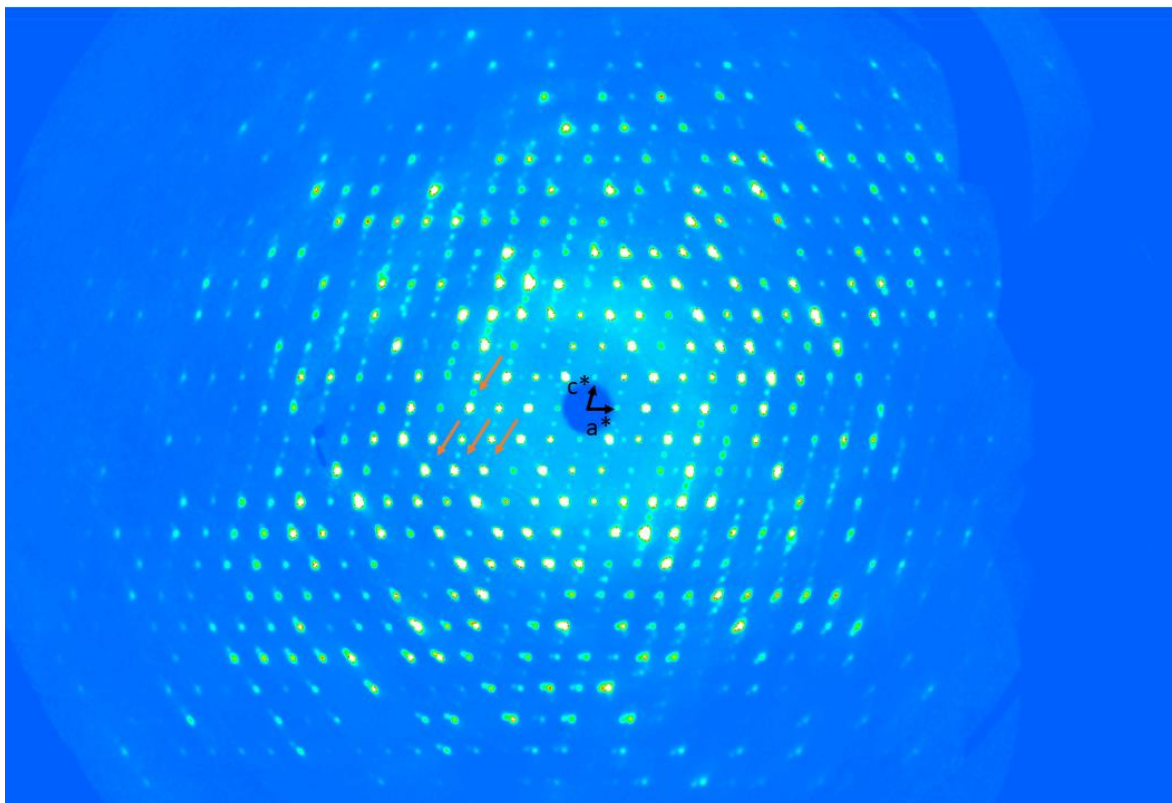
Supplemental Fig. 19. Reciprocal $h0l$ layer after soaking **S-11b-hydroxy-praziquantel** and **R-11b-hydroxy-praziquantel** into the crystalline sponge. Absence of $h=\text{odd}$ and $l=\text{odd}$ reflexes is clearly visible.

Crystallographic data for 1a•R-11b-hydroxy-praziquantel (R-M6) (after solvent masking)

Crystal size: 236 × 168 × 103 μm³, refined formula: C_{81.5}H_{59.78}I₁₂N₂₅O_{1.5}Zn₆, formula weight (M_r) = 3328.34 g/mol, light yellow needle, crystal system: Monoclinic, space group C2, Z = 4, 28422 unique reflections merged from recorded 185893 ones (2.575° < θ < 67.078°) were used for structural analysis (R_{int} = 0.0369). Lattice parameters, R-factor on F² > 2σ(F²), weighted R-factor, and goodness-of-fit are as follows: a = 35.2910(6) Å, b = 14.8009 (2) Å, c = 32.3794 (5) Å, β = 103.507(2)°, V = 16445.2(5) Å³, R = 0.0732, wR₂ = 0.2394, S = 1.092. Calculated density is 1.344 gcm⁻³. Linear absorption coefficient (μ) is 18.930 mm⁻¹. Residual electron density (max/min) is 1.75/-0.96 eÅ⁻³. The Flack parameters for R-11b-hydroxy praziquantel before and after using solvent masking were χ = 0.166(11) and χ = 0.221(8), respectively. CCDC number 2129663. The ORTEP diagram of the asymmetric unit of the framework and R-M6 praziquantel is shown in Supplemental Fig. 20.

The framework is refined using the constraint EADP for some disordered ZnI₂ moieties and carbon atoms. DFIX and SADI was used for some tpt parts. Five ZnI₂ moieties are disordered and refined using the disorder model. One guest molecule (A) can be found in the asymmetric unit near the center of symmetry (C2 axis) and is refined using PART -1 command with s.o.f. = 0.5. The analyte occupancy was modeled to 100%. AFIX 66 was applied to the benzene ring, and SADI and DANG were used for some bonds and angles of the guest (Supplemental Fig. 20). The guest molecule was refined by applying SIMU. A solvent mask was calculated and 422 electrons were found in a volume of 1538 Å³ in one void per asymmetric unit. This is consistent with the presence of 8.5 cyclohexane molecules per asymmetric unit. Additional electron density was observed in position 11b of the non-aromatic ring system and was assigned as hydroxylation (+16 Da) (Supplemental Fig. 21).

The reciprocal space of **1a•R-M6** was inspected for the *h0l* layer, revealing Bragg spots *h=2n* and *l=n* (Supplemental Fig.22).

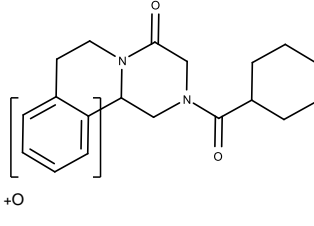
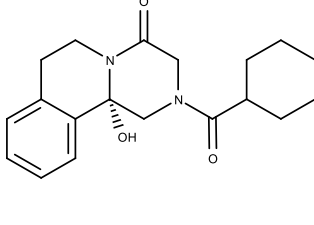
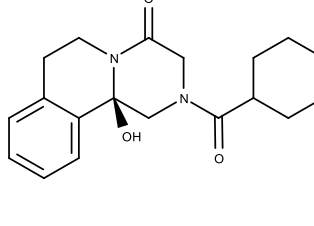


Supplemental Fig. 22. Reciprocal $h0l$ layer after soaking **R-11b-hydroxy-praziquantel** into the crystalline sponge. Reflexes at $h=2n$ and $l=n$ (highlighted with orange arrows) visible.

Ultra-performance liquid chromatography - quadrupole time-of-flight mass spectrometry

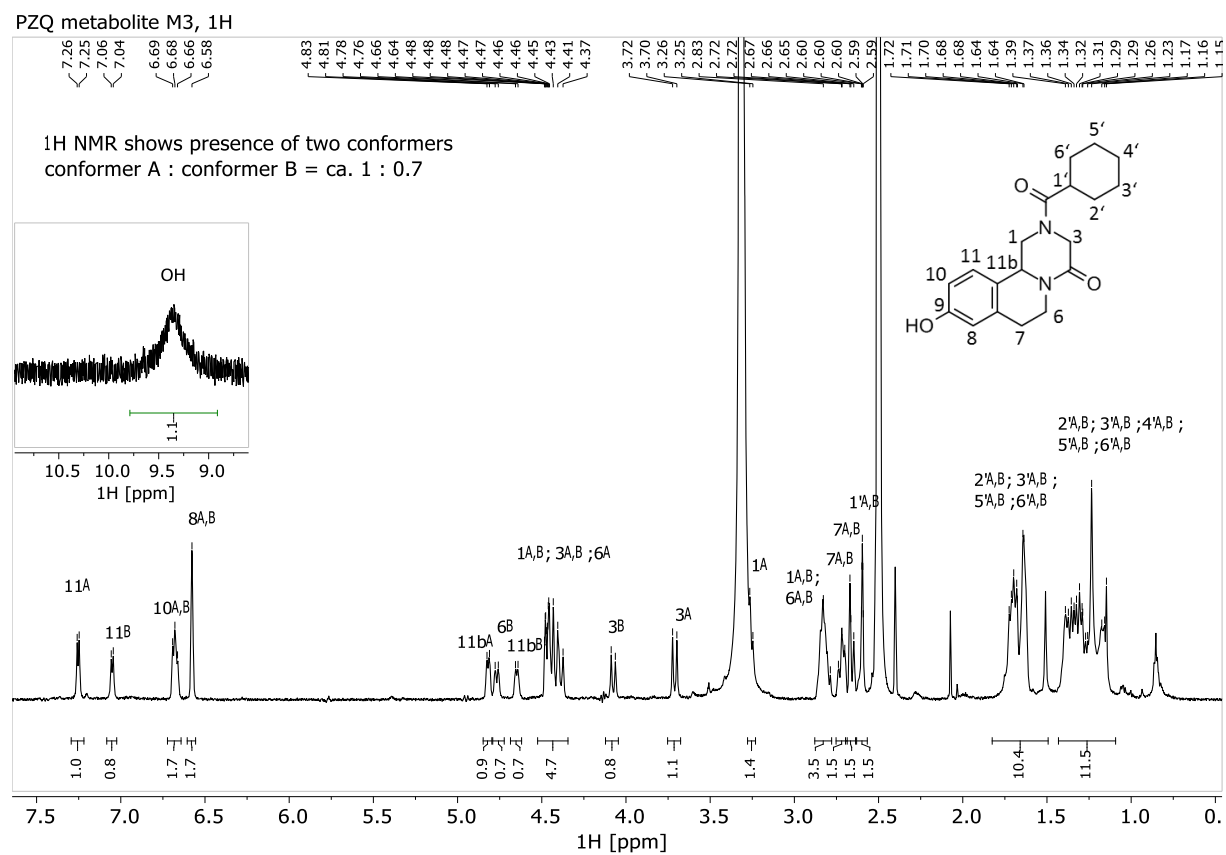
ID	Name	Retention time [min]	Elemental Composition (ion formula)	[M+H] ⁺ [m/z]	Main fragment ions [m/z]	Mass error [mDa]	Structure proposal
S-PZQ	S-praziquantel	11.19	[C ₁₉ H ₂₄ N ₂ O ₂ + H] ⁺ [C ₁₂ H ₁₄ N ₂ O + H] ⁺ [C ₁₂ H ₁₂ N ₂ O + H] ⁺ [C ₁₁ H ₁₁ NO + H] ⁺ [C ₁₀ H ₁₁ N + H] ⁺ [C ₉ H ₉ N + H] ⁺ [C ₁₀ H ₈ + H] ⁺	313.1915	203.1181 201.1024 174.0917 146.0966 132.0810 129.0698	0.2 0.2 0.3 0.1 0.1 -0.2	
M1	S-trans-4'-hydroxy-praziquantel	5.06	[C ₁₉ H ₂₄ N ₂ O ₃ + H] ⁺ [C ₁₉ H ₂₂ N ₂ O ₂ + H] ⁺ [C ₁₂ H ₁₄ N ₂ O + H] ⁺ [C ₁₁ H ₁₁ NO + H] ⁺ [C ₁₀ H ₁₁ N + H] ⁺ [C ₉ H ₉ N + H] ⁺ [C ₁₀ H ₈ + H] ⁺	329.1861	311.1756 203.1180 174.0916 146.0966 132.0811 129.0698	0.2 0.1 0.2 0.1 0.3 -0.1	
M2	S-cis-4'-hydroxy-praziquantel	5.33	[C ₁₉ H ₂₄ N ₂ O ₃ + H] ⁺ [C ₁₉ H ₂₂ N ₂ O ₂ + H] ⁺ [C ₁₂ H ₁₄ N ₂ O + H] ⁺ [C ₁₂ H ₁₂ N ₂ O + H] ⁺ [C ₁₁ H ₁₁ NO + H] ⁺ [C ₁₀ H ₁₁ N + H] ⁺ [C ₉ H ₉ N + H] ⁺ [C ₁₀ H ₈ + H] ⁺	329.1864	311.1758 203.1181 201.1025 174.0916 146.0966 132.0810 129.0698	0.4 0.2 0.3 0.2 0.1 0.2 -0.1	
M3	S-9-hydroxy-praziquantel	7.05	[C ₁₉ H ₂₄ N ₂ O ₃ + H] ⁺ [C ₁₂ H ₁₄ N ₂ O ₂ + H] ⁺ [C ₁₁ H ₁₁ NO ₂ + H] ⁺ [C ₁₀ H ₁₁ NO + H] ⁺ [C ₉ H ₉ NO + H] ⁺ [C ₈ H ₈ O + H] ⁺	329.1860	219.1129 190.0862 162.0906 148.0753 121.0637	0.1 -0.1 -0.7 -0.4 -1.1	
M4	S-7-hydroxy-S-praziquantel	7.13	[C ₁₉ H ₂₄ N ₂ O ₃ + H] ⁺ [C ₁₉ H ₂₂ N ₂ O ₂ + H] ⁺ [C ₁₂ H ₁₂ N ₂ O + H] ⁺ [C ₁₀ H ₉ N + H] ⁺ [C ₉ H ₇ N + H] ⁺ [C ₉ H ₆ + H] ⁺	329.1857	311.1753 201.1017 144.0801 130.0646 115.0531	-0.1 -0.5 -0.7 -0.5 -1.2	

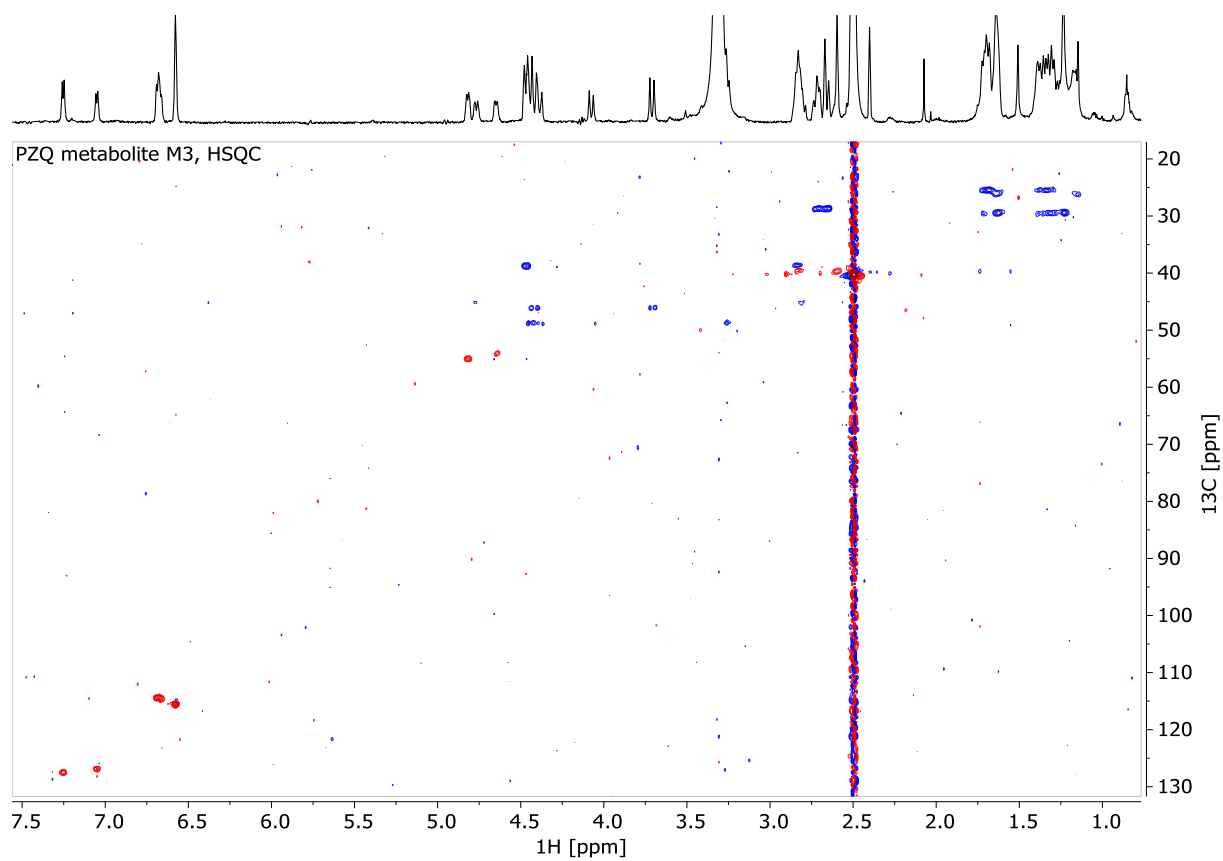
Appendix

ID	Name	Retention time [min]	Elemental Composition (ion formula)	[M+H] ⁺ [m/z]	Main fragment ions [m/z]	Mass error [mDa]	Structure proposal
M5	?-hydroxy-praziquantel	7.37	[C ₁₉ H ₂₄ N ₂ O ₃ + H] ⁺ [C ₁₂ H ₁₄ N ₂ O ₂ + H] ⁺ [C ₁₁ H ₁₁ NO ₂ + H] ⁺ [C ₁₀ H ₁₁ NO + H] ⁺ [C ₉ H ₉ NO + H] ⁺	329.1859	219.1127 190.0860 162.0906 148.0748	0.0 -0.3 -0.7 -0.9	
M6	S-11b-hydroxy-praziquantel	7.49	[C ₁₉ H ₂₄ N ₂ O ₃ + H] ⁺ [C ₁₉ H ₂₂ N ₂ O ₂ + H] ⁺ [C ₁₂ H ₁₂ N ₂ O + H] ⁺ [C ₁₀ H ₉ N + H] ⁺ [C ₉ H ₇ N + H] ⁺ [C ₉ H ₆ + H] ⁺	329.1859	311.1754 201.1023 144.0812 130.0653 115.0545	0.0 0.1 0.4 0.2 0.3	
M6	R-11b-hydroxy-praziquantel	11.85	[C ₁₉ H ₂₄ N ₂ O ₃ + H] ⁺ [C ₁₉ H ₂₂ N ₂ O ₂ + H] ⁺ [C ₁₂ H ₁₂ N ₂ O + H] ⁺ [C ₁₀ H ₉ N + H] ⁺ [C ₉ H ₇ N + H] ⁺ [C ₉ H ₆ + H] ⁺	329.1858	311.1753 201.1022 144.0808 130.0651 115.0542	-0.1 0.0 0.0 0.0 -0.1	

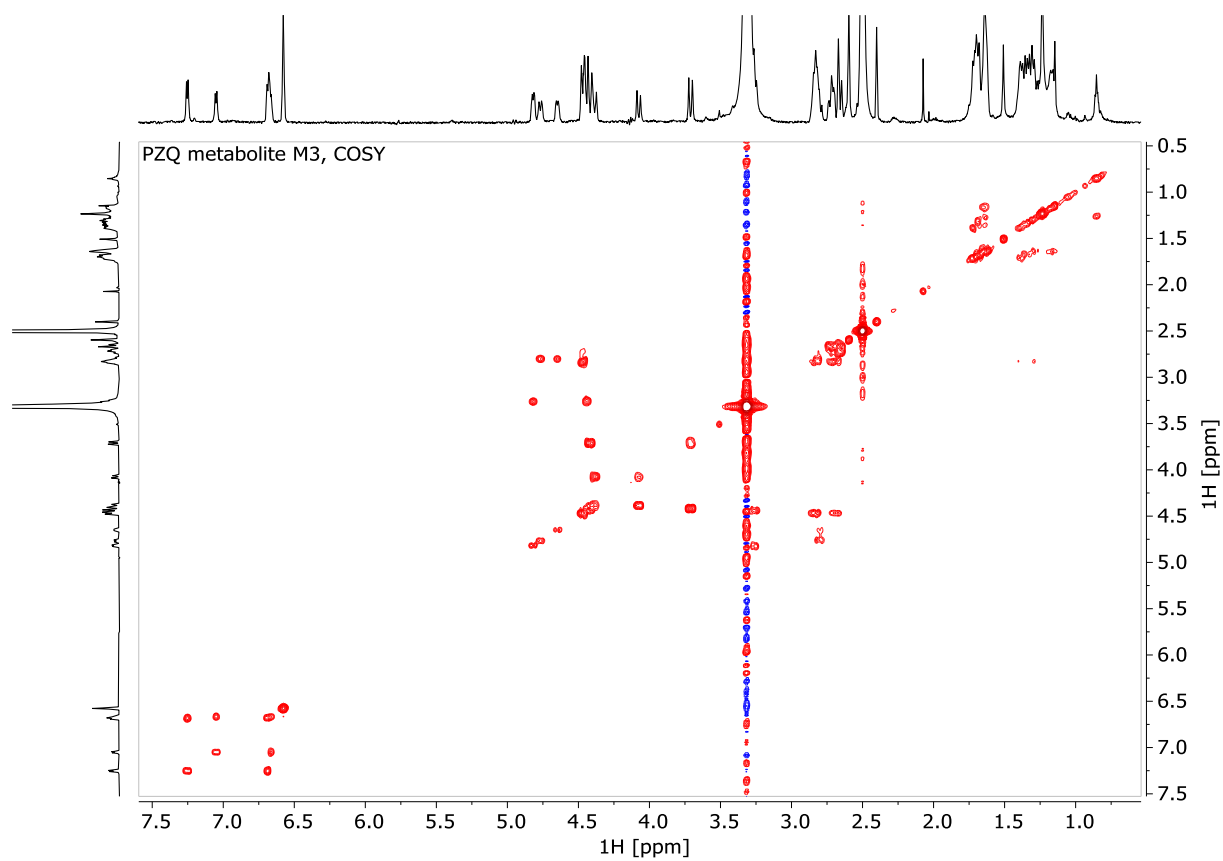
Supplemental Table 1. Mass spectral analysis of hydroxylated metabolites formed *in vitro* from **S-praziquantel**

Nuclear Magnetic Resonance

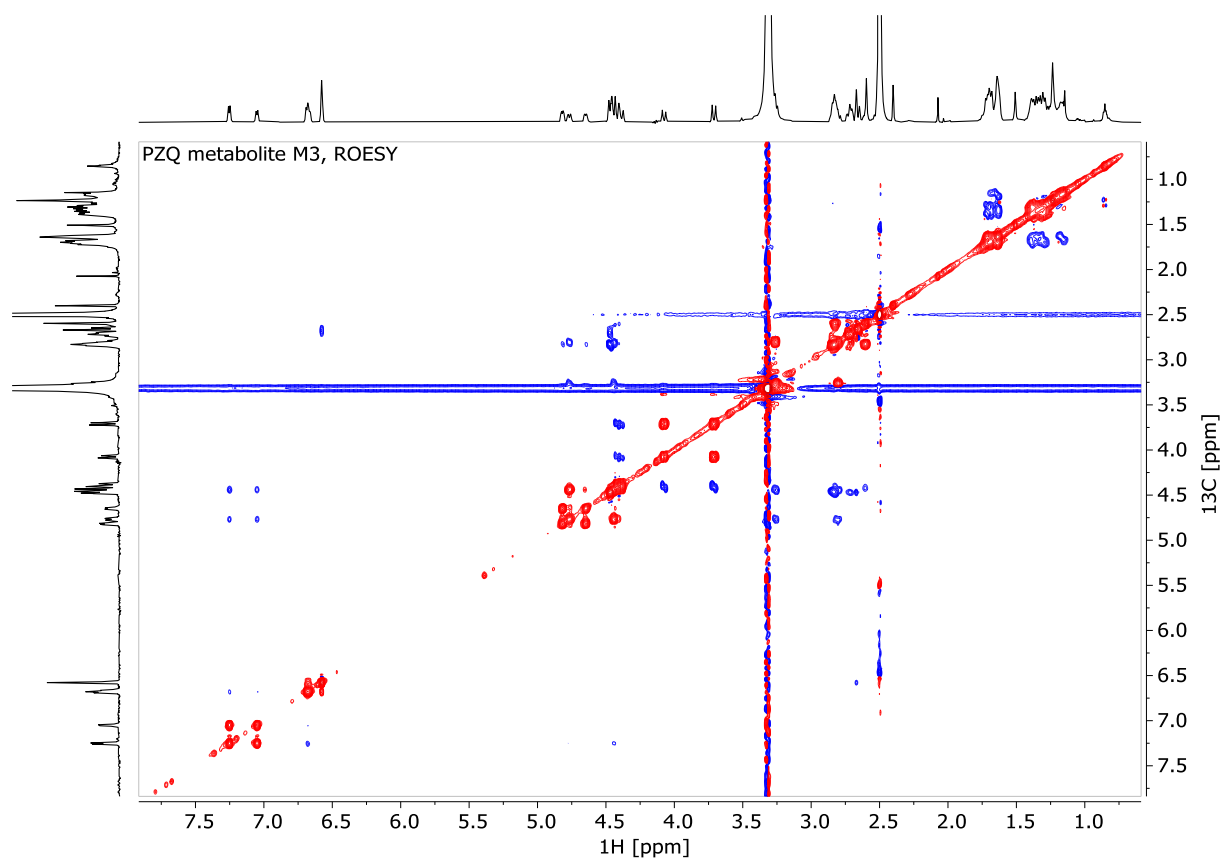
Supplemental Fig. 23. Assigned ^1H NMR spectrum of **S-9-hydroxy-praziquantel (M3)**



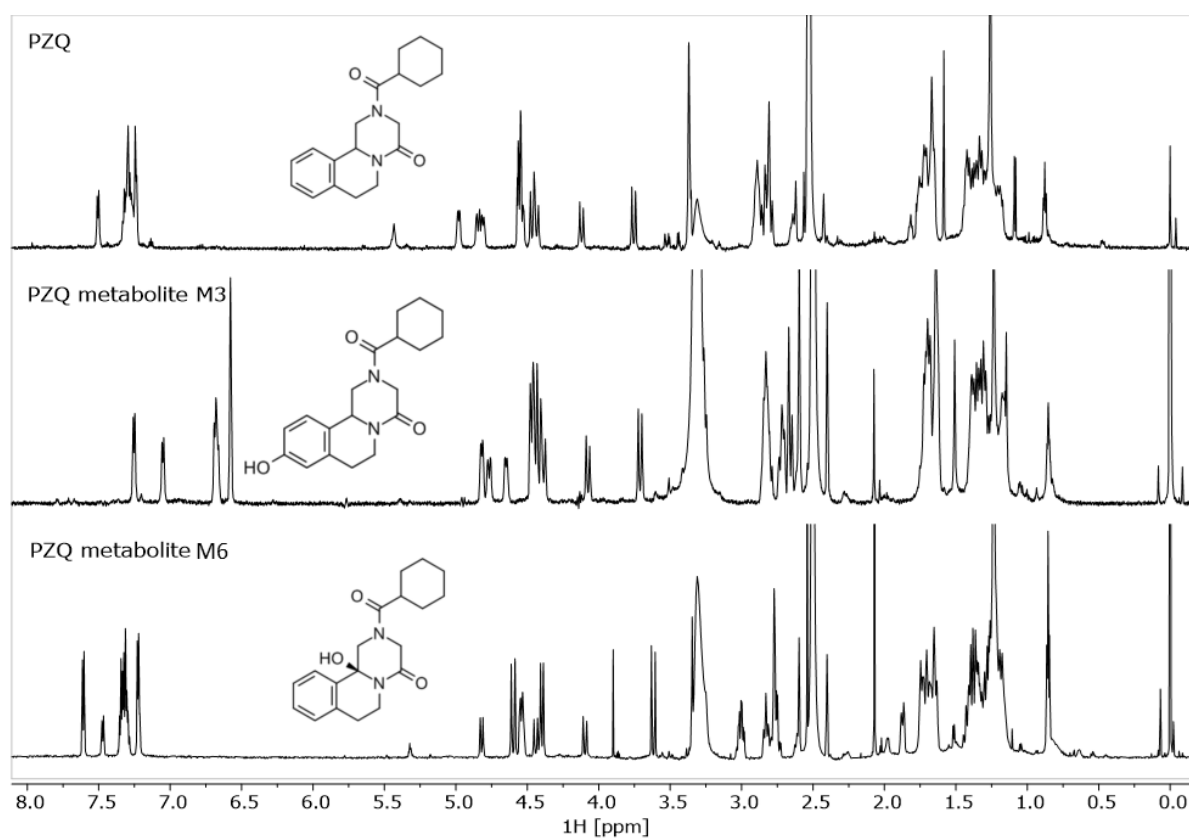
Supplemental Fig. 24. Edited heteronuclear single quantum coherence (HSQC) NMR spectrum of **S-9-hydroxy-praziquantel** (M3). Red: CH/CH₃, blue: CH₂



Supplemental Fig. 25. Edited homonuclear correlation spectroscopy (COSY) NMR spectrum of **S-9-hydroxy-praziquantel (M3)**



Supplemental Fig. 26. Edited rotating frame Overhauser enhancement effect spectroscopy (ROESY) NMR spectrum of **S-9-hydroxy-praziquantel** (M3). Blue: cross-peaks due to spatial proximity, red: cross-peaks due to chemical exchange, i.e. interconversion of conformers



Supplemental Fig. 27. Comparison of ^1H NMR spectra of **praziquantel** (PZQ), **9-hydroxy-praziquantel** (M3) and **11b-hydroxy-praziquantel** (M6) (^1H NMR spectra of PZQ and M6 from Vendrell-Navarro *et al.*, 2020)

References

- Biradha, K., Fujita, M., 2002. A springlike 3D-coordination network that shrinks or swells in a crystal-to-crystal manner upon guest removal or readsorption. *Angew. Chem. Int. Ed. Engl.* 41, 3392–3395.
- Dolomanov OV, Bourhis LJ, Gildea RJ, Howard JAK, and Puschmann H (2009) *OLEX2*: a complete structure solution, refinement and analysis program. *J Appl Crystallogr* 42: 339–341.
- Hoshino, M., Khutia, A., Xing, H., Inokuma, Y., Fujita, M., 2016. The crystalline sponge method update. *I.U.Cr.J.* 3, 139-151.
- Hübschle CB, Sheldrick GM, and Dittrich B (2011) *ShelXle*: a Qt graphical user interface for SHELXL. *J Appl Crystallogr* 44(Pt 6): 1281–1284.
- Ramadhar, T.R., Zheng, S.L., Chen, Y.S., Clardy, J., 2015. Analysis of rapidly synthesized guest-filled porous complexes with synchrotron radiation: practical guidelines for the crystalline sponge method. *Acta Crystallogr. A Found. Adv.* 71(Pt 1), 46–58.
- Sheldrick GM (2015) Crystal structure refinement with SHELXL. *Acta Crystallogr C Struct Chem* 71: 3–8.
- Vendrell-Navarro G, Scheible H, Lignet F, Burt H, Luepfert C, Marx A, Abla N, Swart P, and Perrin D (2020) Insights into Praziquantel Metabolism and Potential Enantiomeric Cytochrome P450-Mediated Drug-Drug Interaction. *Drug Metab Dispos* 48: 481–490.
- Zigon, N., Hoshino, M., Yoshioka, S., Inokuma, Y., Fujita, M., 2015. Where is the Oxygen? Structural Analysis of α -Humulene Oxidation Products by the Crystalline Sponge Method. *Angew. Chem. Int. Ed.* 54, 9033–9037.